

Wireless Communications and Mobile Computing

Advanced Intelligent Computing for Location-aware Services and Mobile Social Networks

Lead Guest Editor: Honghao Gao

Guest Editors: Walayat Hussain and Yuyu Yin





Advanced Intelligent Computing for Location-aware Services and Mobile Social Networks

Wireless Communications and Mobile Computing

**Advanced Intelligent Computing for
Location-aware Services and Mobile
Social Networks**

Lead Guest Editor: Honghao Gao

Guest Editors: Walayat Hussain and Yuyu Yin




Copyright © 2021 Hindawi Limited. All rights reserved.

This is a special issue published in “Wireless Communications and Mobile Computing.” All articles are open access articles distributed under the Creative Commons Attribution License, which permits unrestricted use, distribution, and reproduction in any medium, provided the original work is properly cited.

Chief Editor






















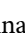

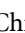


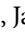





Zhipeng Cai , USA

Associate Editors

Ke Guan , China
Jaime Lloret , Spain
Maode Ma , Singapore

Academic Editors

Muhammad Inam Abbasi, Malaysia
Ghufran Ahmed , Pakistan
Hamza Mohammed Ridha Al-Khafaji ,
Iraq
Abdullah Alamoodi , Malaysia
Marica Amadeo, Italy
Sandhya Aneja, USA
Mohd Dilshad Ansari, India
Eva Antonino-Daviu , Spain
Mehmet Emin Aydin, United Kingdom
Parameshchhari B. D. , India
Kalapaveen Bagadi , India
Ashish Bagwari , India
Dr. Abdul Basit , Pakistan
Alessandro Bazzi , Italy
Zdenek Becvar , Czech Republic
Nabil Benamar , Morocco
Olivier Berder, France
Petros S. Bithas, Greece
Dario Bruneo , Italy
Jun Cai, Canada
Xuesong Cai, Denmark
Gerardo Canfora , Italy
Rolando Carrasco, United Kingdom
Vicente Casares-Giner , Spain
Brijesh Chaurasia, India
Lin Chen , France
Xianfu Chen , Finland
Hui Cheng , United Kingdom
Hsin-Hung Cho, Taiwan
Ernestina Cianca , Italy
Marta Cimitile , Italy
Riccardo Colella , Italy
Mario Collotta , Italy
Massimo Condoluci , Sweden
Antonino Crivello , Italy
Antonio De Domenico , France
Floriano De Rango , Italy


Antonio De la Oliva , Spain
Margot Deruyck, Belgium
Liang Dong , USA
Praveen Kumar Donta, Austria
Zhuojun Duan, USA
Mohammed El-Hajjar , United Kingdom
Oscar Esparza , Spain
Maria Fazio , Italy
Mauro Femminella , Italy
Manuel Fernandez-Veiga , Spain
Gianluigi Ferrari , Italy
Luca Foschini , Italy
Alexandros G. Fragkiadakis , Greece
Ivan Ganchev , Bulgaria
Óscar García, Spain
Manuel García Sánchez , Spain
L. J. García Villalba , Spain
Miguel Garcia-Pineda , Spain
Piedad Garrido , Spain
Michele Girolami, Italy
Mariusz Glabowski , Poland
Carles Gomez , Spain
Antonio Guerrieri , Italy
Barbara Guidi , Italy
Rami Hamdi, Qatar
Tao Han, USA
Sherief Hashima , Egypt
Mahmoud Hassaballah , Egypt
Yejun He , China
Yixin He, China
Andrej Hrovat , Slovenia
Chunqiang Hu , China
Xuexian Hu , China
Zhenghua Huang , China
Xiaohong Jiang , Japan
Vicente Julian , Spain
Rajesh Kaluri , India
Dimitrios Katsaros, Greece
Muhammad Asghar Khan, Pakistan
Rahim Khan , Pakistan
Ahmed Khattab, Egypt
Hasan Ali Khattak, Pakistan
Mario Kolberg , United Kingdom
Meet Kumari, India
Wen-Cheng Lai , Taiwan

Jose M. Lanza-Gutierrez, Spain
Pavlos I. Lazaridis , United Kingdom
Kim-Hung Le , Vietnam
Tuan Anh Le , United Kingdom
Xianfu Lei, China
Jianfeng Li , China
Xiangxue Li , China
Yaguang Lin , China
Zhi Lin , China
Liu Liu , China
Mingqian Liu , China
Zhi Liu, Japan
Miguel López-Benítez , United Kingdom
Chuanwen Luo , China
Lu Lv, China
Basem M. ElHalawany , Egypt
Imadeldin Mahgoub , USA
Rajesh Manoharan , India
Davide Mattera , Italy
Michael McGuire , Canada
Weizhi Meng , Denmark
Klaus Moessner , United Kingdom
Simone Morosi , Italy
Amrit Mukherjee, Czech Republic
Shahid Mumtaz , Portugal
Giovanni Nardini , Italy
Tuan M. Nguyen , Vietnam
Petros Nicolaitidis , Greece
Rajendran Parthiban , Malaysia
Giovanni Pau , Italy
Matteo Petracca , Italy
Marco Picone , Italy
Daniele Pinchera , Italy
Giuseppe Piro , Italy
Javier Prieto , Spain
Umair Rafique, Finland
Maheswar Rajagopal , India
Sujan Rajbhandari , United Kingdom
Rajib Rana, Australia
Luca Reggiani , Italy
Daniel G. Reina , Spain
Bo Rong , Canada
Mangal Sain , Republic of Korea
Praneet Saurabh , India

Hans Schotten, Germany
Patrick Seeling , USA
Muhammad Shafiq , China
Zaffar Ahmed Shaikh , Pakistan
Vishal Sharma , United Kingdom
Kaize Shi , Australia
Chakchai So-In, Thailand
Enrique Stevens-Navarro , Mexico
Sangeetha Subbaraj , India
Tien-Wen Sung, Taiwan
Suhua Tang , Japan
Pan Tang , China
Pierre-Martin Tardif , Canada
Sreenath Reddy Thummaluru, India
Tran Trung Duy , Vietnam
Fan-Hsun Tseng, Taiwan
S Velliangiri , India
Quoc-Tuan Vien , United Kingdom
Enrico M. Vitucci , Italy
Shaohua Wan , China
Dawei Wang, China
Huaqun Wang , China
Pengfei Wang , China
Dapeng Wu , China
Huaming Wu , China
Ding Xu , China
YAN YAO , China
Jie Yang, USA
Long Yang , China
Qiang Ye , Canada
Changyan Yi , China
Ya-Ju Yu , Taiwan
Marat V. Yuldashev , Finland
Sherali Zeadally, USA
Hong-Hai Zhang, USA
Jiliang Zhang, China
Lei Zhang, Spain
Wence Zhang , China
Yushu Zhang, China
Kechen Zheng, China
Fuhui Zhou , USA
Meiling Zhu, United Kingdom
Zhengyu Zhu , China


Contents

Joint Modeling of User Behaviors Based on Variable-Order Additive Markov Chain for POI Recommendation

RuiChang Li 


Research Article (13 pages), Article ID 4359369, Volume 2021 (2021)

Attribute Extraction Study in the Field of Military Equipment Based on Distant Supervision

Xindong You, Meijing Yang, Junmei Han, Jiangwei Ma, Gang Xiao, and Xueqiang Lv 




Research Article (13 pages), Article ID 2549488, Volume 2021 (2021)

The Mobile Water Quality Monitoring System Based on Low-Power Wide Area Network and Unmanned Surface Vehicle

Wei Chen, Xiao Hao, Kui Yan , JianRong Lu, Jin Liu, ChenYu He, Feng Zhou, and Xin Xu



Research Article (16 pages), Article ID 1609612, Volume 2021 (2021)

Applying Deep Learning Technologies to Evaluate the Patent Quality with the Collaborative Training

Xindong You , Jiaqi Liu, Zhe Wang, Zhaonan Liu, Xueqiang Lv , and Jung Yoon Kim 

Research Article (23 pages), Article ID 5006974, Volume 2021 (2021)

An Experiment to Design an Operation and Maintenance System Integrating Apriori Association Rules for a Telecom Platform

Chengfan Li , Lan Liu , Junjuan Zhao, and Yuejun Liu



Research Article (14 pages), Article ID 1185584, Volume 2021 (2021)

An Implicit Preference-Aware Sequential Recommendation Method Based on Knowledge Graph

Haiyan Wang , Kaiming Yao , Jian Luo , and Yi Lin 





Research Article (12 pages), Article ID 5206228, Volume 2021 (2021)

A Novel Approach of Intelligent Computing for Multiperson Pose Estimation with Deep High Spatial Resolution and Multiscale Features

Haiquan Wang, Xiangyang Wang, Yijie Shi, Yanping Li , Chunhua Qian , and Rui Wang 




Research Article (11 pages), Article ID 4948067, Volume 2021 (2021)

Research on Named Entity Recognition of Electronic Medical Records Based on RoBERTa and Radical-Level Feature

Yue Wu , Jie Huang , Caie Xu, Huilin Zheng , Lei Zhang, and Jian Wan 

Research Article (10 pages), Article ID 2489754, Volume 2021 (2021)

Story Generation Using Knowledge Graph under Psychological States

Feifei Xu , Xinpeng Wang , and Shanlin Zhou 

Research Article (12 pages), Article ID 5530618, Volume 2021 (2021)

Research Article

Joint Modeling of User Behaviors Based on Variable-Order Additive Markov Chain for POI Recommendation

RuiChang Li 

Beijing Key Lab of Intelligent Telecommunications Software and Multimedia, Beijing University of Posts and Telecommunications, and the School of Computer Science (National Pilot Software Engineering School), Beijing University of Posts and Telecommunications, Beijing 100876, China

Correspondence should be addressed to RuiChang Li; lrc@bupt.edu.cn

Received 20 August 2021; Revised 8 October 2021; Accepted 25 October 2021; Published 23 November 2021

Academic Editor: Yuyu Yin

Copyright © 2021 RuiChang Li. This is an open access article distributed under the Creative Commons Attribution License, which permits unrestricted use, distribution, and reproduction in any medium, provided the original work is properly cited.

The POI recommendation system has become an important means to help people discover attractive and interesting places. Based on our data analysis, we observe that users pay equal attention to conservatism and curiosity. In particular, adopting analysis corresponding to different time intervals, we find that users lean towards old POIs in the short term and look for new POIs with the increase of the time interval. However, existing approaches usually neglect users' conservatism and curiosity preferences. Therefore, they are confronted with a bottleneck of depicting accurate user needs, making it difficult to improve the recommendation performance further. Besides, we further find that the number of user daily check-ins has uneven distribution, which is not conducive to capture the accurate transition patterns of user behaviors. In light of the above, we design a single POI sequential method. On this basis, we propose a recommendation method of the variable additive Markov chain. We consider the user sequential preferences, especially liking old and pursuing new features. In addition, our model exploits the geographical tendency of user behaviors. Finally, we conduct abundant experiments on four cities in the two real datasets, i.e., Foursquare and Jiebang. The experimental results show its superiority over other competitors.

1. Introduction

Recommender systems are valuable tools that play a crucial role in mitigating information overload problems. Today, such systems are used in many application domains [1–3]. With the increasing popularity of WSN [4] and location-based social networks (LBSNs), such as Foursquare, Gowalla, and Yelp, unlimited possibilities are provided for users to share their highlights. Users not only explore location-aware information but also write reviews and share their experiences [5]. In LBSNs, user-generated trajectory data contains rich information, such as POI location, category, content, visited time, and trajectory sequence, which can be used to exploit user's preferences for providing personalized POI recommendation for the target user. There are huge business opportunities. So the academic and industry has invested a great deal of enthusiasm and energy in studies of recommendation, such as location-based activity recommendation [6], friend recommendation [1, 7], and location rec-

ommendation [8, 9]. In these studies, providing location recommendations becomes an important application with the rapid emergence of LBSNs, such as POIs recommendation [10–16] and routes recommendation [17, 18].

Existing researches mainly study how to use time influence, geographical influence, social relationship, and other characteristics for POI recommendation. For example, a user is more likely to choose a restaurant for dinner at noon. A POI closer to the current location is more popular with the user, and friends may have similar preferences. However, these studies mainly provide POI recommendations based on common sense analysis and fail to notice that users' past experiences that will affect their attitudes towards POI. For example, the pursuit of familiarity and novelty is also an important factor. Through data analysis and reasoning, we found some interesting phenomena to consider POI recommendations from a new perspective.

In a limited geographic space, users tend to like the old and pursue the new. We define POIs that users have visited

as old POIs and that have not been visited in the previous period as new POIs. Due to time and distance constraints, the user choice space and the number of new POIs are limited. For a user, he chooses a POI considering his available time and the acceptable transfer distance. For example, if the user only has half an hour, POIs that take longer than an hour are not considered. If the user likes to walk, then POIs within 1 km are more popular. Long-distance movement requires more time and financial support, which limits users' desire to visit it. The POIs that users frequently visit are not evenly distributed geographically but clustered around limited centers [19, 20]. For example, users have more check-ins near their homes, workplaces, and popular areas. Taylor's first law of geography also confirms this phenomenon [21]. Obviously, the category and number of POIs are limited in a limited geographic area. After repeated exploration by users, new POIs will gradually become old. Therefore, users can only choose POIs on the premise that the new is less and the old is more.

The POI alternates between the old and the new, driving users to like the old and pursue the new POIs. As we all know, users often visit the same POI multiple times, and each visit has a different experience. For example, it is impossible for the user to taste all dishes of a restaurant at one time. For scenic spots, users will find discoveries during repeated visits. For example, climbing the Great Wall from different roads has different sceneries, and the view in the morning and evening is also different. In addition, the POI is also changing. For example, POIs may be updated irregularly, and the surrounding environment may also vary. Just as it is impossible for a person to step into the same river, all the POIs constantly change. Changes of the POI and the surrounding environment will make the old POI glow with new appeal. Intuitively, users will prefer the new POI to the old one. For example, if a restaurant leaves a good memory to the user, the user's experience of going to this restaurant again for dinner will not be worse than the last time and may be better. The user will not wander in the corridor as he revisited the museum the first time, he will be more confident, and the second visit will be smoother than the initial visit [22].

Sparse trajectories affect the acquisition of POI relationships. We define a sequence containing multiple POIs as a dense trajectory, and correspondingly, the other holding a single POI is called a sparse trajectory. Intuitively, a user sometimes generates multiple check-ins a day. Occasionally, they check in only one POI, and even worse, they do not do that for several days. Some studies believe that there is an association relationship between POIs that a user visits continuously, and this relationship reflects the law of co-occurrence between them. Intuitively, due to the continuity of user behavior, the smaller the time interval between check-ins, the more the influential impact on the next behavior. In practice, there are studies that use hours, days, weeks, months, etc., as time intervals [23]. No matter what time interval is used, there will be dense and sparse trajectories coexisting. Currently, two methods are usually used to deal with sparse trajectories: (1) filter out the check-in records of a single POI and only retain the dense trajectories

that visit multiple POIs in a day and (2) increase the time threshold between adjacent POIs to expand the coverage of a single trajectory. For example, we can adjust the time interval so that POIs of several consecutive days are formed a trajectory. However, both of them have drawbacks. The first method will make user data more sparse, which is not conducive to accurately obtaining user preferences. Correspondingly, although the second method reduces data loss, it introduces some additional noise. Obviously, additional noise may interfere with the accuracy of user preferences.

In this paper, we propose a variable-order additive Markov chain based on sequential patterns, the influence of liking the old and pursuing the new, and geographical restriction (SONG). In SONG, the model consists two components: POI transition and variable influence. The POI transition probability model is used to obtain the one-step transition probability between any POIs. The variable influence model is used to extract the joint influence of three factors. We first construct a POI-POI transition graph based on the user-POI interaction sequence contained in check-in trajectories of all users. The transition probabilities can be deduced by dividing transition degrees by outgoing degrees of the graph vertex. Then, we jointly model the variable effects of liking old, pursuing new, and geographical restriction based on the mere exposure effect [24], depreciation theory [25], and Taylor's first law [21], respectively. We finally provide TOP-N POI recommendations. The main contributions of this paper can be summarized:

- (1) User check-in behavior has an apparent feature of liking the old and pursuing the new. Currently, there is no research on this feature. We found that it is mainly due to the unbalanced distribution of interest POIs and user likes to pursue familiarity and novelty, which provides new ideas for POI recommendations
- (2) The check-in number of a user is very uneven every day. For example, there may be only one or no record in a day. This imbalanced situation influences acquiring the sequence pattern implied by the user's check-in behavior. We propose a method to serialize sparse trajectories, which alleviates the problems caused by the neglect of a single POI or the introduction of additional noise by extending the sequence and better obtain user preferences
- (3) Based on the above discovery and the results of single POI serialization, we propose a variable-order additive Markov chain model to capture the influence of historical sequences on subsequent POIs. Then, we use the mere exposure effect and depreciation theory to jointly model the users' preference of preferring old, pursuing new, and combine the geographical restriction to provide personalized recommendations
- (4) We conducted extensive experiments on four city subsets of real trajectory datasets, Foursquare and Jiebang. Experimental results show that our model outperforms other state-of-the-art methods.

The remainder of the paper is organized as follows. In Section 2, we review related work on POIs recommendation. In Section 3, we first describe and define the task we are tackling. Then, we make data analysis on four subdatasets of two real-world datasets. In Section 4, we present our proposed model SONG for POI recommendation in detail. In Section 5, we describe our experiment settings for evaluating the performance of SONG against the state-of-the-art POI recommendation techniques. Finally, Section 6 concludes this paper.

2. Related Work

POI recommendation based on trajectories is a hot topic in LBSNs, and it has attracted increasing attention in both academia and industry. Therefore, we briefly introduce three lines of researches related to our task: (a) POI recommendation based on temporal; (b) recommendation based on geographical influence; and (c) sequential POI recommendation. All of these factors are closely related to acquiring user preferences [26].

2.1. POI Recommendation Based on Temporal. Temporal influence plays a vital role in POI recommendation. Yuan et al. [10] found out that most users tend to visit different POIs at a different time in a day, and the check-in behaviors between neighbor time slots are similar. In addition to that, Zhang et al. [27] pointed out that POI may be not available in all time, for example, POIs are only accessible during their opening hours. He et al. [28] investigated the temporal popularity of a POI and the temporal check-in trends to provide personalized POI recommendation. He et al. [28] propose a spatial-temporal topic model (STM), which embedded the temporal and spatial patterns in users check-in activities. Oppokhonov et al. [29] develop a recommendation system based on a directed graph. The algorithm of the system considers both the temporal factor and the distance for recommending a new POI for next hours. Gao et al. [30] put forward four temporal aggregation strategies, such as sum, mean, maximum, and voting, to integrate a user's check-in preferences of different temporal states. The method using the strategy greatly improves the POI recommendation performance. Ji et al. [31] proposed a social-period-aware topic model (SPATM) to learn the influence weights of both user interests and her social preferences on making-decision for each check-in time automatically. Actually, the time law of users' behaviors include two different patterns, i.e., periodic and aperiodic. For example, a user may like to find a restaurant for dinner at noon, which is periodic. Since the historical experience will affect the user's choice of the target POI, this influence is generally believed to be related to the interval between visiting two POIs. For convenience, we use the interval hops between POIs instead of specific time to model aperiodic effects.

2.2. Recommendation Based on Geographical Influence. In LBSNs, the geographical influence is an important factor that distinguishes the POI recommendation from other rec-

ommendations because physical interactions are required for users to visit POIs [32]. For example, users prefer to select POIs near to their homes or offices and also may be fond of exploring the nearby POIs of their current locations. Several studies have attempted to leverage the geographical influence to improve POI recommendation systems [33, 34]. Ye et al. [35] proposed a power-law distribution model to capture the geographical influence, and proposed a collaborative POI recommendation algorithm based on geographical influence via naive Bayesian. Because it is difficult to find an anchor point to derive a reasonable distance for the new POI, Zhang et al. [32] develop a kernel function to model the geographical influence. The kernel function on two-dimensional is more reasonable than the one-dimensional distance power-law distribution. For users' check-ins is unevenly distribution. Some exiting studied assume that user checked locations conform to the Gaussian distribution of multiple centers. Chenget al. [19] proposed a multicenter Gaussian model to capture the geographical influence for POI recommendation. In addition to directly using geographical influences, there are some joint model methods. Liu et al. [13] develop a general geographical probabilistic factor model (Geo-PFM) to capture the geographical influence on user mobility behaviors, and then combine the influence with Bayesian nonnegative matrix factorization (BNMF) to model user preferences. Finally, POIs are recommended for users by combining the effects of multiple factors. Yin et al. [12] propose a joint probabilistic generative model to integrate geographical-social influence, temporal and word-of-mouth effect for solving check-in data sparsity in the out-of-town recommendation scenario. Griesner et al. [15] propose a augmenting matrix factorization model (GeoMF-TD) for POI recommendation by combining geographical and temporal influences. Li et al. [16] put forward a ranking based geographical factorization method (Rank-GeoFM) model to provide POIs prediction. Specifically, the proposed model can easily combine geographical influence and temporal influence. In this paper, we use power-law distribution to capture the influence of distance on the user's choice of POI.

2.3. Sequential POI Recommendation. In the real world, users' behaviors usually happen in succession, and the next action is often related to the previous one. In recent years, studies have focused on various sequential recommendation tasks, such as next POI recommendation [29, 36]. Early studies were typically based on the Markov chain models for sequential recommendation [32, 36]. For example, He and McAuley [36] proposed fossil that fuses similarity-based models with the Markov chains to predict personalized sequential behavior. Cheng et al. [8] developed a matrix factorization method, which embeds the personalized Markov chains and the localized regions for solving the sequential recommendation task. The order of the Markov chain model decides the scale-free parameters. A higher order will increase the computation cost. Following the development of machine learning, a lot of complex models have been proposed: recurrent neural networks (RNNs) [37], convolutional neural networks (CNNs) [38, 39], translation-based

methods [40], and attention mechanism [41]. Approaches based RNN are popular models for sequential recommendation due to their performance on sequential works. Liu et al. [42] extend RNN and propose a novel method to model temporal and spatial contexts for different time intervals and distance-specific transition matrices for different geographical distances. However, existing RNN methods neglect some details of users preferences, thus making the recommendation results unreliable. To address the above limitations, Sun et al. [43] proposed a method named LSTPM for next POI recommendation. Li et al. [44] introduce a novel neural network model named TMCA that employed the LSTM-based encoder-decoder framework for the next POI recommendation. In this paper, we use a variable high-order Markov chain to model the relationship between preceding POI to the posterior in trajectory.

3. Task Definition and Data Analysis

In this section, we first describe and define the task we are tackling. Then, we make data analysis on four subdatasets of two real-world datasets, which serve as the foundation of our model.

3.1. Task Definition. A notation U denotes the collection of users $U = \{u_1, u_2, \dots, u_{|U|}\}$, and the notation V represents the collection of POIs $V = \{v_1, v_2, \dots, v_{|V|}\}$. We use the v to represent a POI identifier and l_v to denote its corresponding geographical attribute in terms of longitude and latitude coordinates. For each user $u \in U$, we sort her historical records by time and subdivided these into trajectories with different lengths relying on the suitable time interval, i.e., $S_u = \{s_u^1, s_u^2, \dots, s_u^n\}$, where n denotes the latest trajectory. The subtrajectory $s_u^j = \{v_1, v_2, \dots, v_t\}$ is the j th trajectory of user u . Given a trajectory set of target user u , our goal is to recommend Top- N POIs, namely $\Pr(v | s_u^j) = \Pr(v | v_n, v_{n-1}, v_2, v_1)$.

3.2. Dataset Description. We conduct analysis on four real-world datasets from the Foursquare [45] and the JiePang [11]. The Foursquare check-in dataset is from 12 April 2012 to 16 February 2013 in New York (NYC) and Tokyo (TKY), while JiePang contains Beijing and Shanghai from April 2011 to April 2013. For all of them, we filter unpopular POIs with less than five user visits.

3.3. Data Analysis. In theory, users can check any locations. However, user behavior is affected by various factors such as available time, geographic distance, and economic support. Users often look for interesting POIs near their living and working centers. Intuitively, users' repeated exploration might make POIs less appealing, but users can always find pleasure in these POIs. It is worth exploring that makes these POIs so appealing.

We divide POIs into two categories. POIs that appeared in the last time period are called old POIs, and the corresponding ones that did not appear are called new POIs. Figure 1 shows the new and old changes of POIs by different time intervals. We use different time intervals to analyze the new and old changes of visited POIs. Traditionally, we

divide a year into 52 weeks. In the figure, "2012-02" indicates the second week of 2012. Figure 1 contains four cities information, and every city has two figures. The left takes one week as an interval, and the right is five weeks. As we can see from the left figure of every city, the old POI is predominant. Especially, the Foursquare dataset shows this more clearly. Comparing the left and right, it is clear that the ratio of new POIs is predominant in JiePang. Although the proportion of old POIs exceeds the new POIs, the new increases and old decreases.

According to the above analysis, we can come to the following conclusion: Users are conservative in the short term and show more curiosity characteristics with the increase of the time interval. Making full use of users' preference features of liking old and pursuing new simultaneously may improve the recommendation performance.

4. The Proposed Model

In this section, we present our proposed model SONG in detail. SONG mainly consists of three parts, which are the sequential recommendation modeling and the old and new influence weight modeling. Our main contribution lies in joint modeling liking the old and pursuing the new influence, the geographical influence for sequential recommendation in a unified way.

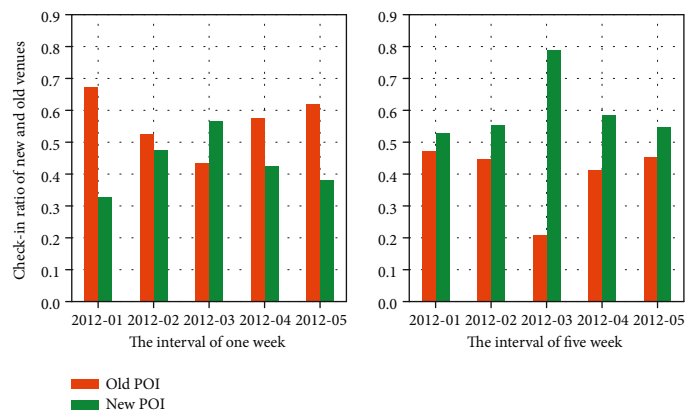
4.1. Modeling Sequential Recommendation Based on Trajectory. For sequential recommendation, the order-based models are used to derive order patterns from items sequences of users', such as using the Markov chains [36, 46]. Inspired by the successful cases of the Markov method in capturing sequence features and the high compatibility [46] with the problem in our paper, we use the high-order Markov chain model to model the sequential recommendation task. The mathematical form of this model is shown by the following equation.

$$\Pr(v_r | s_u^j) = \Pr(v_r = v_{t+1} | v_t, v_{t-1}, \dots, v_2, v_1). \quad (1)$$

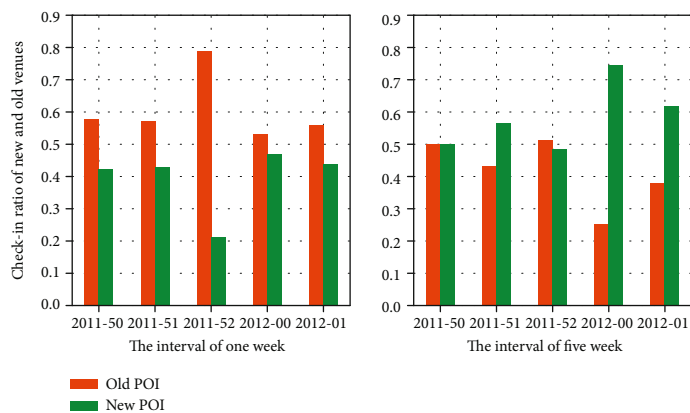
However, as [47] points out, if the k -order Markov chain has n possible states, it usually leads to exponential expansion on the number of states, e.g., $(n-1)n^k$. Moreover, high-order Markov chains also suffer from the sparsity of transitions in the given dataset, which discourages people from using a higher-order Markov chain directly and leads to ineffectiveness in modeling the behaviors of users. Inspired by [32, 47], a higher-order Markov chain model involves only one additional parameter for each one-step transition probability. The model can be written as follows:

$$\Pr(v_r | s_u^j) = \Pr(v_r = v_{t+1} | s_u^j) \approx \sum_{i=1}^t w_u \Pr(v_{t+1}, v_{t+1-i}), \quad (2)$$

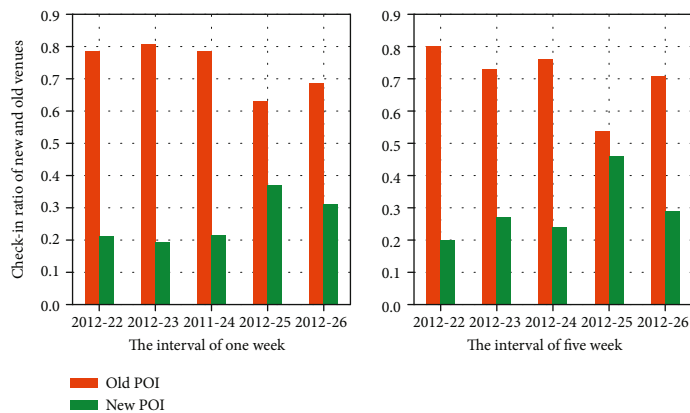
where $\Pr(v_{t+1}, v_{t+1-i})$ denotes the one-step transition probability from POI v_{t+1-i} to POI v_{t+1} and w_u is the additional parameter.



(a)

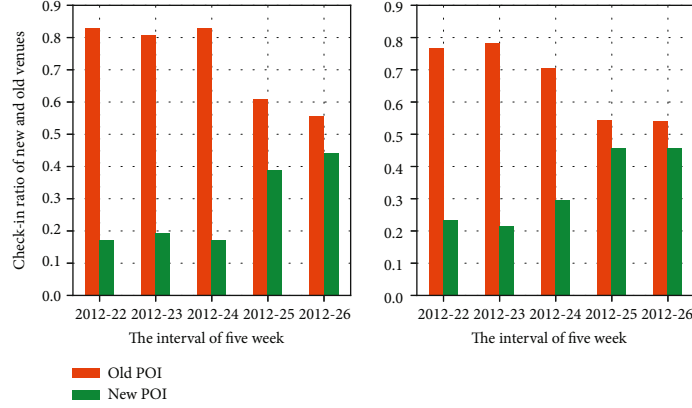


(b)



(c)

FIGURE 1: Continued.



(d)

FIGURE 1: Changes of the ratio of new and old POIs on four datasets at different time intervals. (a) Beijing (Jiepan). (b) Shanghai (Jiepan). (c) NYC (Foursquare). (d) TKY (Foursquare).

Input: Training trajectories of user u : $S_u, s_u^j \in S_u, u \in U$.
Output: Dense trajectories set of user u : S'_u

- 1: for ($u = 0; u < |U|; u++$) **do**
- 2: Get the trajectories count of u : $|S_u|$;
- 3: Set trajectory index: $p = 0$;
- 4: **while** $p < |S_u|$ **do**
- 5: Get the length of trajectory $|s_u^p|$;
- 6: **if** $|s_u^p| > 2$ **then**
- 7: $p \leftarrow p + 1$
- 8: **else if** $|s_u^p| \leq 1$ and $p = 0$ **then**
- 9: Add the current trajectory to the next one
- 10: **else if** $|s_u^p| \leq 1$ and $p < (|S_u| - 1)$ **then**
- 11: Get the time interval of $T_{s_u^p - s_u^{p-1}}$ and $T_{s_u^{p+1} - s_u^p}$.
- 12: **if** $T_{s_u^p - s_u^{p-1}} \leq T_{s_u^{p+1} - s_u^p}$ **then**
- 13: Insert s_u^p to s_u^{p-1} , $p \leftarrow p + 1$
- 14: **else**
- 15: Insert s_u^p to s_u^{p+1} , $p \leftarrow p + |s_u^{p+1}| + 1$
- 16: **end if**
- 17: **else**
- 18: Insert s_u^p into s_u^{p-1} , $p \leftarrow p + 1$
- 19: **end if**
- 20: **end while**
- 21: **end for**
- 22: Return S'_u .

ALGORITHM 1: Serialization algorithm.

4.1.1. One-Step Transition Probability. The number of POIs that a user visits every day is unevenly distributed, and sparse trajectories containing a single POI are sometimes ignored in mining POIs transition patterns. In order to make reasonable use of these sparse trajectories, we propose a method to serialize sparse trajectories. The core idea is as follows. We first split the user's training data by one day and then determine whether it needs to be serialized according to the length of the trajectory. When the user's trajectory

length of a day is greater than 2, this trajectory does not need to be processed. The processing flow is shown in the pseudocode on lines 5-7. When the trajectory length is equal to 1, it needs to be dealt with in three cases: (1) If it is the first trajectory of the user, insert this one into the next one; (2) if it is the last trajectory of the user, add this trajectory to the previous one; and (3) in other cases, it needs to judge the time interval to the previous and the subsequent trajectories and insert the current trajectory into the closer trajectory. The insert operation is relatively simple, it only needs to modify the inserted trajectory's date to the date of the target trajectory, and the time remains unchanged. For example, the date of the target trajectory is October 6, 2016, and the date and time of the trajectory to be inserted is October 7, 2016, 13:23:11. It only needs to change the date to October 6, 2016. Comparing S'_u with S_u , only the date of some trajectories in S'_u has changed, and the time remains the same to retain the user's time-related preferences. The time remains unchanged at 13:23:11. The specific operation process is shown in the following algorithm.

Inspired by [32], the one-step transition probabilities between two POIs are derived by employing the first-order Markov chain. They are supposed to be fixed, which can be represented by the following equation:

$$\Pr(v_{t+1} | s_u^j) = \Pr(v_{t+1} | v_t) = \frac{\text{ToDegree}(v_t, v_{t+1})}{\text{AoDegree}(v_t)}, \quad (3)$$

when $\text{AoDegree}(v_t) > 0$, where $\text{AoDegree}(v_t)$ is out degree of POI v_t and $\text{ToDegree}(v_t, v_{t+1})$ is the degree from v_t to v_{t+1} . When $\text{AoDegree}(v_t) = 0$, $\Pr(v_{t+1} | v_t)$ denotes the following:

$$\Pr(v_{t+1} | v_t) = \begin{cases} 1, & v_{t+1} = v_t \\ 0, & v_{t+1} \neq v_t. \end{cases} \quad (4)$$

4.1.2. Modeling the Influence Weight of User Pursuing Old. It is common that the more exposure something is in front of

us, the more it will strengthen our attitude towards it. Users' attitudes towards things can be divided into three categories: like, neutral, and dislikes. Since the neutral attitude does not change the user's opinion, it can be classified into the other two categories, or ignored. According to this assumption, users' attitudes can be divided into two categories: like and dislike. A user's check-in record is positive feedback. For example, a user who checks in a restaurant indicated that he likes the restaurant.

If a user repeatedly checks in a POI, it indicates that the user likes the POI more. Similarly, if the user does not like it, the record of it will not exist. We assume that if the user checks in to the current POI multiple times, the probability of the POI being checked in again will increase. Based on this hypothesis, we use the following equation to express the exposure effect in the subtrajectory of user u . Multiple exposures of POI v may make the user's loving old preference to be enhanced.

$$\Gamma(u, v_\kappa)_{s_u^j} = 1 + \left(\frac{\sum_{r=1}^{|s_u^j|} \mathbb{1}_{v_r=v_\kappa}}{R} \right)_{v_\kappa \in s_u^j}^{\phi_u}, \quad (5)$$

where $\mathbb{1}_{\text{cond}}$ is the indicator function, and it returns 1 if cond is satisfied, or otherwise returns 0. R is the maximum number that the user checked in repeatedly in all trajectories. ϕ_u is u 's personalized parameter for exposure. The exposure influence $\Gamma(u, s_u^j, v)$ monotonically increases as the POI is visited repeatedly.

4.1.3. Modeling the Influence Weight of User Pursuing New. In real life, visiting a POI is a consumable activity. For example, users need to spend time or move a certain distance to enjoy the happiness brought by POI-related activities [18]. The memory of the user's access to the POI will affect the novelty of the subsequent POI, and the impact is related to the time interval. Like depreciation in economics, the residual value is smaller when the time is longer, and the possibility of purchasing new equipment is greater [25]. We assume that the POI currently checked in by the user will affect the utility of subsequent POIs, and this effect is related to the time interval. The larger the interval, the weaker the impact, making users more likely to choose a new POI. For convenience, we use interval hops instead of time intervals. For example, for the sequence "a, b, c, d," the number of hops between ab, ac, and ad are 1, 2, and 3. We assume that the influence of the current POI on the rear target POI is inversely proportional to the total number of hops between them, and we use the following equation to express the pursuit of newness.

$$\Psi(u, \kappa)_{s_u^j} = \frac{c_u}{\kappa^{\alpha_u} e^{\beta_u \kappa}}, \quad (6)$$

where c_u , α_u , and β_u are personalized parameters and κ refers to the intervals between the current POI to the target POI visited by the same user.

4.1.4. Modeling Geographical Influence. Some existing studies show that the geographical proximities of POIs have a significant influence on users' check-in behavior. To better understand this geographical influence on users, Ye et al. [35] performed a spatial analysis on user check-in activities records collected from the Foursquare. A significant percentage of two consecutive POIs visited by the same user appear to be within a short distance. There are three tendencies: (1) people tend to select POIs near their homes or workplaces; (2) people may prefer to explore POIs from current location; and (3) the POI visited by the user conforms to the Gaussian distribution of multiple centers, which means that the POI visited by the user is not evenly distributed but concentrated in several areas [48]. Based on the above conclusions, it can be seen that distance is the core of geographic influence. There are many mature models for modeling geographic influence, for example, power-law, exponential, and hyperbolic [34]. Thus, we also use power-law distribution to model the check-in probability to the distance between two POIs visited by the same user.

$$Y(d) = a_u \times d^{-b_u}, \quad (7)$$

where a_u and b_u are parameters of a power-law distribution and d refers to the distance between the current POI to the target POI visited by the same user.

4.2. Integrating Model and Inferring Model Parameters. According to the above submodel representation, we change Equation (2) to Equation (8). The weight w_u^i becomes a combination of distance, liking the old, and pursuing the new.

$$\begin{aligned} \Pr(v_r | s_u^j) &\approx \sum_{i=1}^t w_u \Pr(v_{t+1}, v_{t+1-i}) \\ &= \sum_{i=1}^t Y(d) \cdot \left[\mu \cdot \Gamma(u, v_i)_{s_u^j} + (1 - \mu) \Psi(u, i)_{s_u^j} \right] \\ &\quad \cdot \Pr(v_{t+1}, v_{t+1-i}), \end{aligned} \quad (8)$$

where μ is the parameter of liking old and $1 - \mu$ is the pursuing new, respectively.

Let θ denote the set of parameters in the personalized SONG framework. Then, we define our optimization problem to obtain the optimal θ^* as follows:

$$\Theta^* = \underset{\Theta}{\operatorname{argmax}} \prod_u \prod_{s_u, s_u^j \in S_u} P_r(v_r | s_u^j; \Theta). \quad (9)$$

The goal of this problem is aimed at maximizing the probability of predicting the last POI given the rest of an observing sequence s_u . To solve this optimization problem, we employ the maximum a posteriori (MAP) estimation on the following log-likelihood function:

$$\begin{aligned}
\Theta^* &= \underset{\Theta}{\operatorname{argmin}} \mathcal{L} = -\sum_u \sum_{s_u, s_u^j \in \mathcal{S}_u} \ln P(v | s_u^j; \Theta) \\
&= -\sum_u \sum_{S_u} \ln \sum_{i=1}^t Y(d) \cdot \left[\mu \cdot \Gamma(u, v_i)_{s_u^j} + (1 - \mu) \Psi(u, i)_{s_u^j} \right] \\
&\quad \cdot \Pr(v_{t+1}, v_{t+1-i}).
\end{aligned} \tag{10}$$

Furthermore, the gradient of the log-likelihood L with respect to the model parameters is given by

$$\begin{aligned}
\frac{\partial \mathcal{L}}{\partial \theta} &= -\sum_u \sum_{s_u} \frac{\sum_{i=1}^t \left[Y(\cdot) \cdot \mu \left(\frac{\partial \Gamma(\cdot)_{s_u^j}}{\partial \theta} \right) \right] \Pr(\cdot)}{\sum_{i=1}^t Y(\cdot) \cdot \left[\mu \cdot \Gamma(\cdot)_{s_u^j} + (1 - \mu) \Psi(\cdot)_{s_u^j} \right] \Pr(\cdot)}, \theta \in \{\phi_u\}, \\
\frac{\partial \mathcal{L}}{\partial \theta} &= -\sum_u \sum_{s_u} \frac{\sum_{i=1}^t \left[Y(\cdot) (1 - \mu) \left(\frac{\partial \Psi(\cdot)_{s_u^j}}{\partial \theta} \right) \right] \Pr(\cdot)}{\sum_{i=1}^t Y(\cdot) \cdot \left[\mu \cdot \Gamma(\cdot)_{s_u^j} + (1 - \mu) \Psi(\cdot)_{s_u^j} \right] \Pr(\cdot)}, \theta \in \{\alpha_u, c_u, \beta_u\}, \\
\frac{\partial \mathcal{L}}{\partial \theta} &= -\sum_u \sum_{s_u} \frac{\sum_{i=1}^t Y(\cdot) \cdot \left(\Gamma(\cdot)_{s_u^j} - \Psi(\cdot)_{s_u^j} \right) \Pr(\cdot)}{\sum_{i=1}^t Y(\cdot) \cdot \left[\mu \cdot \Gamma(\cdot)_{s_u^j} + (1 - \mu) \Psi(\cdot)_{s_u^j} \right] \Pr(\cdot)}, \theta \in \{\mu\}, \\
\frac{\partial \mathcal{L}}{\partial \theta} &= -\sum_u \sum_{s_u} \frac{\sum_{i=1}^t (\partial Y(d) / \partial \theta) \cdot \left[\mu \cdot \Gamma(\cdot)_{s_u^j} + (1 - \mu) \Psi(\cdot)_{s_u^j} \right] \Pr(\cdot)}{\sum_{i=1}^t Y(d) \cdot \left[\mu \cdot \Gamma(\cdot)_{s_u^j} + (1 - \mu) \Psi(\cdot)_{s_u^j} \right] \Pr(\cdot)}, \theta \in \{a_u, b_u\}.
\end{aligned} \tag{11}$$

In order to make the formula easier to understand and save space, $Y(d)$, $\Gamma(u, v_i)_{s_u^j}$, $\Psi(u, i)_{s_u^j}$, and $\Pr(v_{t+1}, v_{t+1-i})$ are abbreviated as $Y(\cdot)$, $\Gamma(\cdot)_{s_u^j}$, $\Psi(\cdot)_{s_u^j}$, and $\Pr(\cdot)$, respectively.

In addition, the set of parameters θ in our method consists of all the personalized parameters in the definitions of liking old and pursuing new POIs, such as ϕ_u , α_u , β_u , c_u , a_u , b_u , and μ . α_u is randomly drawn from absolute $N(0, 0.1)$. μ is initialized to 0.5. The other parameters are randomly initialized in the range $[0.0, 1.0]$.

Given a training set containing observing sequences of agents, we can iteratively update the parameters θ using the gradient ascent method. Once the (near) optimal Θ is obtained, our SONG framework allows for personalized recommendations based on Equation (8).

5. Experiments Evaluation

In this section, we describe our experiment settings for evaluating the performance of SONG against the state-of-the-art POI recommendation techniques.

5.1. Experiment Settings. Each dataset is divided into the training and testing set in terms of visit time rather than random partition methods in the experiments. In practice, we can only utilize the past data to predict future check-in events. For each user, we select 80% of her check-ins to constitute a training dataset for learning the parameters of the

proposed model. The remaining portions are used as ground truth for testing.

5.2. Evaluation Metrics. To study the effectiveness of the methods, we use two popular metrics, i.e., Recall ($\text{Rec}@k$) and normalized discounted cumulative gain ($\text{NDCG}@k$). While the Recall is defined as the ratio of recovered POIs to the number of POIs generated by the recommendation model, $\text{NDCG}@N$ is a measure to indicate the ranking quality of the recommendation models.

To produce a TOP- k recommendation list for a query user, we compute a preference score for each POI and sort them by score. The Recall@ k for each user is defined as

$$\text{Rec}@k = \frac{tp}{tp + tn}, \tag{12}$$

where tp is the number of POIs visited by a user u and also in the TOP- k recommendations and tn is the number of POIs visited by u but not in the TOP- k recommendations. The $\text{NDCG}@k$ for each user is defined as

$$\text{NDCG}@k = \frac{\text{DCG}@k}{\text{IDCG}@k}, \tag{13}$$

where

$$\text{DCG}@k = \sum_{i=1}^k \frac{2^{\text{rel}_i} - 1}{\log_2(i+1)}, \tag{14}$$

and rel_i refers to the graded relevance of the result ranked at the position. We use the binary relevance in our work, i.e., $\text{rel}_i = 1$ if the result is in the test set, and 0, otherwise. $\text{IDCG}@k$ is the $\text{DCG}@k$ value when the recommended POIs are ideally ranked. The average of recall and NDCG values overall users are reported as the final $\text{Rec}@k$ and $\text{NDCG}@k$ ($k = 1, 5, 10, 15$). These two metrics are both in the range $[0, 1]$, and a higher value means better results.

5.3. Comparison Methods

5.3.1. FPMC-LR. Cheng et al. [8] observed two prominent properties in the check-in sequence: personalized Markov chain and region localization. Then, they proposed a matrix factorization method, which embeds the personalized Markov chains and the localized regions for solving the recommendation task.

5.3.2. TMCA. Li et al. [44] proposed an encoder-decoder-based neural network model named TMCA to capture the complex spatial and temporal dependencies among historical check-in activities automatically. The model leverages the embedding method to incorporate heterogeneous contextual factors to boost recommendation performance. Furthermore, they introduce the temporal and multilevel context attention mechanisms to dynamically select the relevant check-ins and discriminative contextual factors for predicting the preferences over POIs to visit next.

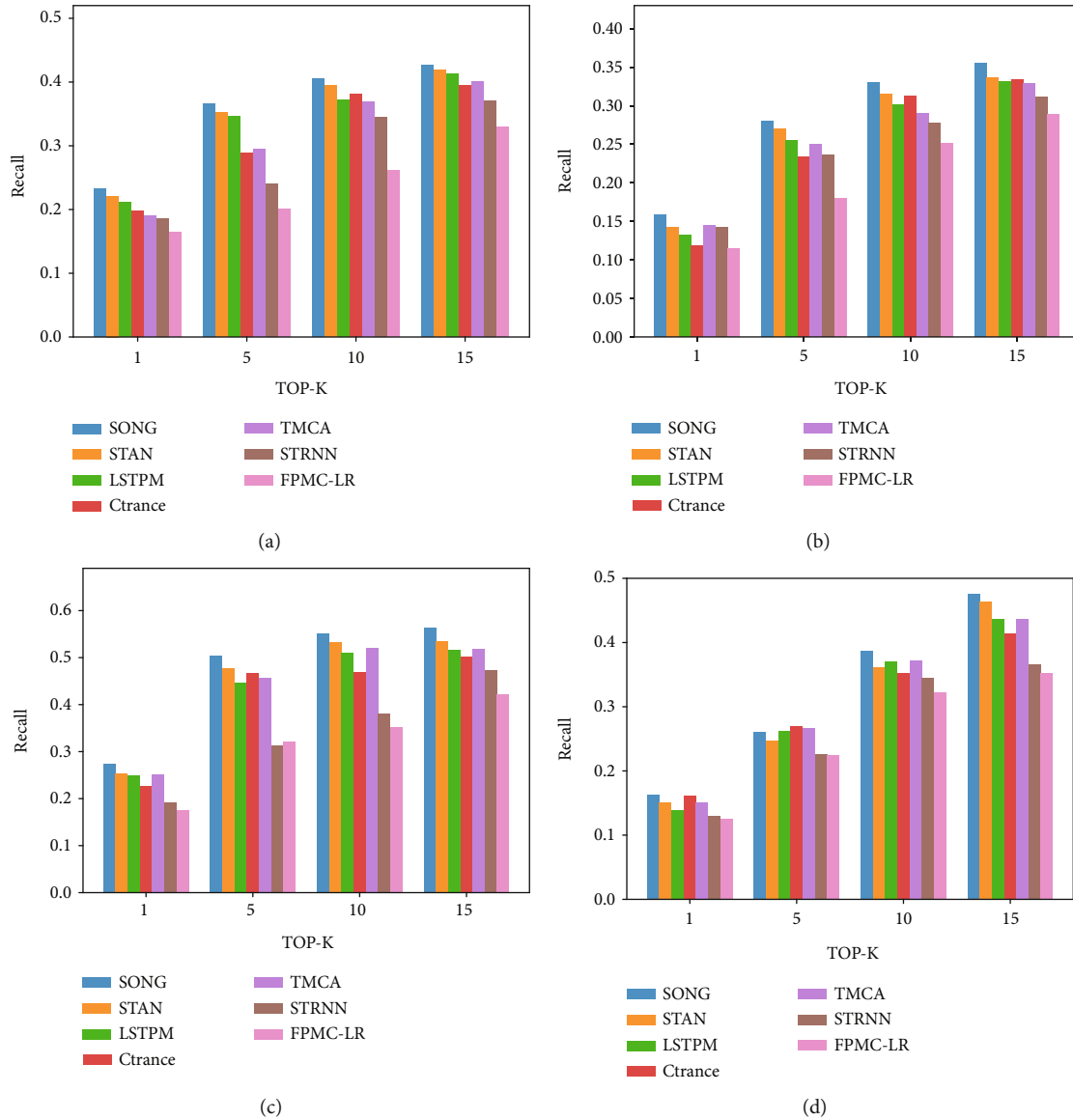


FIGURE 2: Recall on four datasets. (a) Beijing (Jiepan). (b) Shanghai (Jiepan). (c) NYC (Foursquare). (d) TKY (Foursquare).

5.3.3. *STRNN*. Liu et al. [42] extend RNN and propose the spatial-temporal recurrent neural networks (STRNN). To capture time interval and geographical distance information, they replace the single-transition matrix in RNN with time-specific transition matrices and distance-specific transition matrices.

5.3.4. *CTransRec*. CTransRec [40] is a translation-based recommender for complex users, which utilizes auxiliary information (item category and timestamp) and category-specific projection and temporal dynamic relaxation in recommender systems to improve the performance of sequential recommendation.

5.3.5. *LSTPM*. Sun et al. [43] proposed a novel method named long-term and short-term preference modeling for

the next POI recommendation. The proposed model consists of a context-aware nonlocal network for long-term preference modeling and a geodilated RNN for short-term preference learning.

5.3.6. *STAN*. Luo et al. [41] adopt a spatiotemporal attention network (STAN) for location recommendation. This allows a point-to-point interaction between nonadjacent locations and nonconsecutive check-ins with explicit spatiotemporal effect. STAN uses a bilayer attention architecture to learn the explicit spatiotemporal correlations.

5.4. *Comparison with Baselines*. We present the comparison results on the four datasets in terms of Recall and NDCG in Figures 2 and 3, respectively. We can make the following important observations.

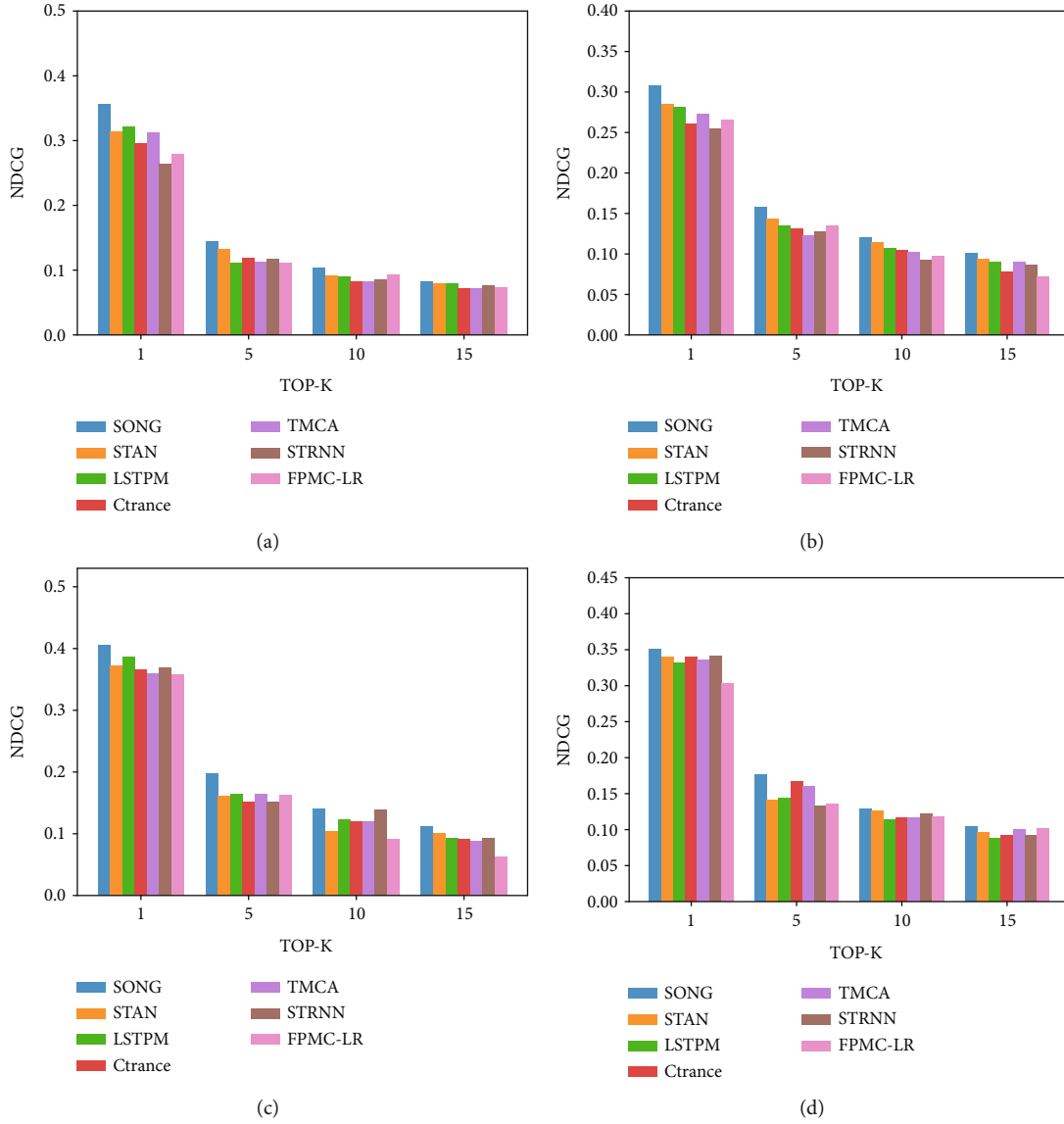


FIGURE 3: NDCG on four datasets. (a) Beijing (JiePang). (b) Shanghai (JiePang). (c) NYC (Foursquare). (d) TKY (Foursquare).

We model users' preference for liking old, assume that repeated check-in POI was the basis of users' liking old, and converted the check-in times into liking old influence. New POIs will bring users unprecedented experience. We calculate the residual value of POIs according to the time interval between check-in POIs, which will serve as the basis for users to pursue new POIs. The lower the residual value, the stronger the incentive to pursue something new. Finally, the combination of liking the old and chasing the new can better reflect the influence of precursor POIs on successor POIs.

Our proposed SONG consistently and significantly outperforms all baselines in terms of every metric on four datasets. For example, on Beijing, Shanghai, NYC, and TKY, compared with the second best method STAN, SONG improves the Recall@1 by 5.22%, 11.17%, 8.22%, and 7.62%, and the NDCG@1 13.55%, 8.17%, 8.88%, and

3.24% by, respectively. The quantitative evaluation clearly demonstrates the superior effectiveness of our method.

Among the baseline methods, STAN performs the best on all datasets. It may be because STAN established the association between nonadjacent locations and nonconsecutive check-ins with explicit spatiotemporal effect, which has alleviated data sparsity. Secondly, the performances of LSTPM and TMCA are better. Specifically, LSTPM performed well on BJ and SH of the JiePang, and TMCA performed well on NYC and TKY of the Foursquare. LSTPM requires dense trajectory support, which is not very good for users with sparse trajectories. In comparison, TMCA adopted an embedding method to incorporate heterogeneous information for mitigating sparsity.

Ctrance used item category and timestamp, and STRNN used time interval and geographic distance. Both methods use time, which shows that time played a role in the

TABLE 1: Performance of SONG_N and SONG on four datasets.

Data	Metric	SONG_N	SONG	Inc
BJ	Rec@1	0.2049	0.2327	14%
	Rec@5	0.3208	0.3662	14%
	Rec@10	0.3577	0.4055	13%
	Rec@15	0.3710	0.4270	15%
SH	Rec@1	0.1488	0.1581	6%
	Rec@5	0.2622	0.2800	7%
	Rec@10	0.3094	0.3297	7%
	Rec@15	0.3291	0.3555	8%
NYC	Rec@1	0.2337	0.2740	17%
	Rec@5	0.4361	0.5042	16%
	Rec@10	0.4800	0.5523	15%
	Rec@15	0.4909	0.5639	15%
TKY	Rec@1	0.1769	0.1994	13%
	Rec@5	0.3364	0.3724	11%
	Rec@10	0.3909	0.4318	10%
	Rec@15	0.4192	0.4623	10%
BJ	NDCG@1	0.3256	0.3564	9%
	NDCG@5	0.1341	0.1440	7%
	NDCG@10	0.0959	0.1030	7%
	NDCG@15	0.0771	0.0832	8%
SH	NDCG@1	0.2978	0.3084	4%
	NDCG@5	0.1522	0.1580	4%
	NDCG@10	0.1170	0.1209	3%
	NDCG@15	0.0972	0.1008	4%
NYC	NDCG@1	0.3580	0.4056	13%
	NDCG@5	0.1785	0.1973	11%
	NDCG@10	0.1280	0.1407	10%
	NDCG@15	0.1024	0.1124	10%
TKY	NDCG@1	0.3248	0.3506	8%
	NDCG@5	0.1649	0.1765	7%
	NDCG@10	0.1199	0.1283	7%
	NDCG@15	0.0977	0.1044	7%

recommendation. Comparing the performance of them, the former is slightly better than the latter. This result may indicate that the item category better reflects the user's preferences.

5.5. Comparison of SONG_N and SONG. Due to the uneven distribution of the number of daily check-ins, dense and sparse trajectories coexist. In order to make full use of user data, this paper proposes a method to serialize sparse trajectories. We test the proposed SONG on the original and the serialized data, and the test results are shown in Table 1. It is found that the effects of Recall and NDCG after serialization (SONG) are significantly higher than those of no serialization (SONG_N). It shows in Table 1. For example, on BJ, SH, NYC, and TKY, Rec@ k ($k = 1, 5, 10, 15$) has increased by more than 13%, 6%, 15%, and 10%, respectively. Comparing

the growth rates of Recall and NDCG of each dataset, NYC and BJ have the best growth rates, followed by TKY and SH. The growth trends of the two indicators are consistent. From this point of view, the sparse trajectory data serialization method we proposed is effective.

6. Conclusions

In this paper, we find out that users' check-in behaviors have an apparent characteristic of liking the old and pursuing the new. After studying the problem of POI recommendation, we proposed a novel sequential prediction method based on the Markov chain model, i.e., SONG. We jointly model users' behaviors and geographical influence with a variable-order additive Markov chain. The experimental results demonstrate that our proposed approach substantially improves the recommendation performance compared with the state-of-the-art methods.

Data Availability

The data used to support the findings of this study are included within the supplementary information file.

Conflicts of Interest

The authors declare that they have no conflicts of interest.

Supplementary Materials

We used two datasets in this paper. They are Foursquare [45] and JiePang [11]. Anyone can freely obtain the dataset from the following URLs, Foursquare (<https://sites.google.com/site/yangdingqi/home/foursquare-dataset>) and JiePang (https://pan.baidu.com/s/1ntXTnuT?_at_=1637459298206). (*Supplementary Materials*)

References

- [1] Y. Zheng, L. Zhang, Z. Ma, X. Xie, and W. Y. Ma, "Recommending friends and locations based on individual location history," *ACM Transactions on the Web (TWEB)*, vol. 5, no. 1, pp. 1–44, 2011.
- [2] H. Gao, X. Qin, R. J. D. Barroso, W. Hussain, Y. Xu, and Y. Yin, "Collaborative learning-based industrial IoT API recommendation for software-defined devices: the implicit knowledge discovery perspective," *IEEE Transactions on Emerging Topics in Computational Intelligence*, pp. 1–11, 2020.
- [3] Y. Xu, Y. Wu, H. Gao, S. Song, Y. Yin, and X. Xiao, "Collaborative APIs recommendation for Artificial Intelligence of Things with information fusion," *Future Generation Computer Systems*, vol. 125, pp. 471–479, 2021.
- [4] H. Gao, C. Liu, Y. Li, and X. Yang, "V2VR: reliable hybrid-network-oriented V2V data transmission and routing considering RSUs and connectivity probability," *IEEE Transactions on Intelligent Transportation Systems*, vol. 22, no. 6, pp. 3533–3546, 2021.
- [5] P. Kefalas, P. Symeonidis, and Y. Manolopoulos, "A graph-based taxonomy of recommendation algorithms and systems in LBSNs," *IEEE Transactions on Knowledge and Data Engineering*, vol. 28, no. 3, pp. 604–622, 2016.

- [6] J. Ye, Z. Zhu, and H. Cheng, "What's your next move: user activity prediction in location-based social networks," in *Proceedings of the 2013 SIAM International Conference on Data Mining*, pp. 171–179, Texas, USA, 2013.
- [7] S. Kim, "Friend recommendation with a target user in social networking services," in *2015 31st IEEE International Conference on Data Engineering Workshops*, pp. 235–239, Seoul, Korea (South), 2015.
- [8] C. Cheng, H. Yang, M. R. Lyu, and I. King, "Where you like to go next: successive point-of-interest recommendation," in *Twenty-Third international joint conference on Artificial Intelligence*, vol. 13, pp. 2605–2611, Beijing, China, 2013.
- [9] W. He, D. Li, T. Zhang, L. An, M. Guo, and G. Chen, "Mining regular routes from gps data for ridesharing recommendations," in *Proceedings of the ACM SIGKDD International Workshop on Urban Computing ACM*, pp. 79–86, Beijing, China, 2012.
- [10] Q. Yuan, G. Cong, Z. Ma, A. Sun, and N. M. Thalmann, "Time-aware point-of-interest recommendation," in *Proceedings of the 36th international ACM SIGIR conference on Research and development in information retrieval ACM*, pp. 363–372, Dublin, Ireland, 2013.
- [11] D. Lian, C. Zhao, X. Xie et al., "Joint geographical modeling and matrix factorization for point-of-interest recommendation," in *Proceedings of the 20th ACM SIGKDD international conference on Knowledge discovery and data mining ACM*, pp. 831–840, New York, USA, 2014.
- [12] H. Yin, X. Zhou, Y. Shao, H. Wang, and S. Sadiq, "Joint modeling of user check-in behaviors for point-of-interest recommendation," in *Proceedings of the 24th ACM International on Conference on Information and Knowledge Management*, pp. 1631–1640, Melbourne, Australia, 2015.
- [13] B. Liu, H. Xiong, S. Papadimitriou, Y. Fu, and Z. Yao, "A general geographical probabilistic factor model for point of interest recommendation," *IEEE Transactions on Knowledge and Data Engineering*, vol. 27, no. 5, pp. 1167–1179, 2015.
- [14] R. Baral and T. Li, "Maps: a multi aspect personalized poi recommender system," in *Proceedings of the 10th ACM Conference on Recommender Systems*, pp. 281–284, Boston Massachusetts, USA, 2016.
- [15] J. B. Griesner, T. Abdesslem, and H. Naacke, "POI recommendation: towards fused matrix factorization with geographical and temporal influences," in *Proceedings of the 9th ACM Conference on Recommender Systems ACM*, pp. 301–304, New York, USA, 2015.
- [16] X. Li, G. Cong, X. L. Li, T. A. N. Pham, and S. Krishnaswamy, "Rank-geofm: a ranking based geographical factorization method for point of interest recommendation," in *Proceedings of the 38th International ACM SIGIR Conference on Research and Development in Information Retrieval ACM*, pp. 433–442, New York, USA, 2015.
- [17] D. Chen, C. S. Ong, and L. Xie, "Learning points and routes to recommend trajectories," in *Proceedings of the 25th ACM International on Conference on Information and Knowledge Management ACM*, pp. 2227–2232, Indianapolis Indiana, USA, 2016.
- [18] Y. Ge, H. Xiong, A. Tuzhilin, and Q. Liu, "Cost-aware collaborative filtering for travel tour recommendations," *ACM Transactions on Information Systems*, vol. 32, no. 1, pp. 1–31, 2014.
- [19] C. Cheng, H. Yang, I. King, and M. Lyu, "Fused matrix factorization with geographical and social influence in location-based social networks," *Proceedings of the AAAI conference on artificial intelligence*, vol. 26, 2012.
- [20] E. Cho, S. A. Myers, and J. Leskovec, "Friendship and mobility: user movement in location-based social networks," in *Proceedings of the 17th ACM SIGKDD international conference on Knowledge discovery and data mining*, pp. 1082–1090, San Diego California, USA, 2011.
- [21] W. R. Tobler, "A computer movie simulating urban growth in the Detroit region," *Economic geography*, vol. 46, pp. 234–240, 1970.
- [22] E. O'Brien, "A mind stretched: the psychology of repeat consumption," *Consumer Psychology Review*, vol. 4, no. 1, pp. 42–58, 2021.
- [23] M. Xie, H. Yin, H. Wang, F. Xu, W. Chen, and S. Wang, "Learning graph-based poi embedding for location-based recommendation," in *Proceedings of the 25th ACM International on Conference on Information and Knowledge Management ACM*, pp. 15–24, Indianapolis Indiana, USA, 2016.
- [24] R. B. Zajonc, "Mere exposure: a gateway to the subliminal," *Current Directions in Psychological Science*, vol. 10, no. 6, pp. 224–228, 2001.
- [25] H. Hotelling, "A general mathematical theory of depreciation," *Journal of the American Statistical Association*, vol. 20, no. 151, pp. 340–353, 1925.
- [26] Y. Huang, H. Xu, H. Gao, X. Ma, and W. Hussain, "SSUR: an approach to optimizing virtual machine allocation strategy based on user requirements for cloud data center," *IEEE Transactions on Green Communications and Networking*, vol. 5, no. 2, pp. 670–681, 2021.
- [27] C. Zhang, H. Liang, and K. Wang, "Trip recommendation meets real-world constraints," *ACM Transactions on Information Systems*, vol. 35, no. 1, pp. 1–28, 2016.
- [28] T. He, H. Yin, Z. Chen, X. Zhou, S. Sadiq, and B. Luo, "A spatial-temporal topic model for the semantic annotation of POIs in LBSNs," *ACM Transactions on Intelligent Systems and Technology*, vol. 8, no. 1, pp. 1–24, 2016.
- [29] S. Oppokhonov, S. Park, and I. K. Ampomah, "Current location-based next POI recommendation," in *Proceedings of the International Conference on Web Intelligence ACM*, pp. 831–836, Leipzig, Germany, 2017.
- [30] H. Gao, J. Tang, X. Hu, and H. Liu, "Exploring temporal effects for location recommendation on location-based social networks," in *Proceedings of the 7th ACM conference on Recommender systems ACM*, pp. 93–100, Hong Kong, China, 2013.
- [31] W. Ji, X. Meng, and Y. Zhang, "SPATM: a social period-aware topic model for personalized venue recommendation," *IEEE Transactions on Knowledge and Data Engineering*, pp. 1–14, 2020.
- [32] J. D. Zhang, C. Y. Chow, and Y. Li, "Lore: exploiting sequential influence for location recommendations," in *Proceedings of the 22nd ACM SIGSPATIAL International Conference on Advances in Geographic Information Systems ACM*, pp. 103–112, Dallas Texas, USA, 2014.
- [33] S. Zhao, I. King, and M. R. Lyu, "A survey of point-of-interest recommendation in location-based social networks," <http://arxiv.org/abs/1607.00647>.
- [34] H. Wang, H. Shen, W. Ouyang, and X. Cheng, "Exploiting POI-specific geographical influence for point-of-interest recommendation," in *Proceedings of the Twenty-Seventh International Joint Conference on Artificial Intelligence*, pp. 3877–3883, Stockholm, Sweden, 2018.

- [35] M. Ye, P. Yin, W. C. Lee, and D. L. Lee, "Exploiting geographical influence for collaborative point-of-interest recommendation," in *Proceedings of the 34th international ACM SIGIR conference on Research and development in Information Retrieval ACM*, pp. 325–334, 2011.
- [36] R. He and J. McAuley, "Fusing similarity models with Markov chains for sparse sequential recommendation," in *2016 IEEE 16th International Conference on Data Mining (ICDM)*, pp. 191–200, Barcelona, Spain, 2016.
- [37] K. Zhao, Y. Zhang, H. Yin et al., "Discovering subsequence patterns for next POI recommendation," in *Proceedings of the Twenty-Ninth International Joint Conference on Artificial Intelligence*, pp. 3216–3222, Yokohama, Japan, 2020.
- [38] J. Xiao, H. Xu, H. Gao, M. Bian, and Y. Li, "A weakly supervised semantic segmentation network by aggregating seed cues: the multi-object proposal generation perspective," *ACM Transactions on Multimedia Computing Communications and Applications*, vol. 17, no. 1s, pp. 1–19, 2021.
- [39] Y. Yin, Z. Cao, Y. Xu, H. Gao, R. Li, and Z. Mai, "QoS prediction for service recommendation with features learning in mobile edge computing environment," *IEEE Transactions on Cognitive Communications and Networking*, vol. 6, no. 4, pp. 1136–1145, 2020.
- [40] H. Li, Y. Liu, N. Mamoulis, and D. S. Rosenblum, "Translation-based sequential recommendation for complex users on sparse data," *IEEE Transactions on Knowledge and Data Engineering*, vol. 32, no. 8, pp. 1639–1651, 2020.
- [41] Y. Luo, Q. Liu, and Z. Liu, "STAN: spatio-temporal attention network for next location recommendation," in *Proceedings of the Web Conference*, pp. 2177–2185, Ljubljana, Slovenia, 2021.
- [42] Q. Liu, S. Wu, L. Wang, and T. Tan, "Predicting the next location: a recurrent model with spatial and temporal contexts," in *Thirtieth AAAI conference on artificial intelligence*, pp. 194–200, Phoenix, Arizona, USA, 2016.
- [43] K. Sun, T. Qian, T. Chen, Y. Liang, Q. V. H. Nguyen, and H. Yin, "Where to go next: modeling long-and short-term user preferences for point-of-interest recommendation," *Proceedings of the AAAI Conference on Artificial Intelligence*, vol. 34, pp. 214–221, 2020.
- [44] R. Li, Y. Shen, and Y. Zhu, "Next point-of-interest recommendation with temporal and multi-level context attention," in *2018 IEEE International Conference on Data Mining (ICDM)*, pp. 1110–1115, Singapore, 2018.
- [45] Dingqi Yang, Daqing Zhang, V. W. Zheng, and Zhiyong Yu, "Modeling user activity preference by leveraging user spatial temporal characteristics in LBSNs," *IEEE Transactions on Systems, Man, and Cybernetics: Systems*, vol. 45, no. 1, pp. 129–142, 2015.
- [46] W. K. Ching, E. S. Fung, and M. K. Ng, "Higher-order Markov chain models for categorical data sequences," *Naval Research Logistics*, vol. 51, no. 4, pp. 557–574, 2004.
- [47] A. E. Raftery, "A model for high-order Markov chains," *Journal of the Royal Statistical Society: Series B (Methodological)*, vol. 47, no. 3, pp. 528–539, 1985.
- [48] C. Su, J. Wang, and X. Xie, "Point-of-interest recommendation based on geographical influence and extended pairwise ranking," in *IEEE INFOCOM 2020 - IEEE Conference on Computer Communications Workshops (INFOCOM WKSHPS)*, pp. 966–971, Toronto, ON, Canada, 2020.

Research Article

Attribute Extraction Study in the Field of Military Equipment Based on Distant Supervision

Xindong You,¹ Meijing Yang,¹ Junmei Han,² Jiangwei Ma,¹ Gang Xiao,² and Xueqiang Lv¹ 

¹Beijing Key Laboratory of Internet Culture Digital Dissemination, Beijing Information Science and Technology University, Beijing, China

²National key Laboratory for Complex Systems Simulation, Institute of Systems Engineering, China

Correspondence should be addressed to Xueqiang Lv; lxq@bistu.edu.cn

Received 6 August 2021; Revised 24 September 2021; Accepted 23 October 2021; Published 23 November 2021

Academic Editor: Honghao Gao

Copyright © 2021 Xindong You et al. This is an open access article distributed under the Creative Commons Attribution License, which permits unrestricted use, distribution, and reproduction in any medium, provided the original work is properly cited.

The effective organization and utilization of military equipment data is an important cornerstone for constructing knowledge system. Building a knowledge graph in the field of military equipment can effectively describe the relationship between entity and entity attribute information. Therefore, relevant personnel can obtain information quickly and accurately. Attribute extraction is an important part of building the knowledge graph. Given the lack of annotated data in the field of military equipment, we propose a new data annotation method, which adopts the idea of distant supervision to automatically build the attribute extraction dataset. We convert the attribute extraction task into a sequence annotation task. At the same time, we propose a RoBERTa-BiLSTM-CRF-SEL-based attribute extraction method. Firstly, a list of attribute name synonyms is constructed, then a corpus of military equipment attributes is obtained through automatic annotation of semistructured data in Baidu Encyclopedia. RoBERTa is used to obtain the vector encoding of the text. Then, input it into the entity boundary prediction layer to label the entity head and tail, and input the BiLSTM-CRF layer to predict the attribute label. The experimental results show that the proposed method can effectively perform attribute extraction in the military equipment domain. The *F1* value of the model reaches 77% on the constructed attribute extraction dataset, which outperforms the current state-of-art model.

1. Introduction

With the continuous development of Internet technology, data from all walks of life is growing rapidly. Organizing these data through knowledge graph technology can effectively improve data utilization efficiency. In the military field, the construction of knowledge graph is not only conducive for the military commanders to quickly and deeply understand certain military equipment but also can be combined with knowledge map and intelligent system for rapid intelligent decision-making assistance [1].

Attribute extraction is an important step in knowledge graph construction, which refers to extracting the attribute name and attribute value of entities from text data. Facing a large amount of text data in the military field, extracting attribute data automatically is one of the keys to study the construction of a military knowledge graph. The traditional

attribute extraction methods are divided into rule-based methods and machine learning-based methods. Zhai and Qiu [2] proposed a rule-based knowledge meta-attribute extraction method based on phrase structure trees. The rule-based method needs to set rules manually according to the data characteristics, so the migration of the method is poor. Jakob and Gurevych [3] fused multiple features and used conditional random fields [4] to extract attributes. However, machine learning methods require a large amount of labelled data and manual features. In recent years, deep learning methods have also been gradually applied to attribute extraction. Toh and Su [5] used a bidirectional recurrent neural network BRNN combined with a conditional random field for attribute value extraction. Cheng et al. [6] used a bidirectional long short-term memory network BiLSTM combined with a gated dynamic attention mechanism for attribute extraction. However, attribute extraction

based on deep learning methods also requires a large amount of annotated data. In the field of weaponry, there is a lack of corresponding annotated datasets. Manual annotation is not only time-consuming but also the level of the annotator will largely affect the quality of the annotated corpus [7]. Through investigation, we found that Baidu Encyclopedia currently contains a large number of weapon and equipment entries. There are a large number of semi-structured and unstructured data in the encyclopedia pages, which contain rich information of entity attributes. We propose a new way of attribute data annotation based on the characteristics of the encyclopedia pages. We annotate the unstructured text data by distant supervision based on the InfoBox data of the encyclopedia pages. At the same time, we convert the attribute extraction task into a sequence annotation task and use the RoBERTa-BiLSTM-CRF-SEL method for attribute data extraction.

In summary, the contribution points of this paper can be divided into the following three points.

- (1) A new way of data annotation is proposed for the characteristics of encyclopedia data. In the annotation process, the subjective is fixed according to the name of the encyclopedia page, and then, its attributes and attribute values are annotated
- (2) Based on Baidu Encyclopedia data, the military domain attribute extraction dataset is automatically constructed by using the idea of distant supervision
- (3) RoBERTa-BiLSTM-CRF-SEL is designed for automatic attribute extraction in the field of weapons. The method obtains entity boundary features through the entity boundary prediction layer. The loss of boundary prediction layer and the loss of attribute prediction layer are weighted and summed as the loss value of the model. In this way, the model entity recognition effect is improved. On the military equipment attribute extraction dataset, the *F1* of the proposed method reaches 0.77, which is better than other existing methods

2. Related Work

Attribute extraction methods can be mainly classified into rule-based methods, machine learning-based methods, and deep learning-based methods. The rule-based approach needs to formulate rules manually for specific situations. This method is simple and usually oriented to specific domains. Although the method has a high accuracy rate, it has a small scope of application and is difficult to migrate to other domains. The method based on machine learning is more flexible, but it needs the support of artificial features and large-scale datasets. The method based on deep learning can automatically mine hidden features between texts through a neural network model, but it also requires large amounts of labelled data for model training and optimization.

In the early studies of attribute extraction, scholars mainly formulated a series of rules to extract attributes. Hu

and Liu [8] extracted commodity attributes from customer reviews by frequent itemset feature extraction. Li et al. [9] presented an automatic method to obtain encyclopedia character attributes, and the speech tagging of each attribute value was used to locate the encyclopedia free text. The rules were discovered by statistical method, and the character attribute information was obtained from encyclopedia text according to rules matching. Yu et al. [10] proposed an approach of extracting maritime information and converting unstructured text into structural data. Ding et al. [11] formed nine types of description rules for attribute extraction by manually constructing rules. They analyzed the quantitative relationship and emotional information of attribute description and finally designed and implemented the academic concept attribute extraction system. Qiao et al. [12] suggested a rule-based character information extraction algorithm. Based on the rules, they researched and developed a character information extraction system and finally realized the automatic extraction of semistructured character attribute information. Kang et al. [1] offered an unsupervised attribute triplet extraction method for the military equipment domain. According to the distribution law of attribute triples in sentences, this method adopts an attribute indicator extraction algorithm based on frequent pattern mining and completes the extraction of attribute triples by setting extraction rules and filtering rules.

In a machine learning-based attribute extraction method, Zhang et al. [13] introduced word-level features in the CRF model and used domain dictionary knowledge as an aid for product attribute extraction. Xu et al. [14] introduced shallow syntactic information and heuristic location information and input them to CRF as features, which effectively improved the attribute extraction performance of the model. Gurumdimma et al. [15] presented the approach to extracting these events based on the dependency parse tree relations of the text and its part of speech (POS). The proposed method uses a machine-learning algorithm to predict events from a text. Cheng et al. [16] broke through the current method of a statistical operation mainly in the scope of sentences in the attribute attribution judgment. They proposed a method of character attribute extraction that is classified from text to sentence with the guidance of text knowledge. Kambhatla [17] employed maximum entropy models to combine diverse lexical, syntactic, and semantic features derived from the text. References [18–20] suggested a weakly supervised automatic extraction method that uses very little human participation to solve the problem of lack of training corpus. Zhang et al. [21] offered a novel composite kernel for relation extraction. The composite kernel consists of two individual kernels: an entity kernel that allows for entity-related features and a convolution parse tree kernel that models syntactic information of relation examples. Liu et al. [22] put a perceptron learning algorithm that fuses global and local features for attribute value extraction of unstructured text. The combination of features makes the model obtain better feature representation ability. Li et al. [23] constructed three kinds of semantic information through word attributes, word dependencies, and word embeddings of words. The three semantic information are

combined with the conditional random field model to realize the extraction of commodity attributes.

In recent years, attribute extraction methods based on deep learning have gradually become mainstream. Wang et al. [24] regarded attribute extraction as a text sequence labelling task. Input the word sequences and lexical sequences into a GRU network, and then, use CRF for sequence label prediction. Xu et al. [25] considered that there is a gap between the meaning of a word expression in general and specialized domains. Therefore, they input both word embeddings from the generic domain and word embeddings from the specialized domain into a convolutional neural network model. The model is used to decide which expression is more preferred to achieve the attribute extraction. For the low performance of slot filling method applied in Chinese entity-attribute extraction at present, He et al. [26] presented a distant supervision relation extraction method based on bidirectional long short-term memory neural network. Wei et al. [27] proposed an attribute extraction-oriented class-convolutional interactive attention mechanism. The target sentence was first input into a bidirectional recurrent neural network to obtain the implicit expression of each word and then underwent class-convolution interactive attention. The force mechanism performed representation learning. To solve the problem that traditional information extraction methods have poor extraction results due to the existence of long and difficult sentences and the diversity of natural language expressions, Wu et al. [28] introduced text simplification as the preprocessing process of extraction. Among them, text reduction is modeled as a sequence-to-sequence (seq2seq) translation process and is implemented with the seq2seq-RNN model in the field of machine translation. Huang et al. [29] proposed a different method, which uses an independent graph based on a neural network as the input and is accompanied by two attention mechanisms to better capture indicative information. Cheng et al. [30] used the advantages of the CRF model to deal with the sequence labelling problem and realized the automatic extraction of journal keywords by integrating the part-of-speech information and the CRF model into the BiLSTM network. Luo et al. [31] proposed a new bidirectional dependency grammar tree to extract the dependency structure features of a given sentence and then combined the extracted grammar features with the semantic features extracted using BiLSTM and finally used CRF for attribute word annotation. Feng et al. [32] introduced an entity attribute value extraction method based on machine reading comprehension model and crowdsourcing verification due to the high noise characteristics of Internet corpus. The attribute extraction task is transformed into a reading comprehension task. Luo et al. [33] introduced a MLBiNet (multilayer bidirectional network) that integrates cross-sentence semantics and associated event information, thereby enhancing the discrimination of events mentioned within. Xi et al. [34] presented bidirectional entity level decoder (BERD) to gradually generate argument role sequences for each entity.

To address the problem of lack of annotation data in the military equipment domain, the attribute extraction dataset

in the military equipment domain is automatically constructed based on distant supervision. The attribute annotation sequence is decoded by RoBERTa model combined with BiLSTM-CRF model, and the entity boundary prediction layer is also added to improve the effect of entity recognition in this paper.

3. Attribute Extraction Methods Based on RoBERTa and Entity Boundary Prediction

The model proposed in this paper is mainly composed of text coding layer, entity boundary prediction layer, and BiLSTM-CRF attribute prediction layer. We first encode the input text through RoBERTa [35] to obtain its hidden layer state vector. Then, input them into the entity boundary prediction layer and the BiLSTM-CRF attribute prediction layer, respectively. At the entity boundary prediction layer, the 0/1 coding method is used to label the entity head and tail, respectively, and then, the `start_loss` and `end_loss` of the two sequence labels are calculated. In the BiLSTM-CRF attribute prediction layer, we take the output result of the entity boundary prediction layer as a feature and splice it with the text vector. Input the splicing results into BiLSTM-CRF to predict the text attribute tag. Next, calculate its loss value `att_loss`. Finally, in the model optimization, we consider the three-loss values together, weigh the summation, and achieve the overall optimization of the model by backpropagation. The model structure diagram is shown in Figure 1.

3.1. Text Encoding Layer. BERT is a pretrained language model proposed by Google in 2018. BERT uses the bidirectional transformer structure as the main framework of the algorithm, which can capture the bidirectional relations in utterances more thoroughly. BERT uses a self-supervised approach to train the model based on a massive corpus, which can learn a good feature representation for words. Therefore, BERT has achieved good results in several downstream tasks such as text classification and sequence annotation. RoBERTa model is an improved version based on the BERT model. Compared with BERT, RoBERTa has improved both the training data and training methods and pretrained the model more adequately.

In terms of training data, RoBERTa uses 160G training text, while BERT only uses 16G training text. RoBERTa also uses a new dataset CCNEWS and confirms that using more data for pretraining can further improve the performance of downstream tasks. At the same time, RoBERTa has increased the batch size. BERT uses 256 batch size. RoBERTa uses a larger batch size in the training process. Researchers have tried batch sizes ranging from 256 to 8000. Liu et al. found through experiments that the performance of certain downstream tasks can be slightly improved after removing the NSP (next sentence prediction, NSP) loss. Therefore, in the training method, RoBERTa deleted the NSP task. In addition, unlike the static masking mechanism of BERT, RoBERTa uses a dynamic masking mechanism to randomly generate a new mask pattern every time. BERT relies on random masks and predicted tokens. The original BERT implementation performs a mask during data

a temporal recurrent neural network, which can better capture the longer distance dependencies in the text. The LSTM model structure is shown in Figure 2.

There are three inputs to the LSTM, which are the hidden layer state vector h_{t-1} at the previous moment, the cell state C_{t-1} at the previous moment, and the input x_t at the current moment. Inside the LSTM, the retention and forgetting of information are decided by three gating mechanisms. The first is the forgetting gate, which is used to decide what information to forget from the cell state. The forgetting gate is used to read h_{t-1} and x_t and outputs data between 0 and 1 to decide which information in C_{t-1} to keep and which to discard, where 1 means fully retained, and 0 means all discarded. The input gate is used to decide which new information is added to the cell state, and the output gate decides which data in the cell state will be output. The calculation formulas of the LSTM model are shown in

$$f_t = \sigma(W_f[h_{t-1}, x_t] + b_f), \quad (1)$$

$$i_t = \sigma(W_i[h_{t-1}, x_t] + b_i), \quad (2)$$

$$o_t = \sigma(W_o[h_{t-1}, x_t] + b_o), \quad (3)$$

$$\tilde{C}_t = \tanh(W_C[h_{t-1}, x_t] + b_C), \quad (4)$$

$$C_t = f_t \cdot C_{t-1} + i_t \cdot \tilde{C}_t, \quad (5)$$

$$h_t = o_t * \tanh(C_t). \quad (6)$$

LSTM can only encode information in one direction. To effectively use the context information, we use a bidirectional LSTM structure for encoding.

By calculating the hidden layer vector output of the LSTM in both positive and negative directions and splicing them together, the hidden layer state vector of BiLSTM is finally obtained. The formulas are shown in

$$\vec{h}_t = \overrightarrow{\text{LSTM}}(\vec{h}_{t-1}, w_t), \quad (7)$$

$$\overleftarrow{h}_t = \overleftarrow{\text{LSTM}}(\overleftarrow{h}_{t-1}, w_t), \quad (8)$$

$$h_t = \text{concat}(\vec{h}_t, \overleftarrow{h}_t). \quad (9)$$

The conditional random field is a conditional probability distribution model of output $Y = (Y_1, Y_2, \dots, Y_n)$ given a set of input variables $X = (X_1, X_2, \dots, X_n)$. CRF is a serialization annotation algorithm, which can consider the dependencies between tags to obtain the globally optimal tag sequence.

For a set of label prediction sequence Y , its scoring formula is shown in

$$\text{score}(x, y) = \sum_{i=0}^n A_{y_i, y_{i+1}} + \sum_{i=1}^n P_{i, y_i}. \quad (10)$$

Among them, P is an $n \times m$ dimensional matrix, m represents the number of labels to be predicted, and P_{ij}

represents the possibility that input i is the label j . A is the transition matrix, and $A_{i,j}$ represents the probability of transition from label i to label j .

Therefore, for all possible prediction sequence sets Y_x of the input sequence X , the conditional probability is as shown

$$P(y | x) = \frac{e^{\text{score}(x, y)}}{\sum_{\tilde{y} \in Y_x} e^{\text{score}(x, \tilde{y})}}. \quad (11)$$

In training, we optimize the model by maximizing the log-likelihood probability of the correct output label in Equation (12). For prediction, we select the sequence with the highest score as the best prediction sequence, which is calculated as shown in Equation (12).

$$y^* = \arg \max_{\tilde{y} \in Y_x} \text{score}(x, \tilde{y}). \quad (12)$$

Take sentences in the dataset as an example, such as ‘‘On November 11-1989, the USS Abraham Lincoln was officially commissioned at Naval Station Norfolk and integrated into the American Atlantic Fleet,’’ ‘‘November 11-1989’’ would be marked as ‘‘B-FY,’’ ‘‘USS’’ would be marked as ‘‘B-ST,’’ ‘‘Abraham’’ would be marked as ‘‘I-ST,’’ ‘‘Lincoln’’ would be marked as ‘‘I-ST,’’ and ‘‘American’’ would be marked as ‘‘B-GJ’’ (please refer to Chapter 4 for label meaning).

3.4. Loss Value Calculation. In terms of loss value calculation, we take the weighted sum of entity boundary loss value and attribute identification loss value as the final loss value. The loss value is used to optimize the overall parameters of the model (as shown in Figure 3).

The loss value calculation formula is shown in Equation (13), where $\text{loss}_{\text{start}}$ and loss_{end} represent the loss values of entity head recognition and entity tail recognition, respectively, and $\text{loss}_{\text{attribute}}$ represents the loss value generated by the attribute sequence labelling. $\alpha, \beta, \gamma \in [0, 1]$ are hyperparameters that control the weighted summation of the three-loss values.

$$\text{loss} = \alpha \text{loss}_{\text{start}} + \beta \text{loss}_{\text{end}} + \gamma \text{loss}_{\text{attribute}}. \quad (13)$$

4. Experimental Results and Analysis

4.1. Acquisition of Military Equipment Attribute Data

4.1.1. Data Acquisition. The experimental data came from the Baidu Encyclopedia website (<https://baike.baidu.com/>), and the data acquisition process is shown in Figure 4. We cannot directly obtain military-related terms from Baidu Encyclopedia, because the website does not classify and index terms. The military channel of <http://globe.com/> has a summary display of various types of weapons and equipment. We get the names of various military equipment from the military channel of the World Wide Web. Then, we expand the rules, splice them with the links of encyclopedia entries, and finally, get the URL links of the required military equipment-related entries. After obtaining the links of military equipment entries in Baidu Encyclopedia, we analyzed

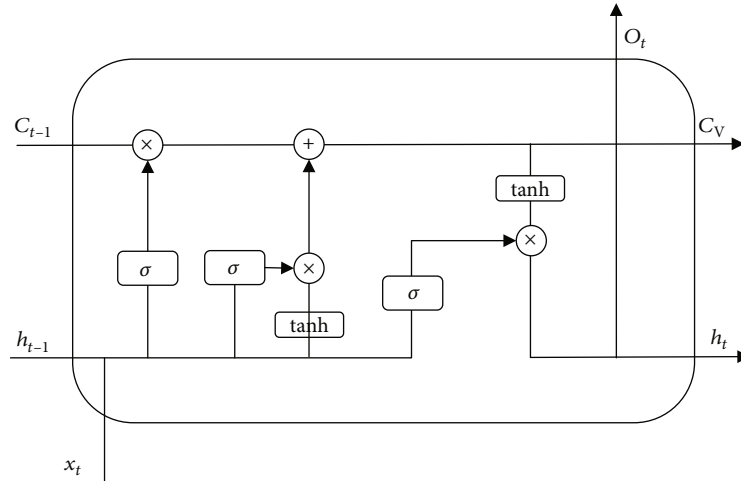


FIGURE 2: LSTM structure diagram.

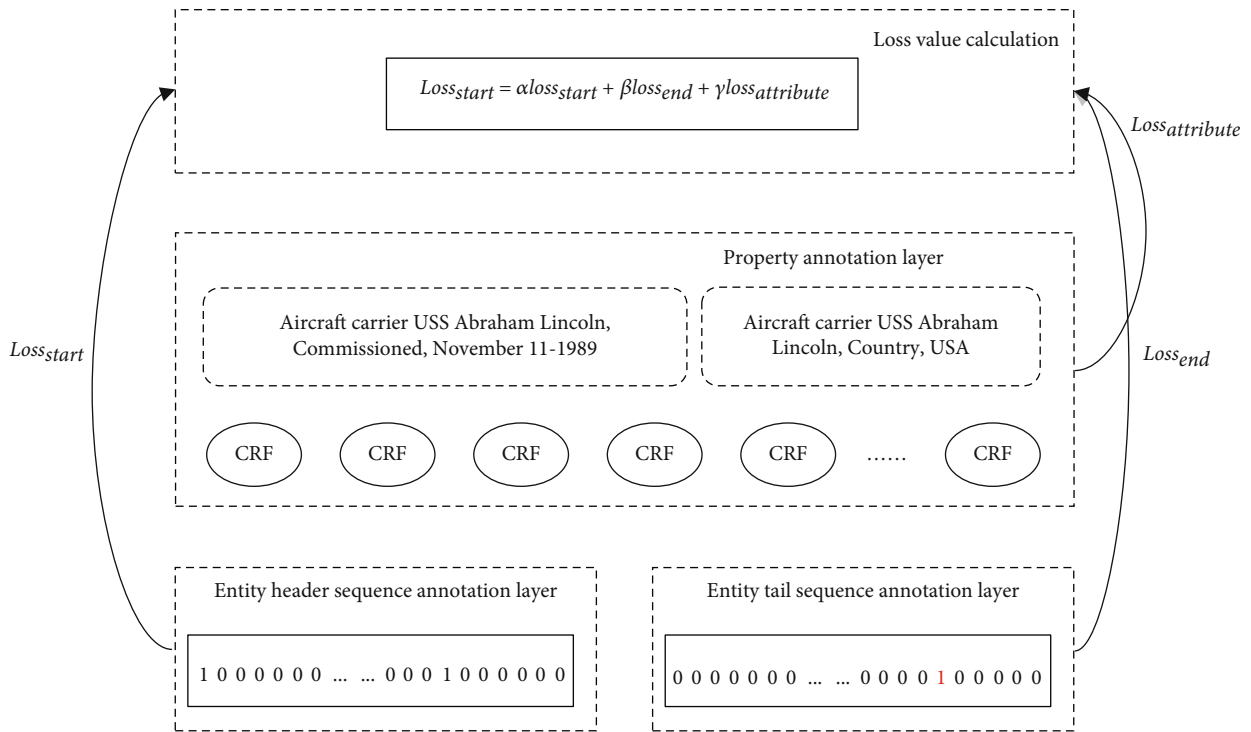


FIGURE 3: Calculation of loss value.

the encyclopedia entry pages and found that the entries mainly consist of entry names, information boxes containing attribute data, and a large amount of unstructured text. We used a crawler to collect the InfoBox data and text data in the Baidu Encyclopedia entry of weapons and equipment and finally collected 1757 encyclopedia data of military equipment.

4.1.2. *Data Annotation.* Data annotation by manual is not only time-consuming and laborious but also different annotators may have different annotation rules for the same piece of data. Therefore, automatic annotation of data has become the focus of current research. Encyclopedia word data

consists of two main parts, which are attribute data in the information frame and unstructured text description data. Taking the “Nimitz aircraft carrier” as an example, the entry information box of the aircraft carrier contains basic attributes such as “English Name,” “Nation,” “pretype/level,” and “subtype/level.” The text data is an introduction to the basic information of the “Nimitz aircraft carrier.” Observing its text data, it can be seen that it contains textual expressions of the “English Name,” “Nation,” and other attribute values of the “Nimitz aircraft carrier.”

For this data feature, the data annotation in this paper is based on the distant supervision hypothesis [33]. The distant supervision hypothesis means that when there is a

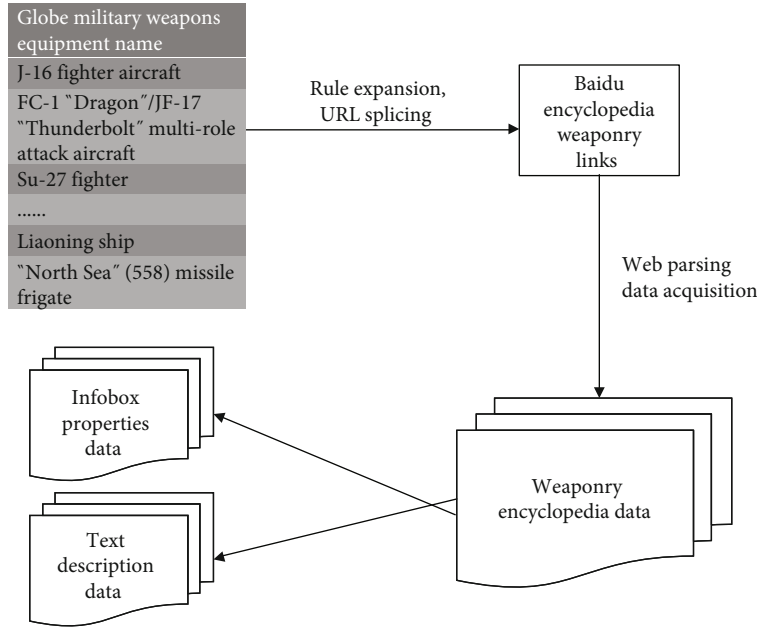


FIGURE 4: Flow chart of attribute data collection.

relationship between two entities, then all sentences containing the pair of entities are considered to express this relationship to some extent. Distant supervision is to provide labels for data with the help of external knowledge bases, to save the trouble of manual labelling [37]. Attributes can also be considered as a type of relationship, so the distant supervision assumption is applied to the annotation of attribute data. Taking the Nimitz aircraft carrier as an example, the information box in Figure 5 shows that the relationship between “Nimitz aircraft carrier” and the attribute “United States” is a “Nation” attribute. Then, based on the distant supervision assumption, all sentences containing “Nimitz aircraft carrier” and “United States” can be labelled with the “Nation” attribute, for example, the sentences “Nimitz Aircraft Carrier (CVN-68) is the first ship of the Nimitz-class aircraft carriers of the United States Navy” and “The Nimitz aircraft carrier started construction in June 1968. It was launched in May 1972 and delivered to the United States Navy in May 1975”. Both of these sentences contain the words “Nimitz aircraft carrier” and “United States,” and the triad (Nimitz aircraft carrier, nation, United States) can be considered to exist in these two sentences when labelling the data. Suppose a dataset $D = \{s_1, s_2, \dots, s_n\}$, where s_i represents sentence and is unstructured text. Train a model F such that $F(s_i; \theta) = [(e_i^t, e_j^t, e_k^t)]$, where θ represents model parameters, and e_i^t, e_j^t, e_k^t represent the T_{th} entity and its corresponding relationship. The idea of the distant supervision algorithm is to use knowledge base to align plain text for annotation and then perform supervised training.

However, Baidu Encyclopedia website is an open knowledge platform, and the editors of entries are not fixed. Therefore, there is a lack of standardization and unity in the naming of attributes, which leads to a variety of expressions of the same attribute. Since the data in the military field has a certain degree of confidentiality, the field itself has data sparsity. Different attribute expressions can lead to a variety of

data labels. If the labels are too scattered, the annotation data of each type of attribute will be small, which is difficult to obtain a good attribute extraction effect. To merge multiple attribute labels’ expressions, we count the distribution of attribute names to select high-frequency words as attribute names. The attribute expressions present in the military equipment data of the encyclopedia website were merged by manual means, and a synonym table of military equipment attribute names was constructed. We merged and normalized the attribute expressions in the encyclopedia data through the synonym table. The synonym table of military equipment attribute names is shown in Table 1.

Normalize the attributes in the information box through the attribute name synonym table in Table 1 to obtain the attribute triplet set. Combined with the introduction text of triplet set and military equipment entries, data annotation is carried out through distant supervision. As shown in Figure 5, the text content in the encyclopedia web pages is expanded and described with the title of the entry as the center. The attribute triad is also composed with the title of the entry as the head entity. Based on the characteristics of this encyclopedia attribute data, a text sentence usually contains a primary entity and multiple attribute values corresponding to the entity. This chapter proposes a new data labelling method. Unlike the previous annotation form, we first annotate subjective according to the entry title and then annotate the attribute values corresponding to the primary entity separately (as shown in Table 2).

The relationship extraction dataset constructed by the distant supervision method often has noisy data (as shown in Table 3). For the relational triad [Obama, born in, United States], “Obama” and “United States” is a relationship of birth, and the distant supervision method is used for “Obama is the 44th president of the United States.” The error occurs when the annotation is performed. For the

USS Nimitz (The first ship of the Nimitz-class aircraft carrier CVN-68)



The USS Nimitz (English: Nimitz Aircraft Carrier, port number: CVN-68 ^[1]), is the first ship of the US Navy's Nimitz-class aircraft carrier and a large nuclear-powered aircraft carrier in active service .

The ship is propelled by nuclear power , equipped with 4 elevators , 4 steam catapults and 4 arresting cables , and can eject a combat aircraft every 20 seconds. The model equipment in the carrier combat wing differs according to the nature of the combat mission. It can carry different purpose carrier aircraft to launch attacks on enemy aircraft, ships, submarines and land targets, and protect the maritime fleet. Kampfgruppe with its core usually consists of 4-6 cruisers , destroyers , submarines and supply ship constituted only.

Construction of the USS Nimitz started in June 1968, launched in May 1972, and delivered to the U.S. Navy in May 1975. The ship was first incorporated into the Atlantic Fleet , and its home port was Norfolk on the east coast of the United States. After being transferred to the Pacific Fleet, the station was changed to Everett Naval Base ^[2] .

Chinese name	USS Nimitz	Service time	May 3, 1975
Foreign name	USS Nimitz CVN-68 ^[1]	nation	U.S
Pre-type/level	Kitty Hawk class aircraft carrier and USS Enterprise ^[1]	Launch time	May 13, 1972
		Homeport	Everett Naval Base
Subtype/level	Ford class aircraft carrier ^[1]	Origin of ship...	Admiral Chester W. Nimitz
Development...	1961-1968	Full load drai...	101196 tons

FIGURE 5: Example of encyclopedia data.

triple [Obama, President, United States], the relationship between “Obama” and “United States” is “President,” and the annotation of “Obama was born in the United States” based on the distant supervision method will result in an annotation error. Since the relationship triad is composed of [entity, relationship, entity] and there may be multiple relationships between entities and entities, the distant supervision method often causes mislabelling problems when constructing relationship extraction datasets.

The attribute triad is composed of [entity, attribute, attribute value]. For military equipment data, the attribute values are usually some numerical information with unit agency names. Therefore, there is less possibility of distant supervision mislabelling problem when labelling the data for the entity and attribute values in military equipment data. For example, for the triad (Nimitz aircraft carrier, total load displacement, 101196 tons), the attribute value “101196 tons” is not a common entity, and it is challenging to generate other attribute relationships with the “Nimitz aircraft carrier.” The automatic annotation of the attribute data in the field of military equipment by the distant supervision method does not generate many mislabelling problems, and the correctness of the dataset can be guaranteed to a certain extent.

4.2. Dataset and Evaluation Index Description

(1) Description of dataset

We use the attribute extraction dataset constructed by the distant supervision method to verify method’s effective-

ness. 4291 attribute extraction corpus was constructed through the distant supervision method and the filtering of rules, including 3432 items in the training set, 429 items in the validation set, and 430 items in the test set. The details are shown in Table 4.

The Military Weaponry Dataset is a text corpus of weapons and equipment extracted from the military channel of the World Wide Web. Combined with the relevant knowledge of the encyclopedia website, the attribute extraction dataset is constructed using distant supervision and annotation. In the labeling process, we first determine the type of attribute contained in the sentence and then label the corresponding head entity and tail entity for each attribute [38]. The specific annotation example of the dataset is shown in Table 5. Among them, O stands for irrelevant words, B stands for the beginning of the entity, I stands for the middle part of the entity, ST stands for the subjective, GJ stands for the nation, QX stands for the pretype, ZL stands for weight, WW stands for foreign name, YZ stands for development time, FY stands for service time, TY stands for retirement time, CX stands for subtype, SF stands for first flight time, and DW stands for construction unit.

(2) Evaluation criteria

The experiment uses accuracy rate, recall rate, and F_1 value as evaluation indicators to evaluate the effectiveness of the method. The calculation method is shown in formula (14) to formula (16). Among them, $TP_{\text{attribute}}$ represents the number of attribute labels correctly identified in the forecast

TABLE 1: List of synonyms for attribute names of military equipment.

Name	Synonym			
Nation	Nation	Nation of origin	Nationality	Nation of manufacture
	Equipment nation	Place of birth	Nation of origin	Nation of construction
	Producing nation	Development nation	Manufacturing nation	Country
	R & D nation	Design nation	Origin	Build nation
Foreign name	Affiliation nation			
	Foreign name	Spanish name	German name	Japanese name
	Latin name	Russian name	English alias	Other translated names
	Japanese alias	French name	English scientific name	Korean name
Development/construction time	English name	Alias	Nickname	
	Development time	Manufacturing time	Development date	Development year
	Start to develop	Start development time	Design time	Construction time
	Build date	Construction year	Start time	
Service time	Year of service	Service	During service	Service date
Decommissioning time	Retirement time	End-time	Retirement date	Time to retire
	Retirement years	Retired		
Pretype/level	Pretype/level	Pretype	Predecessor	Former model
Subtype/level	Prestage			
	Subtype/level	Subtype	Secondary	
Launch/first flight time	Launch time	Launch date	Launch	First flight time
	First test flight	First flight	First flight date	Maiden flight
Development/construction unit	Development unit	R & D unit	Development company	Development organization
	Developer	Manufacturer	Production unit	Construction unit
Weight	Weight	Full load drainage	Full load displacement	Standard displacement
	Standard drainage	Displacement		

TABLE 2: Example of data annotation.

Example one	The [458 Sebari/subjective] commenced construction in [1990/construction time], was launched on [August 27, 1991/launch time] and commissioned on [August 4, 1992/commissioning time].
Example two	On [11 November 1989/service time], the [USS Abraham Lincoln/Subjective] was officially commissioned at Naval Station Norfolk as part of the [American/National] Atlantic Fleet.

TABLE 3: Example of distant supervision error labelling.

[Obama, born in, United States]	[Obama] was the 44th president of the [United States].	False
	[Obama] was born in the [United States].	True
[Obama, president, United States]	[Obama] was the 44th president of the [United States].	True
	[Obama] was born in the [United States].	False

TABLE 4: Description of attribute extraction dataset.

Dataset	Military equipment attribute extraction dataset
Training set	3432
Validation set	429
Test set	430

$$P = \frac{TP_{\text{attribute}}}{TP_{\text{attribute}} + FP_{\text{attribute}}}, \quad (14)$$

$$R = \frac{TP_{\text{attribute}}}{TP_{\text{attribute}} + FN_{\text{attribute}}}, \quad (15)$$

$$F_1 = \frac{2 \times PR}{P + R}. \quad (16)$$

output, $FP_{\text{attribute}}$ represents the number of attribute labels incorrectly identified in the forecast output, and $FN_{\text{attribute}}$ represents the number of unidentified attribute labels.

4.3. *Experimental Parameter Settings.* The experimental parameter settings are shown in Table 6. The batch size is

TABLE 5: Data annotation example.

T-44 tank (English: T-44 medium tank) is a medium tank developed by the Soviet Union on the basis of the T-34/85 tank in the mid-1940s.							
T-44	B-ST	Is	O	On	O	Mid-1940s	O
Tank	I-ST	a	O	The	O		
(O	Medium	O	Basis	O		
English	O	Tank	O	Of	O		
:	O	Developed	O	The	O		
T-44	B-WW	By	O	T-34/85	B-QX		
Medium	I-WW	The	O	Tank	I-QX		
Tank	I-WW	Soviet	B-GJ	In	O		
)	O	Union	I-GJ	The	O		

TABLE 6: Attribute extraction parameter settings.

Parameter	Parameter value
Batch size	8
Learning rate	$5e-5$
RoBERTa hidden layer size	768
LSTM hidden layer size	128
Sentence length	256
Training rounds	20
Dropout	0.5

set to 8, the learning rate is set to $5e-5$, the hidden layer size of RoBERTa is set to 768 according to the pretraining model, and the hidden layer size of LSTM is set to 128.

4.4. Description of Comparison Experiments and Analysis of Experimental Results. In this paper, the attribute extraction task is converted into a sequence annotation task. The current mainstream sequence annotation method is BiLSTM-CRF method. To obtain richer text vector information, we adopt RoBERTa for text encoding. At the same time, to be able to increase the entity recognition accuracy and improve the model extraction effect, we also add an entity boundary prediction layer. To verify the effectiveness of the methods, we design a total of five methods as the baseline models for attribute extraction from the perspective of the ablation experiment [39], as shown below. At the same time, we replace RoBERTa with BERT(base) for comparison experiments based on the following 5 methods. The details are shown in Tables 7 and 8.

The first experiment only uses the public pretraining model RoBERTa to label the attribute sequence. RoBERT uses longer time, larger batch size, and more data for training. This model has achieved good results. The $F1$ value of this experiment reached 0.719. The second experiment is RoBERTa+CRF model, which adds a conditional random field model to label the attribute sequence based on RoBERTa. Adding the CRF layer can add some constraints to the final predicted label to ensure that they are valid. These constraints can be automatically learned by the CRF layer from the training dataset during the training process. The third experiment uses RoBERTa+CRF+SEL model.

TABLE 7: Comparison experiment of attribute extraction (RoBERTa).

Model	Precision	Recall	$F1$
RoBERTa	0.662	0.786	0.719
RoBERTa+CRF	0.691	0.775	0.731
RoBERTa+CRF+SEL	0.745	0.780	0.762
RoBERTa+BiLSTM+CRF	0.721	0.751	0.735
RoBERTa+BiLSTM+CRF+SEL	0.740	0.803	0.770

TABLE 8: Attribute extraction comparison experiment (BERT).

Model	Precision	Recall	$F1$
BERT(base)	0.640	0.731	0.682
BERT(base)+CRF	0.670	0.752	0.709
BERT(base)+CRF+SEL	0.746	0.771	0.758
BERT(base)+BiLSTM+CRF	0.687	0.751	0.718
BERT(base)+BiLSTM+CRF+SEL	0.729	0.776	0.752

The entity boundary prediction layer is added on top of RoBERTa+CRF, splice it as features with hidden layer vector, and consider the loss value of entity boundary prediction layer and attribute labelling loss value in the process of model optimization. The accuracy of this experiment reached 0.745, which is the highest compared to the accuracy of the other four experiments. The fourth is RoBERTa+BiLSTM+CRF model, which uses RoBERTa to vectorize the input text. The traditional BiLSTM+CRF model is used to predict the text attribute sequence. The last model adds features of the entity boundary prediction layer based on RoBERTa+BiLSTM+CRF and comprehensively considers the entity boundary prediction layer loss and the BiLSTM-CRF attribute prediction layer loss when optimizing the model. The recall rate of this experiment reached 0.803, and the $F1$ value reached 0.77, which is better than the existing model.

It can be seen from Table 7 that the model effect has been improved to a certain extent after decoding with CRF. This may be that CRF can restrict the predicted label results and ensure that label "I" appears after label "B" with a high probability, which improves the effect of entity

TABLE 9: Comparison of extraction results of different attribute categories.

Attributes	Precision	Recall	<i>F1</i>	Number of training set samples
Subjective	0.80	0.87	0.83	3004
Nation	0.90	0.95	0.92	3032
Foreign name	0.63	0.64	0.64	716
Development time/construction time	0.50	0.48	0.49	311
Service time	0.39	0.51	0.44	423
Decommissioning time	0.50	0.14	0.22	31
Pretype/level	0.38	0.36	0.37	317
Subtype/level	0.26	0.29	0.27	105
Launch time/first flight time	0.49	0.60	0.54	293
Development unit/construction unit	0.54	0.68	0.60	556
Weight	0.70	0.84	0.76	60

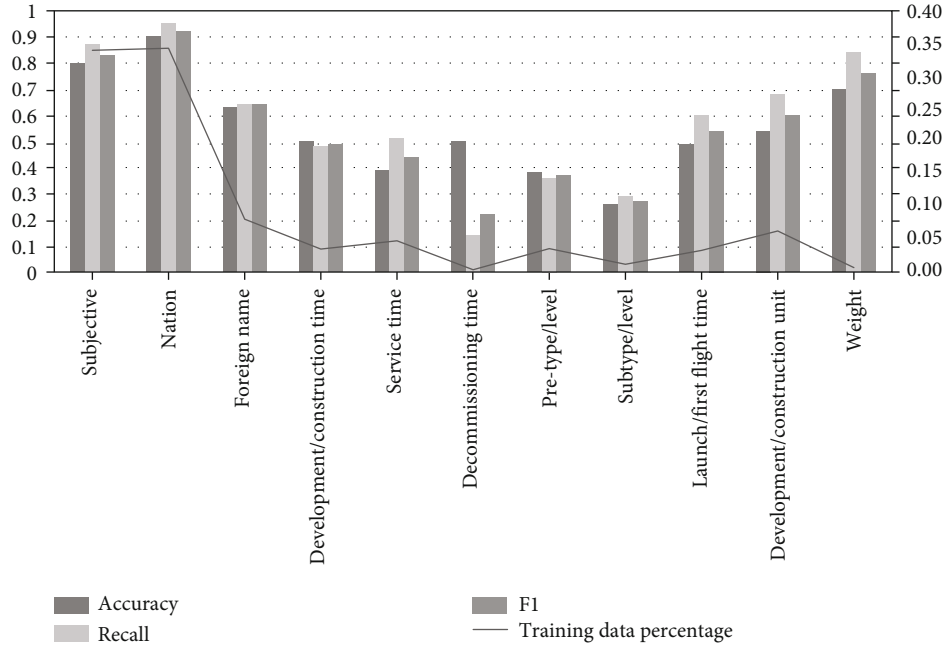


FIGURE 6: Comparison of the combination of the extraction results of different attribute categories for attribute extraction.

recognition to a certain extent. The *F1* value of the model is increased by 0.28 to 0.31 after adding the entity boundary prediction layer SEL. It may be that the increase of the entity boundary prediction layer helps to improve the effectiveness of the entity and attribute value boundary recognition. The overall effect has been improved. After adding BiLSTM for encoding, the model product has a slight improvement compared with the previous one, which may be due to the powerful encoding ability of RoBERTa has more fully obtained the contextual semantic information in the vector. So, the change is smaller after adding BiLSTM.

As shown in Table 8, the results of all five comparison experiments decrease after replacing RoBERTa with BERT(base), which indicates that RoBERTa is more effective in text vector representation and is more suitable for the mil-

itary equipment domain. Comparing BERT(base)+CRF+SEL with BERT(base)+BiLSTM+CRF+SEL, it can be seen that the effect of adding BiLSTM layer may not be greatly improved when the semantic information obtained by contextual encoding through BERT is richer. With the addition of BiLSTM, the recall of the model increase slightly, but the accuracy and *F1* both decrease to some extent.

To further study the recognition effect of RoBERTa+BiLSTM+CRF+SEL method on each different attribute, we test the accuracy, recall, and *F1* of the model on different attributes in the military equipment attribute dataset (as shown in Table 9). At the same time, to show the experimental results more clearly, a combined graph is drawn to show the model extraction effect and the number of samples in the training set. The histogram shows the accuracy, recall, and

F1. The number of samples in the training set is shown by the line graph.

As can be seen from Table 9, the F1 of the model varies considerably for different categories. For example, for the categories of “Subjective” and “Nation,” the F1 reach 0.83 and 0.92. For the categories of “Decommissioning Time,” “Pretype/Level,” and “Subtype/Level,” the F1 are around 0.2 to 0.3. It can be shown in Figure 6 that the recognition effect is better for the categories with more samples in the training set and worse for the categories with fewer samples in the training set. Therefore, it can be speculated that the large difference in the recognition effect of different categories may be caused by the uneven distribution of samples in the training set. For “Nation,” the description of “Nation” often appears in the sentence and every weapon information box in the encyclopedia entry. Therefore, the attribute can obtain more training corpus and a better extraction effect. As for “Decommissioning Time,” many pieces of equipment may be in active service, and there is less description of retirement. Therefore, the available corpus is far smaller than that of other attributes, and the model recognition effect is less satisfactory. The number of training samples for the attribute “Weight” is smaller, but the extraction effect is better. The reason may be that the attribute value of this attribute is usually numerical type, with obvious characteristics and easy to identify.

5. Conclusions

To address the problem of sparse data in the field of weaponry, a distant supervision approach is used to automatically annotate the weaponry data on Baidu Encyclopedia. The method reduces the working time of manual annotation and constructs a weaponry attribute extraction dataset. Based on the characteristics of the encyclopedia data, a data annotation approach is proposed. The annotation of the subjective is performed first, followed by the annotation of the attribute values corresponding to the subjective. For the constructed weapon and equipment dataset, we use the method of RoBERTa+BiLSTM+CRF+SEL to extract attributes and input text sentences into the pretrained attribute extraction model for attribute recognition. The method first uses RoBERTa to vectorize the text and then input it to the entity boundary prediction layer to obtain entity boundary features. This feature is spliced with the hidden layer state vector output by RoBERTa and input to the BiLSTM-CRF attribute prediction layer. Entity attribute triples are predicted through a sequence labeling method. The F1 value of this method is 0.763, which is better than other baseline models.

The attribute extraction of weapons and equipment is one of the important steps to construct the knowledge graph of weapons and equipment. We only consider Baidu Encyclopedia data in terms of data source, which has the problems of insufficient data, less partial attribute data, and unbalanced sample distribution. In future work, we should consider using more sources of data for distantly supervised annotation to expand the data scale. We should also try to solve the problem of uneven data distribution to improve the effect of model extraction.

Data Availability

The data used to support the findings of this study have not been made available because military data is classified.

Conflicts of Interest

The authors declare that they have no conflicts of interest.

Acknowledgments

The authors also acknowledge the Natural Science Foundation of Beijing under grant no. 4212020, National Natural Science Foundation of China under grant no. 62171043, Defense-Related Science and Technology Key Lab Fund Project under grant no. 6412006200404, Qin Xin Talents Cultivation Program of Beijing Information Science and Technology University under grant no. QXTCP B201908, and Research Planning of Beijing Municipal Commission of Education under grant no. KM202111232001.

References

- [1] K. Ruizhi, H. Wenning, K. Cheng, and Z. Donghui, “Attribute extraction for military equipment entity,” *Application Research of Computers*, vol. 33, no. 12, pp. 3721–3724, 2016.
- [2] Z. H. A. I. Jie and Q. I. U. Jiang-nan, “Research on the rule-based knowledge unit attributes extraction method,” *Information Science*, vol. 34, no. 4, pp. 43–47, 2016.
- [3] N. Jakob and I. Gurevych, “Extracting opinion targets in a single and cross-domain setting with conditional random fields,” in *Proceedings of the 2010 Conference on Empirical Methods in Natural Language Processing*, pp. 1035–1045, MIT, Massachusetts, USA, 2010.
- [4] J. Lafferty, A. McCallum, and F. C. N. Pereira, “Conditional random fields: probabilistic models for segmenting and labeling sequence data,” in *Proceedings of the 18th International Conference on Machine Learning 2001 (ICML 2001)*, pp. 282–289, 2001.
- [5] Z. Toh and J. Su, “Nlangp at semeval-2016 task 5: improving aspect based sentiment analysis using neural network features,” in *Proceedings of the 10th international workshop on semantic evaluation (SemEval-2016)*, pp. 282–288, San Diego, California, 2016.
- [6] C. Meng, H. Yu, T. Jian, Z. Jiashuo, Z. Bowei, and Y. Jianmin, “Gated dynamic attention mechanism towards aspect extraction,” *Pattern Recognition and Artificial Intelligence*, vol. 32, no. 2, pp. 184–192, 2019.
- [7] M. Jin, Y. Yifan, and C. Wenliang, “Distant supervision for person attribute recognition,” *Journal of Chinese Information Processing*, vol. 34, no. 6, pp. 64–72, 2020.
- [8] M. Hu and B. Liu, “Mining and summarizing customer reviews,” in *Proceedings of the tenth ACM SIGKDD international conference on Knowledge discovery and data mining*, pp. 168–177, Seattle, Washington, U.S.A, 2004.
- [9] H. Li, Y. Yang, H. Yin, and Z. Jia, “Rules-based character attributes extraction from Baidu Encyclopedia,” *Journal of Integration Technology*, vol. 3, 2013.
- [10] C. Yu, Z. Mao, and S. Gao, “An approach of extracting information for maritime unstructured text based on rules,” *Traffic Information and Safety*, vol. 35, no. 2, pp. 40–47, 2017.

- [11] D. Junjun, Y. Zheng, and H. Bolin, "Rule-based attribute extraction of academic concepts," *Information Theory and Practice*, vol. 34, no. 12, pp. 10–14, 2011.
- [12] L. Qiao, C. Li, Z. Zhong, J. Wang, and D. Liu, "Research on people's information extraction based on rules," *Journal of Nanjing Normal University(Natural Science Edition)*, vol. 35, no. 4, pp. 134–139, 2012.
- [13] S. Zhang, W. Jia, Y. Xia, Y. Meng, and H. Yu, "Opinion analysis of product reviews," in *2009 Sixth International Conference on Fuzzy Systems and Knowledge Discovery*, pp. 591–595, Tianjin, China, 2009.
- [14] X. Bing, Z. Tie-Jun, W. Shan-Yu, and Z. De-Quan, "Extraction of opinion targets based on shallow parsing features," *Acta Automatica Sinica*, vol. 37, no. 10, pp. 1241–1247, 2011.
- [15] N. Y. Gurumdimma, D. B. Bisandu, and E. Ojedayo, "Event extraction from textual data," *Journal of Computer Science and Its Application*, vol. 26, no. 1, 2020.
- [16] N. Cheng, Y. Zou, Y. Teng, and M. Hou, "On the method of personal attributes extraction based on textual knowledge and hierarchical classification," *Applied Linguistics*, vol. 1, pp. 125–134, 2019.
- [17] N. Kambhatla, "Combining lexical, syntactic, and semantic features with maximum entropy models for information extraction," in *Proceedings of the ACL Interactive Poster and Demonstration Sessions*, pp. 178–181, Barcelona Spain, 2004.
- [18] Y. Yufei, D. Qi, J. Zhen, and Y. Hongfeng, "Weakly supervised method for attribute relation extraction," *Journal of Computer Applications*, vol. 34, no. 1, pp. 64–68, 2014.
- [19] C. Liwei, F. Yansong, and Z. Dongyan, "Extracting relations from the web via weakly supervised learning," *Journal of Computer Research and Development*, vol. 50, no. 9, pp. 1825–1835, 2013.
- [20] J. Zhen, Y. Yang, and D.-k. He, "Attribute extraction of Chinese online encyclopedia based on weakly supervised learning," *Journal of University of Electronic Science and Technology of China*, vol. 43, no. 5, pp. 758–763, 2014.
- [21] M. Zhang, J. Zhang, J. Su, and G. Zhou, "A composite kernel to extract relations between entities with both flat and structured features," in *Proceedings of the 21st International Conference on Computational Linguistics and 44th Annual Meeting of the Association for Computational Linguistics*, pp. 825–832, Sydney, Australia, 2006.
- [22] L. Qian, D. Wu, L. Yue, X. Cheng, and P. Lin, "Extracting attribute values for named entities based on global feature," *Journal of Computer Research and Development*, vol. 53, no. 4, pp. 941–948, 2016.
- [23] L. Chengliang, Z. Zhongying, L. Chao, Q. Liang, and W. Yan, "Extracting product properties with dependency relationship embedding and conditional random field," *Data Analysis and Knowledge Discovery*, vol. 4, no. 5, pp. 54–65, 2020.
- [24] R. Wang, M. Xianru, and Q. Kong, "Entity-attribute extraction with GRU+CRF method," *Journal of Modern Information*, vol. 38, no. 10, pp. 57–64, 2018.
- [25] H. Xu, B. Liu, L. Shu et al., "Double embeddings and CNN-based sequence labelling for aspect extraction," in *Proceedings of the 56th Annual Meeting of the Association for Computational Linguistics (Volume 2: Short Papers)*, pp. 592–598, Melbourne, Australia, 2018.
- [26] Z. He, Z. Zhou, L. Gan, J. Huang, and Y. Zeng, "Chinese entity attributes extraction based on bidirectional LSTM networks," *Journal of Computational Science and Engineering*, vol. 18, no. 1, p. 65, 2019.
- [27] W. Zhenkai, C. Meng, Z. Xiabing et al., "Convolutional interactive attention mechanism for aspect extraction," *Journal of Computer Research and Development*, vol. 57, no. 11, pp. 2456–2466, 2020.
- [28] W. Cheng, W. Chaokun, and W. Muxian, "Entity attributes extraction based on text simplification," *Computer Engineering and Applications*, vol. 56, 2020.
- [29] C. Bin, S. Shuicai, Y. Du, and X. Shibin, "Keyword extraction for journals based on part-of-speech and BiLSTM-CRF combined model," *Data Analysis and Knowledge Discovery*, vol. 5, no. 3, pp. 101–108, 2020.
- [30] H. Luo, T. Li, B. Liu, B. Wang, and H. Unger, "Improving aspect term extraction with bidirectional dependency tree representation," *IEEE/ACM Transactions on Audio, Speech, and Language Processing*, vol. 27, no. 7, pp. 1201–1212, 2019.
- [31] S. Feng, J. Liu, H. Jiang, and Y. Xiao, "Attribute value extraction method based on machine reading comprehension model and crowdsourcing verification," *Computer Engineering*, vol. 47, no. 5, pp. 97–103, 2021.
- [32] Y. Liu, M. Ott, N. Goyal et al., "Roberta: a robustly optimized bert pretraining approach," <http://arxiv.org/abs/1907.11692>.
- [33] D. Lou, Z. Liao, S. Deng, N. Zhang, and H. Chen, "MLBiNet: a cross-sentence collective event detection network," <http://arxiv.org/abs/2105.09458>.
- [34] X. Xi, W. Ye, S. Zhang, Q. Wang, H. Jiang, and W. Wu, "Capturing event argument interaction via a bi-directional entity-level recurrent decoder," <http://arxiv.org/abs/2107.00189>.
- [35] M. Mintz, S. Bills, R. Snow, and D. Jurafsky, "Distant supervision for relation extraction without labelled data," in *Proceedings of the 47th Annual Meeting of the ACL and the 4th IJCNLP of the AFNLP*, pp. 1003–1011, Suntec, Singapore, 2009.
- [36] Y. Zhu, W. Zhang, Y. Chen, and H. Gao, "A novel approach to workload prediction using attention-based LSTM encoder-decoder network in cloud environment," *EURASIP Journal on Wireless Communications and Networking*, vol. 2019, no. 1, p. 18, 2019.
- [37] J. Xiao, H. Xu, H. Gao, Y. Li, and Y. Li, "A weakly supervised semantic segmentation network by aggregating seed cues: the multi-object proposal generation perspective," *ACM Transactions on Multimedia Computing Communications and Applications*, vol. 17, no. 1s, pp. 1–19, 2021.
- [38] X. Ma, H. Gao, H. Xu, and M. Bian, "An IoT-based task scheduling optimization scheme considering the deadline and cost-aware scientific workflow for cloud computing," *EURASIP Journal on Wireless Communications and Networking*, vol. 2019, no. 1, p. 19, 2019.
- [39] Y. Huang, H. Xu, H. Gao, X. Ma, and W. Hussain, "SSUR: an approach to optimizing virtual machine allocation strategy based on user requirements for cloud data center," *IEEE Transactions on Green Communications and Networking*, vol. 5, no. 2, pp. 670–681, 2021.

Research Article

The Mobile Water Quality Monitoring System Based on Low-Power Wide Area Network and Unmanned Surface Vehicle

Wei Chen,¹ Xiao Hao,² Kui Yan ,¹ JianRong Lu,³ Jin Liu,¹ ChenYu He,² Feng Zhou,¹ and Xin Xu²

¹Industrial Center/School of Innovation and Entrepreneurship, Nanjing Institute of Technology, Nanjing, Jiangsu 211100, China

²Graduate School, Nanjing Institute of Technology, Nanjing, Jiangsu 211100, China

³Jiangsu Aviation Vocational and Technical College, Zhenjiang, Jiangsu 212134, China

Correspondence should be addressed to Kui Yan; yankui@njit.edu.cn

Received 12 August 2021; Revised 26 September 2021; Accepted 27 September 2021; Published 21 October 2021

Academic Editor: Yuyu Yin

Copyright © 2021 Wei Chen et al. This is an open access article distributed under the Creative Commons Attribution License, which permits unrestricted use, distribution, and reproduction in any medium, provided the original work is properly cited.

The increasingly serious water pollution problem makes efficient and information-based water quality monitoring equipment particularly important. To cover the shortcomings of existing water quality monitoring methods, in this paper, a mobile water quality monitoring system was designed based on LoRa communication and USV. In this system, the USV carrying water quality sensors was used as a platform. Firstly, the LoRa network is used to monitor water quality over a large area. Secondly, the unmanned surface vessel controls the position error within ± 20 m and the velocity error within ± 1 m/s based on the Kalman filter algorithm. Thirdly, the genetic algorithm based on improved crossover operators is used to determine the optimal operational path, which effectively improves the iterative efficiency of the classical genetic algorithm and avoids falling into local convergence. In the actual water surface test, its packet loss probability within a working range of 1.5 km was below 10%, and the USV could accurately navigate according to the preset optimal path. The test results proved that the system has a relatively large working range and high efficiency. This study is of high significance in water pollution prevention and ecological protection.

1. Introduction

Today, the water quality in coastal and inland lakes is deteriorating under the influence of increasing human social and economic activities. The ill-being water environment has caused irreparable losses to human health, production, and living, so that the protection of the water ecological environment demands immediate attention [1].

The data collection and monitoring of the water area take an important part in the protection and management decision-making of the water ecosystem. In spite of the research achievements, several problems in the field of water quality monitoring still need to be tackled.

- (i) Monitoring scope: for large natural reserves of hundreds or even thousands of square kilometers,

expensive economic costs will be incurred if monitoring and sensing device is arranged.

- (ii) Remote location of the monitored area: special communication infrastructure should be erected for monitoring device in such areas.
- (iii) Daily maintenance of device: a traditional monitoring device needs manual inspection and maintenance one by one, which will cause high human resource costs [2]. To address these issues, this paper investigates efficient water quality monitoring methods.

2. Related Works

There are three main approaches to current water quality monitoring: labor-intensive manual sampling, construction

of fixed monitoring stations in monitoring waters, and mobile water quality monitoring through autonomous robots such as unmanned boats. Current water quality monitoring methods based on the second approach are many; for example, Ruan and Tang combined solar charging and wireless sensor network technology to design an energy-saving low-carbon water quality monitoring system [3]. Nam et al. designed a wireless sensor network system based on CDMA (Code Sector Multiple Access) and ZigBee technology when monitoring the water environment inhabited by coastal fish [4]. Wiebke et al. [5] deployed a wireless sensor network in coastal fishing grounds with low-cost compact buoys equipped with water quality monitoring sensors to analyze the impact of water quality parameters on aquaculture. These methods above have significant drawbacks; they can only monitor fixed locations and still require manual repositioning of node locations if the monitoring target is to be changed.

In response to above drawbacks, many studies have been made on the application of unmanned vessels for water quality monitoring. Cao et al. designed a 4G technology-based automatic navigation water quality monitoring unmanned boat, which can navigate to the preset monitoring point and collect water quality information at the location [6]. Siyang and Kercharoen realized the upload and storage of water quality monitoring data from unmanned boat based on Zigbee network, and the effective monitoring distance is about within 300 m [7]. Yang et al. in Taiwan designed a double-hulled water quality monitoring unmanned boat, which is stable and able to conduct water sampling on the basis of water quality collection. Bălănescu et al. combined blockchain technology with unmanned boat water quality monitoring work, providing a high security data collection, transmission, and management scheme [8]. However, these current research results are either limited by the shortcomings of ZigBee or WiFi, such as short communication distance and weak anti-interference ability, or limited by the high power consumption of 4G or GPRS, and the need for additional fees.

To cope with these existing problems, the emerging LoRa technology that boasts low cost, long communication distance, and strong endurance was introduced in this paper [9]. Further, the USV can navigate autonomously on the water surface, by which the efficiency of water surface working can be enhanced to a great degree [10]. In this paper, a mobile water quality monitoring system that works based on USV and LoRa was designed to effectively cover the shortcomings of existing methods. Featuring good energy-saving performance, low cost, and wide monitoring range, this system can be used to collect and monitor the data of the target water area by any environmental protection agency and individual, presenting extremely important research significance in the prevention and treatment of water pollution and the construction of a good aquatic ecology.

3. Architecture of the Mobile Water Quality Monitoring System

The mobile water quality monitoring system proposed in this paper integrates path planning, autonomous navigation,

real-time water quality monitoring, and remote monitoring. This system is composed of parts: shipboard system, LoRa gateway, and monitoring terminal. The system architecture is shown in Figure 1.

First, the shipboard system mainly consists of positioning and navigation system, power system, LoRa communication system, and main control board. It has the functions of obtaining GPS positioning coordinates, reading heading, and speed information of unmanned surface vessels. The shipboard system interacts with the shore-based monitoring platform for data commands through LoRa network and with the water quality monitoring system for control commands through RS232 interface. The shipboard system according to the shore-based monitoring platform to send control commands for independent cruise or remote control action controls the water quality monitoring system for water quality testing.

Second, the water quality detection system consists of a main control board and four elements of water quality sensors such as temperature, turbidity, pH, and conductivity. It receives the instructions that sent by the shipboard system to collect water body information on a regular basis.

Third, the shore-based platform is mainly developed based on windows operating system, including monitoring software programs and data processing algorithms. The host computer is mainly based on the human-computer interaction interface, completing LoRa communication, algorithm call, map display, data sending and receiving, and display functions; the algorithm application is mainly through the C++ call MATLAB algorithm, sending the calculated operation path coordinates to the unmanned ship, so as to achieve the application of multipoint monitoring path planning.

The shipboard system of the USV is designed with a catamaran with a length of 0.8 m, a width of 0.68 m, and a maximum speed of 8 km/h. Structured with two parallel hulls of equal size, the catamaran has a wider beam and a shallower draft than a monohull, making the course of the entire ship more stable [11]. The structure of the unmanned surface vessel is shown in Figure 2.

Two DC motors are provided to serve as the kinetic drive device of the USV and coordinated with the motor driver; the hull steering can be adjusted through the differential control method. The USV is equipped with the positioning module ATK1218-BD and the attitude detection module MPU9250. The loose coupling integrated navigation algorithm was introduced to calculate the hull attitude and position. To meet the basic monitoring requirements, temperature, pH, turbidity, and conductivity were selected as the monitoring elements in this paper. The E-201C pH-water temperature composite sensor, the TSW-30 turbidity sensor, and the DJS-12 conductivity electrode sensor are employed and paralleled via RS485 communication protocol, and these sensors can be replaced and configured according to actual use condition. STM32F103ZET6 acts as the central controller to complete data collection and calculation.

The LoRa communication technology used for USV can effectively expand the monitoring scope and save costs. In this paper, close attention was paid to the design of the ship-shore LoRa communication system and the path

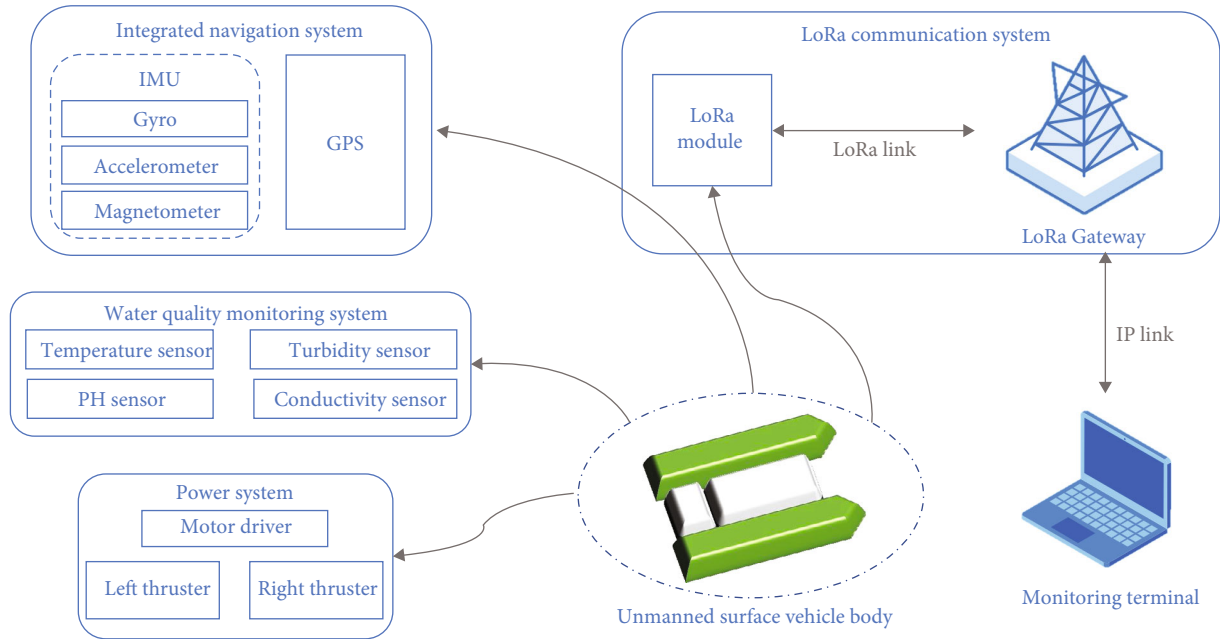


FIGURE 1: Architecture of the mobile water quality monitoring system.

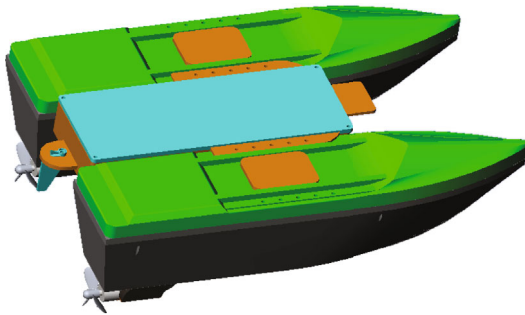


FIGURE 2: The mechanical structure of USV.

planning algorithm of USV was improved. In addition, ONENET—China Mobile IoT Development Platform—was used as the monitoring terminal of this system to help realize the device monitoring and configuration, real-time data monitoring, data storage, and other functions [12].

4. LoRa Communication System

4.1. Shipboard LoRa Nodes

4.1.1. Communication Node Hardware. This system is designed with LoRa radio frequency module to receive and transmit the water quality data. The programming was conducted in the MCU to control the LoRa module and send the encoded information through the module. The integrated +20 dBm power amplifier is provided to ensure that the long-distance wireless communication is available under the condition of sensitivity as low as -148 dBm. The circuit schematic diagram of the LoRa communication module is shown in Figure 3.

4.1.2. Communication Node Software. In this study, the control program of the STM32 single-chip microcomputer was designed in the Keil integrated development environment and finally programmed to the MCU to complete the development after compilation, simulation, and debugging. The program was written to complete such functions as data collection, signal conversion, and uploading data. The flow of node program is shown in Figure 4. After the program starts, it is divided into the following steps: first, initialize the device and make the LoRa module connect to the network; second, enter the main program and wait for the timer to trigger the detection task; third, complete the trigger and collect the water body data; fourth, carry out MCU data processing and ADC conversion; fifth, store the data in the buffer after processing is completed and wait for sending; sixth, after sending, enter the sleep state and wait for the timer to trigger the detection command again.

4.2. Shore-Based LoRa Gateway

4.2.1. Gateway Hardware. The embedded gateway designed in this study was composed of an industrial-control core board, a LoRa gateway module, and a 4G LTE mobile data board, as shown in Figure 5.

In order to cope with large-scale distributed monitoring scenarios, it is necessary to extend the downlink channel of gateway. A symmetrical channel processor refers to the coexistence of multiple SX1278s by combiners based on a communication channel provided by the existing SX1278 RF chip. Connect the module with the serial port of LoRa gateway, and control frequency band, power, spreading factor, and other RF parameters of each channel by application program to operate the serial port, and fix all channels of modules as downlink channels. This makes up for the lack

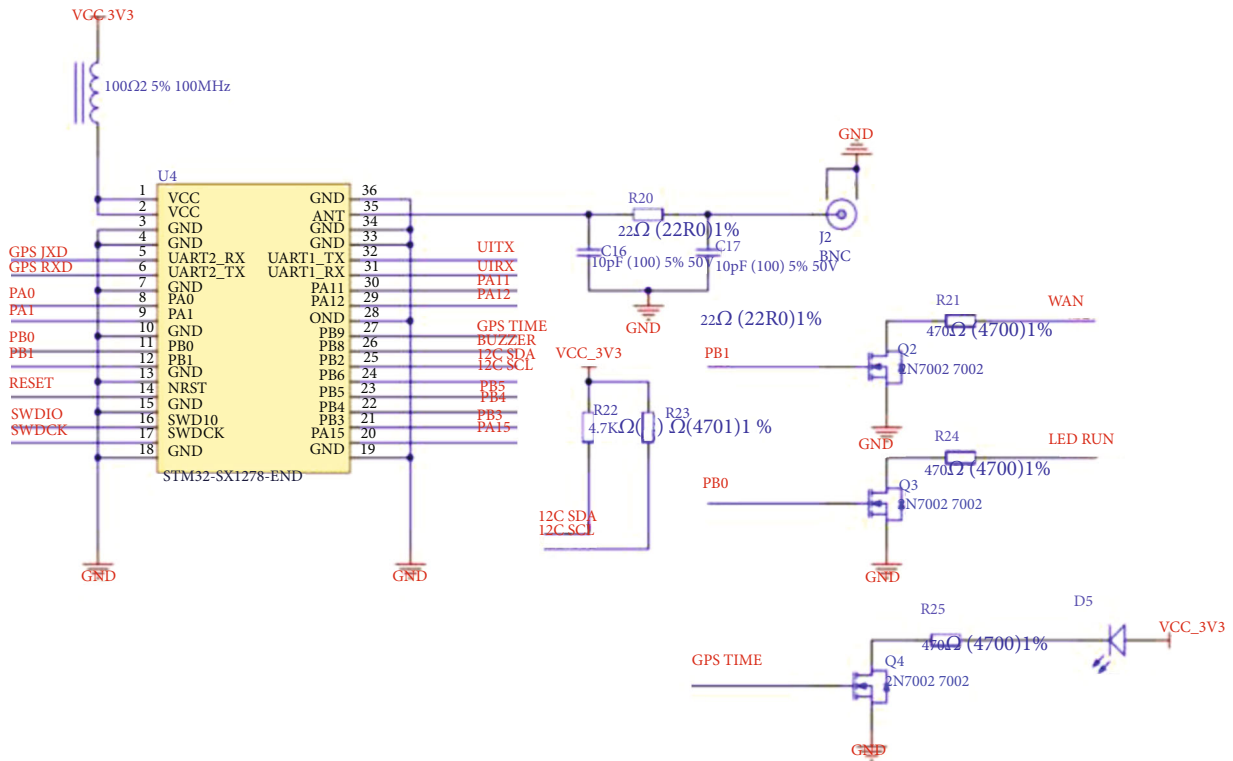


FIGURE 3: Schematic diagram of LoRa RF module.

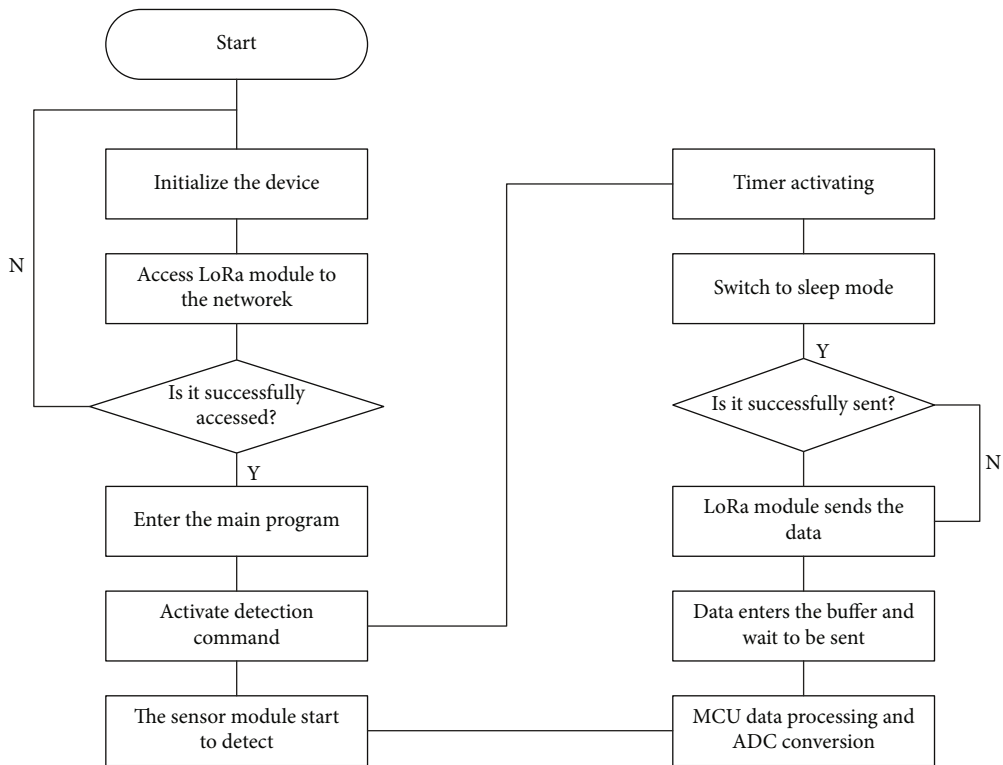


FIGURE 4: Flow of sensing layer node program.

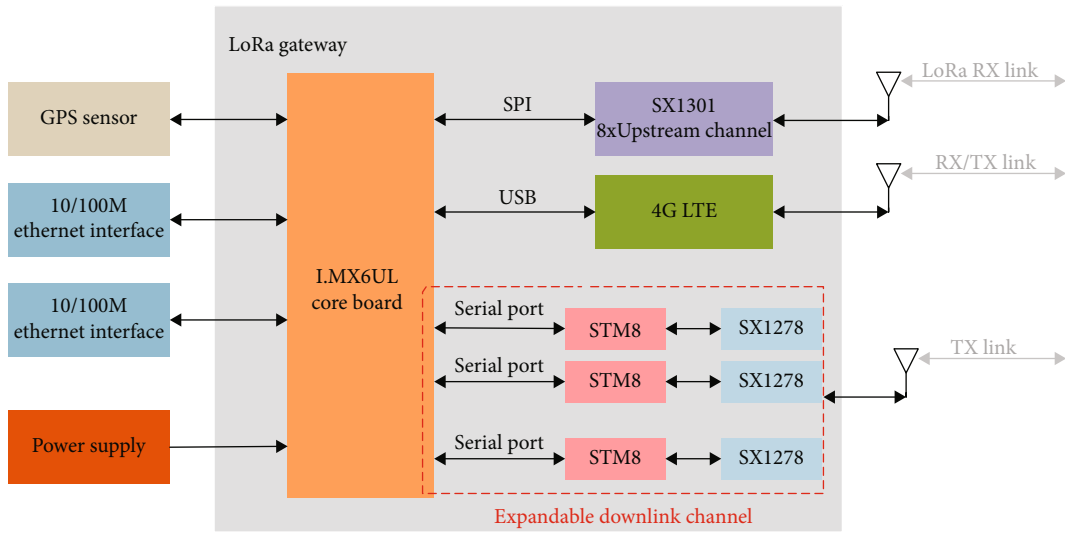


FIGURE 5: Architecture of gateway hardware.

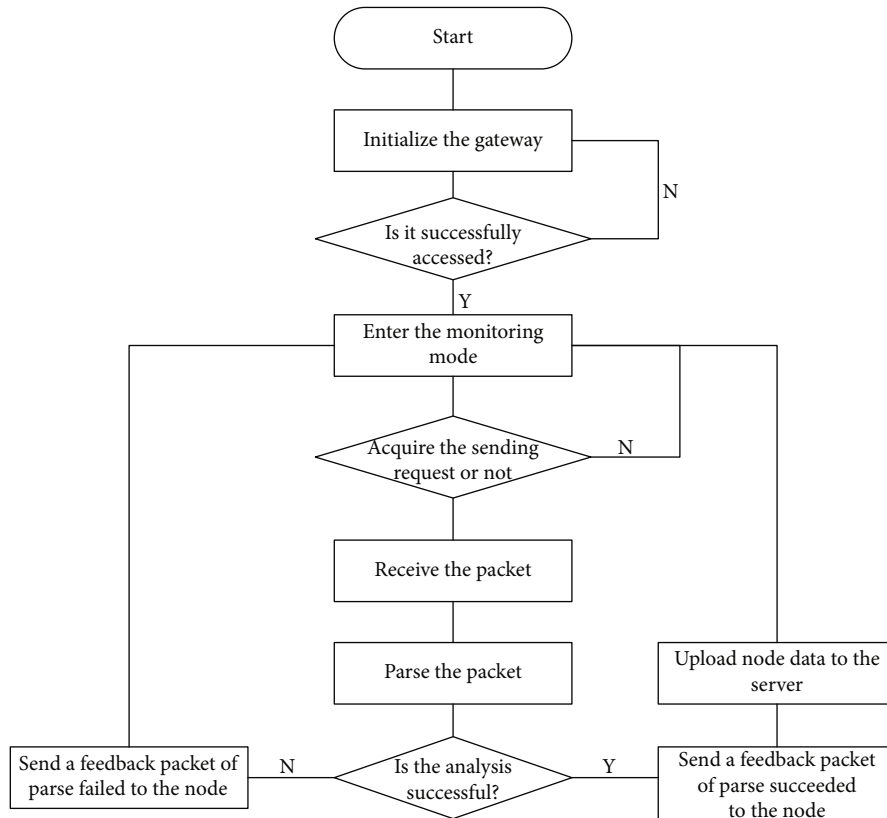


FIGURE 6: Flow of gateway program.

of one downlink channel of existing LoRa gateway and realizes a LoRa gateway structure under multichannel symmetrical channel, which can alleviate transmission congestion and packet loss caused by large-scale data access.

4.2.2. *Gateway Software.* The workflow of the gateway in this study is shown in Figure 6. After the gateway program starts,

it is divided into the following steps: first, initialize the gateway device and check whether the initialization is successful; second, the gateway enters listening mode; third, determine whether to obtain the send request; fourth, receive the packet after successfully obtaining the send request, otherwise continue listening; fifth, parse the packet and determine whether the parsing is successful; sixth, if the parsing is

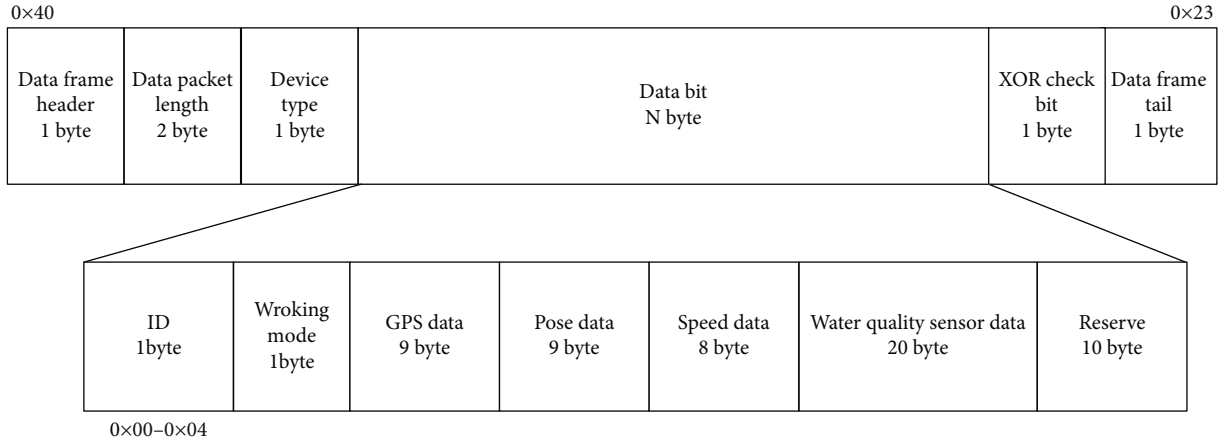


FIGURE 7: Format of protocol frame sent by monitoring terminal.

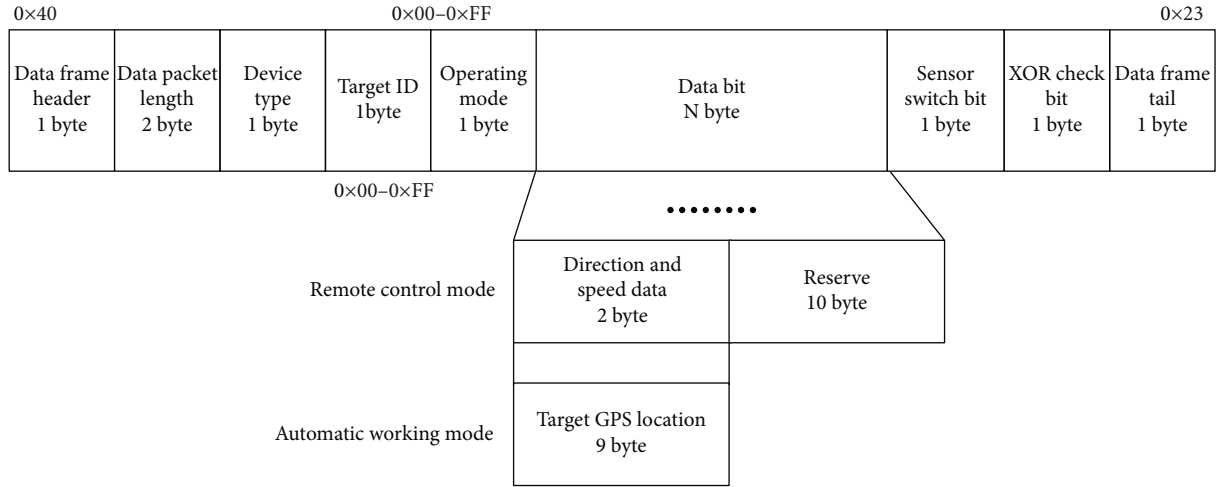


FIGURE 8: Flow of gateway program.

successful, upload the data to the user monitoring platform. Otherwise, send the feedback packet to the node for failed parsing.

4.3. Ship-Shore Interaction LoRa Communication Protocol. The parsing of the communication protocol by the on-board system is mainly implemented by a finite state machine. We preset three states: stop, autonomous, and remote control. When the shipboard system receives the protocol frame from the shore-based monitoring platform, it parses the operation mode field in the protocol. The finite state machine further processes the data in the data frame by the different operational states. In the case of remote control mode, the speed and heading information in the data frame is parsed and the remote control procedure is executed. In the case of autonomous mode, the GPS coordinates of the target point in the data frame are resolved. Then, the heading is calculated based on the current GPS coordinates, and navigation to the target point is performed. In case of stop mode, the operation is terminated. During the operation of the unmanned surface vessel, water body data and navigation status are regularly collected and uploaded

to the user monitoring platform. The user monitoring platform receives the data packets and parses, displays, and stores them.

4.3.1. USV Node Sends Protocol Frame. The communication when the USV node sends data to the LoRa gateway was in line with the protocol frame format shown in Figure 7.

This protocol frame contains 64 bytes, composed of data frame header, data packet length, device type, target ID number, operating mode, GPS data, pose data, speed data, water quality sensor data, reserved bits, XOR check bit, and data frame tail.

4.3.2. Protocol Frame Sent by Monitoring Terminal. The communication when the monitoring terminal sends data to the USV node was in line with the protocol frame format shown in Figure 8.

The protocol frame contains 21-28 bytes, composed of data frame header, data packet length, device type, target ID number, operating mode, direction and speed data, target GPS position, reserved bit, sensor switch bit, XOR check bit, and data frame tail.

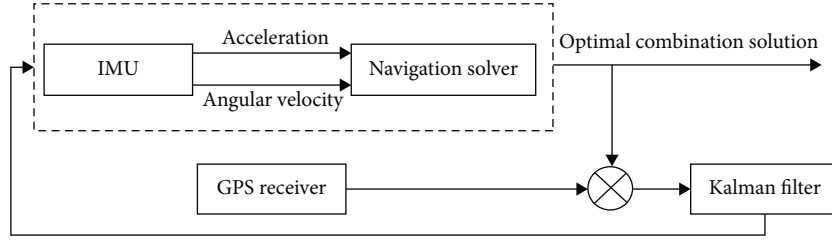


FIGURE 9: Improved combination method.

The protocol frame is a data frame with variable length. When the remote control mode is selected as the working mode, the direction and speed data were transmitted in the data bit, and when the automatic working mode was selected, the target GPS location data were transmitted in the data bit.

5. Integrated Navigation Method for USV

For water quality monitoring cruise operations, the navigation algorithm is crucial. GPS navigation is vulnerable to interference from the external environment and limited by the low update frequency. It cannot meet the demand for continuous and stable positioning. The inertial navigation method calculates position and velocity by direct integration of inertial module measurement information data, and the accumulated error will occur and gradually increase with time. To address the above problems, we use an improved integrated navigation method based on the Kalman filter to achieve the fusion of GPS and inertial data. It can overcome the shortcomings of inertial sensor dispersion over time. The inertial sensors provide the acceleration and angular velocity of the ship, and the speed and position information of the ship can be calculated using the laws of physics. The Kalman filtering algorithm reduces the effect of cumulative errors while reducing the complexity of implementation. This improved integrated navigation method has the advantages of simple structure and small computational effort, which is well suited for low-cost unmanned ship navigation applications. Its schematic block diagram is shown in Figure 9.

Neglecting the velocity error and position error of the sky direction, the state variables of the combined navigation are:

$$X = [\varphi_E, \varphi_N, \varphi_U, \partial V_E, \partial V_N, \partial L, \partial \lambda, \varepsilon_{bx}, \varepsilon_{by}, \varepsilon_{bz}, \Delta_x, \Delta_y, \Delta_z]^T, \quad (1)$$

where $\varphi_E, \varphi_N, \varphi_U$ denote the platform angle error in the east, north, and sky directions, respectively; $\partial V_E, \partial V_N$ denote the velocity error in the east and north directions, respectively; $\partial L, \partial \lambda$ denote the longitude and latitude error, respectively; $\varepsilon_{bx}, \varepsilon_{by}, \varepsilon_{bz}$ denote the constant drift of gyroscope in the east, north, and sky directions, respectively; and $\Delta_x, \Delta_y, \Delta_z$ denote the constant drift of acceleration in the east, north, and sky directions, respectively.

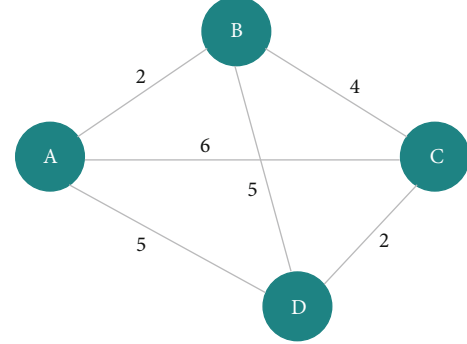


FIGURE 10: Example of weighted completely undirected graph for TSP problem.

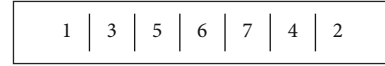


FIGURE 11: Chromosome representation method.

The system noise vectors are

$$W = [\omega_{\varepsilon E}, \omega_{\varepsilon N}, \omega_{\varepsilon U}, \omega_{aE}, \omega_{aN}, 0, 0, 0, 0, 0, 0, 0, 0]^T, \quad (2)$$

where $\omega_{\varepsilon E}, \omega_{\varepsilon N}, \omega_{\varepsilon U}$ denote the random drift of the gyroscope in the east, north, and sky directions, respectively, and ω_{aE}, ω_{aN} denote the random drift of the accelerometer in the east and north directions, respectively.

Assume that the gyroscope and accelerometer drift obey Gaussian distribution, that is,

$$\varepsilon = 0, \Delta = 0, \quad E[W(t)W(t)^T] = Q(t). \quad (3)$$

Also considering the unmanned ship work actual, the system works in the horizontal plane; then, the system state equation is

$$\begin{aligned} \phi_E = & -\frac{\partial V_N}{R_m + h} + \left[\omega_{ie} \sin L + \frac{V_E}{R_n + h} \tan L \right] \phi_N \\ & - \left[\omega_{ie} \cos L + \frac{V_E}{R_n + h} \tan L \right] \phi_U + C_b^t(1, 1)\varepsilon_{bx} \\ & + C_b^t(1, 2)\varepsilon_{by} + C_b^t(1, 3)\varepsilon_{bz} + \omega_{\varepsilon E}, \end{aligned} \quad (4)$$

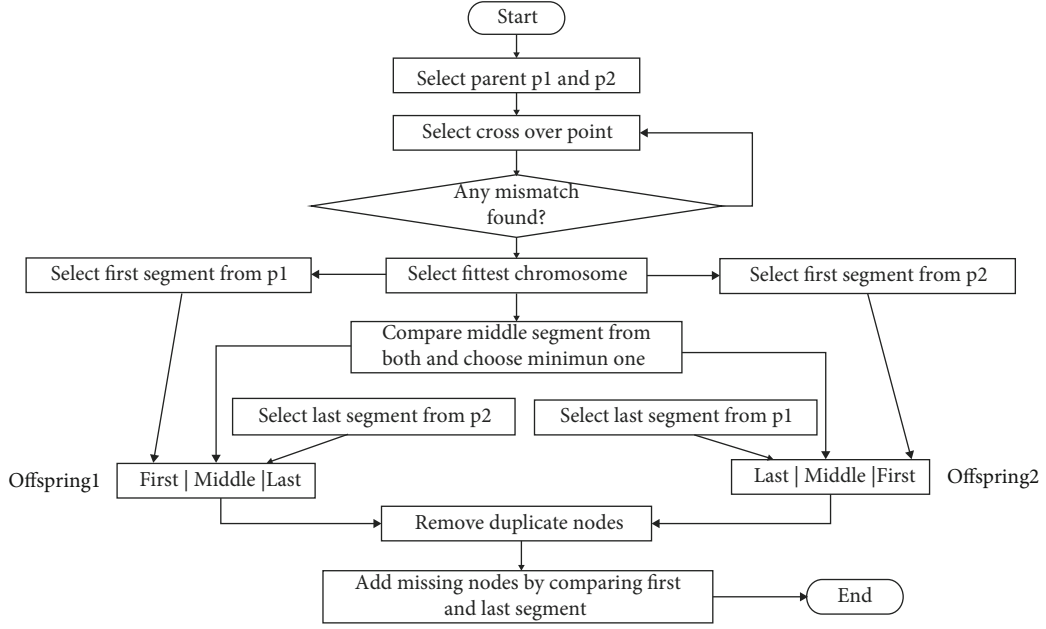


FIGURE 12: Cross process diagram.

$$\phi_N = \frac{\partial V_E}{R_n + h} - \omega_{ie} \sin L \partial L - \left[\omega_{ie} \sin L + \frac{V_E}{R_n + h} \tan L \right] \phi_E - \frac{V_N}{R_m + h} \phi_{U+C_b^i(2,1)\varepsilon_{bx}+C_b^i(2,2)\varepsilon_{by}+C_b^i(2,3)\varepsilon_{bz}+\omega_{eN}}, \quad \partial \lambda = \frac{\sec L}{R_n + h} \partial V_E + \frac{V_E \sec L \tan L}{R_n + h} \partial L, \quad (10)$$

$$\phi_U = \left[\omega_{ie} \cos L + \frac{V_E}{R_n + h} \right] \phi_E + \frac{V_E}{R_m + h} \phi_N + \frac{\tan L}{R_n + h} \partial V_E + \omega_{ie} \sin L \partial L + \left[\omega_{ie} \cos L + \frac{V_E}{R_n + h} \sec^2 L \right] \partial L + C_b^t(3, 1)\varepsilon_{bx} + C_b^t(3, 2)\varepsilon_{by} + C_b^t(3, 3)\varepsilon_{bz} + \omega_{eU}, \quad (6)$$

$$\partial V_E = \left[2\omega_{ie} \sin L + \frac{V_E}{R_n + h} \tan L \right] \partial V_N + \frac{V_N}{R_m + h} \tan L \partial V_E + f_U \phi_N - f_N \phi_U - \left[2\omega_{ie} \cos L + \frac{V_E V_N}{R_n + h} \sec^2 L \right] \partial L + C_b^t(1, 1)\Delta_x + C_b^t(1, 2)\Delta_y + C_b^t(1, 3)\Delta_z + \omega_{aE}, \quad (7)$$

$$\partial V_N = 2 \left[\omega_{ie} \sin L + \frac{V_E}{R_n + h} \tan L \right] \partial V_E + f_U \phi_E - f_E \phi_U - \left[2\omega_{ie} \cos L + \frac{V_E}{R_n + h} \sec^2 L \right] \partial L + C_b^t(2, 1)\Delta_x + C_b^t(2, 2)\Delta_y + C_b^t(2, 3)\Delta_z + \omega_{aE}, \quad (8)$$

$$\partial L = \frac{1}{R_m + h} \partial V_N, \quad (9)$$

where V_E, V_N indicate the speed of the unmanned ship in the east and north directions, respectively; ω_{ie} indicates the angular velocity of the earth's rotation; and f_E, f_N, f_U indicate the specific force felt by the accelerometer in the east, north, and sky directions, respectively.

Combining the above equations, the system equation of state can be written as

$$\hat{X}(t) = F(t)X(t) + W(t), \quad (11)$$

where $\hat{X}(t)$ indicates the estimated state, $F(t)$ indicates the state matrix, $X(t)$ indicates the current state, and $W(t)$ indicates the noise vectors.

In the navigation system, there are two groups of observation equations: one group is the position observation value, which is the difference between the latitude and longitude information given by the inertial guidance system and the corresponding position information given by the GPS receiver; the other group of observation value is the difference between the velocity in each direction given by the two systems.

The position measurement information of INS can be expressed as the sum of the true value and the error:

$$\begin{bmatrix} L_I \\ \lambda_I \end{bmatrix} = \begin{bmatrix} L_t + \partial L \\ \lambda_t + \partial \lambda \end{bmatrix}. \quad (12)$$

TABLE 1: Example cost matrix.

Node	1	2	3	4	5	6	7
1	Inf	29	82	46	68	52	15
2	29	Inf	55	46	42	43	43
3	82	55	Inf	68	63	20	23
4	46	46	68	Inf	82	15	72
5	68	42	63	82	Inf	74	23
6	52	43	20	15	74	Inf	61
7	15	43	23	72	23	61	Inf

Offspring1 $\boxed{4 \mid 3 \mid 5 \mid 7 \mid 6 \mid 1 \mid 2}$ Cost = 296

Offspring2 $\boxed{4 \mid 5 \mid 6 \mid 1 \mid 3 \mid 7 \mid 2}$ Cost = 356

FIGURE 13: Representation of father generation chromosome.

Offspring1 $\boxed{4 \mid 3 \mid 5 \mid 7 \mid 6 \mid 7 \mid 2}$

Offspring2 $\boxed{4 \mid 5 \mid 5 \mid 7 \mid 6 \mid 1 \mid 2}$

FIGURE 14: Representation of the offspring chromosome obtained after Step 2.

Similarly, the position information of GPS can be expressed as the sum of the true value and the error:

$$\begin{bmatrix} L_G \\ \lambda_G \end{bmatrix} = \begin{bmatrix} L_t + N_N \\ \lambda_t + N_E \end{bmatrix}. \quad (13)$$

Then, the position observation equation is

$$\begin{aligned} Z_p(t) &= H_p(t)X(t) + V_p(t), \\ H_p(t) &= [0_{2 \times 5} \quad \text{diag} [1 \quad 1] \quad 0_{2 \times 6}], \\ V_p(t) &= [N_N \quad N_E]. \end{aligned} \quad (14)$$

Similarly, the velocity observation equation of INS is

$$\begin{aligned} \&Z_v(t) &= H_v(t)X(t) + V_v(t), \\ H_v(t) &= [0_{2 \times 3} \quad \text{diag} [1 \quad 1] \quad 0_{2 \times 8}], \\ V_v(t) &= [M_N \quad M_E]. \end{aligned} \quad (15)$$

By combining the position observation equation and the velocity observation equation, the observation equation of the combined INS/GPS navigation system can be obtained as

$$Z(t) = \begin{bmatrix} H_p(t) \\ H_v(t) \end{bmatrix} X(t) + \begin{bmatrix} V_p(t) \\ V_v(t) \end{bmatrix}. \quad (16)$$

Offspring1 $\boxed{4 \mid 3 \mid 5 \mid 7 \mid 6 \mid 2 \mid \bigcirc}$

Offspring2 $\boxed{4 \mid 5 \mid 7 \mid 6 \mid 1 \mid 2 \mid \bigcirc}$

FIGURE 15: Representation of the offspring chromosomes after Step 3. \bigcirc represents to the missing node to be supplemented.

Offspring1 $\boxed{4 \mid 3 \mid 5 \mid 7 \mid 6 \mid 2 \mid 1}$ Cost = 287

Offspring2 $\boxed{4 \mid 5 \mid 7 \mid 6 \mid 1 \mid 2 \mid 3}$ Cost = 302

FIGURE 16: Representation of the offspring chromosomes after Step 3.

6. Study on USV Path Planning Based on Improved Genetic Algorithm

6.1. Problem Description. Path planning is the key technology for a mobile water quality monitoring system to work efficiently. The available optional paths from the starting point to the end point in the water quality monitoring were countless. This paper is aimed at finding out the optimal working path with high efficiency and energy saving as indicators.

Based on the working characteristics of the USV traversing multiple monitoring points over the course of water quality monitoring, the water quality monitoring process was abstracted as the Traveling Salesman Problem (TSP) in this paper. Observe Figure 10; the essence of the problem is to find a Hamilton loop with the smallest weight in a weighted completely undirected graph.

The classic TSP could be described as follows: when the number of target cities N and the distance between any cities are all known, the shortest path traversed all cities once and only once and returned to the starting city [13]. The problem can be described via the following mathematical model.

$$D = (d_{ij})_{N \times N} \begin{cases} d_{ij}, i \neq j, \\ Inf, i = j, \end{cases} \quad (17)$$

$$\begin{cases} \text{Tour} = \{T_1, T_2, \dots, T_p, \dots, T_{(n-1)}\}, \\ n! = n \cdot (n-1) \cdot \dots \cdot 2 \cdot 1, \end{cases} \quad (18)$$

$$\text{Len}(T_p) = \left(\sum_{l=1}^{N-1} d_{T_p(l)T_p(l+1)} \right) + d_{T_p(N)T_p(1)}, \quad (19)$$

where N is the number of cities, D is the distance matrix, d_{ij} is the distance between two cities, Inf is a large enough positive number, i, j are the city numbers, Tour is the set of paths, $T_p(l)$ is the l th city in the path, and $\text{Len}(T_p)$ is the total length of the path T_p . It can be seen that the optimal solution of TSP is the minimum value of solving $\text{Len}(T_p)$. Then, an

```

Genetic algorithm with improved crossover operator
Input:  $N, G, F(t)$ 
Output: Achieve the chromosome with the best fitness value
1: Initialize the population
2:  $t \leftarrow 0$ 
3: while  $t \leq G$  do
4:   for  $i = 0 \rightarrow N$  do
5:     Calculate fitness  $F(t)$ 
6:   end for
7:   for  $i = 0 \rightarrow N$  do
8:     Selection operations
9:   end for
10:  for  $i = 0 \rightarrow N/2$  do
11:    Get parent chromosomes  $p1, p2$ 
12:    Select the crossover point and cut the parent chromosome into three segments
13:    Select the first segment of  $p1$  and the last segment of  $p2$  insert into offspring 1
14:    Select the first segment of  $p2$  and the last segment of  $p1$  insert into offspring 2
15:    Calculate the local adaptation of the intermediate segments of  $p1$  and  $p2$ 
16:    Select the intermediate segment with high fitness as the intermediate segment of the offspring
17:    Remove duplicate nodes
18:    Insert missing nodes in the first or last segment according to the fitness value
19:    Obtain offspring 1 and 2
20:  end for
21:  for  $i = 0 \rightarrow N$  do
22:    Mutation operation
23:  end for
24:  for  $i = 0 \rightarrow N$  do
25:     $F(t+1) = F(t)$ 
26:  end for
27:   $t = t + 1$ 
28: end while

```

ALGORITHM 1: Pseudocode for the method proposed.

improved genetic algorithm was introduced in this paper to solve this problem.

6.2. Basic Genetic Algorithm Principle. In this paper, the basic genetic algorithm is improved so as to calculate the optimal path of the unmanned ship. The basic genetic algorithm is one kind of iterative algorithm, which is an intelligent computational model to complete the simulation of biological evolution process in nature with the help of computer technology. Compared with the traditional algorithms, the genetic algorithm not only has the characteristics of self-learning, self-organization, and self-adaptation but also has high robustness and wide applicability, which can effectively deal with the complex problems that are difficult to be solved by traditional optimization algorithms without the limitation of problem nature.

The main operators that manipulate chromosomes in genetic algorithms are as follows: population initialization operator, selection operator, crossover operator, and mutation operator. The population initialization operator prepares for the improvement of the feasible solution and the iterative process of the algorithm, mainly for the task of transforming the feasible solution of the problem into the corresponding chromosomes based on the coding scheme. The purpose of the selection operator is to select individuals of good breed. The operator is based on the evaluation of the

fitness of the individuals and, according to a specific method, selects a part of the contemporary population with high fitness in preparation for the generation of the new generation. The crossover operator is an important operator that enables genetic algorithms to search for new solutions over a very wide space, in order to obtain new and better individuals. The crossover process is a process performed by a certain probability to replace and reorganize some genes of the chromosomes of the individuals already selected from the population into new individuals. The mutation operator ensures the diversity of individuals in the population, thus suppressing to some extent the problem of early convergence in the genetic algorithm.

The basic execution steps of the genetic algorithm are as follows:

- (Step 1) In population initialization, first, complete the setting of the control parameters of the genetic algorithm, and then establish the first generation population using the population initialization operator.
- (Step 2) Calculate the individual fitness. Construct the corresponding fitness function, and calculate the fitness of all individuals in the population according to the problem being addressed.

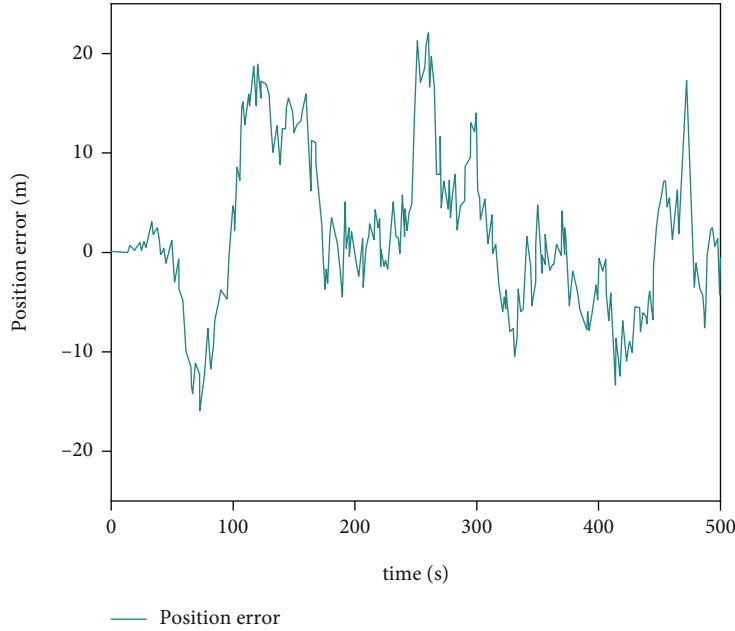


FIGURE 17: Position error convergence range after combined navigation filtering.

- (Step 3) Determine whether to terminate the iteration. When the number of evolutionary generations is less than the maximum number of iterations, Step 4 is executed; otherwise, the iteration is terminated and the optimal individuals in the population are output.
- (Step 4) Execute the selection operation. Use the selection operator to select some individuals from the population.
- (Step 5) Execute the crossover operation. Compare the crossover probability, and perform the update operation on the selected individuals using the crossover operator.
- (Step 6) Perform the variation operation. In contrast to the mutation probability, a new generation of population is obtained by performing the mutation operation on the selected individuals, updating the evolutionary generation and moving to Step 2.

In order to be able to make the offspring obtained by crossover jump out of the local optimal solution while retaining the excellent genes of the parent, this paper proposes an improved triple crossover operator, which divides the parent chromosome into three segments and then compares the recombination, so as to obtain better individuals.

6.3. Improved Genetic Algorithm. The high efficiency of the basic genetic algorithm is mainly attributed to its operators: replication, crossover, and mutation [14]. But the basic genetic algorithm is still exposed to such shorting such as poor local search ability and slow convergence speed [15]. In this paper, the iterative efficiency of genetic algorithm in

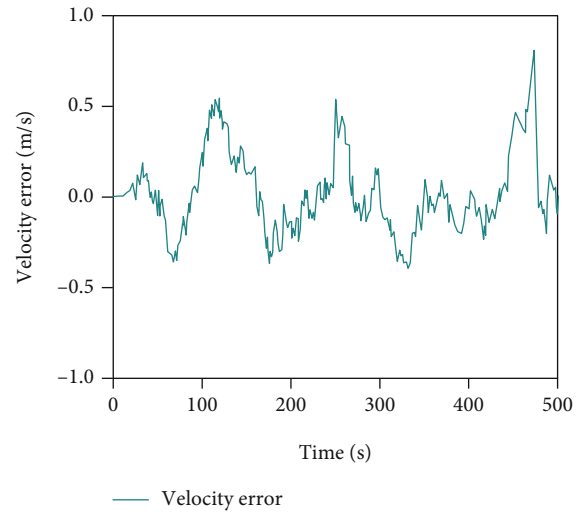


FIGURE 18: Velocity error convergence range after combined navigation filtering.

the path planning of USVs was lifted by improving the multipoint crossover operator.

In the process of species initializing, each chromosome was described as a series of nodes (each node was a monitoring target point). If there were seven monitoring target points in the job, the length of the chromosome would be set to 7, as shown in Figure 11. The cost matrix could be used to calculate the distance cost between two monitoring target points.

The fitness function that used the basic genetic algorithm was reserved:

$$F(x) = \frac{1}{f(x)}, \quad (20)$$

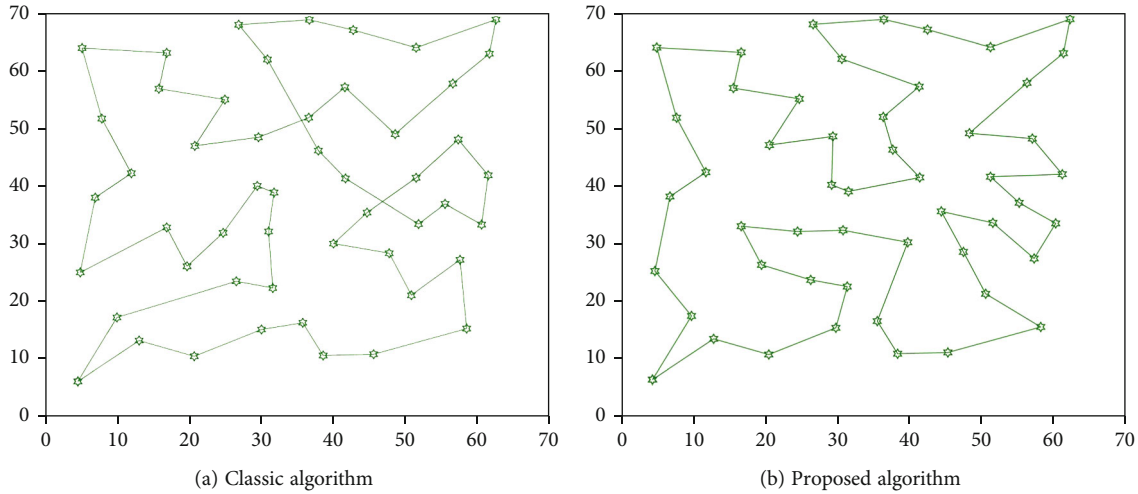


FIGURE 19: Path planning results solved by two algorithms.

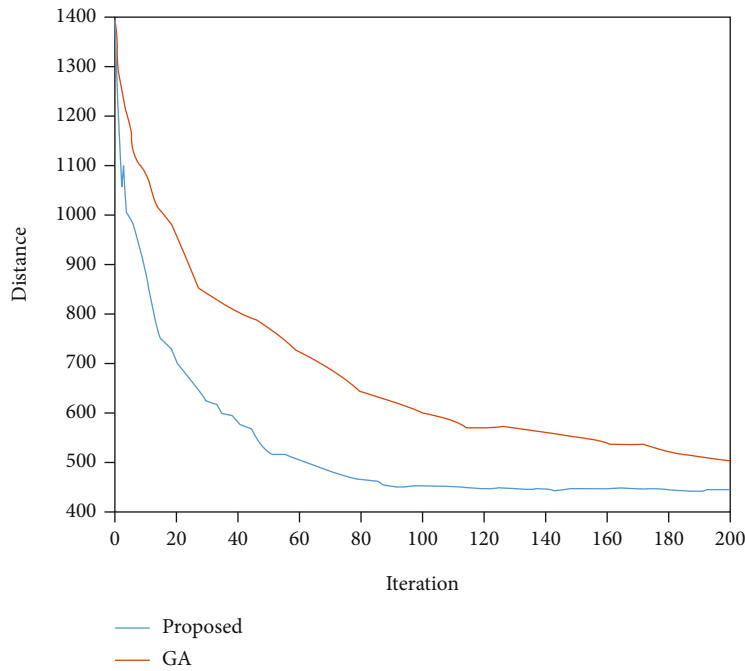


FIGURE 20: Convergence curve of the proposed algorithm and the classical algorithm.

where $f(x)$ is the objective function of the monitoring path cost described by the chromosome. The smaller objective function value would lead to the larger fitness function value and would be closer to the desired optimal solution.

The new solution space could be completed by crossover operations. First, the father generation was randomly selected, and then position 3 and position 7 were set as the intersection point; the father generation chromosome was cut into three segments and named as the first segment, the middle segment, and the tail segment. To determine the optimal chromosome part of the father generation, these three segments were calculated and compared, and finally, the relatively good offspring was acquired. The flow chart

of the entire improved crossover process is shown in Figure 12.

(Step 1) Select p1 and p2 from the father generation randomly, and measure their costs. The cost matrix is shown in Table 1, and the random generation chromosomes are shown in Figure 13.

(Step 2) Select the first segment of p1, 4-3, and use it as the first segment of offspring 1. Compare the middle segments of p1 and p2 to select the

TABLE 2: Calculation results and contrast for two algorithms.

Algorithm	Convergence time (s)	Path cost	Number of iterations
Proposed algorithm	9.2	458	106
Classic algorithm	8.8	512	192

group with the lower cost (for example, in 5-7-6 and 6-1-3, the former that had a lower cost was selected) as the middle section of offspring 1. Select the tail segment from p2 again to fill in the size of the chromosome. Then, create offspring 2 in the same way. Select the first segment of p2 to compare, and select the smaller middle segment of p1 and p2, and finally select the last segment of p1. The offspring changes are shown in Figure 14.

(Step 3) Delete the duplicate nodes in the offspring. As shown in Figure 15, delete node 3 of offspring 1 and node 1 of offspring 2.

(Step 4) Search for the missing node. Insert the missing node 1 in offspring 1, and compare it with the first and last nodes to acquire the one with a smaller cost. For example, the cost of 1-4 was 46, and the cost of 2-1 was 29. Therefore, node 1 was inserted after node 2, and the same steps were applied to offspring 2. The resulting offspring is shown in Figure 16.

The pseudocode of the algorithm is shown in Algorithm 1, where N is the number of individuals in the population, G is the number of iterations, and $F(t)$ is the fitness value.

7. Experimental Results and Analysis

In this chapter, we mainly conducted 4 sets of experiments. First, we conducted computer simulations on the integrated navigation algorithm and path planning algorithm proposed above; second, we controlled the communication distance and conducted experiments on the LoRa communication quality; third, we used unmanned surface vessels for actual surface operations. And we compared and analyzed the actual path and the expected path; fourth, we collected a set of water quality data at the target point in the actual operation and made an analysis of the experimental results.

7.1. Computational Simulations. The computing environment of algorithms is in Win10 Matlab2018b RAM16GB Core (TM) i5CPU.

7.1.1. Simulation of Integrated Navigation Algorithm. Based on the mathematical model of the combined INS/GPS sys-

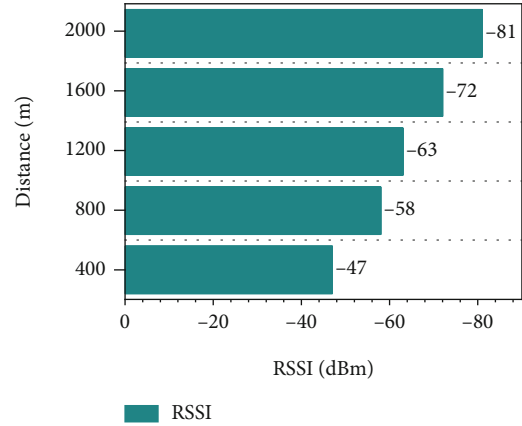


FIGURE 21: The relationship between transmission distance and RSSI.

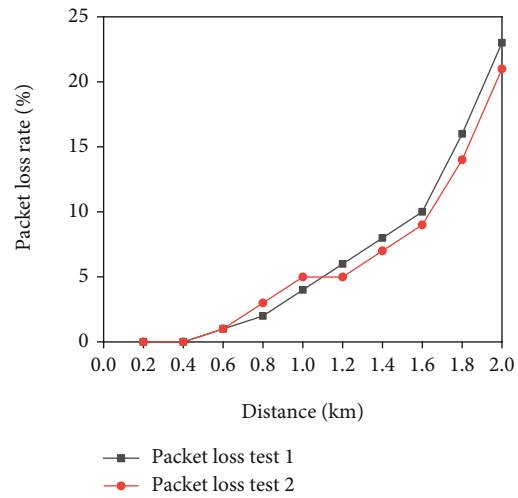


FIGURE 22: The relationship between transmission distance and packet loss probability.

tem designed above, a simulation study was carried out to illustrate the simulation results with actual data. Assume that the first order Markov drift of gyroscope is $30^\circ/\text{h}$, the first order Markov zero bias of accelerometer is 0.5 mg , the root mean square value of GPS position white noise is 10 m , the root mean square value of GPS velocity white noise is 0.2 m/s , the root mean square value of random drift of gyroscope is $30^\circ/\text{h}$, the root mean square value of random zero bias of accelerometer is 0.5 mg , and the simulation time is 500 s . water motion, so the height channel is not simulated in the build simulation. The results are as follows:

The results are shown in Figures 17 and 18, in the presence of noise and zero drift, the GPS correction of the inertial guidance through the Kalman filter is obvious, and the velocity and position can be stabilised within $\pm 1 \text{ m/s}$ and $\pm 20 \text{ m}$ and remain stable. The feasibility of the optimised combination has been verified and can guide the programming design accordingly. Therefore, the simplified GPS/INS combination can be used by unmanned ships.

TABLE 3: Table for water quality data of target points.

Node	Coordinate	Temperature (°C)	pH	Turbidity (FTU)	Conductivity (s/m)
1	118.8861°E, 31.9237°N	7.123	7.92	187.12	82.50
2	118.8861°E, 31.9232°N	7.094	7.93	187.09	82.60
3	118.8868°E, 31.9234°N	7.013	8.04	185.33	82.30
4	118.8869°E, 31.9230°N	7.051	7.95	185.67	82.40
5	118.8875°E, 31.9235°N	7.070	7.98	186.88	82.40
6	118.8868°E, 31.9242°N	7.106	8.02	186.72	82.50

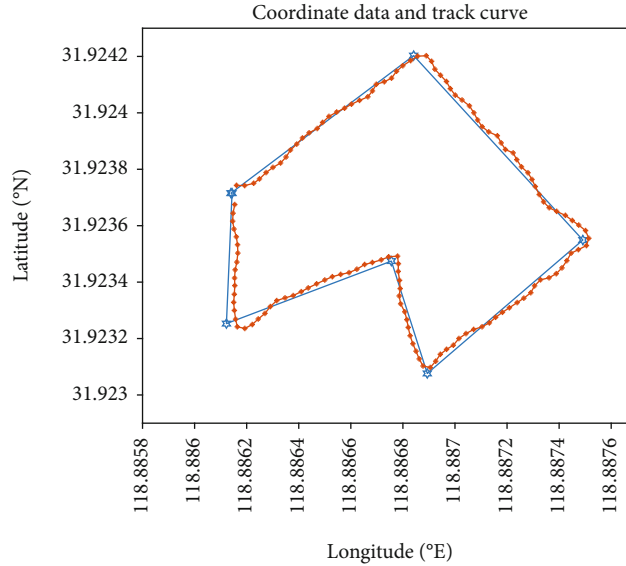


FIGURE 23: Coordinate data and trajectory curve.

7.1.2. Simulation of Path Planning Algorithm. In order to theoretically verify the effectiveness of the proposed algorithm for the TSP model of water quality monitoring operations, we choose the classical genetic algorithm to compare with the proposed algorithm [16]. The USV passes 50 points in the 70×70 simulated water area, and then the USV returns to the initial point to form a closed loop. The parameters of the algorithm are set as follows.

- (i) Classic algorithm: $M = 30$, $T_m = 200$, Crossover = 0.8, Mutation = 0.8
- (ii) Proposed algorithm: $M = 30$, $T_m = 200$, Crossover = 0.8, Mutation = 0.8

In the above, M is the population size, T_m is the number of iteration terminations, Crossover is the crossover probability, and Mutation is the mutation probability.

As shown in Figures 19 and 20, the global path planning results and convergence curves corresponding to the two algorithms can be obtained. It is observed that the proposed algorithm quickly converges to the global minimum fitness value in Figure 20. The path calculated by the proposed algorithm is a closed loop, and there is no cross path. Fewer crossing points mean stronger traversal and less travel waste. Figure 20 and Table 2 show that the shortest path distance

obtained by the proposed algorithm is 458, the calculation time of the proposed algorithm is 9.2 s, and the number of iterations is 106. Although the calculation time of the classical genetic algorithm is similar, it does not reach the minimum number of iterations and distance. In short, the proposed algorithm is acceptable in terms of computing time and has better computing performance than the classic algorithm.

7.2. Communication Quality Experiment. The data transmission quality of the USV and the gateway was changed at an interval of 400 m to test the pack loss probability of the LoRa communication link deteriorates with the distance increasing [17]. Therefore, the RSSI and packet loss probability were tested at different distances in this paper. The data size of each packet was 9 bytes and checked based on CRC, the test distance was 0-2 km, the transmitting power of the radio frequency module was 20 dBm, and the antenna gain was 3 dBi. 1000 data packets were sent and received for each test distance, and the test was performed twice. The experiment results are shown in Figures 21 and 22.

From Figures 21 and 22, it can be seen that the RSSI of the shipboard LoRa node is greater than -81 dBm within 2 km, and the signal reception strength is reliable and stable. From the packet loss rate, there is no packet loss within



FIGURE 24: Environment of the field test.

400 m, and the packet loss rate does not exceed 10% within 1600 m, and the packet loss rate is effectively controlled within 25% within 1600-2000 m.

Through the above experimental analysis, it can be concluded that the water quality monitoring unmanned boat designed in this paper, based on LoRa network, can achieve a long distance and reliable data transmission link within 2 km, fully enhancing the monitoring range and reliability of the unmanned boat water quality monitoring operation.

7.3. Surface Operation Experiment. In order to verify the reliability of the unmanned surface vessel in actual operation, we set six target monitoring points (these point coordinates are shown in Table 3) in advance in Tianyin Lake of Nanjing Institute of Technology. The user monitoring platform calculates the optimal traversal sequence through the proposed path planning algorithm and sends it to the unmanned surface vessel. After the unmanned surface vessel receives the coordinate set, it traverses one by one and returns to the current coordinate regularly. By fitting the coordinate points, the trajectory diagram of the USV was obtained, as shown in Figure 23.

USV adopts an integrated navigation algorithm based on the Kalman filter and PID heading control algorithm to achieve access to all target detection points. When turning from the current coordinate to the next coordinate, the USV's motion trajectory will show a small deviation, but it can be adjusted to the correct route in time. In short, the unmanned surface vessel designed in this paper can complete the water quality monitoring operation according to the preset path.

7.4. Water Quality Monitoring Results and Analysis. In January 2021, a field test was performed in a local lake. The field test environment is shown in Figure 24.

The USV was set to return its GPS coordinates at an interval of 1 s and collect water quality information when it arrived at the monitoring point. The water quality data collected at each monitoring point is shown in Table 3.

The experimental site is located in the nature reserve inside the school, and monitoring points 3 and 4 are located in the center of the lake. According to the water quality monitoring results in Table 3, it can be seen that the turbidity of monitoring points 3 and 4 is lower compared to other monitoring points, and it can be seen that the water in the middle of the lake is clearer, and the water quality of other monitoring points, although slightly worse, is in the normal water quality range, and it can be concluded that the overall water quality of the lake is relatively good.

8. Conclusion

To cover the deficiencies of the existing water quality monitoring system, a mobile water quality monitoring system has been designed based on LoRa communication and USV in this paper. The USV in this system is equipped with LoRa nodes and water quality sensors, and the data is transmitted through the LoRa gateway on the shore, by which the real-time monitoring in large areas are realized. Moreover, an improved genetic algorithm is introduced to plan the working path. The test results have proved that the mobile water quality monitoring system designed in this paper can complete the autonomous cruise work in large areas and can monitor the water quality at the target point in real time. Compared with the traditional water quality monitoring mode, the mobile water quality monitoring system proposed in this paper can save costs and labor, enhance working efficiency, and expand the monitoring scope to a great extent.

In the future, we plan to equip the unmanned surface vessel with solar charging panels to improve endurance. And a more complete information-based monitoring platform will be designed around it.

Data Availability

The data included in this paper are available without any restriction.

Conflicts of Interest

The authors declare that there is no conflict of interest regarding the publication of this paper.

Acknowledgments

This work was supported by the Postgraduate Research & Practice Innovation Program of Jiangsu Province (No. SJCX20_0698) and School-level Scientific Research Fund of Nanjing Institute of Technology (QKJ201808).

References

- [1] Y. Y. Fu, "Analysis on marine pollution and marine fishery resources protection," *Technology Wind*, vol. 33, no. 4, p. 133, 2020.
- [2] T. H. Yang et al., "Development of unmanned surface vehicle for water quality monitoring and measurement," in *2018 IEEE International Conference on Applied System Invention (ICASI)*, pp. 566–569, Chiba, Japan, April 2018.
- [3] R. Yue and T. Ying, "A novel water quality monitoring system based on solar power supply & wireless sensor network," *Procedia Environmental Sciences*, vol. 12, no. A, pp. 265–272, 2012.
- [4] H. Nam, S. An, C. Kim, S. Park, Y. Kim, and S. Lim, "Remote monitoring system based on ocean sensor networks for offshore aquaculture," in *2014 Oceans - St. John's*, pp. 1–7, St. John's, NL, Canada, September 2014.
- [5] W. Schmidt, D. Raymond, D. Parish et al., "Design and operation of a low-cost and compact autonomous buoy system for use in coastal aquaculture and water quality monitoring," *Aquacultural Engineering*, vol. 80, pp. 28–36, 2018.
- [6] H. Cao, Z. Guo, Y. Gu, and J. Zhou, "Design and implementation of unmanned surface vehicle for water quality monitoring," in *2018 IEEE 3rd Advanced Information Technology, Electronic and Automation Control Conference (IAEAC)*, pp. 1574–1577, Chongqing, China, October 2018.
- [7] S. Siyang and T. Kerdcharoen, "Development of unmanned surface vehicle for smart water quality inspector," in *2016 13th International Conference on Electrical Engineering/Electronics, Computer, Telecommunications and Information Technology (ECTI-CON)*, pp. 1–5, Chiang Mai, Thailand, June 2016.
- [8] M. Bălănescu, G. Suci, A. Badicu et al., "Study on unmanned surface vehicles used for environmental monitoring in fragile ecosystems," in *2020 IEEE 26th International Symposium for Design and Technology in Electronic Packaging (SIITME)*, pp. 94–97, Pitesti, Romania, October 2020.
- [9] A. Lavric and V. Popa, "Internet of Things and LoRa™ low-power wide-area networks: a survey," in *2017 International Symposium on Signals, Circuits and Systems (ISSCS)*, pp. 1–5, Iasi, Romania, 2017.
- [10] Y. Wang, J. Cui, B. Zhao, W. Zhao, and K. Liu, "Observation and communication platform design of USV for marine environmental parameters," in *Global Oceans 2020: Singapore – U.S.*, pp. 1–5, Gulf Coast, Biloxi, MS, USA, 2020.
- [11] S. L. Yang and D. M. Yang, "Performance advantages of small waterplane area catamaran and its application overview," *Marine Technology*, vol. 3, pp. 1–4, 2000.
- [12] Z. Sun, S. Pan, and L. Yang, "Remote monitoring system for multiple mobile robot based on OneNet cloud platform," in *2018 Chinese automation congress (CAC)*, pp. 3977–3980, Xi'an, China, 2018.
- [13] J. W. Wang, G. M. Dai, B. Q. Xie, and Q. Y. Zhang, "Overview of algorithms for solving TSP problems," *Computer Engineering and Science*, vol. 36, no. 2, pp. 72–74+155, 2008.
- [14] J. Stender, "Introduction to genetic algorithms," in *IEE Colloquium on Applications of Genetic Algorithms*, pp. 1/1–1/4, London, UK, 1994.
- [15] Y. P. Shen, X. J. Zhang, P. Wu, and C. Z. Wang, "Solving traveling salesman problems based on genetic algorithm," *Computer CD Software and Applications*, vol. 5, no. 10, pp. 21–22+115, 2012.
- [16] D. N. Mudaliar and N. K. Modi, "Design and application of m-mutation operator in genetic algorithm to solve traveling salesman problem," in *2019 International Conference on Computation of Power, Energy, Information and Communication (ICCPEIC)*, pp. 094–096, Melmaruvathur, India, March 2019.
- [17] Z. Y. Wang, Z. H. Yu, Q. Q. Wang, and Z. H. Liang, "Study on the coverage and propagation loss of LoRa technology in urban environments," *Telecommunications Information*, vol. 58, no. 6, pp. 26–31, 2021.

Research Article

Applying Deep Learning Technologies to Evaluate the Patent Quality with the Collaborative Training

Xindong You ¹, Jiaqi Liu,¹ Zhe Wang,¹ Zhaonan Liu,¹ Xueqiang Lv ¹,
and Jung Yoon Kim ²

¹Beijing Key Laboratory of Internet Culture Digital Dissemination, Beijing Information Science and Technology University, Beijing, China

²Department of Game Media, College of Future Industry, Gachon University, Seongnam-si, 13120, Gyeonggi-do, Republic of Korea

Correspondence should be addressed to Xueqiang Lv; icddtxy@163.com and Jung Yoon Kim; kjyoon@gachon.ac.kr

Received 13 May 2021; Revised 20 August 2021; Accepted 14 September 2021; Published 21 October 2021

Academic Editor: Yu Yinyu

Copyright © 2021 Xindong You et al. This is an open access article distributed under the Creative Commons Attribution License, which permits unrestricted use, distribution, and reproduction in any medium, provided the original work is properly cited.

As the country vigorously promotes the development of science and technology and tries to enhance independent innovation capabilities, more and more attention is paid on the protection of technology ownership. In recent years, China has developed rapidly in many scientific and technological fields, and the number of patent applications increased year by year. However, various patent quality problems including immature patent technology and low patent authorization rate appear. The indicators of patent quantification and quality evaluation are studied in this paper. First, we quantify the patent quality evaluation indicators and combine the content of the patent text to build a patent evaluation model. US patents with patent grade labels are used for training with multitask learning technology. Second, the evaluation model is transferred from the English patents to the Chinese patents, in which the active learning technology and transfer learning technology are used to minimize the work of manual labeling. Finally, a Chinese patent quality evaluation model based on collaborative training was designed and implemented. Methods used in this experiment have notably improved the prediction effect of the model and achieved a better migration effect. A large number of experimental results show that the Chinese patent quality evaluation model has achieved good evaluation results. This research uses deep learning and natural language processing technology to carry out research on patent quality evaluation models from different perspectives, to provide patent decision support for related companies, and to point out research directions for research institutions and patent inventors.

1. Introduction

Since the 18th CPC National Congress, the cause of intellectual property has entered a new era of vigorous development driven by policies. Patent applications are trending year by year. As of 2020, the State Intellectual Property Office has authorized a total of 530,291 disclosed invention patents, an increase of 18% over 2019. According to data published by the State Intellectual Property, in 2020, 683,000 invention patent applications were discovered; a total of 217,000 invention patents were authorized. In order to implement the guiding ideology and effectively promote my country's transformation from a country of intellectual property rights to a country of cre-

ativity, from the pursuit of quantity to the improvement of quality, recently, the National Intellectual Property "Notice on Further Strictly Regulating Judges' Applicants for Understanding" (Guo) Fabaozi 2021 No. 1 during the project verbally promoted the improvement of patent quality, strengthened quality orientation, and strengthened the standardization and supervision of patent transactions. How to quickly, automatically, fairly, press, openly, and scientifically evaluate the quality and value of patents will become a problem that needs to be resolved.

Patent and other intellectual property intangible assets have become an important force in national development, with the development of intellectual property-related technologies at home and abroad and the improvement of their

status in the economic field. In recent years, the patent pledge financing project has gradually taken shape, which has provided a great boost to the growth of small and medium-sized enterprises. In 2020, the total amount of national patent and trademark pledge financing reached 218 billion yuan, an increase of 43.9% year on year. This fully demonstrates that there is a huge demand for patent value evaluation in China and the world, and it is increasingly not negligible in the fields of science and society. While strengthening innovation, my country should also promote the transformation of scientific and technological achievements. Therefore, in recent years, with the country's high requirements on the speed and efficiency of the transformation of the results of authorized national invention patents, how to objectively and automatically evaluate the value of massive Chinese patents has become a hot research topic and a scientific problem that needs to be solved urgently.

Many scholars have been exploring the construction of models based on quantitative indicators and automatic quality assessment. However, there are still the following shortcomings in the evaluation of Chinese patent quality:

- (1) The Chinese patent quality evaluation index system is not sound enough and difficult to quantify: in current research, on the one hand, most of the evaluation indexes of patent quality are still at the theoretical stage, which is far from practical applications; on the other hand, the system is not sound more index dimensions should be considered. Important factors affecting patent quality: the content of the patent text itself, the knowledge information mined in the patent text, and the domain knowledge information mined are not included in the existing patent quality evaluation indicator system
- (2) The difficulty of quantification of the Chinese patent quality evaluation index system and the lack of data make it impossible to implement automatic evaluation: there is no relevant research on the automatic evaluation model of Chinese patent quality in China. On the one hand, due to the aforementioned reasons, most of the Chinese patent quality evaluation indexes are still stuck at the theoretical level; it cannot be quantified, and thus cannot support the automatic evaluation of Chinese patents. On the other hand, due to the lack of data on Chinese patent quality levels, it is impossible to construct a data-driven automatic model of Chinese patent quality

In order to make the most of effective role of patent quality assessment and identify high-quality patents, it is urgent to adopt certain technical means to make this process easier. Faced with the three common problems in the field of patent quality evaluation, this article mainly uses data mining and natural language processing technology to extract indicators from a large number of patent information data of different dimensions and uses deep learning methods to predict patent quality. In addition, multitask learning

method is used to improve the accuracy of patent quality evaluation and prediction. The constructed patent quality evaluation model (PQE-MT) can automatically evaluate the quality of patents with a high accuracy rate (83.9%), saving a lot of valuable manpower and material resources. Regarding the lack of data labeling of Chinese patents, a large number of US patents with patent quality grade are used to construct basic training data. Therefore, a Chinese patent evaluation method based on transfer learning and active learning method is proposed in this paper. Then, the model is divided into two feature spaces, Chinese and English, and a network model is trained on these two features, respectively, to form collaborative training. The results of the evaluation show that the article method achieved a good migratory effect, with micro-F1 reaching 74%.

2. Related Work

2.1. Related Work of Patent Quality Index Quantification. In recent years, scholars have begun to summarize existing indicators from different dimensions and propose a more comprehensive evaluation system. Li et al. (2007) [1] summarized the technology cycle, technical scope, scientific relevance, and claims item number as for the professional indicators. On the other hand, the number of patent applications, patents home race number amount, and patents survival time is summarized as a comprehensive index and litigation. Through the above indicators, comparisons are made in terms of time, difficulty, and cost. Jin et al. (2011) [2] constructed a patent attribute network to optimize the prediction effect of algorithms from the aspects of patent content standardization, innovation, technology relevance, market value, patent inventors, and patentees. Han and Sohn (2015) [3] predicted the remaining effective time of the patent by constructing the similarity feature between the patent abstract and the claims and combining it with 14 other quantitative indicators. The article began to combine the text features of patents with patent attributes to make predictions. Yang et al. (2016) [4] broaden the patent quality impact indicator choice from the patent field correlation and life cycle stages. Leng and Zhai (2017) [5] constructed patent quality evaluation indicators, used the analytic hierarchy process to obtain the importance of the indicators to obtain the corresponding weight results, and used the comprehensive fuzzy evaluation algorithm to evaluate the patents in the medical field. In this article, different indicators are weighted to make them more targeted. Li (2018) [6] quantified patent quality evaluation indicators from the three dimensions of technology, law, and economy. The technical dimension mainly uses dependence, novelty, monopoly, and maturity; the economic dimension uses patent revenue and market evaluation, patent survival time, and other indicators; the legal dimension refers to factors such as patent legal status and litigation conditions. Finally, a comprehensive evaluation of the patent value is carried out in three dimensions. The above article explained and elaborated the patent quality impact indicators at the theoretical level, taking into account indicators of different dimensions and different levels, but some indicators are poor in

availability and difficult to express using algorithms. Meng (2018) [7] conducted a comparative analysis of patent data, combined with traditional patent quality evaluation methods, and quantified patent evaluation indicators in hierarchical levels, set up technical, economic, and legal levels, and further subdivided them into 14 different levels. At two levels, the weights of indicators at different levels are calculated through rough sets, and the final evaluation is performed through cloud models. The article summarizes the advantages and disadvantages of different indicator systems and summarizes the indicators, but the data discretization process and cloud model limit the generalization ability of the method. In general, the abovementioned scholars have put forward numerous patent quality evaluation indicators at the theoretical and application levels, and the topic optimizes and summarizes related indicators and further includes multiple dimensions from time, quantity, technology, law, inventor and agent, and text content. Quantify indicators, compare, and select key indicators as input to the patent quality evaluation model.

2.2. Related Work on Patent Quality Assessing. In terms of patent quality evaluation models, scholars gradually began to apply neural networks to patent quality evaluation. Chen and Chang (2009) [8] extracted indicators from medical patents in the United States, trained deep learning network models, and predicted the market value of patents. Trappey et al. (2011) [9] used the principal component analysis algorithm to obtain the impact factors of different indicators and used them as the input parameters of the backpropagation neural network model to judge the patent quality. As a preliminary screening scheme, the proposed patent quality evaluation method can automatically and effectively evaluate the quality of patents and save the time spent by domain experts on research and development of high-value patents. Wang (2012) [10] and others used indicators such as the actual benefits of patents as input parameters of the algorithm to construct a decision tree for prediction. First, use the analytic hierarchy process to get the value of the patent, then use the decision tree to get the risk of the patent, and combine the two to get the patent status. Zhao et al. (2013) [11] extract numerical indicators such as the number of patent citations and use decision trees, SVM, and deep learning methods to predict patent quality. Articles consider a variety of impact indicators progress in different model experiments; however, due to the use of only numeric attributes, the experimental structure is greatly restricted. Wu et al. (2016) [12] use the self-organizing mapping (SOM) method to cluster the patents to be tested with related patents published in the same field and perform nonlinear space transformation through kernel principal component analysis (KPCA), using SVM established a patent quality classification model, and proposed the somo-kpca-svm model to predict patent quality. The classification method proposed in the article can effectively display the analysis results, but the correctness of the results lacks the reference to the actual categories. Qiu et al. (2017) [13] use CART to extract evaluation indicators, optimize input parameter items, reduce model scale, and improve fitting effect. This method pro-

vides practical methods and theoretical support for the selection of patent indicators. The article uses classification regression trees to solve the patent evaluation problem, but the indicators used in the article are all basic patent attributes, and many influencing factors have not been fully considered. The above three articles did not take into account the textual content of the patent, so that the prediction model lacks vital influencing factors. Lin (2018) [14] applied neural networks to the quality evaluation research of patents and proposed the DLPQE model. The model is composed of two-part vector of the attribute representation structure ANE composed of the patent citation network and the text sequence feature represented by the convolutional neural network connected with the attention mechanism. The article proposes for the first time that the deep learning method is used for patent document analysis, taking into account different indicators and text content, but due to lack of the deep quantification of patent indicators, the convolutional neural network will lose the time series characteristics of the text. The subject combines quantitative indicators with text content and applies multitask learning to the patent quality evaluation model for the first time.

2.3. Related Work on Transfer Learning and Active Learning. Since data labeling is very time-consuming and labour-intensive, high-quality labeling data is scarce. The learning of transfer attracted increasing attention from the academy. Banea et al. (2008) [15] proposed a method of learning to transfer to a foreign language because of the numerous English entry data in this document, and a corpus of English data is used to generate the source domain data set of the target language through automatic translation, which demonstrates the feasibility of using automatic translation for learning to transfer through languages. Pan and Yang (2009) [16] propose transferring domains with sufficient training data to domains with similar data distribution and avoiding costly data annotation tasks via knowledge migration to greatly improve the learning effect and discuss transfer learning and domain adaptation, sample selection, the relationship between deviation, and other related machine learning technologies. Xu and Yang (2011) [17] use transfer learning and multitask learning to extract and transfer useful knowledge from auxiliary domain data. Weiss et al. (2016) [18] introduced the latest developments in the field of biological information and explained the information on learning and transfer solutions and discussed possible future research work. Transfer learning solution has nothing to do with the size of the data. Yosinski et al. (2017) [19] conducted research on the transferability of deep neural networks. Perform finetune experiments layer by layer in different layers to explore network transferability. Note that adding an end-to-end to the deep migration network will improve the effectiveness and overcome better data differences. Migration of the number of layers of the network can speed up learning and network optimization, general characteristics of the low-level network learning, and the high-level network learning field feature.

In order to make the model conform to the data distribution characteristics of the target area, a small number of

materials still need to be marked. Active learning can predict the results and select samples according to the model, and it is most helpful to improve the model. Thompson et al. (1999) [20] use active learning to try to select the most useful example as training data for transfer learning. Experimental results show that skilled learning can significantly reduce the number of samples labeled when the algorithm achieves the same effect. Tong and Koller (2001) [21] use pool-based active learning. The algorithm does not need a randomly selected training group and can request samples for marking. The new algorithm of support vector machine is used for active learning, which provides a theoretical basis for the concept usage algorithm of space version. Experimental results show that the use of the active learning method in the article can significantly reduce the need for labeled samples. Active learning, literature reviews, and less labelled training examples were introduced by Settles (2009) [22]. Discuss the query plan and analyze the experience and theoretical evidence of active learning. Li et al. (2016) [23] propose an active multigrade multilabel learning based on the minimum SVM classification range to take the minimum SVM classification distance as the confidence of the selected example, effectively reduce the number of sample annotations, and improve classification performance. Zhou et al. (2017) [24] propose the impact of active and transfer learning, data expansion, fault selection, continuous information extraction, and other methods on remote data and diagnosis. According to Zhu and Bento (2017) [25], GAN is used for active learning, and an object-oriented learning model GAN and a learning algorithm for motion value samples are given. Konyushkova (2017) [26] tried to transform active learning into a regression problem and dealt with the overfitting of previous query schemes. The experimental results show that the order reduction of data points is feasible in multivariable finite element analysis.

2.4. Related Work on Collaborative Training. After the transfer learning and active learning are used to promote the model to adapt to the feature distribution of the new data set, since the patent data has two views in Chinese and English, the experiment is carried out collaborative training in the remaining unlabeled sample set, making full use of the different learning features of the model on the two views. Features enhance the overall effect of the model. Blum and Mitchell (1998) [27] first tried collaborative training on web content prediction, learning from different views according to the model, using feature differences in different views to predict the labeled samples, and selecting high-confidence data as algorithms in other views training data. Wan (2009) [28], according to the feature difference between Chinese and English bilinguals, combined English data sets with a large number of emotional labels and unlabeled Chinese data, using machine translation technology to translate each other, training models for the two languages separately, and predicting based on the model the probability of each category of the sample is obtained, and the sample with high confidence is obtained as the training data of other models to achieve the purpose of bilingual collaborative training. Guo et al. (2012) [29] first proposed the use of graph-

based confidence estimation semisupervised collaborative training algorithm, which improved the speed of collaborative training in obtaining the data to be labeled to a certain extent. According to the information of the sample itself, the probability of the category of the unlabeled sample is calculated, and the confidence of the unlabeled data is estimated by a multiclassifier, which improves the effect of the collaborative classification algorithm, and proves the effectiveness of the algorithm on the UCI data set. Qiao et al. (2018) [30] use a collaborative training method on the neural network model to divide the sample features into multiple different views and fit the corresponding network parameters in different views. Experiments found that different models learned different characteristics of the data. The characteristics learned by different models are generally complementary. Gong and Lv (2019) [31] jointly use active learning, density peak clustering, and collaborative training to increase the amount of information in the data to be labeled and to a certain extent alleviate the mislabeling of fuzzy samples. Huang and Huang (2019) [32] use collaborative training for machine translation technology to improve the translation effect of the model. The experimental comparison shows that after the use of collaborative training, the results of machine translation are more accurate. When there are fewer labeled samples, there are still better results and translation quality. This topic makes full use of the unique Chinese-English bilingual features of the research and applies collaborative training to the Chinese patent quality evaluation model.

3. Patent Quality Evaluation Model

This paper uses transfer learning and active learning methods based on the PQE-MT model built with English patent data, further proposes a cross-language transfer of patent quality evaluation model based on active learning data expansion, and transfers the original model to Chinese patents. Finally, cooperative training is carried out. We will introduce the model from these three parts.

3.1. Patent Quality Evaluation Model Based on Multitask Learning. We first proposed the PQE-MT_USA model to predict the quality of US patents and selected the best-performing model structure through the comparison of different algorithms to facilitate the migration to Chinese patents in subsequent research. The related technologies involved in this part of the content are as follows, among which Word2vec and Bert are used for vector representation of text content to extract more semantic information; LSTM is used for learning the long-term dependence of the sequence, and Bi-LSTM also considers the information of the article context; CRF can improve the effect of named entity recognition based on the dependence of label results; multitask learning combines named entity recognition tasks with patent quality level prediction tasks to speed up model training and improve model fitting effects; TextCNN is used as comparison experiment of the effect of product neural network and recurrent neural network in this research.

3.1.1. Construction and Quantification of Patent Quality Evaluation Indicators. Due to the lack of systematic and fair evaluation grades and evaluation methods for Chinese patents for a long time, there is no clear quality grade. Grading the quality of patents requires professional knowledge and analysis of a large number of related patents, making it difficult to obtain the labels of Chinese patent data, and there is no reference scale for the evaluation process. Through research, it is found that the US patent has a patent quality grade, and the patent quality grade is recognized by scholars. Therefore, the experiment selected US patents in the field of new energy as the research object.

The experiment analyzes the information contained in the patent and specifically removes redundant information (such as patent application number: a numerical combination of other patent information) and overly complex information (such as patent specification: the text of the detailed description of the patent). Part, the content is tens of thousands of words, most of the content is the detailed introduction of the patent, which contains less effective information, and most of the main information exists in the abstract and claims of the patent and image information (patent drawing: prototype of the patent). As shown in the figure, this experiment mainly conducts research in the direction of natural language processing, focusing on patented text and numerical data. Part of the image information will not be considered for the time being.

The original attribute information obtained after screening is shown in Table 1 based on the attributes of these existing patents, and the experiment will quantify patent quality evaluation indicators in multiple dimensions and directions.

The experiment carried out in-depth processing of the above data items, mainly quantified and combined the following dimensions, including time dimension, quantity dimension, technical dimension, legal dimension, inventor, and agent dimension, and obtained related to patent quality quantitative indicators. And Figure 1 shows the division of some related attributes in different dimensions.

- (1) *Time Dimension.* The experiment will process the various time attributes of the patent and convert it into computable numerical data. In the end, indicators such as the time from patent application to publication, the time from application to approval, the time from publication to approval, the survival time, and the remaining time to termination are obtained
- (2) *Quantity Dimension.* The change in the number of patent applications in a certain field shows the development trend of patents to a large extent. The increase in the number of patent applications means good prospects, and the decline in the number of patent applications indicates that this field is gradually being replaced
- (3) *Technical Dimension.* CPC is the joint patent classification, and IPC is the international patent classification. Both have different partitions for different parts in detail, but the overall structure is similar. Each level is a more detailed classification of the previous level

- (4) *Legal Dimension.* Different legal status indicates the degree of importance the assignee of the patent attaches to the patent, including survival, revocation, withdrawal, reissue, and termination. Since the patent right was granted, the assignee has to pay a certain fee every year to maintain the validity of the patent, and the fee increases year by year. When the patent cannot satisfy the interests of the assignee, the assignee will stop paying the fees, resulting in the cancellation of the patent
- (5) *The Dimensions of Inventor and Assignee.* A good inventor and assignee means a good patent. We get the sum of the number of patents invented by all inventors in the field; the average number of invention patents per inventor in the field, etc. In addition to the same indicators as the inventor, the patent assignee also extracts whether the assignees of previous and future generations have changed, the type of organization, and so on. The assignee involves different organizations, including companies, research institutes, universities, colleges, foundations, and individuals
- (6) *Combined Indicators.* We combine the feature of different dimensions to get combination indexes. Such as the proportion of patent survival, withdrawal and expiration of inventors, the number of patents in different technical fields and different years, and so on. The following is a list of the combination indexes of the assignment. In a specific patent agent and a specific field, Num_Application means the experimental definition: the number of patents applied; Num_Approval means the number of patent approved, Q_2 means the number of IPC and CPC, Q_3 means the size of patent family, and Q_4 means the average patent quotation rate. There are the following quantitative indexes.

$$\text{Research_Focus}_i = \frac{\text{Num_Application}_{\text{filed}}}{\sum_{i=\text{filed}1}^{\text{filed}n} \text{Num_Application}_i}, \quad (1)$$

$$Q_1 = \frac{\text{Num_Approval}}{\text{Num_Application}}, \quad (2)$$

$$\text{Strength} = \text{Num_Apply} * \sum_{i=1}^4 Q_i, \quad (3)$$

$$\text{Technical_Portion}_i = \frac{\text{Strength}_{\text{inventor}}}{\sum_{i=\text{inventor}1}^{\text{inventor}n} \text{Strength}_i}. \quad (4)$$

In addition, the experiment adds long text description type attributes. On the one hand, the experiment takes the publication time of the patent as the node, uses the TF-IDF algorithm to calculate the text similarity of other patents before and after the node, and selects the top 50 with the highest similarity as the result of the similarity before and after the publication of the patent. The smaller

TABLE 1: Filtered patent raw data information.

Attributes	Value
Patent title	Automated electric vehicle charging system and method
Quality grade	6
Legal status	Alive
Country of origin	US
Agent	Interim Design Inc.
Inventor	Haddad; Joseph C.; Elizabethtown; Lysak; Daniel B.; state college
Application date	2016.01.29
Public day	2016.05.26
Approval date	2018.10.23
Expiry date	2032.04.25
IPC	H02J-007/00; B60L-011/18
CPC	B60L11/1835; B60L53/14; B60L53/35; Y04S30/12; Y04S30/14
International patent documentation center	6
Number of families	
Number of ordinary families	5
Cited by other patents	3
Number of cited patents	4
Number of references	0
Cited by other documents	0
Abstract	A system and method for charging an electric vehicle include identifying vehicle information corresponding...
Claims	A system for charging an electric vehicle, comprising: a camera configured to acquire an electronic image of the electric vehicle...

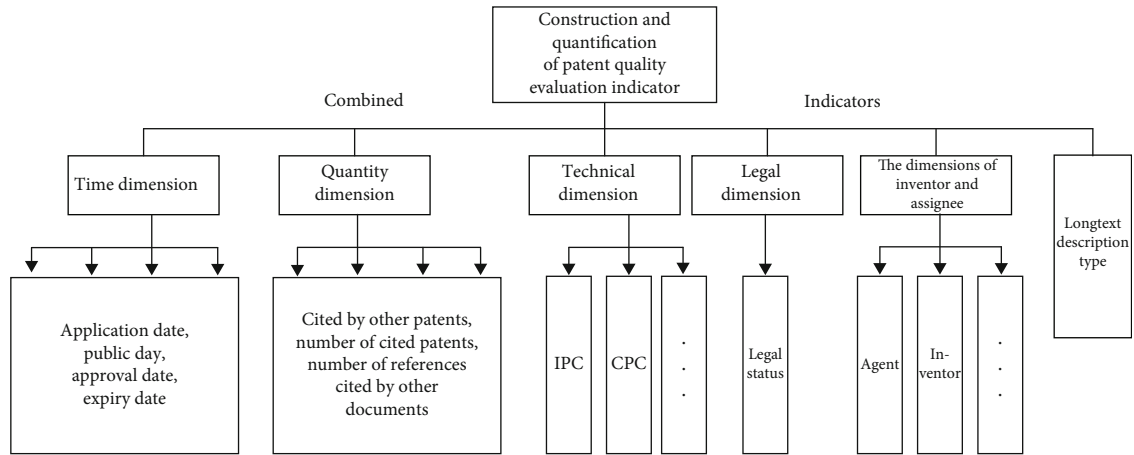


FIGURE 1: Construction and quantification of patent quality evaluation indicator.

the similarity result before the node, the more novel the patent; the greater the similarity result after the publication time node is, it indicates that the patent is groundbreaking and has been used for reference by other related patents, as well as the number of technical elements (field terms) in the main claim and the positive words (can, enable, so as to, etc.). On the other hand, the patent name, patent abstract, and patent claims are input into the sequence model to participate in the final prediction.

The PQE-MT_USA model mainly involves two parts: a quantitative index model and a sequence model. The sequence model uses a multitask learning structure. Next, we will introduce the model from these two parts.

3.1.2. Patent Quality Evaluation Model Based on Quantitative Indicators. The patent quality evaluation model mainly includes input, index quantification, fully connected layer, softmax layer, and output. Its structure is shown in Figure 2.

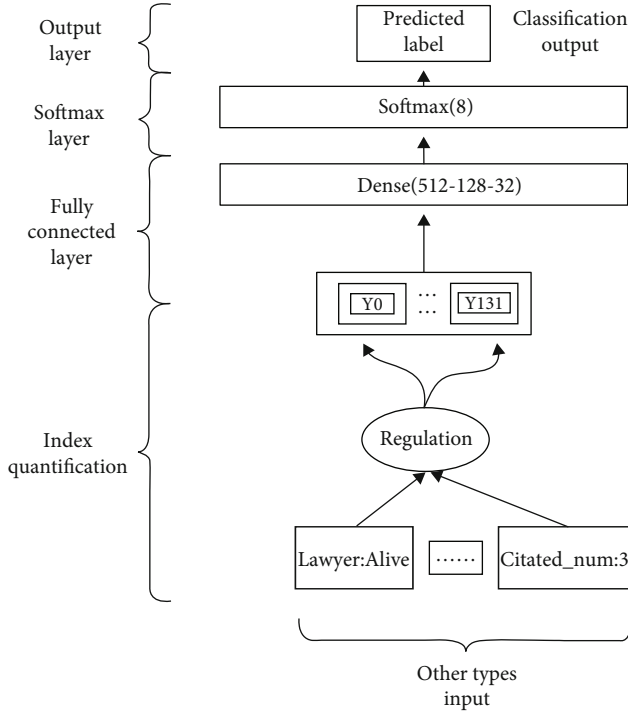


FIGURE 2: Quantitative index model structure.

First, we enter the initial patent attributes, including legal status and number of citations. According to relevant rules, 15 initial indicators and 117 quantitative indicators in different dimensions are constructed, which together constitute 132 indicators. We combine the patent text with 132 indicators into a fully connected layer composed of 512-128-32 nodes. Finally, multiple classifications are performed through the softmax layer to predict the patent quality level. Patent quality levels are divided into eight categories. Take the “Dynamic power supply management system for electric vehicle” patent as an example, its legal status is “Alive,” the number of citations is “4,” and other patent attributes and 132 evaluation indicators are combined to finally get its patent quality grade prediction result. The result is 8.

3.1.3. Multitask Learning Model

(1) *Task 1: Text Classification Model.* This task preprocesses the title, abstract, and claims of the patent and predicts the quality of the patent through the deep learning model described below. The detailed structure of the text classification model is as follows.

The model takes the three parts of patent title, abstract, and claims as input and first performs text processing on it, including splicing the input items, removing stop words, removing special symbols, converting to lowercase, and converting to word roots. The experiment uses Word2vec and Bert as the initial vector representation of words. The processed data is fine-tuned in Bert to obtain the word vector of a specific field as a word embedding. Next, through the Bi-LSTM layer, fusing the attention mechanism, LSTM can

learn long-term dependencies, and after bidirectional splicing, it can effectively use the context information of the text to dig out more hidden features.

The Bi-LSTM in this model is equivalent to inputting the sequence into a forward LSTM and a back-end LSTM, respectively, and the output result is used as the result. The structure of LSTM is shown in Figure 3. Taking the title part of the patent text “Test system for battery management system” as an example, the basic unit of LSTM is used to encode the text. First, input the word vector “Test” and pass through the forget gate, memory gate, and output gate. The calculation generates a new hidden state h_t (test) corresponding to it. The calculation process of the three gates is as follows:

$$f_t = \sigma_g(W_f x_t + U_f h_{t-1} + b_f), \quad (5)$$

$$i_t = \sigma_g(W_i x_t + U_i h_{t-1} + b_i), \quad (6)$$

$$o_t = \sigma_g(W_o x_t + U_o h_{t-1} + b_o), \quad (7)$$

$$c_t = f_t \circ c_{t-1} + i_t \sigma_c(W_c x_t + U_c h_{t-1} + b_c), \quad (8)$$

$$h_t = o_t \circ \sigma_h(c_t). \quad (9)$$

Among them, x_t is the input of LSTM, f_t is the forget gate, it is the input gate, o_t is the output gate, h_t is the hidden gate, c_t is the cell state, W , U , and b are the matrices in training and the network learning calculation element value, and σ is the sigmoid function, which ensures that the output result is between 0-1, which is used to control the proportion of information passing.

The second word vector “system” and the hidden state h_{t-1} (test) output at the previous moment are used as new inputs. After three gate calculations again, the updated hidden state h_t (system), h_t (system) is obtained. Contains information about the characters entered in the preceding text. Repeat the above coding process until the end of the patent text.

When the input sequence is very long, it is difficult for the model to learn a reasonable vector representation. The attention mechanism [33] retains the intermediate results of the LSTM encoder on the input sequence, selectively learns the input and associates it with the output sequence, so that the model focuses on the words that are considered more important in the input sequence. Then, through a fully connected layer network composed of 512, 128, and 32 nodes, the softmax layer is used for multiclassification to predict and output the patent quality level. The specific structure is shown in Figure 4.

(2) *Task 2 (NER Task): Sequence Labeling Model.* This task is used to identify the terms in the patent text. The first few layers of the model are the same as task 1. Here, we focus on the CRF layer and the output layer.

In the NER task, the decoding layer usually uses the conditional random field (CRF) model to perform label

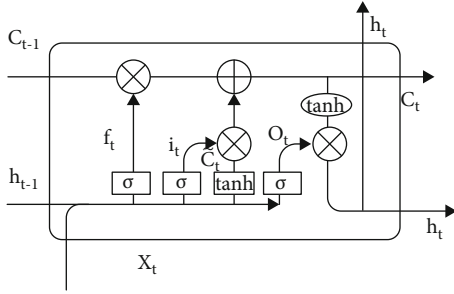


FIGURE 3: LSTM structure diagram.

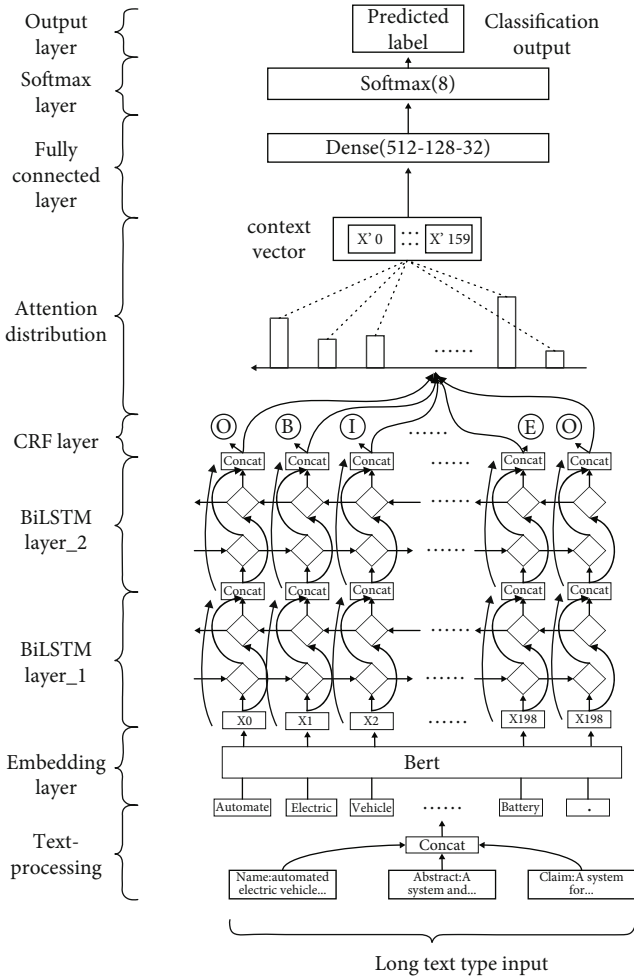


FIGURE 4: Text classification model.

inference on the entire character sequence in turn. The decoding process is as follows.

For an input sequence, the input vector is obtained after embedding to the LSTM, and the score on the label corresponding to each word is obtained after the linear layer is applied. According to the label transition matrix T , we can get the score of the label at the previous moment as y_i and the label at the next moment as y_{i+1} , namely, $T[y_i, y_{i+1}]$. For a sequence x , if the length of the sequence x is n and there are m possible labels, then there are a total of m^n possible labeling results. We can use the LSTM + CRF model to

calculate the score (y) of each possible annotation result, and then use softmax to normalize to find the probability of a certain annotation result, and choose the one with the largest probability as the annotation result. The specific calculation process is as follows:

$$\phi_t(y', y | x) = \exp(w_{y', y}^T h_t + b_{y', y}), \quad (10)$$

$$p(y | x; \theta) = \frac{\prod_{t=1}^n \phi_t(y_{t-1}, y_t | x)}{\sum_{y' \in Y_{(x)}} \prod_{t=1}^n \phi_t(y'_{t-1}, y'_t | x)}. \quad (11)$$

Among them, $w_{(y', y)}$ and $b_{(y', y)}$ are the training parameters of the label pair (y', y) , h_t represents the output of the coding layer at time t , θ represents the model parameters, $Y_{(x)}$ represents all possible tag sequences corresponding to the character sequence x . In the tag reasoning process, CRF needs to find the tag sequence y^* that maximizes the conditional probability given the input sequence x :

$$y^* = \operatorname{argmax}_{y \in Y_{(x)}} p(y | x; \theta). \quad (12)$$

The search problem of the tag sequence y^* can be solved efficiently using the Viterbi algorithm.

The experiment defines the label space as $\{B, I, E, O\}$. “B” indicates that the element is the beginning of a domain term, “I” indicates that the element is the middle part of a domain term, “E” indicates that the element is the end of a domain term, and “O” indicates that this element does not belong to the domain term part. The CRF layer can determine the domain terms in the sequence data according to the label sequence output by the model. In the final output, each element is marked as a label in $\{B, I, E, O\}$. Take the patent text of “Test system for battery management system” as an example, the sequence length is 6, there are four possible tags for BIEO, and a total of 6^4 possible tagging results, including $y = (OOBIE)$, $y = (BEOOBI)$, \dots , after the calculation (OOBIE) marked the highest score, that is to identify “battery management system” as a patent term. The specific structure of the model is shown in Figure 5.

The experiment considers that the two tasks overlap greatly, and the domain terms in the text sequence are the part that has a greater impact on the patent level. The sequence labeling task backpropagates to update the parameters, which is conducive to the model to obtain a better sequence representation and pay more attention to the learning of domain terms. The two tasks together form a multitask learning structure, which promotes each other and simplifies the overall task complexity and prediction time. Take the patent text of “Automated electric vehicle” as an example, its specific structure is shown in Figure 6.

This figure combines the previous two models. The left side is the sequence model part of multitask learning, and the right side is the quantitative index model part. The PQE_MT_USA model is obtained after the two parts of vectors are spliced to predict the final result and used for subsequent migration training of Chinese patents.

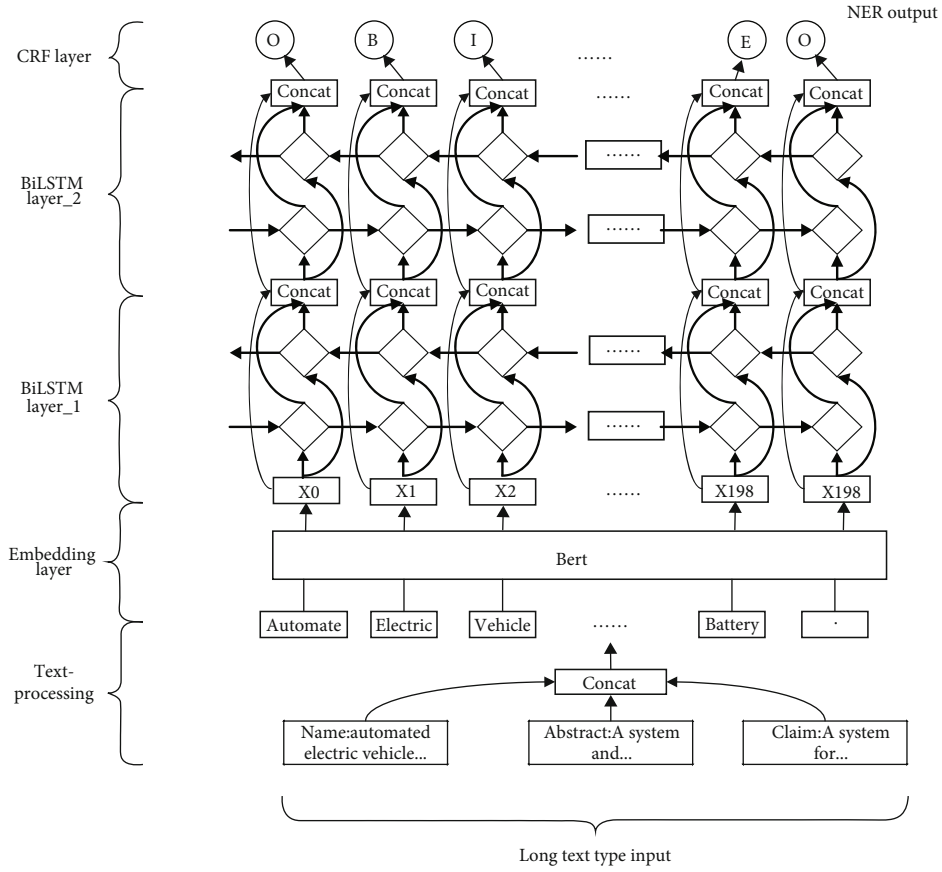


FIGURE 5: Sequence labeling model.

3.2. Patent Quality Evaluation Model Based on Transfer Learning. If the model PQE_MT_USA trained by the US patent is directly applied to the Chinese patent, the predicted patent rating result will have a large error. The reason is that if you use traditional machine learning methods, you need the data to obey the same distribution and sufficient labeled data. On the issue of labeling data, the process of labeling data consumes a lot of manpower and time costs; on the issue of data distribution, on the one hand, there are cultural differences in the writing process of Chinese and English patents. On the other hand, there are differences in the distribution of various attributes and quantitative indicators of Chinese and US patents. By comparing Chinese and American patent data, it is found that the inventors, attorneys, IPC classification numbers, and CPC classification numbers of Chinese and American patents have the same expression. Although the inventors and agents of the Chinese and American patents belong to two different sets, the experiment quantifies the indicators based on the overall situation in the field, and the training model will not be affected by the specific values. The differences in patents between the two countries are mainly reflected in the following four aspects: (1) the legal status of patents is different; (2) there are differences in the distribution of patents between the two countries in the following 6 attributes: number of cited patents, number of citations by other patents, number of common families, number of citations by other documents, number of references, and international patent docu-

mentation center; (3) the patent origination level is different; and (4) the content of the text type is different, including the title, abstract, and claims of the patent. The writing language of the US patent is English, and the Chinese is Chinese. In terms of related indicators, US patents are generally higher than Chinese patents.

Because the US patent has the patent strength label required for experimentation, the Chinese patent has the contradiction between a large amount of data and a small amount of labeling. At the same time, the impact of various attributes and indicators on patent strength has the same trend, with only the difference in feature distribution. Transfer learning breaks the same distribution assumption of traditional machine learning and can adapt to the requirements of experiments well.

Transfer learning mainly involves domains and tasks. Given a labeled source domain, that is, an English patent text with a large number of labeled data sets: $D_s = \{x_i, y_i\}_{i=1}^n$, and an unmarked target domain, that is, the Chinese patent text without data annotation: $D_t = \{x_j\}_{j=n+1}^{n+m}$. The data distribution of these two fields $P(x_s)$ and $P(x_t)$ are different, $P(x_s) \neq P(x_t)$ [34]. The purpose of transfer learning is to use the knowledge of D_s to learn the knowledge (label) of the target domain D_t . That is to say, the process of transfer learning is to transfer knowledge from the source domain to the target domain, complete the model update, and predict the target domain label. Transfer learning can be divided into different

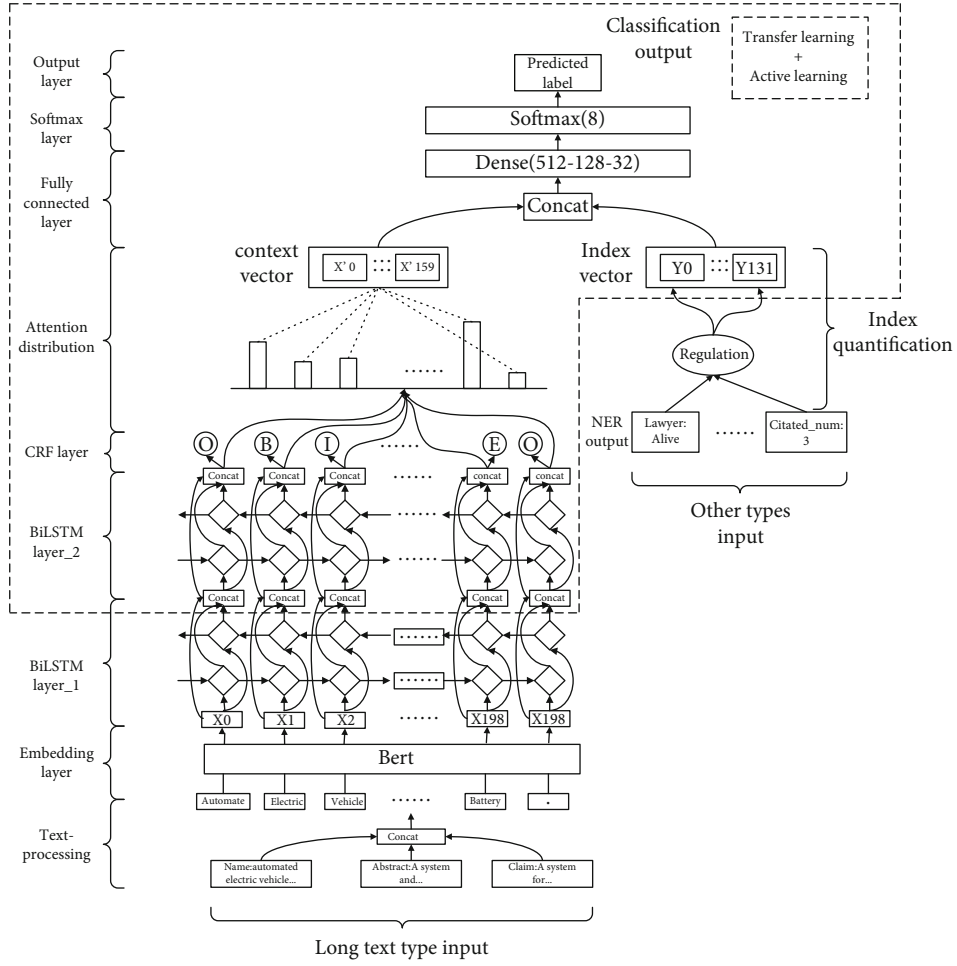


FIGURE 6: PQE_MT_USA model structure.

types, and there are many classification methods. This article mainly uses the model-based transfer learning method, that is, based on the self-adaptation of model parameters to find new parameters θ , and the transfer of parameters makes the model better at the target work on the domain to minimize its loss. The calculation formula is as follows:

$$\min \frac{1}{n} \sum_{i=1}^n L(x_i^s, y_i^s, \theta). \quad (13)$$

The experiment uses US patents as a domain of origin and Chinese patents as a reference domain. It is impossible to transfer directly between the different languages. This concerns the problem of the classification of texts in the cross language. The experiment uses automatic translation to translate the text of Chinese and English patents and marks the patent levels of some Chinese patents. The model adapts to the distribution of indices and to the linguistic characteristics of Chinese patents. Figure 7 shows the transfer learning process.

To put it simply, taking the patent text in the field of new energy vehicles used in the experiment as an example, the process of transfer learning is to first translate the English

patent text in the United States (source domain data) into Chinese patent text (target domain data) and use it as the input of the PQE_MT_USA model mentioned in the previous section is vectorized using Bert, and the model is retrained through the Bi-LSTM encoding layer and CRF decoding layer. The initial parameters are the final parameters obtained by PQE_MT_USA training English text. After the training is completed, new parameters suitable for the Chinese patent grade prediction model are obtained, and then other Chinese patent texts (target domain data) are tested and adjusted to obtain the transferred parameters.

Through comparative experiments, try to freeze the parameters of different layers to obtain the best migration effect. The specific experimental process and results will be described in detail in the fourth part of the experimental results and analysis. The final experiment selects the part shown by the dotted line in Figure 5 to transfer the model parameters.

Although migration learning requires less data, too little migration data for larger networks will still cause overfitting problems in the model. The model needs more migration samples to make the network model have better generalization capabilities. The experiment contains more than 20,000 Chinese patent data. Labeling a large number of data

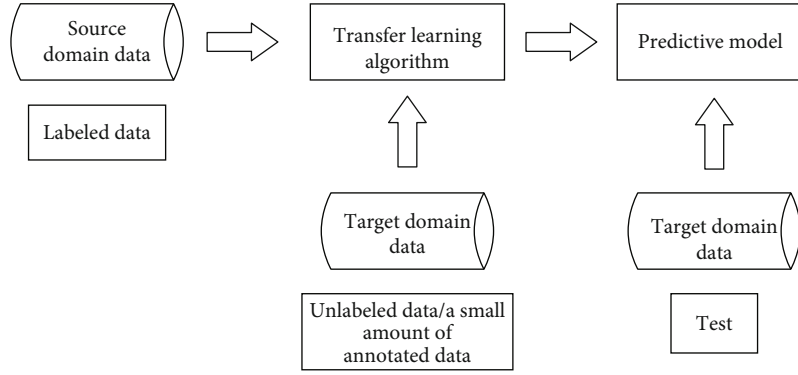


FIGURE 7: Transfer learning flowchart.

samples requires a lot of manpower and material resources. In the process of transfer learning, which patents should be selected for labeling has a greater impact on the results of the transfer. With the same amount of target domain data, selecting samples that are difficult for the model to choose has a better effect than selecting samples that can be clearly classified by the model. The process of letting the model actively propose which data needs to be labeled is active learning. Transfer learning reduces the amount of sample labeling, and active learning improves the quality of labeling samples.

The proposal of active learning is mainly due to the different amount of information provided by each sample in the training set for model training, that is, different samples have different contributions to the improvement of the model effect. Active learning mainly includes classifiers, labeled training data sets, unlabeled data sets, query functions used to extract samples with large amounts of information in unlabeled data sets, and supervisors who label the extracted samples.

The experiment selects more efficient and mature methods based on uncertainty reduction. The main query functions include methods based on classification uncertainty $U(x)$, classification margin $M(x)$, and classification entropy $H(x)$. The specific calculation method is shown in the following equations.

$$U(x) = 1 - P(\hat{x} | x), \quad (14)$$

$$M(x) = P(\hat{x}_1 | x) - P(\hat{x}_2 | x), \quad (15)$$

$$H(x) = -\sum_k p_k \log(p_k). \quad (16)$$

The experiment uses the most effective method based on classification margin for multiclassification problems, namely, the best versus second best (BVSB) strategy [35] to calculate the uncertainty of the sample. This method calculates the difference of the category with the highest probability among the sample prediction results as a measure of sample selection. The smaller the difference, the greater is the uncertainty. Figure 8 lists the two real samples in the experiment. In contrast, the sample on the right has a smaller probability difference and greater uncertainty, and

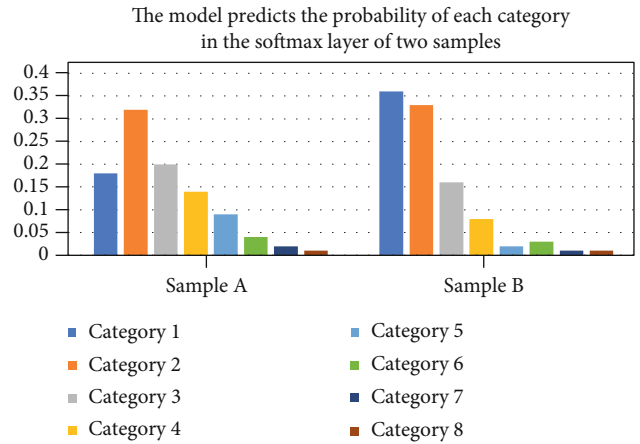


FIGURE 8: The model predicts the probability of each category in the softmax layer of two samples.

the model is more inclined to select it as the sample to be labeled.

By analyzing the output value of each category of the two samples, it is observed that the highest probability of sample A is category 2, its probability is 0.32, the category with the highest probability of sample B is category 1, and its probability is 0.36. Although the final predicted result of sample B is more probable, it can be observed from the overall probability of each category that the model is more confusing for sample B because the difference between the highest category probability and the second highest category probability is smaller, based on classification, the active learning algorithm of margin is good at extracting samples with higher uncertainty for multiclassification problems.

The following is a detailed introduction to the process of transfer learning and active learning algorithms based on the Chinese patent.

First, the English text Patent_USA_En in the source domain data set is translated into Chinese text Patent_USA_Ch, the Chinese patent quality evaluation model PQE-MT_Ch based on the US patent is obtained by Patent_USA_Ch training, and the frozen model PQE-MT_Ch does not require a training layer. Next, we use the unlabeled target domain Chinese patent data set Patent_CHN_Ch as the training set to continue training the model PQE-MT_

Ch. Then, we use this model to classify and predict the sample set Patent_CHN_Ch, calculate the probabilities C1 and C2 of the two categories with the highest predicted probability for each sample, and get the set S of 100 samples with the largest uncertainty, that is, the smallest C1-C2. Then remove the set S from the sample set Patent_CHN_Ch, manually mark the samples in the set S, add the marked set S to the training set, repeat the above training process, and finally get the migration model PQE-MT-CHN_Ch. This model comprehensively utilizes transfer learning and active learning algorithms and is suitable for the English patent quality assessment of Chinese patents. Figure 9 is a diagram of the overall process of transfer learning and active learning.

3.3. Patent Quality Evaluation Model Based on Collaborative Training. In the experiment of the above transfer model, it is not difficult to find that different languages make the model have different effects. The following research will start to use the difference in feature space between Chinese and English languages, and the different features and knowledge learned by the models in different languages, resulting in different prediction effects for different samples, and use bilingual collaborative training to improve the prediction results of the models.

Collaborative training is the mainstream semisupervised machine learning algorithm. The theoretical basis is by training classifiers under multiple views; under the existing small amount of annotated corpus, different features of samples can be learned according to different classifiers, and a large amount of category information of data to be annotated can be further obtained, thus, achieving the purpose of learning by using unlabeled data. The cooperative training process is similar to clustering hypothesis; on the whole, it can be explained that the classification model trained by a small amount of labeled data can only roughly describe the distribution of data, and it is difficult to accurately divide most samples. By using a large amount of unlabeled data, the most accurate data can be found based on the classification of the trained model, so that the model can further find a more accurate classification surface.

In the process of cross-language transfer learning, there is a language barrier between Chinese and English, and the feature spaces of the two languages are different, so it is impossible to transfer the model directly. The experiment used machine translation to unify the languages of the patents of the two countries, so the patents of both countries have two language versions. The experiment hopes to make full use of both Chinese and English feature spaces to further improve the prediction effect of the model.

The experiment trains Chinese patent quality evaluation model PQE_MT_CHN_Ch based on Chinese and Chinese patent quality evaluation model PQE_MT_CHN_En based on English. Through mutual supervision of the two models, a Chinese patent quality evaluation model PQE_MT_CHN_Co based on collaborative training is obtained.

In the experiment, the collaborative training algorithm used machine translation to translate the Chinese text of Chinese annotation data into English text. Train the Chinese-based Chinese patent quality evaluation model

PQE_MT_CHN_Ch on the Chinese text of the labeled Chinese patent data set. In the same way, the English-based Chinese patent quality evaluation model PQE_MT_CHN_En is trained on the English text of the labeled Chinese patent data set. Use these two models to label the unlabeled patent texts in the corresponding data sets and select high-confidence data from them to add to the labeled data set collection. Iterate the above training process. Next, the prediction results of the two evaluation models PQE_MT_CHN_Ch and PQE_MT_CHN_En are combined according to weights, and finally, the Chinese patent quality evaluation model PQE_MT_CHN_Co based on collaborative training is obtained. The overall flow of the algorithm is shown in Figure 10. The algorithm ensures that the sample data distribution is balanced with the real situation by setting the number m_i of the data obtained under each category.

4. Experimental Results and Analysis

4.1. Experimental Corpus. 59147 patents are used in the experiment, and the number of patents with different grades is shown in Figure 11. The experiment randomly shuffled the data set to ensure the uniform distribution of different label samples. 90% samples (53475) are for training and 10% samples (5942) are for testing. The verification method chooses k -fold cross-validation for model optimization. The $k - 1/k$ of the data set is used as the train set, and the rest is used as the validation set. The result is the average of k times. The value of k is set to 10.

There are 21611 Chinese patents, of which 308 are in the United States, which means that the two countries have applied for 308 patents; at the same time, this led to the formation of a monopoly family belonging to the same patent family, in order to meet quality standards, corresponding to Chinese patents. In this paper, 100 Chinese patents with patent grade are taken as the samples of the final model test, 208-as the original data for migration, and the remaining 21303 Chinese unmarked patents are used as the active learning pool for data screening, Mark.

All experimental data are random, and the extraction method is random. In order to ensure the uniform distribution of different label samples and the accuracy and fairness of experimental results, this paper involves Google's machine translation, and this is the most accurate translation system at present.

4.2. Experimental Settings. The accuracy, recall, $f1$ -score, accuracy, microaveraging, and macroaveraging used in the text classification evaluation are used for evaluation. The calculation process is as equations (17)–(26). For category C, the classification results can be divided into the following situations:

- (1) The original type C is classified as type C, and the quantity is recorded as a
- (2) The original non-C category is classified as C category, and the quantity is recorded as b

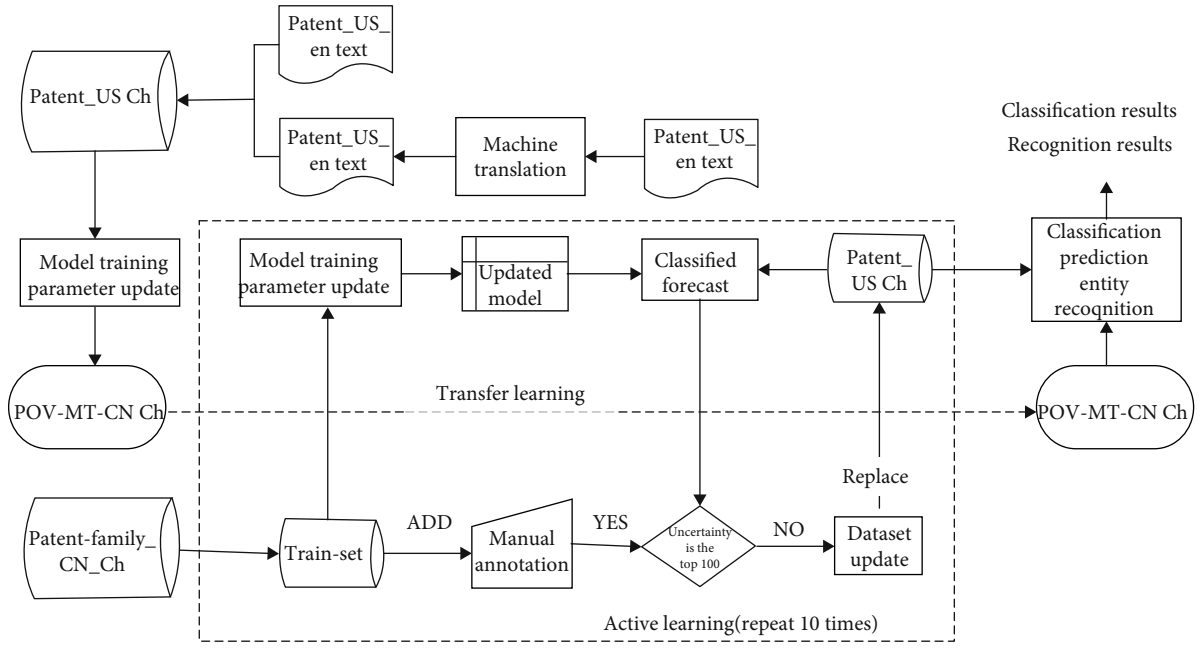


FIGURE 9: Overall process diagram of transfer learning and active learning.

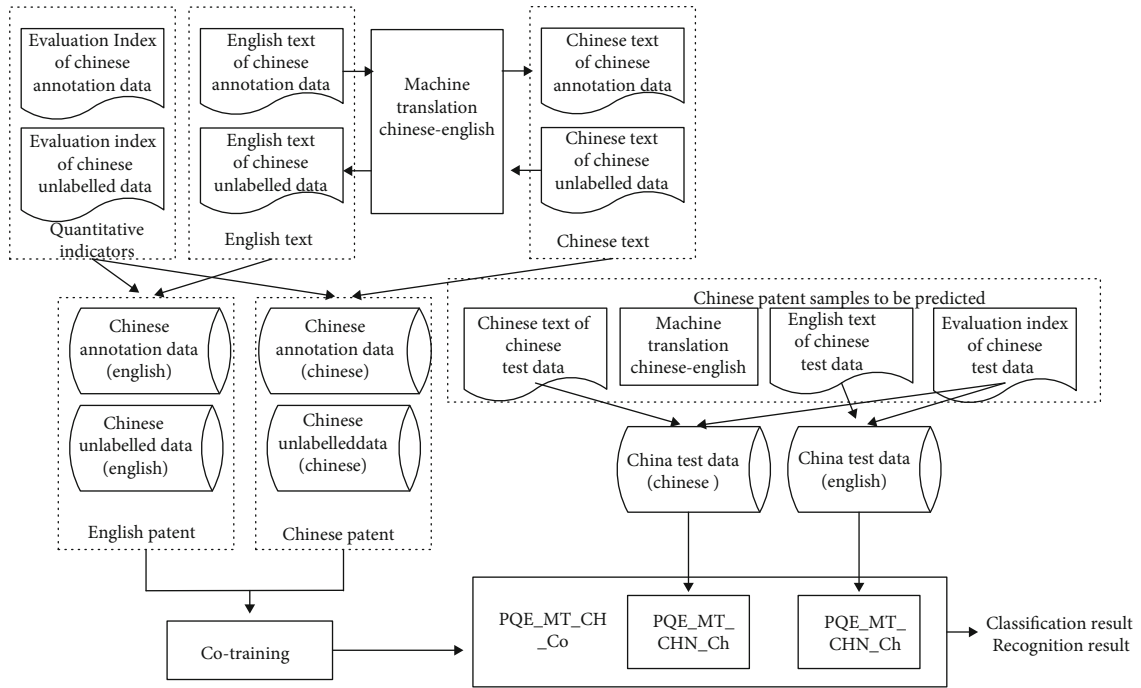


FIGURE 10: Bilingual collaborative training flowchart.

(3) Originally C is classified as non-C, and the quantity is recorded as c

$$R = \frac{a}{a+c} \times 100\%, \quad (18)$$

(4) The original non-C category is classified as non-C category, and the quantity is recorded as d

$$F = \frac{2 \times P \times R}{P + R} \times 100\%, \quad (19)$$

$$P = \frac{a}{a+b} \times 100\%, \quad (17)$$

$$A = \frac{a+d}{a+b+c+d} \times 100\%, \quad (20)$$

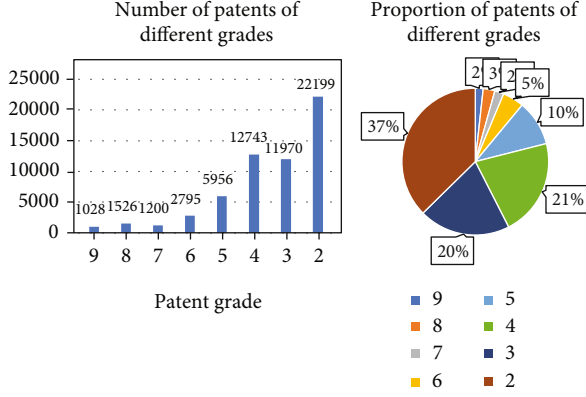


FIGURE 11: Number and proportion of patents with different ratings.

$$\text{Micro}_P = \frac{\sum_{i=1}^n a_i}{\sum_{i=1}^n a_i + \sum_{i=1}^n b_i}, \quad (21)$$

$$\text{Micro}_R = \frac{\sum_{i=1}^n a_i}{\sum_{i=1}^n a_i + \sum_{i=1}^n c_i}, \quad (22)$$

$$\text{Micro}_{F1} = \frac{2 * \text{Micro}_P * \text{Micro}_R}{\text{Micro}_P + \text{Micro}_R}, \quad (23)$$

$$\text{Macro}_P = \frac{1}{n} \sum_{i=1}^n P_i, \quad (24)$$

$$\text{Macro}_R = \frac{1}{n} \sum_{i=1}^n R_i, \quad (25)$$

$$\text{Macro}_{F1} = \frac{2 * \text{Macro}_P * \text{Macro}_R}{\text{Macro}_P + \text{Macro}_R}. \quad (26)$$

4.3. Experimental Results and Analysis of Patent Quality Evaluation Model

4.3.1. *Experimental Results and Analysis of Patent Quality Evaluation Model Based on Multitask Learning.* The experiment tested 15 initial patent indexes, 117 quantified indexes, and 132 indexes combined with the two, respectively. The results are shown in Table 2. The results show that both the initial attributes of patents and the quantitative index parameters in the experiment have influence on the evaluation of patent quality, but the evaluation effect is still poor and cannot meet the final demand. It will be combined with sequence model tasks to improve the effect.

The experimental sequence model and multitask learning model (PQE-MT) training results are shown in Table 3. For readability, the model is defined as follows:

- (i) *Model_1.* word2vec as the embedded layer of the model connects with Bi-LSTM
- (ii) *Model_2.* On the basis of Model_1, attention mechanism is added to form patent quality evaluation model

TABLE 2: Accuracy of initial patent attributes and quantitative index models.

Model input (size)	Train	Dev	Test
Initial index (15)	0.4809	0.4811	0.4813
Quantitative indicators (117)	0.6292	0.6248	0.6156
Combine (132)	0.6604	0.6609	0.6555

- (iii) *Model_3.* On the basis of Model_1, using the Bert after fine-tuning by all patent text data instead of word2vec
- (iv) *Model_4.* On the basis of Model_2, CRF is added to identify patent terms, forming a patent quality evaluation model based on multitask learning
- (v) *Model_5.* On the basis of Model_3, CRF is added to identify patent terms, forming a patent quality evaluation model based on multitask learning
- (vi) *PQE_MT_USA.* Model_5 combined with quantitative index model

The detailed results of our proposed PQE_MT_USA model on different indicators in each category are shown in Table 4.

Through the analysis of the experimental results, it can be concluded that

- (i) Model_2, which uses word2vec as embedding layer and Bi-LSTM as sequence layer, can achieve 58.25% accuracy on train set, 56.52% accuracy on validation set, and 55.22% accuracy on test set
- (ii) After adding the attention mechanism, the accuracy of the model is improved by nearly 2 percentage points, which proves the effectiveness of attention mechanism
- (iii) After replacing the embedding layer with BERT, the accuracy of the model has been greatly improved, but the generalization ability has slightly decreased
- (iv) After using the sequence model based on multitask learning, the effect of model is further optimized and the evaluation effect is further improved. Although multitask learning increases the scale of the model, but the training time of the model does not significantly increase because two tasks share learning parameters, only more 4128 parameters are trained. Each epoch in word2vec and BERT models only increases 54 s and 62 s, indicating that the model has better usability
- (v) The final model combines features of two parts and achieves good results in classification tasks. The accuracy of train set, validation set, and test set is 87.29%, 82.29%, and 83.90%, respectively. It shows that two parts of the model in this paper have an important impact on the evaluation of patent quality

TABLE 3: Results of models.

Model	Text classification			Train	NER		Time s/epoch
	Train	Val	Test		Val	Test	
Model_1	0.5825	0.5652	0.5522	N/A	N/A	N/A	1420
Model_2	0.6026	0.5805	0.5734	N/A	N/A	N/A	1526
Model_3	0.6373	0.5910	0.5962	N/A	N/A	N/A	1922
Model_4	0.6326	0.6054	0.6024	0.8461	0.8457	0.8490	1580
Model_5	0.6890	0.6253	0.6220	0.8541	0.8584	0.8566	1984
PQE_MT_USA	0.8729	0.8292	0.8390	0.8689	0.8795	0.8788	2310

TABLE 4: Results of PQE_MT.

Category	Precision	Train set			Precision	Test set		
		Recall	F1	Support		Recall	F1	Support
1	0.98	0.99	0.98	19967	0.96	0.98	0.97	2232
2	0.93	0.92	0.92	10743	0.89	0.87	0.88	1227
3	0.93	0.87	0.90	11534	0.89	0.81	0.85	1209
4	0.77	0.82	0.80	5330	0.65	0.72	0.68	626
5	0.58	0.80	0.67	2502	0.53	0.65	0.58	293
6	0.54	0.50	0.52	1087	0.48	0.36	0.41	113
7	0.53	0.67	0.60	1382	0.44	0.59	0.50	144
8	0.69	0.74	0.72	930	0.57	0.53	0.55	98
Micro	0.89	0.90	0.89	53475	0.84	0.85	0.84	5942
Macro	0.74	0.79	0.76	53475	0.67	0.69	0.68	5942

- (vi) The model has a good effect on a large number of categories, but a little worse effect on a small number of categories, and the result is positively correlated with the size of the categories as a whole

4.3.2. *Experimental Results and Analysis of Patent Quality Evaluation Model Based on Multitask Learning.* Different layers of the neural network model usually learn the characteristics of different levels of the sample. “Visualizing and Understanding Convolutional Networks” [36, 37] visualizes the layers of CNN and shows the above theory more clearly. The bottom layer 1 and 2 of the model network can usually learn the basic color and edge features of the object; the third layer of the model network generally learns the texture features of the object; the fourth layer that continues upward can learn local features, such as wheels; the top level learns more discernible overall characteristics.

For the image training model, the results of each network layer are easy to observe. In contrast, the knowledge learned by the text training sequence model is difficult to clearly display, but the above rules are also met on the whole. The underlying structure of the network learns the text the part-of-speech and word-sense characteristics of the word; high-level results learn semantic and syntactic characteristics. In response to this phenomenon, experiments try to perform transfer learning in different layers of the model and compare the optimal transfer part.

In the process of transfer learning, the bottom part of the model is usually kept intact to reduce the risk of model over-

fitting. At the same time, for the model in this article, the corpus is first converted into the same language through machine translation. In this process, there is usually no major change in part of speech and word meaning. Due to the differences in culture and writing habits, the migration part is closer to semantics, context, and syntax. At the same time, it meets the requirements of coping with the high-level migration of the network model. The detailed information of each layer of the model PQE_MT_USA is shown in Table 5.

According to the structural characteristics of the network model, the experiment gradually freezes at the bottom of the network, compares the results of different parts of the migration, and obtains the final-migration part. Since only 308 Chinese patents have American patents, they have quality ratings. Take the English data migration results as an example to show and use a total of 308 Chinese patent samples to translate into English text and then perform model migration. Use 100 of them as a test set to compare the effects of different models. Actually, the Chinese patent data used for migration are only 208 articles. The experimental results, respectively, enumerate the microaverage and macroaverages of the accuracy, recall, and F1 value on the training set and the test set. The results are shown in Table 6.

It can be seen from the experimental results that as the low-level parameters of the network gradually freeze, the indicators of the training set show a downward trend, and the indicators of the test set, especially the macroaverage, have a process of first increasing and then decreasing. The main reason for this phenomenon is that the new data set

TABLE 5: PQE-MT layer information.

Number of layers	Type	Output shape	Number of parameters
0	Text input layer	(None, 200)	0
1	Embedding layer	(None, 200, 768)	17999616
2	Bidirectional LSTM_1	(None, 200, 160)	543360
3	Bidirectional LSTM_2	(None, 200, 160)	154240
4	Attention	(None, 160)	32400
5	Number input layer	(None, 132)	0
6	Concatenate layer	(None, 292)	0
7/9/11	Dense layer_1/2/3	(None, 512/128/32)	150016
8/10/12	Dropout layer_1/2/3	(None, 512/128/32)	65664
13	CRF layer	(None, 200, 4)	4128
14	Softmax layer	(None, 8)	668

TABLE 6: Final results of different migration parts.

Migration layer	Training set (microavg/macroavg)						Test set (microavg/macroavg)					
	Precision		Recall		F1-score		Precision		Recall		F1-score	
0-14	0.85	0.70	0.85	0.68	0.85	0.69	0.61	0.38	0.60	0.44	0.60	0.41
2-14	0.83	0.70	0.83	0.63	0.83	0.66	0.66	0.43	0.65	0.46	0.65	0.44
3-14	0.82	0.66	0.82	0.65	0.82	0.65	0.66	0.61	0.66	0.54	0.66	0.57
7-14	0.78	0.66	0.77	0.60	0.77	0.63	0.60	0.44	0.60	0.38	0.60	0.41
9-14	0.60	0.43	0.60	0.39	0.60	0.41	0.58	0.44	0.58	0.36	0.58	0.40
11-14	0.53	0.37	0.53	0.34	0.53	0.35	0.52	0.42	0.52	0.35	0.52	0.38

is small. The larger the migration part of the network during the migration process, the better the fitting effect in the training set, but the problem of overfitting occurs. In the end, the experiment freezes the training of the parameters of the 0-2 layers and selects the 3-14 layers of the network for migration. According to the parameter items in Table 6, freezing the underlying model training can reduce a large number of parameter updates, which improves the model effect and reduces the migration time.

In addition, only the English text of the Chinese patent has experimented with training data, and the patent of model migration was not used. Results of the two experiments are shown in Tables 7 and 8.

From the comparison of Tables 7 and 8, it can be verified that the transfer learning has a certain degree of improvement in each indicator of the model. Due to the lack of training samples in normal supervised learning, the entire TEM model has two obvious problems: first, model TEM poor forecast results in categories with a small number of samples. The results of the accuracy, collection, and f value of the main measurement indicators in category 7 and category 8 were all 0; second, the capacity to generalize the model is very poor, and the problem of overadaptation is obvious. The test set is about 35% lower than the training set in both micro and macroaverages. Comparing results after forwarding learning results in both problems improved. For a few categories of samples, the model has better adaptation, the gap between the microaverage indicators is reduced to 17% on the training set and the test set, and the three indicators of the macroaverage, respectively, reduce to 10%, 16%, and

15%. These two problems have been solved to some extent thanks to the model having learned how the relevant characteristics affect the results of a large number of US patents. Although the distribution of characteristics is different, the overall trend is approximately the same. The model adapts even more to changes in several Chinese patent indicators based on the trend initially learned. Although the model has improved, the effect still cannot meet the final requirements for patent assessment. Hope to improve the model effect by increasing migration data.

We randomly selected 200 unlabeled Chinese patents and manually labeled them as data_random and used the active learning algorithm to obtain the top 200 Chinese patents with the largest classification margin and labeled them as data_active_learning. The experiment starts from 0 and increments each time by 20 on these two data sets, until it reaches 200. Compare the effects of randomly selected data and active learning to select data on model migration. The comparison of the prediction accuracy of the model in the two cases is shown in Figure 12.

By comparing the two trends, it has been found that using the active learning method to select data is better than randomly selected data. The effect of the model that used active learning to select about 140 data to be labeled is equivalent to the effect of randomly selecting 200 data labels. Then, the experiment uses active learning to further expand the labeled data, and active learning can get the most informative data. And each round obtained the first 200 data with the largest classification margin for manual labeling. A total of 2000 samples labeled as new migration data were

TABLE 7: Results of training the network using only Chinese patent data.

Category	Training set				Test set			
	Precision	Recall	F1-score	Support	Precision	Recall	F1-score	Support
1	0.92	1.00	0.96	61	0.55	0.66	0.60	35
2	0.79	0.70	0.74	33	0.41	0.39	0.40	18
3	0.80	0.82	0.81	49	0.18	0.19	0.19	21
4	0.61	0.69	0.65	29	0.30	0.30	0.30	10
5	0.42	0.65	0.51	17	0.33	0.38	0.35	8
6	1.00	0.80	0.89	5	0.00	0.00	0.00	3
7	0.00	0.00	0.00	9	0.00	0.00	0.00	3
8	0.00	0.00	0.00	5	0.00	0.00	0.00	2
Microavg	0.76	0.76	0.76	208	0.40	0.40	0.40	100
Macroavg	0.57	0.58	0.57	208	0.22	0.24	0.23	100

TABLE 8: Data transfer learning results of the initial 208 Chinese patent English.

Category	Training set				Test set			
	Precision	Recall	F1-score	Support	Precision	Recall	F1-score	Support
1	1.00	0.92	0.96	61	1.00	0.77	0.87	35
2	0.83	0.91	0.87	33	0.54	0.78	0.64	18
3	0.82	0.92	0.87	49	0.78	0.67	0.72	21
4	0.81	0.72	0.76	29	0.20	0.20	0.20	10
5	0.50	0.76	0.60	17	0.35	0.75	0.48	8
6	0.40	0.40	0.40	5	0.33	0.33	0.33	3
7	0.60	0.33	0.43	9	0.67	0.33	0.44	3
8	0.75	0.60	0.67	5	1.00	0.50	0.67	2
Microavg	0.83	0.83	0.83	208	0.66	0.66	0.66	100
Macroavg	0.71	0.70	0.70	208	0.61	0.54	0.57	100

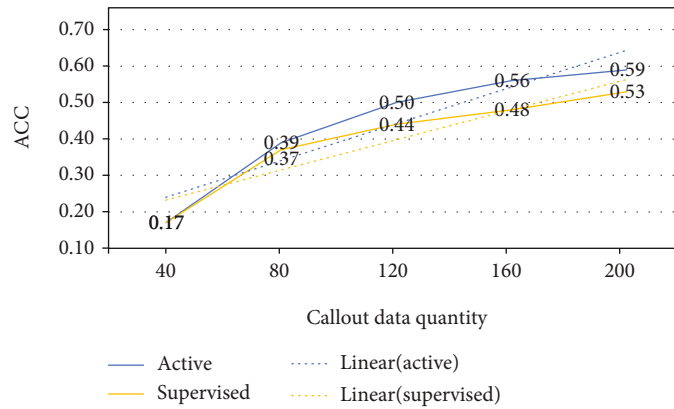


FIGURE 12: Comparison of the accuracy of transfer learning between active learning and randomly selected labeled data.

obtained, the model uses 2-14 levels with the best migration effect obtained from the experimental comparison as a migration part, and the result of the migration of 2208 Chinese patent data obtained after active learning is shown in Table 9. Furthermore, the experiment was conducted in the same way using the patented English language, and the results are given in Table 10.

Experimental results in Tables 8 and 9 are compared to observe the effect of enabled learning on the effect of the data expansion model. Using the initial data migration model, micro-F1 values in the training set and in the test set were 83% and 66%, and macro-F1 values were 70 and 57%. After active learning for data expansion, the values of micro-F1 were 79% and 74% and the macro-F1 values were 68% and

TABLE 9: Data transfer learning results of 2208 Chinese patent English text data after active learning expansion.

Category	Training set				Test set			
	Precision	Recall	F1-score	Support	Precision	Recall	F1-score	Support
1	0.93	0.96	0.95	676	0.93	0.83	0.88	35
2	0.85	0.71	0.77	404	0.88	0.78	0.82	18
3	0.79	0.85	0.81	506	0.74	0.81	0.77	21
4	0.59	0.77	0.67	258	0.39	0.70	0.50	10
5	0.61	0.64	0.62	154	0.50	0.38	0.43	8
6	0.41	0.54	0.47	69	0.33	0.33	0.33	3
7	0.63	0.54	0.58	87	0.33	0.67	0.45	3
8	0.78	0.37	0.50	54	1.00	0.50	0.67	2
Microavg	0.79	0.80	0.79	2208	0.74	0.74	0.74	100
Macroavg	0.70	0.67	0.68	2208	0.64	0.63	0.63	100

TABLE 10: Data transfer learning results of 2208 Chinese patent Chinese text data after active learning expansion.

Category	Training set				Test set			
	Precision	Recall	F1-score	Support	Precision	Recall	F1-score	Support
1	0.95	0.89	0.92	676	0.87	0.79	0.83	35
2	0.68	0.68	0.68	404	0.51	0.54	0.53	18
3	0.65	0.79	0.71	506	0.52	0.64	0.57	21
4	0.55	0.52	0.53	258	0.45	0.42	0.43	10
5	0.45	0.28	0.34	154	0.36	0.22	0.27	8
6	0.43	0.36	0.39	69	0.33	0.67	0.45	3
7	0.56	0.71	0.48	87	0.33	0.33	0.33	3
8	0.70	0.65	0.67	54	1.00	0.50	0.67	2
Microavg	0.73	0.71	0.72	2208	0.62	0.61	0.61	100
Macroavg	0.61	0.61	0.61	2208	0.55	0.51	0.53	100

63%. Due to the increase in the amount of migrated data, the ability to generalize the model became stronger, and the effect of the FOI model improved to a certain extent by providing the test set data.

The results of Table 9 were compared with Table 10, and the effects of Chinese and English were observed on the model effect. The model transition effect for English texts is generally better than Chinese text. The authors believe that the use of machine translated Chinese data leads to degradation of the initial model effect in the case of using source models trained by U.S patents due to the limitations of machine translation techniques, resulting in the final effect of the transfer model is reduced; the number of Chinese patent translations used for the target model has a lower overall influence factor; in addition, the differences in the Chinese and English writing specifications and feature spaces also cause difference in model learning effects.

4.3.3. Experimental Results and Analysis of Patent Quality Evaluation Model Based on Multitask Learning. The article uses SVM as a classification model and Chinese patent text as an example to compare and demonstrate the use of TF-IDF feature vectors and the bag-of-words method for feature word extraction using mutual information, information gain, and chi-square, as well as the three

TABLE 11: Forecast accuracy of different algorithms.

Method	Threshold	Accuracy (train)	Accuracy (test)
TF-IDF	N/A	0.68	0.60
MI	0.1	0.59	0.53
IG	0.03	0.66	0.61
CHI	3	0.67	0.64
Union	N/A	0.71	0.62

methods to extract feature words take the result of the union. The SVM classification algorithm based on bag-of-words is very critical in the selection of feature words. The experiment uses feature extraction formulas for different types of patents to calculate, by manually setting a threshold as a reference value, and extracting words higher than this value as the input features of the bag of words [38]. Table 11 shows the accuracy of algorithm prediction in different situations.

The experimental results show that the SVM classification algorithm based on TF-IDF achieves 68% accuracy on the training set, but in contrast, the prediction result on the test set is reduced by nearly 10%, showing a trend of overfitting. Although the bag-of-words method has a lower accuracy in the training set compared with the TF-IDF method, the accuracy in the test set has been greatly improved. Due to the

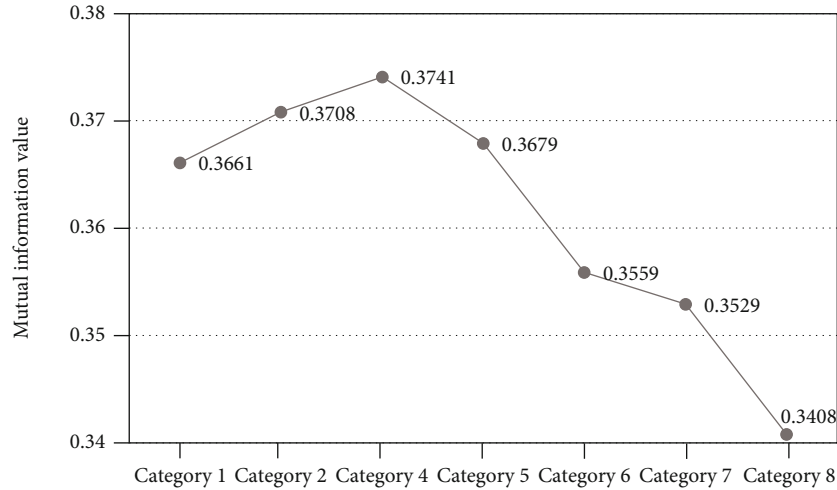


FIGURE 13: Mutual information value between category 3 and other categories.

higher dimension of the union set, it is easy to cause overfitting, which reduces the accuracy of the test set. The experiment finally uses the chi-square algorithm for feature extraction. In addition, the experiment uses the mutual information value that can calculate the similarity between the categories to test different categories. The mutual information value of category 3 and other categories is selected as the display. The test results are shown in Figure 13.

It can be observed that the closer the distance between the samples, the greater the mutual information value. This result fully demonstrates the effectiveness of the training set data annotation. Experiments with different numbers of feature words, the number of feature words with the best model effect is obtained, and the result is shown in Figure 14. The figure shows the dimensions of feature words, and the input of the model is a vector of word bag features and quantitative indicators.

A comparative analysis of the experimental results shows that the accuracy of the model in the training set increases as the dimension of the feature word increases. When the dimension of the feature word is too high, overfitting problems will occur. The effect of the model on the test set gradually decreases. Use the 400-dimensional bag-of-words vector with the best comprehensive results to further test different classification algorithms. The results are shown in Table 12.

It can be seen that the classification accuracy of Bayesian and kNN algorithms is poor, and the decision tree algorithm is not suitable for patent quality evaluation classification due to the overfitting problem caused by the complexity of the sample. Finally, SVM is selected as the classification method for classification.

In the experiment, CHI with better results is selected as the feature word extraction method. Extract 400-dimensional bag-of-words vectors, perform SVM classification on the text, perform collaborative training with the migrated deep learning model PQE_MT_CHN at the same time, and finally compare the prediction effects of the two methods.

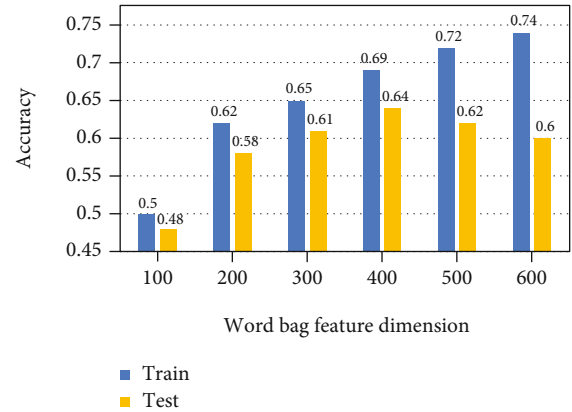


FIGURE 14: SVM classification results of different dimensional bag-of-words vectors.

TABLE 12: CHI extracts the classification results of 400-dimensional bag-of-words vectors combined with quantitative indicators in different algorithms.

Model	Train			Test		
	Precision	Recall	F1	Precision	Recall	F1
Naive Bayes	0.66	0.65	0.65	0.62	0.60	0.61
kNN	0.62	0.58	0.60	0.56	0.54	0.55
SVM	0.70	0.69	0.69	0.64	0.63	0.63
Decision tree	0.74	0.71	0.72	0.59	0.57	0.58

In the experiment, the proposed collaborative training method was compared with the following benchmark methods:

- (i) *SVM_Ch*. Use the combination of Chinese features and quantitative indicators as input, and use SVM for classification. There is no need for text translation in the process, only the marked data is used
- (ii) *SVM_En*. Use the combination of English features and quantitative indicators as input and use SVM for classification. The process requires a Chinese-

TABLE 13: Classification results of PQE_MT_CHN_Co and other benchmark models.

Model	Train			Test		
	Precision	Recall	F1	Precision	Recall	F1
SVM_Ch	0.70	0.69	0.69	0.64	0.63	0.63
SVM_En	0.66	0.61	0.63	0.60	0.57	0.58
SVM_Ch + En	0.75	0.67	0.71	0.62	0.60	0.61
SVM_Co	0.75	0.70	0.72	0.68	0.67	0.67
PQE_MT_CHN_Ch	0.73	0.71	0.72	0.62	0.61	0.61
PQE_MT_CHN_En	0.79	0.80	0.79	0.74	0.74	0.74
PQE_MT_CHN_Ch + En	0.81	0.79	0.80	0.67	0.66	0.66
PQE_MT_CHN_Co	0.84	0.82	0.83	0.78	0.77	0.77

English translation, and only the marked data is used

- (iii) *SVM_Ch + En*. Use the combination of Chinese and English bilingual features and quantitative indicators as input and use SVM for classification. The process requires a Chinese-English translation, and only the marked data is used
- (iv) *SVM_Co*. Use SVM_Ch and SVM_En for collaborative training, and sample prediction is obtained by weighting the results of the two models. The process requires translation from Chinese to English, using unlabeled data for collaborative training
- (v) *PQE_MT_CHN_Ch*. Use the combination of Chinese features and quantitative indicators as input, and use Chinese text transfer learning to obtain the model PQE_MT_CHN for classification. There is no need for text translation in the process, only the marked data is used
- (vi) *PQE_MT_CHN_En*. Use the combination of English features and quantitative indicators as input and use English text transfer learning to obtain a model for classification. The process requires a Chinese-English translation, and only the marked data is used
- (vii) *PQE_MT_CHN_Ch + En*. Use the combination of Chinese and English bilingual features and quantitative indicators as input and use the Chinese and English bilingual text transfer learning model for classification. The process requires a Chinese-English translation, and only the marked data is used
- (viii) *PQE_MT_CHN_Co*. Use PQE_MT_CHN_Ch and PQE_MT_CHN_En for collaborative training, and the sample prediction is obtained by weighting the results of the two models. The process requires Chinese-English translation, using unlabeled data for collaborative training

The results of the above model are shown in Table 13. In addition, the experiment compares the number of samples

of each category and optimizes the experimental parameters for the iteration rounds of collaborative training and each iteration process. The specific results of the model are shown in Figures 15 and 16. The following text will analyze and summarize the results of this part.

Experimental results show

- (1) From the comparison of the various data in Table 13, it can be concluded that the Chinese patent quality evaluation model constructed by the experiment using transfer learning is better than the best-performing SVM in traditional machine learning in the overall transfer effect on the small training set. It proves the feasibility of using transfer learning in this field
- (2) After combining the Chinese and English features of the two models, the prediction effect of the training set has been improved, but due to the lack of training corpus, certain overfitting problems have occurred, resulting in the model's effect on the test set decline. It further proves the necessity of using collaborative training instead of splicing Chinese and English directly
- (3) The proportion of each type of data selected in each iteration of collaborative training has a greater impact on the improvement of the training effect. It can be observed from Figure 15 that when the data proportions of each category are the same, the sample space of model learning will change, leading to the reduction of model prediction effect, and the model is the most stable when the data with the same proportion of each category in the initial data set is selected
- (4) After using the collaborative training algorithm, the semisupervised training method further optimizes the fitting effect of the model on the small training set, and all the evaluation indicators of the model are further improved. The PQE_MT_CHN_Co proposed in the article reaches the highest level in all indicators. Figure 14 can analyze that collaborative training can improve the effect of both Chinese and English models at the same time. Initially, the effect

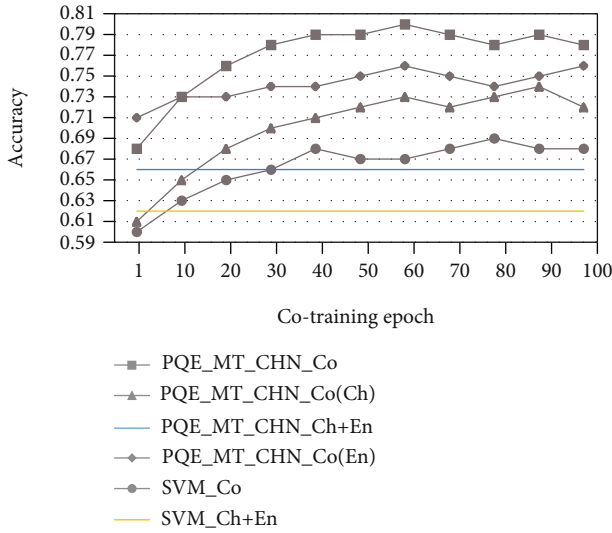


FIGURE 15: Cotraining iterative process model effect changes.

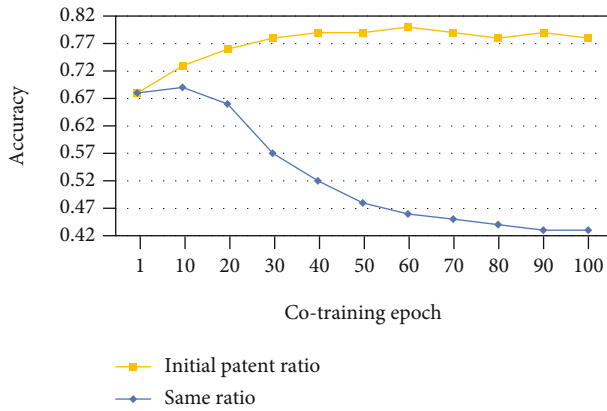


FIGURE 16: The impact of the proportion of data obtained in each category on cotraining.

of the two models is quite different, resulting in a lower effect of the model's joint prediction. However, after multiple rounds of iterations, the prediction effects of the two models gradually approached, and the joint prediction effect of the two models is better than that of one of the models. The micro- F_1 value of the final model reached 83% on the training set and 77% on the test set. It shows that the method proposed in the article has improved the effect of quality evaluation to a certain extent

5. Conclusion and Future Work

Patent quality evaluation model-PQE_MT is proposed in this paper by quantifying the patent indexes from different dimensions and taking the long text part of the patent as one kind of index. The proposed model combines quantitative index model and sequence model based on multitask learning to predict the quality rating of patent. The advantage of this model is that it combines the numerical attribute

part with the text part of the patent as the evaluation indexes. Therefore, the feature extracted from the patent is more comprehensive. In addition, multitask learning is added to train two tasks together, so that the process of updating parameters by backpropagation can promote each other and improve the effectiveness of the model. Compared with the baseline model, the PQE_MT model improves the accuracy of English patent quality assessment.

The migration process mainly includes three parts: the selection of migrant parts, the cross-sectoral transition, and the use of active learning to enlarge data. The advantage of this model is to select the data labeled from the maximum information quantity using the transition learning technology and the positive learning and to reduce the time cost of manual annotation. In the experimental process, the prediction effect of the model gradually improved, and finally, the Chinese patent quality evaluation model achieved good accuracy. At the end of the experiment, we compared the effects of transmission learning between Chinese and English and found that the results were different and the model learned different features. In the follow-up task, we consider two different character models to have different characteristics that may affect each other to improve different results.

In the future, more comprehensive and more meaningful indexes should be quantified. Patent information such as patent drawings, patent research and development cycle, and other internal information of the company are still unused in the experiment, which may improve the predicted results and be more convincing. Moreover, we will try different data expansion methods or semisupervised algorithms to improve the effect of the migration process.

Data Availability

The data used to support the finding of this study are available from the corresponding author upon request.

Conflicts of Interest

The authors declare that there is no conflict of interest regarding the publication of this paper.

Acknowledgments

Regarding the content of the experiment in the article, we previously published the research results of the active learning part in the EAI conference [39]. Based on the research results, we have carried out more innovations, expansions, and more details on the patent quality evaluation research. The authors also acknowledge the National Natural Science Foundation of China under grant no. 62171043, Natural Science Foundation of Beijing under grant no. 4212020, Defense-related Science and Technology Key Lab Fund project under grant no. 6412006200404, Qin Xin Talents Cultivation Program of Beijing Information Science and Technology University under grant no. QXTCP B201908, and Research Planning of Beijing Municipal Commission of Education under grant no. KM202111232001.

References

- [1] L. Qinghai, L. Yang, S. Wu, and X. Xu, "Overview and AHP of patent value evaluation indexes," *Studies in Science of Science*, vol. 2, pp. 281–286, 2007.
- [2] X. Jin, S. Spangler, Y. Chen et al., "Patent maintenance recommendation with patent information network model," in *2011 IEEE 11th International Conference on Data Mining*, Vancouver, BC, Canada, 2011.
- [3] E. J. Han and S. Y. Sohn, "Patent valuation based on text mining and survival analysis," *Journal of Technology Transfer*, vol. 40, no. 5, pp. 821–839, 2015.
- [4] S. Yang, Y. Wang, C. Hang, Z. Lijuan, L. Baizhi, and D. Lei, "Research on the evaluation of patent legal value," *High Technology News*, vol. 26, no. Z1, pp. 815–823, 2016.
- [5] L. Xionghui and Z. Fuyuan, "Research on the evaluation of invention patent value based on fuzzy comprehensive evaluation method," *Journal of Gannan Normal University*, vol. 38, no. 3, pp. 26–30, 2017.
- [6] L. Dan, "The determination of market dominance in the field of patents—from the perspective of patent value evaluation," *Electronic Intellectual Property*, vol. 5, pp. 21–29, 2018.
- [7] M. Yuying, *Comprehensive Evaluation of Patent Value Based on Rough Set and Cloud Model*, Capital University of Economics and Business, 2018.
- [8] Y. S. Chen and K. C. Chang, "Using neural network to analyze the influence of the patent performance upon the market value of the US pharmaceutical companies," *Scientometrics*, vol. 80, no. 3, pp. 637–655, 2009.
- [9] A. J. C. Trappey, C. V. Trappey, C. Y. Wu, and C. W. Lin, "A patent quality analysis for innovative technology and product development," *Advanced Engineering Informatics*, vol. 26, no. 1, pp. 26–34, 2012.
- [10] J. Wang, Y. Wu, and S. Dashuai, "Research on non-commercial patent value evaluation method based on decision tree model," *Economic Forum*, vol. 10, pp. 131–136, 2012.
- [11] Z. Yunhua, Z. Jing, L. Yan, and Y. Xucheng, "Research on patent value evaluation method based on machine learning," *Information Science*, vol. 31, no. 12, pp. 15–18, 2013.
- [12] J. L. Wu, P. C. Chang, C. Tsao, and C. Y. Fan, "A patent quality analysis and classification system using self-organizing maps with support vector machine," *Applied Soft Computing*, vol. 41, no. C, pp. 305–316, 2016.
- [13] Q. Yihui, Z. Chiyu, and C. Shuixuan, "Research on patent value evaluation index system based on classification regression tree algorithm," *Journal of Xiamen University (Natural Science Edition)*, vol. 56, no. 2, pp. 244–251, 2017.
- [14] H. Lin, *Research on Patent Value Evaluation Method Based on Deep Learning*, University of Science and Technology of China, 2018.
- [15] C. Banea, R. Mihalcea, J. Wiebe, and S. Hassan, "Multilingual subjectivity analysis using machine translation," in *Proceedings of the 2008 Conference on Empirical Methods in Natural Language Processing*, pp. 127–135, Honolulu, Hawaii, 2008.
- [16] S. J. Pan and Q. Yang, "A survey on transfer learning," *IEEE Transactions on Knowledge and Data Engineering*, vol. 22, no. 10, pp. 1345–1359, 2010.
- [17] Q. Xu and Q. Yang, "A survey of transfer and multitask learning in bioinformatics," *Journal of Computing Science and Engineering*, vol. 5, no. 3, pp. 257–268, 2011.
- [18] K. Weiss, T. M. Khoshgoftaar, and D. D. Wang, "A survey of transfer learning," *Journal of Big Data*, vol. 3, no. 1, p. 9, 2016.
- [19] J. Yosinski, J. Clune, Y. Bengio, and H. Lipson, "How transferable are features in deep neural networks?," 2014, <https://arxiv.org/abs/1411.1792>.
- [20] C. Tohompson, M. E. Califf, and R. Mooney, "Active learning for natural language parsing and information extraction," in *Proceedings of the Sixteenth International Conference on Machine Learning*, pp. 406–414, San Francisco: Morgan Kaufmann, 1999.
- [21] S. Tong and D. Koller, "Support vect or machine active learning with applications to text classification," *Journal of Machine Learning Research*, vol. 2, pp. 45–66, 2001.
- [22] B. Settles, *Active Learning Literature Survey*, University of Wisconsin-Madison Department of Computer Sciences, 2009.
- [23] L. Jielong, X. Yanshan, H. Zhifeng, R. Yibang, and Z. Liyang, "Multi-instance multi-label active learning based on SVM," *Computer Engineering and Design*, vol. 37, no. 1, pp. 254–258, 2016.
- [24] Z. Zhou, J. Shin, L. Zhang, S. Gurudu, M. Gotway, and J. Liang, "Fine-tuning convolutional neural networks for biomedical image analysis: actively and incrementally," in *Proceedings of the IEEE conference on computer vision and pattern recognition*, pp. 7340–7351, Honolulu, HI, USA, 2017.
- [25] J. J. Zhu and J. Bento, "Generative adversarial active learning," 2017, <https://arxiv.org/abs/1702.07956>.
- [26] K. Konyushkova, R. Sznitman, and P. Fua, "Learning active learning from data," 2017, <https://arxiv.org/abs/1703.03365>.
- [27] A. Blum and T. M. Mitchell, "Combining labeled and unlabeled data with co-training," in *Proceedings of the eleventh annual conference on Computational learning theory*, pp. 92–100, the University of Wisconsin, Madison, Wisconsin, 1998.
- [28] X. Wan, "Co-training for cross-lingual sentiment classification," in *Proceedings of the Joint Conference of the 47th Annual Meeting of the ACL and the 4th International Joint Conference on Natural Language Processing of the AFNLP*, pp. 235–243, Beijing, China, 2009.
- [29] G. U. O. Tao, L. I. Guiyang, and L. A. N. Xia, "Graph-based semi-supervised cooperative training algorithm," *Computer Engineering and Design*, vol. 33, no. 9, pp. 3584–3587 +3621, 2012.
- [30] S. Qiao, W. Shen, Z. Zhang, B. Wang, and A. Yuille, "Deep co-training for semi-supervised image recognition," in *Proceedings of the European Conference on Computer Vision (ECCV)*, pp. 135–152, Munich, 2018.
- [31] Y.-l. Gong and J. Lv, "Cooperative training algorithm combining active learning and density peak clustering," *Computer Applications*, vol. 39, no. 8, pp. 2297–2301, 2019.
- [32] J.-y. Huang and D.-y. Huang, "Improving the translation performance of neural machine translation system by cooperative training," *Journal of Xiamen University (Natural Science Edition)*, vol. 58, no. 2, pp. 176–183, 2019.
- [33] H. Gao, K. Xu, M. Cao, J. Xiao, Q. Xu, and Y. Yin, "The deep features and attention mechanism based method to dish healthcare under social IoT systems: an empirical study with a hand-deep local-global net," *IEEE Transactions on Computational Social Systems (TCSS)*, vol. 2021, no. 8, pp. 1–12, 2021.
- [34] H. Gao, X. Qin, R. J. D. Barroso et al., "Collaborative learning-based industrial IoT API recommendation for software-defined devices: the implicit knowledge discovery perspective,"

- IEEE Transactions on Emerging Topics in Computational Intelligence (TETCI)*, vol. 2020, no. 9, pp. 1–11, 2020.
- [35] Y. Huang, H. Xu, H. Gao, X. Ma, and W. Hussain, “SSUR: an approach to optimizing virtual machine allocation strategy based on user requirements for cloud data center,” *IEEE Transactions on Green Communications and Networking*, vol. 5, no. 2, pp. 670–681, 2021.
- [36] M. D. Zeiler and R. Fergus, “Visualizing and understanding convolutional networks,” in *European Conference on Computer Vision*, Springer, Cham, 2014.
- [37] J. Xiao, H. Xu, H. Gao, M. Bian, and Y. Li, “A weakly supervised semantic segmentation network by aggregating seed cues: the multi-object proposal generation perspective,” *ACM Transactions on Multimedia Computing Communications and Applications*, vol. 17, no. 1s, pp. 1–19, 2021.
- [38] Z. Wang, “A study on the subject classification of the NBA match reports,” in *Proceedings of 2018 2nd International Conference on Electronic Information Technology and Computer Engineering (EITCE 2018)*, pp. 104–121, Shanghai University of Engineering Science, China, 2018.
- [39] J. Liu, X. You, Z. Wang, and X. Lv, “Cross-language transferring the patent quality evaluation model based on active learning data extension,” in *International Conference on Testbeds and Research Infrastructures: Tools for Design, Implementation and Verification of Emerging Information Technologies*, Lecture Notes of the Institute for Computer Sciences, Social Informatics and Telecommunications Engineering, Springer, Cham, 2020.

Research Article

An Experiment to Design an Operation and Maintenance System Integrating Apriori Association Rules for a Telecom Platform

Chengfan Li ¹, Lan Liu ², Junjuan Zhao,¹ and Yuejun Liu¹

¹School of Computer Engineering and Science, Shanghai University, Shanghai 200444, China

²School of Electronic and Electrical Engineering, Shanghai University of Engineering Science, Shanghai 201620, China

Correspondence should be addressed to Lan Liu; liulan@sues.edu.cn

Received 13 April 2021; Revised 15 August 2021; Accepted 16 September 2021; Published 30 September 2021

Academic Editor: Simone Morosi

Copyright © 2021 Chengfan Li et al. This is an open access article distributed under the Creative Commons Attribution License, which permits unrestricted use, distribution, and reproduction in any medium, provided the original work is properly cited.

The operation and maintenance management of telecom platforms puts more emphasis on operation and alarm monitoring and less on business flow, and it is difficult to have a seamless connection between operation and maintenance and sales. To improve the cooperative efficiency and the informatization level of telecom platform operation and maintenance, a new operation and maintenance system integrating Apriori association rules for a telecom platform is proposed. In this paper, the Apriori algorithm is firstly used to analyse the fault correlation of the operation and maintenance system of the telecommunications platform to get the alarm message. Then, the fault risk of the operation and maintenance platform is evaluated intelligently by the system-business alarm causality model. Finally, based on the fixed end and the mobile end, the dynamic presentation of the system running state and alarm monitoring, device query and positioning, and online and offline inspection are implemented and designed, respectively. Experimental results show that the proposed operation and maintenance systems integrating Apriori association rules for the telecom platform innovate the cooperative mode between the operations and sales team, and the average time reduces to 3.9 minutes from 4.7 minutes and the risk forecasting accuracy increases from 8% to 26%. The assumed method can significantly improve the operational efficiency and intelligent level of the telecom platform's system and business.

1. Introduction

With the booming development of mobile Internet, there are many new products and services constantly launched by telecom operators, and it strives to form their own unique advantages in the competition [1, 2]. At present, a telecom operation pattern with the coexistence of fixed and mobile basic services has been formed based on their respective business platforms [3–6]. Different from the basic platform, the operation and maintenance of the business platform include platform hardware (system level) and business data (business level), namely, the combination of operation and maintenance. The operation and maintenance method of a traditional telecom platform not only is time-consuming and inefficient but also have too many process steps and are prone to errors [7–10]. Due to the number of operation and maintenance personnel of the telecom platform which is constantly decreasing under the background of intensifica-

tion and integration and the current cooperative mode between the front end and back end of the telecom platform, there is generally a shortage of an effective coordination mechanism between operation and maintenance and sales. All these greatly limit the efficiency of operation and maintenance and intelligent management of the telecom platform.

On the one hand, with the continuous capacity expansion of key business and efficiency improvement of operation and maintenance in the telecom platform, the problems and fault alarm in the process of system operation are constantly increasing [11]. However, there is a prominent contradiction increasingly between traditional operation and maintenance means and management requirements because of the reducing gradually of back-end operation and maintenance personnel and high costs of subsequent development for network management [12–14]. On the other hand, the traditional information transmission

methods on the telecom platform, such as paper, e-mail, and telephone, have the characteristics of long process flow, extracorporeal circulation, asymmetry between information input and output, etc. It is easy to cause errors and reduce the information construction of telecom operation and maintenance management. In addition, the knowledge-based maintenance has been introduced to the related areas, and the expert system, knowledge base system, and knowledge modelling [15–17] have been explored deeply and extensively.

As an important technology in the field of data mining, association rules can effectively mine the implicit association features in data [18–21]. In these common methods, the Apriori algorithm is one of the most basic data mining methods of association rules, which finds out the association relationship among different data via mining the datasets that frequently appear in the data. At present, the Apriori algorithm has already been successfully applied in business, network security, mobile communication, and other similar studies [22, 23]. The operation and maintenance process of the telecom platform involves many links, complex information, and diverse types, and the correlation between different types and departments of information transmission is obvious [24]. The mining and detection of the associated information in the operation and maintenance of the telecom platform improve the efficiency and quality of the business platform maintenance and solve the collaboration between the platform operation and sale, and it has become an urgent issue to be solved in the telecom industry.

In this paper, we propose the Apriori algorithm to analyse the fault correlation and intelligently evaluate the fault risk of the telecom platform and to implement the system running status and alarm monitoring by HTML5, Ajax, and quick response (QR) code recognition. Limited by the time and length of the text, this paper mainly discusses the Apriori association rules and the conduction of a preliminary experiment to design an operation and maintenance system integrating Apriori association rules for a telecom platform. The results show that the designed telecom operation and maintenance system based on Apriori association rules in this paper can significantly shorten the time of fault determination and improve the accuracy of risk prediction, which is conducive to realizing seamless and high-speed flow of services and information and improving the efficiency of business processing.

The major contributions of this paper are as follows.

- (1) We propose to operate and maintenance the telecom platform based on Apriori association rules; to some extent, it improves the cooperative efficiency and the informatization level of telecom platform operation and maintenance
- (2) We propose to analyse the fault correlation of the operation and maintenance system by the Apriori algorithm to get the alarm message. Then, the system-business alarm causality model evaluates the fault risk of the operation and maintenance platform intelligently

- (3) We propose to construct the system running state and alarm monitoring based on the fixed end and the mobile end and present the device query and positioning and online and offline inspection

The rest of this paper is organized as follows. Section 2 describes different related works. Section 3 shows the detailed Apriori algorithm with association rules. Sections 4 and 5 illustrate the experiments and the corresponding results and application. Section 6 presents the discussion of our paper. Section 7 gives conclusions and future works in the paper.

2. Related Work

Association rules, a method primarily used to mine interesting rules from large amounts of original data, are one of the main research directions of data mining in recent years, aimed at the different fields, such as university scientific research projects [25], hidden abstraction mining of text data [26], data itemset [27], and product and service fusion [28]. To some extent, these achievements extend the usage field of the Apriori algorithm. In addition, different rule sets are obtained via the data mining by Cui and then the cross-selling model of telecom value-added services is constructed [29]. An enterprise financial risk analysis model based on interactive mining of association rules from financial indicators is proposed by Lin and Chen [30]. In the field of disaster monitoring, based on digital aerial images and the landslide caused by heavy rainfall event in the southwest of South Korea in 1998, the uncertainty of unlabelled features in the landslide is accomplished by t-SNE clustering and Apriori algorithms, and the results can provide the reference for the classification of missing or outdated spatial attribute information [31]. The correlation among tax data is mined by association rules and then established the identification path of tax evasion [32]. Via mining on microblog comment behaviour, a microblog recommendation model was constructed based on sentiment-weighted association rules from the above conducted association rule [33].

In the field of electricity and architecture, key inducements in power production safety accidents were extracted by the Apriori algorithm from the deep association rule [34], the association rules among entities are mined by the Apriori algorithm in view of the large number of concrete dam construction documents, and it significantly improved the intelligent and refined management level of concrete dam construction documents [35]. Correlation analysis on cigarette physical indicators was conducted by the Apriori association rules and pointed out that the weight was the key factor affecting suction resistance and total ventilation rate; it provided an effective reference for stability control of cigarette physical indicators [36]. In the field of finance, the shareholder association of companies was mined by the Apriori algorithm and provides effective reference suggestions for the industry shareholder association [37]. In the transportation field, the prior perception of railway network security was completed by the improved Apriori algorithm and expands the early warning means of railway network

monitoring [38]. A parking space idle pattern mining method was proposed based on Hadoop platform, and the association rule is mined by MapReduce parallel computing framework, which improves the computational efficiency [39]. In the personal communications, the indicators including mobile device types, mobile phone apps of the same type, and advertising investment were analysed and mined by the Apriori algorithm and further explore the association rules among users, different types of apps, and advertising investment [40]. Therefore, for many different research fields and specific application requirements, the generality, predictive and prescriptive of the constructed model, is crucial. To some extent, this determines the application value of the constructed model. In this paper, we mainly discuss the Apriori association rules and the conduction of a preliminary experiment to design an operation and maintenance system for a telecom platform due to the time and length of the text.

In view of operation and maintenance of the telecom platform, there are not only a small number of telecom service platforms in mainland China at present but also a general lack of a comprehensive information support system with complete functions. In the implementation method of the fixed end of the integrated operation and maintenance system of the telecom platform, the B/S architecture could not only eliminate the need for users to install special client software but also facilitate the development and maintenance of the system, which is conducive to unified deployment and automatic upgrade and update [41]. At present, with the web technologies developing rapidly, the possibility of HTML5 and lightweight web to develop mobile applications is discussed [42, 43]. The results show that the telecom platform with web technology can achieve richer system functions and a more humanized human-computer interaction interface, with strong experience and practicability. Meanwhile, in the operation monitoring of the telecom platform, it is necessary to find the correlation among various faults and quickly determine the cause of the faults, which requires the correlation analysis of a large number of alarm data. At the same time, the frequent itemsets of Boolean association rules were mined by the Apriori algorithm and then constructed the alarm system [44, 45]. Subsequently, the telecom alarm system was analysed by the association rules and then provided relevant tips for operation and maintenance personnel [46, 47].

3. Apriori Methods with Association Rules

The Apriori algorithm is one of the most basic methods in association rule mining, which mainly includes two parts including finding frequent itemsets and exploring association rules. The core of the Apriori algorithm is the support degree from frequent itemsets and the confidence from association rules.

Let us assume that $I = \{i_1, i_2, \dots, i_m\}$ is the set of all the items and $D = \{T_1, T_2, \dots, T_m\}$ is the object database. The elements that make up object T_i are called terms, the collection of items is called an itemset, and an itemset containing k items is called a k -itemset.

Definition 1. The support degree of itemset A is the proportion of the number of objects containing A in the object database D . Namely,

$$S(A) = \frac{\text{number}(A)}{\text{number}(\text{all samples})} = P(A). \quad (1)$$

Definition 2. If the support degree of itemset A is not less than the preset minimum support threshold (min_sup), namely, $S(A) \geq \text{min_sup}$, the itemset A is called the frequent itemset and the frequent itemset containing k items is called the frequent k -itemset.

Definition 3. An association rule can be represented as a logical expression $A \Rightarrow B$, whereinto A and B are the two non-empty subitemsets of I , respectively. Namely, $A \subset I$, $B \subset I$, $A \neq \emptyset$, $B \neq \emptyset$, and $A \cap B = \emptyset$. The measurement of association rules is usually expressed as the degree of support (S), confidence (C), and lift (L).

For the $A \Rightarrow B$, the support degree is defined as the proportion of the number of $A \cup B$ contained in the object database D . Namely,

$$S(A \Rightarrow B) = \frac{\text{number}(A \cup B)}{\text{number}(\text{all samples})} = P(A \cup B), \quad (2)$$

Confidence is defined as the proportion of objects that contain itemset A that also contains itemset B . Namely,

$$C(A \Rightarrow B) = P(B | A) = \frac{P(A \cup B)}{P(A)} = \frac{\text{number}_{s_count}(A \cup B)}{\text{number}_{s_count}(A)}, \quad (3)$$

where $\text{number}_{s_count}(A \cup B)$ and $\text{number}_{s_count}(A)$ are the number of objects $A \cup B$ in the object databases D and A , respectively.

The lift degree is defined as the ratio of the proportion of objects in the object database D that contains itemset A and also contains itemset B to the proportion of objects that contain itemset B . Namely,

$$L(A \Rightarrow B) = \frac{P(A \cup B)}{P(A)P(B)} = \frac{P(B | A)}{P(B)}. \quad (4)$$

Based on (4), it can be seen that (1) the correlation between itemset A and itemset B is negative when $L < 1$. That is, the occurrence of itemset A will inhibit the occurrence of itemset B . (2) It is independent of each other between the itemset A and itemset B and has no correlation with each other when $L = 1$. (3) The correlation between itemset A and itemset B is positive when $L > 1$. That is, the appearance of itemset A can promote the appearance of itemset B , and the greater the value, the stronger the promoting effect.

The detailed flowage structure of the Apriori algorithm is illustrated in Figure 1.

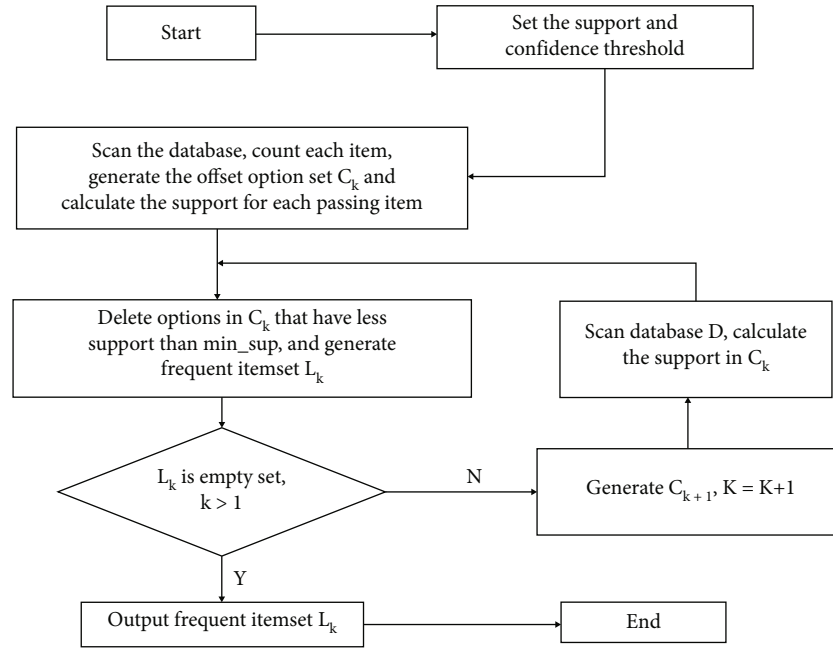


FIGURE 1: The detailed flowage structure of the Apriori algorithm.

To sum up, the Apriori algorithm mainly includes the following steps:

Step 1. Look for a frequent itemset, i.e., items whose occurrence frequency is greater than the support degree threshold.

Step 2. Generate strong association rules from a frequent itemset, and the support and confidence of these rules should be greater than the set threshold.

Step 3. Generate the expected rules using the frequent itemset obtained in Step 1, and further generate all the rules that contain the collection items.

Step 4. In the generated rules, only those rules that satisfy a confidence level greater than the given confidence level are left. The nonfrequent itemset in the candidate set is removed, and then, all frequent itemsets are generated by the recursive method.

4. Experiments

4.1. Experimental System and Deployment Environment. The hardware and software environment in this experiment includes the server side of the supporting system, the data acquisition side of the platform, the fixed client, the mobile client, etc.

4.1.1. Server Side of the Supporting System. The system is implemented by Intel Xeon 4-core CPU, 8 GB RAM, 1 TB hard disk, Apache2.4 or IIS7, PHP5.5, MySQL 5.5, and x86 Server with the Windows Server 2008R2 and Linux system. In addition, the transmission rates of Internet access bandwidth or enterprise Intranet access bandwidth are greater than 1 Mbps in the server.

4.1.2. Acquisition Side of Platform Data. The data acquisition side is deployed on the server of the business platform with

the UNIX or Linux operating system and can connect with the server of the supporting system remotely by intranet and extranet.

4.1.3. Fixed-End Client. The fixed-end client is run in a web browser on a PC. In order to better be compatible with the system running state, alarm information, and interactive experience in the operation and maintenance module of the fixed end of the telecom platform, in the experiment, it is recommended to use Chrome, Firefox, and Internet Explorer with version 9.0 or above.

4.1.4. Mobile-End Client. The client is run on the apps with Android, iOS, and Windows systems. The smartphone should have the connection capability of cellular network data and Wi-Fi data, and the camera can support the scanning function of the QR code.

Taking business data collection as an example, the collected data contains the number of users, active users, calls, CRM account opening records, the call success rate, etc. When collecting the above data of the number of users, the business data acquisition script `usernum.sh` accessed the background Oracle database of the encrypted communication platform by the `SQLPlus` command and conducted data query processing on the internal data tables of multiple platforms and saved the obtained results in the record file.

Some of the core code in data collection includes the following:

On all servers where the capture scripts are deployed, the `crontab` is set to periodically execute the appropriate shell script. For example, on the processing interface machine, the server is used to update the system running status data every minute and the platform business data every 5 minutes.

```
#!/bin/bash.
[process data and time variables]
#connect to the platform backend database
USERNUM=`sqlplus -s [database user name]/[database password] <<EOF
[SQLstatement]
#output the results to a log file
echo filedate$yy-$mm >./record/$yy-$mm-usernum.rec
echo lastdate$yy2-$mm2 >>./record/$yy-$mm-usernum.rec
echo $USERNUM >>./record/$yy-$mm-usernum.rec
```

ALGORITHM 1: Some of the core code in data collection.

```
***** ./report/sysmonitor/report_sysmonitor.sh &
*/5 * 1 ** ./report/report_business.sh &
```

ALGORITHM 2: Some of the core code in planning tasks.

4.2. Experimental Details

4.2.1. Fault Correlation Mining. In order to reduce the number of itemsets, in this paper, the alarm snapshot stored in the database at the same time interval when the alarm occurs is taken as the data source, that is, the alarm set at the same time. Correspondingly, in the experiment, the most recent 100 alarm snapshots with alarms to be calculated were selected as the original data (D).

Candidate itemset 1 (i.e., C_1) is obtained by scanning the original data and further calculating the number of each alarm in the original data. The candidate itemset includes the support degree of each itemset. Frequent itemset 1 (i.e., L_1) was generated by comparing the candidate itemset, and then, the minimum support (MinSup) was set as 10%. That is, the itemset with the support degree less than 10% in the candidate itemset was removed, and finally, L_1 was got.

In the next, candidate itemset 2 (i.e., C_2) was generated by joining and pruning operations on L_1 . In the process of computing, the join operation is to lexicographically join the itemset in L_1 to C_2 , and the pruning operation is to delete the itemset containing the infrequent subset after joining. Frequent itemset 2 (i.e., L_2) was generated by comparing C_2 , and the minimum support (MinSup) was set at 10%. That is, the itemset with the support less than 10% in C_2 was removed to get L_2 . Meanwhile, item-associated alarm set 2 (i.e., A_2) was obtained via comparing L_2 , and the minimum support (MinSup) is set to 50%. That is, there is half of the alarm snapshots in the original data appearing in itemset A_2 .

Similarly, candidate itemset 3 (i.e., C_3) is generated by joining and pruning operations on L_2 , and then, frequent itemset 3 (i.e., L_3) is generated by comparing C_3 ; finally, item correlation alarm set 3 (A_3) is obtained after comparison of L_3 , and so on until the new frequent sets was no longer generate to it. In the method, the MinSup for comparing and generating frequent sets L_K is set to 10%, while the MinSup for comparing and generating associated alarm sets is differ-

TABLE 1: Relationship between the MinSup and the number of items in the itemset.

Number of items (K)	MinSup (L_k)	MinSup (A_k)
1	10%	/
2	10%	50%
3	10%	35%
4	10%	20%
>4	10%	10%

ent. The relationship between the MinSup and the number of items in the itemset is shown in Table 1.

Figure 2 shows the alarm calculation process based on the Apriori algorithm. Candidate itemset 1 is generated by scanning the original data D , and the frequent itemset K is generated by comparing the frequent itemset. And then, the candidate itemset $K + 1$ is generated further by connecting and pruning the frequent itemset. Finally, the management alarm sets A_2 and A_3 are generated by comparing L_2 and L_3 , respectively. The general collection of A_2 and A_3 (i.e., $\{A, C\}$ and $\{A, B, C\}$) is the relevant alarm set, namely, the alarm set of all items obtained from the original data D .

4.2.2. Fault Risk Assessment. The fault alarm types of the telecom platform usual include system alarm and service alarm. The former is caused by the abnormal state of system hardware and software, while the latter is caused by the abnormal business indicators of the platform.

In the experiment, the key to the fault risk assessment model based on system-business alarm causality lies in the potential causality between system faults and business alarms. That is, in the related alarm set obtained by the Apriori algorithm, to some extent, the service alarm is regarded as being caused by the system alarm in the same itemset.

In terms of the proposed model, the number and level of the associated business alarms together determine the risk level of the alarm for a single system alarm.

To quantify the alarm risk of the system, in the experiment, the fault risk is evaluated by the risk degree score model, as shown in

$$R_{\Sigma} = \sum_{i=0}^n R_i, \quad (5)$$

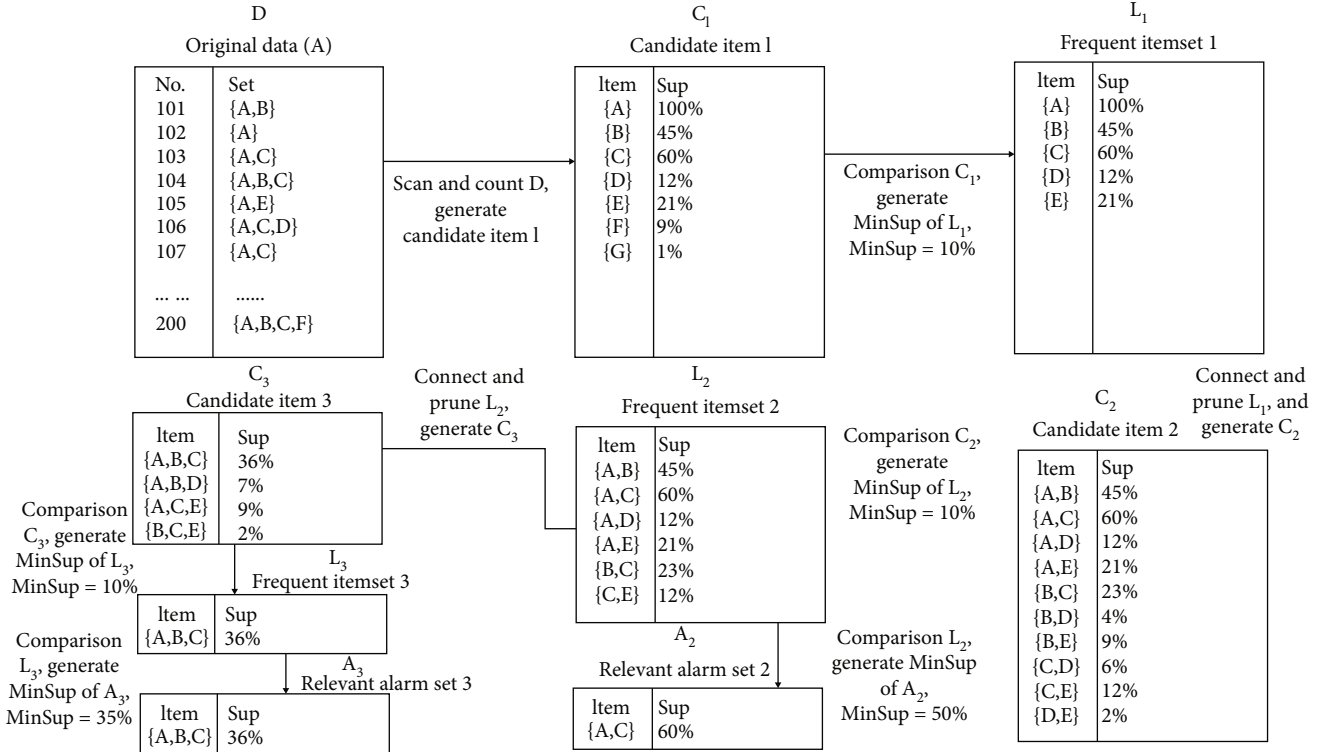


FIGURE 2: Alarm calculation process based on the Apriori algorithm.

where R_i is the score of business alarm level related to the system alarm, N is the total number of related business alarm, and R_Σ is the risk score of system alarm.

Since the score of alarm risk varies with the number of items, the different alarm level scores are designed as equation (5). And the alarm level score of different numbers of the items is shown in Table 2.

As shown in Table 2, there are three types of alarm level including severe, serious, and general with the number of items. For the same number of item value, the alarm level score is not exactly the same. For example, when the number of items reaches 4, the same alarm level score means the different alarm level.

Since the itemset $\{A, B, C\}$ of the associated alarm set to which A and B belong is a 3-item associated alarm itemset (i.e., $K = 3$), $R_i = 3$, $n = 1$, and then $R_\Sigma = 3$, we conclude that the risk assessment level corresponding to alarm A is medium, as shown in Table 3.

In Table 3, the operation and maintenance system integrating the Apriori algorithm for the telecom platform proposed in this paper has the preliminary function of alarm and alarm risk assessment, which helps to improve the fault judgment and response efficiency of the operation and maintenance of the telecom platform.

4.2.3. Monitoring Visualization of System Operation. Figure 3 shows the updating process of web page information based on Ajax and HTML technologies.

As shown in Figure 3, the program of a web front end regularly calls a jQuery function without the human intervention and accesses the operation and maintenance module

TABLE 2: Different types of business alarm level.

Number of items (K)	Alarm level	Alarm level score (R_i)
2	Severe	5
	Serious	3
	General	1
3	Severe	3
	Serious	2
	General	1
≥ 4	Severe	2
	Serious	1
	General	1

TABLE 3: Different risk assessment levels.

R_Σ	Risk assessment level
≥ 5	High
$3 \leq R_\Sigma < 5$	Medium
$1 \leq R_\Sigma < 3$	Low
< 1	Very low

of the web back end in the manner of HttpRequest. Via accessing the system running state and alarm information table of the system database, the web back end obtains data, and then, the assembled JSON format data is returned to the web front end by HTTP. After inputting JSON data, the

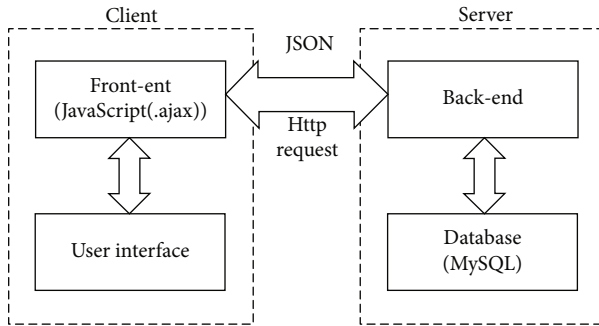


FIGURE 3: Updating process of web page information.

jQuery function in the web front end is used to identify and update HTML elements of the user interface (UI).

Some of the core code in function calls and data access includes the following:

4.2.4. Inspection Report and Mobile End. In the experiment, the inspection report of the abnormal situation is accomplished by the method of combining the fixed end and mobile end, which can scan the QR code of the equipment in the machine room with mobile phones. In the method, the key to realize the mobile-end inspection and reporting process is the identification and location of the QR code for equipment. That is, after the user scans the QR code of the device with the mobile app, the telecom platform pushes the XML message to the back end of the mobile by HTTP, and the format of the XML message is the following:

When the above XML message is received at the back end of the mobile, the XML message is parsed by the `simplexml:load_string()` function, and then, the link and page to report the inspection information of the room and equipment are pushed to the user.

5. Results and Application

The detailed software structure and implementation process are shown in Figure 4.

As shown in Figure 4, the whole software structure contains a user interaction layer, business logic layer, operation environment layer, and basic resource layer. There are fixed-end UI and mobile-end UI in the operation and maintenance system.

5.1. Monitoring System of Operation and Maintenance. In the operation and maintenance of the telecom platform, the operation monitoring page of the fixed-end platform displays the running state and alarm overview of the platform, and the main index information is displayed by switching of the tab page. Meanwhile, the mobile end binds customer information and displays system running status and alarm overview information. There is an alarm message produced in line with the push standards, the mobile end can also receive the fault push message and display the relevant alarm and risk assessment information. In the process of pushing alarm message, the mobile end is mainly to scan the QR code of equipment and report the inspection information,

while the fixed end in a machine room is mainly to carry out inspection records, data screening, and inspection of the equipment.

Figure 5 shows the operation monitoring interface of the telecom platform in this paper.

As shown in Figure 5, the operation and maintenance staff can monitor the disk space of the system, such as network element IP, results, and pass, whereinto the `XX.XX.XX.XX`. indicates the IP address that hides specific information.

Figure 6 shows the inspection reporting interface of the telecom platform based on the mobile end in this paper.

5.2. Auxiliary System of Operation and Maintenance. In the auxiliary system of operation and maintenance, the management page of monthly report in the fixed end can generate and download the monthly report; the management page of the knowledge base can view and search the knowledge experience classification. Meanwhile, the mobile end can share the experience and query the knowledge base.

Figure 7 shows the auxiliary system interface of the operation and maintenance in the telecom platform in this paper.

Figure 8 shows the monthly report generated by the auxiliary system of operation and maintenance in this paper.

Figure 9 shows the management interface of the knowledge base by the auxiliary system of the operation and maintenance in this paper.

As can be seen from Figures 8 and 9, the knowledge and experience sharing and the query of the knowledge base can be carried out normally on mobile terminals; the management page of the knowledge base in the fixed terminal platform can be smoothly classified, viewed, and searched for knowledge and experience.

5.3. Business Management and Support System. In the business management and support system, the statistics page of fixed-end business data shows the statistical charts of user development and call situation in the last month. The management page of the support order shows the view, feedback, statement, and other operations. Users can create, feedback, settle, and evaluate the service support order on the mobile end.

By taking the test data as an example, Figure 10 shows the statistical interface of business data in the business management and support system in this paper.

As shown in Figure 10, the business management and support system clearly displays the monthly business statistics (Figure 10(a)) and change trend (Figure 10(b)) of the whole year in 2020.

5.4. Management System. In the management system, the administrator can enter the back end of the system module. The user account can create, modify, and delete users in the management page. In the management page of the device, the device list can be displayed, and further create, modify, and delete the device and generate the QR code. Figure 11 shows the management interface of the system user.

As shown in Figure 11, in the management page of the fixed end, the administrator can edit, delete, review, and

```
dataread_alarmlist = function(){
    $.ajax({
        url: "../json/dataread_alarmlist.php",
        cache: false,
        dataType : "json",
        data:{
        },
        ifModified:true,
        success: function(data){
        }
    })
    setTimeout(dataread_alarmlist,60000);
}
```

ALGORITHM 3: Some of the core code in function calls and data access.

```
<xml>
<ToUserName><![CDATA[toUser]]></ToUserName>
<FromUserName><![CDATA[FromUser]]></FromUserName>
<CreateTime>216568821</CreateTime>
<MsgType><![CDATA[event]]></MsgType>
<Event><![CDATA[scan]]></Event>
<EventKey><![CDATA[SCENE_VALUE]]></EventKey>
<Ticket><![CDATA[TICKET]]></Ticket>
</xml>
```

ALGORITHM 4: The format of the XML message by HTTP.

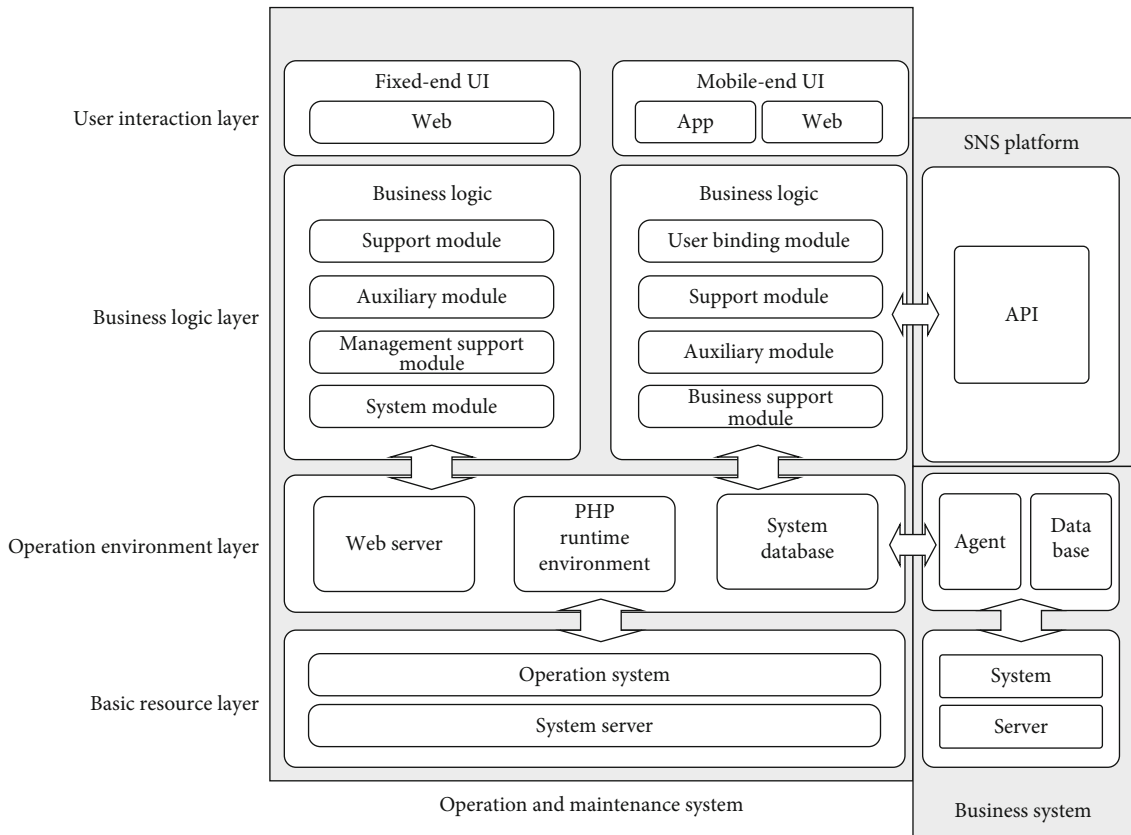


FIGURE 4: Software structure and implementation process.

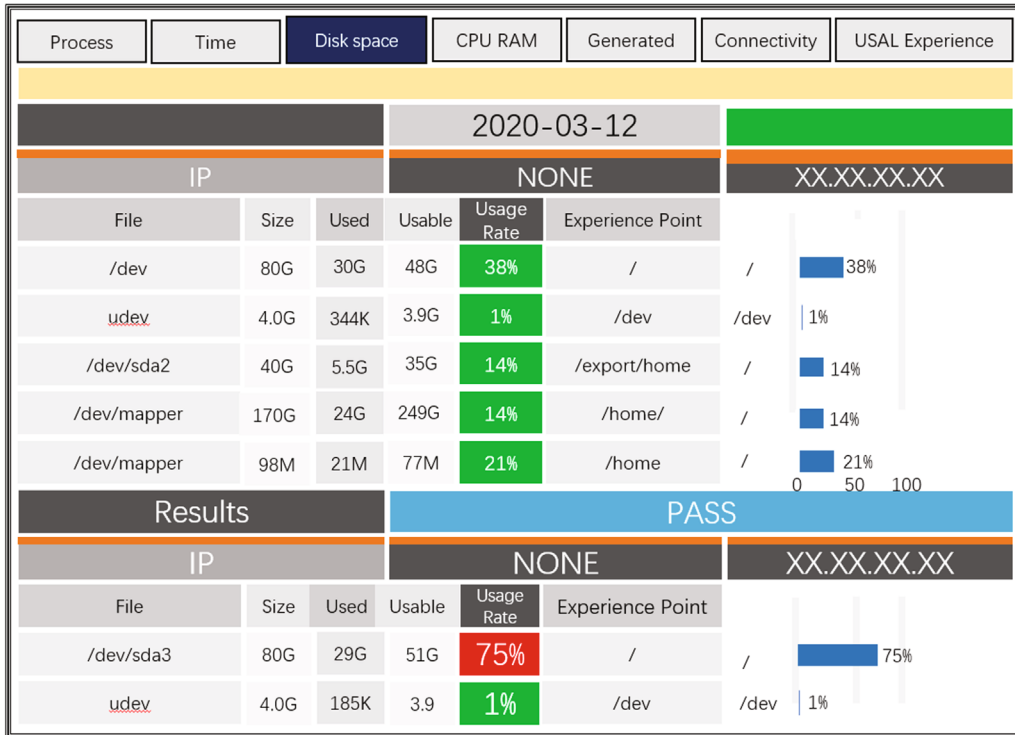


FIGURE 5: Operation monitoring interface of the telecom platform.



FIGURE 6: Inspection reporting interface based on the mobile end.

delete the basic information displayed on the main interface and delete and modify the operation log. In the management page of the mobile end, the administrator can set the menu of the mobile-end official account and modify the level of fault information push in the mobile end.

6. Discussions

6.1. Comparison with the Traditional Network Management Platform. Compared with the traditional network management platform, the proposed operation and maintenance system integrating Apriori association rules for the telecom platform in this paper has many benefits. It breaks through the limitations of the traditional network management system including structure, function, and cooperation mode of users.

6.1.1. Constructing the System Architecture Based on the Fusion Model of the Fixed End and Mobile End. In this system, it not only enables the operation and maintenance team to check the platform running status and alarm information by the mobile phone anytime and anywhere but also then reports the abnormal situation of equipment in real time in the machine room and receives and pushes the fault information in time. In addition, it also enables the sales team to collaborate closely with the operation and maintenance team anytime and anywhere to get timely technical support. To some extent, it overcomes the limitation that the traditional network management system can only be used in a fixed environment.

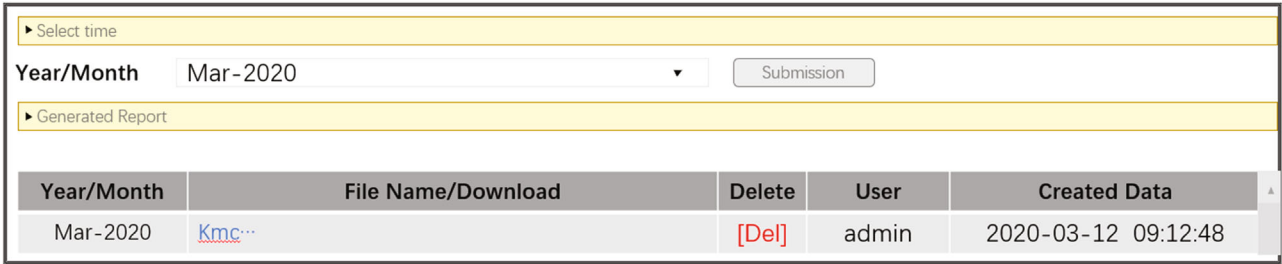


FIGURE 7: Auxiliary system interface of the operation and maintenance.

Analysis report (test data)
(May, 2020)

Number of account users

Total accounts	
133 DNSEG	200
153 DNSEG	300
180 DNSEG	500
181 DNSEG	100
189 DNSEG	200
Number of new users/month	20
Number of accounts closed/month	10
Number of accounts net additions/month	10

FIGURE 8: Monthly report generated by the auxiliary system.

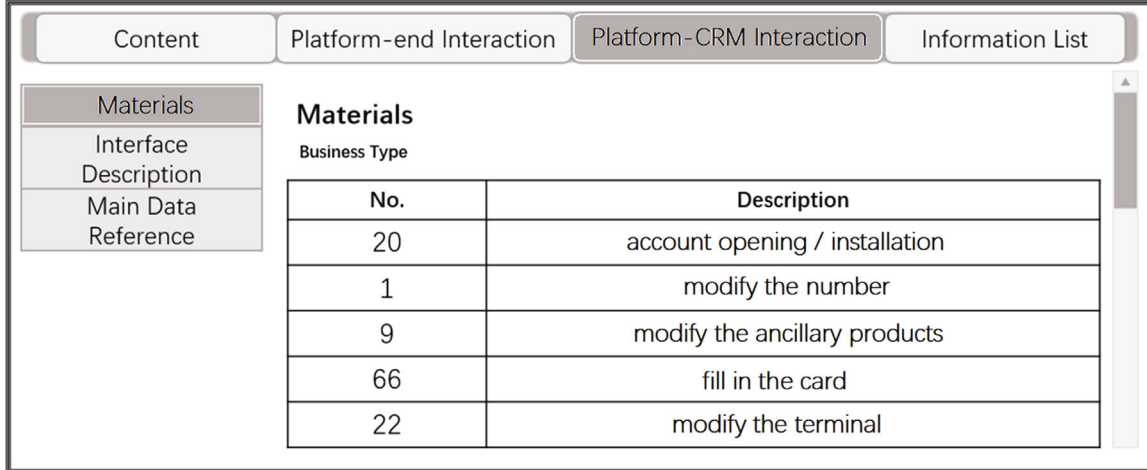


FIGURE 9: Management interface of the knowledge base.

6.1.2. *Realizing the Comprehensive Coverage of System Operation and Maintenance and Business Support Functions.* In this system, it mainly includes operation and maintenance support, auxiliary system of operation and maintenance, business management and support, and other functions. In view of the operation flow, it covers the data and business process of the whole telecom platform, such as daily monitoring and fault processing, auxiliary system, business data analysis, and team collaboration of the front end and back end. It overcomes the limitation that the tradi-

tional network management system can only monitor the system running state and alarm.

6.1.3. *Building the Collaborative Mode of Comprehensive Support for the Telecom Platform.* Via the development of the mobile end, in this system, it connects the platform operation and sales support team together, initially realizes the cooperation between knowledge experience sharing and business support, and promotes the working efficiency of the front end and back end in the telecom platform. It

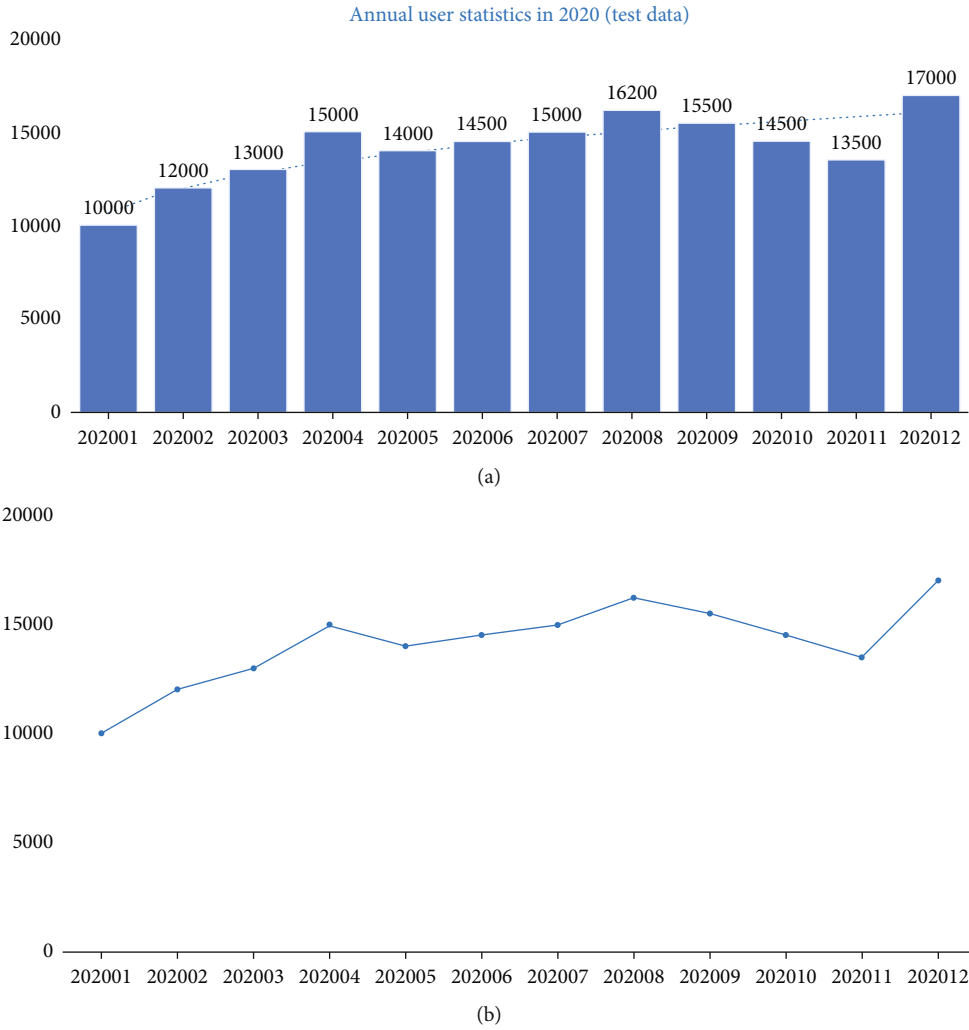


FIGURE 10: Statistical interface of business data (a) and the corresponding line chart (b).

▶ Create Account

Nickname User Right Normal User

Password English/Numbers/Special Characters

Name Please Insert Real Name

Advise set a strong password and fill in your real name

Restore the original value

Append

#Total 3 users#

id	Nickname	Name	Password	User Right	Revise	Delete
1	John	Test admin	asd12h0ty5nmj325tyq1sr52gj63m	Amin	Revise	Del
2	Kitty	Test user	asd12h0ty5nmj325tyq1sr52gj63m	User	Revise	Del
3	David	Test admin	asd12h0ty5nmj325tyq1sr52gj63m	Admin	Revise	Del

Page 1/Page 1

FIGURE 11: Management interface of the system user.

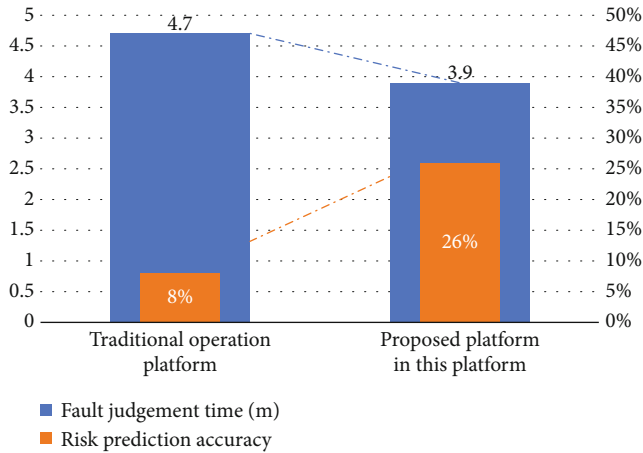


FIGURE 12: Comparison of fault judgment time and risk prediction accuracy.

overcomes the limitations of the traditional network management only supporting the operation and maintenance team.

6.2. Comparison with Traditional Alarm Analysis. To improve the accuracy and timeliness of the alarm impact and risk judgment for the operation and maintenance support team, in this system, it displays not only the alarm information but also the alarm and the related risk assessment of the alarm. Figure 12 shows the comparison of fault judgment time and risk prediction accuracy between the traditional operation platform and the proposed platform in this paper.

As shown in Figure 12, compared with the traditional alarm analysis that relies on manual analysis of historical alarms, the experiment to design operation and maintenance system integrating the Apriori association rule for the telecom platform in this paper effectively improves the judgment efficiency of the operation and maintenance support team on the cause of the fault. Thus, the time of risk determination reduced from 4.7 minutes to 3.9 minutes. At the same time, it also significantly improved the accuracy of risk prediction, and the risk prediction increased from 8% to 26%.

7. Conclusions and Future Work

In this paper, we have followed the experiment of operation and maintenance system integrating the Apriori algorithm to discover the association rules in large-scale data and we have developed an operation and maintenance system integrating the Apriori association rule for the telecom platform via designing the system architecture, database, front end, and back end. The experimental results show that the system can effectively overcome the limitations of the architecture, function, and user collaboration mode of the traditional operation platform and improve the judgment efficiency of the fault cause for the operation and maintenance support team and the accuracy of risk prediction.

Compared with the current operation and maintenance system of the telecom platform, although this work has certain characteristics and advantages, it still has many short-

comings due to the limitation of development time and computing resources. As a future work, we are planning to improve the existing work from the following aspects:

- (1) *Mobile-end security.* The operation and access of the system are mainly achieved via the network; although the system has done security design for the user access rights, there are still some security problems; e.g., it is possible to bypass user authentication for the collaboration features of the social network. In the future, we will introduce the more robust authentication mechanism of the mobile end to overcome the security risks
- (2) *Multiplatform adaptability.* This work suffers from a lack of data acquisition capacity for the non-Linux/UNIX server's platform and external network management system, and the multiplatform adaptability is weak. In the future, we will enhance the capacity of data acquisition and improve the external interface functions
- (3) *Fault risk assessment.* Although this work has improved the accuracy of fault risk prediction affecting the business level, there is also misjudgement of the risk level in actual operation. In the future, we will continuously optimize the evaluation model based on the application experience and further reduce the probability of alarm misjudgement
- (4) *Model construction of predictive and prescriptive maintenance.* This work mainly uses Apriori association rules to conduct a preliminary experiment of the operation and maintenance system for the telecom platform, so in the experimental design and test, there is not much involved in model prediction and system standardization and other factors. To some extent, it determines the generality and portability of the built model

In addition, we would also like to continue experimenting with other implementation techniques based on the telecom platform and others specific for fixed-end and mobile-end devices.

Data Availability

Data sharing is not applicable to this article as no datasets were generated or analysed during the current study.

Conflicts of Interest

The authors declare that they have no conflicts of interest.

Acknowledgments

This work was partially supported by the Science and Technology Commission of Shanghai Municipality (No. 19142201600) in China and the Graduate Innovation and Entrepreneurship Program in Shanghai University in China (No. 2019GY04).

References

- [1] J. Mulongo, M. Atemkeng, T. Ansah-Narh, R. Rockefeller, G. M. Nguengang, and M. A. Garuti, "Anomaly detection in power generation plants using machine learning and neural networks," *Applied Artificial Intelligence*, vol. 34, no. 1, pp. 64–79, 2020.
- [2] M. Sorrentino, V. Cirillo, D. Panagrosso, A. Trifiro, and F. Bedogni, "Development of free-cooling detection procedures to support energy intelligence actions within telecommunication environments," *Applied Thermal Engineering*, vol. 144, pp. 1037–1048, 2018.
- [3] S. Van Rossem, W. Tavernier, D. Colle, M. Pickavet, and P. Demeester, "Introducing development features for virtualized network services," *IEEE Communications Magazine*, vol. 56, no. 8, pp. 184–192, 2018.
- [4] C. Heracleous, P. Kolios, C. G. Panayiotou, G. Ellinas, and M. M. Polycarpou, "Hybrid systems modeling for critical infrastructures interdependency analysis," *Reliability Engineering and System Safety*, vol. 165, pp. 89–101, 2017.
- [5] R. Kaur, V. Krishnasamy, and N. K. Kandasamy, "Optimal sizing of wind-PV-based DC microgrid for telecom power supply in remote areas," *IET Renewable Power Generation*, vol. 12, no. 7, pp. 859–866, 2018.
- [6] R. Kaur, V. Krishnasamy, K. Muthusamy, and P. Chinnamuthan, "A novel proton exchange membrane fuel cell based power conversion system for telecom supply with genetic algorithm assisted intelligent interfacing converter," *Energy Conversion and Management*, vol. 136, pp. 173–183, 2017.
- [7] X. Chen, "Optimizing MPBSM resource allocation based on revenue management: a China mobile Sichuan case," *Mobile Information Systems*, vol. 2015, Article ID 892705, 10 pages, 2015.
- [8] L. Bennacer, Y. Amirat, A. Chibani, A. Mellouk, and L. Ciavaglia, "Self-diagnosis technique for virtual private networks combining Bayesian networks and case-based reasoning," *IEEE Transactions on Automation Science and Engineering*, vol. 12, no. 1, pp. 354–366, 2015.
- [9] N. Lu, G. Q. Zhang, and J. Lu, "Concept drift detection via competence models," *Artificial Intelligence*, vol. 209, pp. 11–28, 2014.
- [10] C. Lozano-Garzon, C. Ariza-Porras, S. Rivera-Diaz, H. Riveros-Ardila, and Y. Donoso, "Mobile network QoE-QoS decision making tool for performance optimization in critical web service," *International Journal of Computers Communications and Control*, vol. 7, no. 5, pp. 892–899, 2014.
- [11] Y. S. Rong and C. F. Li, "Design of integrated operation and maintenance support system of telecommunication platform based on web and light app," *Electronic Technology and Software Engineering*, vol. 20, no. 1, pp. 46–47, 2015.
- [12] X. J. Geng, Y. Liang, and L. M. Jiao, "EARC: evidential association rule-based classification," *Information Sciences*, vol. 547, pp. 202–222, 2021.
- [13] M. S. Bashkari, A. Sami, and M. Rastegar, "Outage cause detection in power distribution systems based on data mining," *IEEE Transactions on Industrial Informatics*, vol. 17, no. 1, pp. 640–649, 2021.
- [14] Y. H. He, Y. X. Zhao, X. Han, D. Zhou, and W. Z. Wang, "Functional risk-oriented health prognosis approach for intelligent manufacturing systems," *Reliability Engineering & System Safety*, vol. 203, article 107090, 2020.
- [15] Q. Jiang, Z. X. Xiao, C. P. Ru et al., "Study on the modeling method of knowledge base system in web environment," *International Journal of Pattern Recognition and Artificial Intelligence*, vol. 33, no. 9, article 1959031, 2019.
- [16] S. Wan, D. B. Li, J. Gao, and J. Li, "A knowledge based machine tool maintenance planning system using case-based reasoning techniques," *Robotics and Computer-Integrated Manufacturing*, vol. 58, pp. 80–96, 2019.
- [17] N. Hai, D. Q. Gong, and S. F. Liu, "Ontology knowledge base combined with Bayesian networks for integrated corridor risk warning," *Computer Communications*, vol. 174, pp. 190–204, 2021.
- [18] J. Y. Jhang, I. S. Tzeng, H. H. Chou et al., "Association rule mining and prognostic stratification of 2-year longevity in octogenarians undergoing endovascular therapy for lower extremity arterial disease: observational cohort study," *Journal of Medical Internet Research*, vol. 22, no. 12, article e17487, 2020.
- [19] J. Y. Liao, S. Wu, and A. L. Liu, "High utility itemsets mining based on divide-and-conquer strategy," *Wireless Personal Communications*, vol. 116, no. 3, pp. 1639–1657, 2021.
- [20] D. Y. Li and Y. L. Liao, "Pollution zone identification research during ozone pollution processes," *Environmental Monitoring and Assessment*, vol. 192, no. 9, p. 591, 2020.
- [21] M. Al-Fayoumi, J. Alwidian, and M. Abusaif, "Intelligent association classification technique for phishing website detection," *International Arab Journal of Information Technology*, vol. 17, no. 4, pp. 488–496, 2020.
- [22] F. Safara, A. Souri, and M. Serrizadeh, "Improved intrusion detection method for communication networks using association rule mining and artificial neural networks," *IET Communications*, vol. 14, no. 7, pp. 1192–1197, 2020.
- [23] S. Raj, D. Ramesh, M. Sreenu, and K. K. Sethi, "EAFIM: efficient Apriori-based frequent itemset mining algorithm on spark for big transactional data," *Knowledge and Information Systems*, vol. 62, no. 9, pp. 3565–3583, 2020.
- [24] B. Shazad, H. U. Khan, M. Zahoor-ur-Rehman et al., "Finding temporal influential users in social media using association rule learning," *Intelligence Automation and Soft Computing*, vol. 26, no. 1, pp. 87–98, 2019.
- [25] L. J. Chen, K. Mao, Y. Zheng, X. Zhou, and C. M. Zhu, "Research on mining association rules in university scientific projects management," *Network Computing and Information Security*, vol. 345, no. 1, pp. 561–567, 2012.
- [26] Y. Xu, M. M. Zeng, Q. Liu, and X. Wang, "A genetic algorithm based multilevel association rules mining for big datasets," *Mathematical Problems in Engineering*, vol. 2014, no. 12, Article ID 867149, p. 9, 2014.
- [27] L. H. Ding, S. S. Xie, S. C. Zhang et al., "Delayed comparison and Apriori algorithm (DCAA): a tool for discovering protein-protein interactions from time-series phosphoproteomic data," *Frontiers in Molecular Biosciences*, vol. 7, article 606570, 2020.
- [28] Z. He and J. H. Chen, "Research on service innovation methods of service-oriented manufacturing enterprises based on product-service integration," *Operations Research and Management Science*, vol. 24, no. 3, pp. 240–247, 2015.
- [29] D. M. Cui, "Empirical analysis of statistical data mining in big data era," *Statistics and Decision*, vol. 48, no. 4, pp. 180–182, 2016.

- [30] Y. H. Lin and C. F. Chen, "Research on enterprise financial risk evaluation based on association rules," *Friends of Accounting*, vol. 16, no. 1, pp. 32–35, 2017.
- [31] O. F. Althuwaynee, A. Aydda, I. T. Hwang et al., "Uncertainty reduction of unlabeled features in landslide inventory using machine learning t-SNE clustering and data mining Apriori association rule algorithms," *Applied Sciences-Basel*, vol. 11, no. 2, p. 556, 2021.
- [32] X. G. Guo and Y. P. Fan, "Research on tax evasion identification path of tax system based on big data," *Mathematics in Practice and Theory*, vol. 48, no. 3, pp. 92–100, 2018.
- [33] T. J. Li and D. W. Yan, "Research on Weibo recommendation based on emotional weighted association rules," *Data Analysis and Knowledge Discovery*, vol. 4, no. 4, pp. 27–33, 2020.
- [34] B. Y. Chen, J. Ding, and S. N. Chen, "Selection of key incentives for power production safety accidents based on association rule mining," *Electric Power Automation Equipment*, vol. 38, no. 4, pp. 68–74, 2018.
- [35] D. Tian, Y. Shen, M. C. Li, and S. Han, "An intelligent data mining approach of text entity knowledge from construction documents of concrete dam," *Journal of Hydroelectric Engineering*, vol. 40, no. 6, pp. 139–151, 2021.
- [36] L. Q. You, X. X. Li, Y. Q. Li, F. Li, and D. Liu, "Correlation analysis of cigarette physical indexes based on Apriori association rules," *Light Industry Science and Technology*, vol. 37, no. 3, pp. 88–92, 2021.
- [37] F. Li, J. L. Guo, and L. M. Tan, "Association analysis of company shareholders based on Apriori algorithm," *Software Guide*, vol. 20, no. 3, pp. 106–109, 2021.
- [38] W. J. Cui, X. N. Ma, and S. Q. Sun, "Railway network security early warning method based on improved Apriori algorithm," *Railway Computer Application*, vol. 30, no. 3, pp. 59–64, 2021.
- [39] Y. Q. Zhang, H. Q. Wang, S. Z. Wang, and L. Q. Gao, "Mining method for parking space idle pattern based on Hadoop," *Journal of Tianjin Normal University (Natural Science Edition)*, vol. 41, no. 1, pp. 69–74, 2021.
- [40] J. W. Xia, B. X. Liu, and C. F. Luo, "Analysis of mobile APP and advertising investment based on Apriori algorithm," *China Management Information*, vol. 24, no. 2, pp. 62–64, 2021.
- [41] R. N. Yang, *Research and software realization of remote supervision and control system based on web*, Tianjin University of Technology Master's Degree, 2008.
- [42] H. A. Kang, "Developing mobile apps in HTML5," *Science and Technology Innovation Herald*, vol. 7, pp. 30–31, 2012.
- [43] X. Qiao, J. Chen, P. Gu, and Y. Li, "Opening up telecom networks with a lightweight web element service cloud for ordinary users in the web 2.0 era," *IEEE Communications Magazine*, vol. 52, no. 10, pp. 127–133, 2014.
- [44] C. Borgelt and R. Kruse, "Induction of association rules: Apriori implementation," *Leukemia Research*, vol. 8, no. 6, pp. 937–944, 1984.
- [45] R. Perego, S. Orlando, and P. Palmerini, "Enhancing the Apriori algorithm for frequent set counting," in *Data Warehousing and Knowledge Discovery*, vol. 2114, pp. 71–82, Springer, Berlin, Heidelberg, 2001.
- [46] Y. Z. Wu, "Design and implementation of improved Apriori algorithm in telecommunication alarm system," *Computer Knowledge and Technology*, vol. 7, no. 36, pp. 9423–94237, 2011.
- [47] Y. Huang, *Research and application of association rule analysis in telecommunication warning system*, University of Electronic Science and Technology of China Master's Degree, 2007.

Research Article

An Implicit Preference-Aware Sequential Recommendation Method Based on Knowledge Graph

Haiyan Wang ^{1,2}, Kaiming Yao ^{1,2}, Jian Luo ¹ and Yi Lin ^{1,2}

¹School of Computer Science, Nanjing University of Posts and Telecommunications, Nanjing 210023, China

²Jiangsu Key Laboratory of Big Data Security and Intelligent Processing, Nanjing 210023, China

Correspondence should be addressed to Haiyan Wang; wanghy@njupt.edu.cn

Received 27 May 2021; Accepted 2 August 2021; Published 16 August 2021

Academic Editor: Honghao Gao

Copyright © 2021 Haiyan Wang et al. This is an open access article distributed under the Creative Commons Attribution License, which permits unrestricted use, distribution, and reproduction in any medium, provided the original work is properly cited.

Sequential recommendation system has received widespread attention due to its good performance in solving data overload. However, most of the sequential recommendation methods assume that user's preferences only depend on specific items in the current sequence and do not consider user's implicit interests. In addition, most of the previous works mainly focus on exploiting relationships between items in the sequence and seldom consider quantifying the degree of preferences for items implied by user's different behaviors. In order to address these above two problems, we propose an implicit preference-aware sequential recommendation method based on knowledge graph (IPAKG). Firstly, this method introduces knowledge graph to exploit user's implicit preference representations. Secondly, we integrate recurrent neural network and attention mechanism to capture user's evolving interests and relationships between different items in the sequence. Thirdly, we introduce the concept of behavior intensity and design a behavior activation unit to exploit the degree of preferences for items implied by a user's different behaviors. Through the activation unit, the user's preferences on different items are further quantified. Finally, we conduct experiments on an Amazon electronics dataset and Tmall dataset to evaluate the performance of our method. Experimental results demonstrate that our proposed method has better performance than those baseline methods.

1. Introduction

With the rapid development of online platforms in recent years, the problem of information overload has become more and more serious. Recommendation systems, aimed at mining user's preferences to recommend personalized goods or services for the user in the massive data, have achieved widespread attention and great success due to its practicality and effectiveness. So far, recommendation systems have been widely used in various fields, including e-commerce, social media, short videos, and searching engines. Traditional recommendation systems mainly focus on static preferences of users. In order to better model the dynamic and evolving interests of users, sequential recommendation is proposed. Sequential recommendation, as a type of recommendation system, recommends personalized items for users based on their historical interaction behaviors [1, 2].

Traditional recommendation methods (such as collaborative filtering and matrix factorization) mainly focus on

the static interaction of user-items, so it is difficult to meet the requirements of sequential recommendation. In order to model the sequential task, a series of models are proposed. The FPMC [3] model is based on Markov chain and matrix factorization. The main problem of this model is that this method is still modeling the static preferences of users. With the rapid development of neural networks, neural network-based models have been widely used in sequential recommendation tasks, such as recurrent neural network-based models [4–6] and convolutional neural network-based models [7]. The recurrent neural network-based model expresses the user's interest as a hidden state vector by encoding the user's historical interaction records. This method can capture the user's dynamic and evolving interest preferences, but due to the characteristics of the recurrent neural network, this method is difficult to capture the long-term dependence of user preferences. The models based on the convolutional neural network express sequential features and capture the complex relevance of items by directly modeling paired item

relationships. The attention mechanism has received widespread attention due to its high efficiency. The sequential recommendation method based on self-attention [8–12] has also been widely proposed. This method uses the attention mechanism to capture the relationship between items in the sequence, solving the problem of long dependence of the recurrent neural network models. The above-mentioned methods have achieved good performance in the sequential recommendation task. However, we emphasize that there are two main problems with the above methods. Firstly, these methods often assume that the user’s interest only depended on the certain item in the current sequence and do not consider the user’s implicit interest. For example, in movie recommendation scenarios, although the user clicks on the movie *Wonder Woman*, this does not mean that the user likes the movie itself, and it is possible that the user is only interested in the actors in the movie. Therefore, it is of great importance to exploit the implicit preferences of users. Secondly, in the sequential recommendation, most of the past work mainly focus on the relationship between different items in current recommendation sequence and seldom consider the information implied by the user’s behavior, let alone quantify this behavioral information. We argue that the user’s behavior plays an important role in the sequential recommendation. Different behaviors imply the degree of the user’s preferences for specific items. For example, if the user bookmarks or purchases an item, it can be considered that the user has a strong interest on the current item; if the user just clicks on a certain item, it can be considered that the user is just interested in this item; and if the user skips an item, it can be considered that the user has no preference for the item at all. The interaction process is shown in Figure 1. Therefore, it is very significant to quantify the user’s different behavior information. We emphasize the integration of users’ implicit preferences and behavioral intensity to improve the performance of the model.

In view of the above analysis, we propose an implicit preference-aware sequential recommendation method based on knowledge graph. Firstly, we introduce knowledge graph-embedding technology. The knowledge graph contains comprehensive auxiliary information about the item, which helps to further expand the item representation space and exploit the user’s deeper implicit preferences, so that we can obtain high-quality entity representation. Secondly, we introduce the concept of behavior intensity and design a behavioral activation unit to exploit the degree of preferences implied by the user’s different behaviors. By introducing the behavioral activation unit, the user’s microbehavior information is further mined and utilized. Finally, we integrate recurrent neural network and attention mechanism to capture the user’s dynamically evolving interests and the relationship between different items in the sequence. In order to evaluate the performance of our proposed IPAKG model, we conduct experiments on two real datasets, and the experimental results proved the efficiency of our proposed model.

The main contributions of this paper are as follows:

- (i) We proposed the IPAKG model, which introduces a knowledge graph to exploit a user’s implicit prefer-

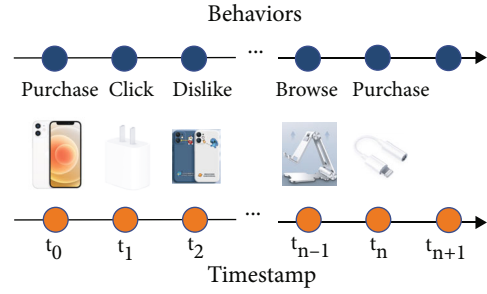


FIGURE 1: An example of user’s interaction process.

ence representations. In addition, we integrate a recurrent neural network and attention mechanism to capture the user’s evolving interest and the relationship between different items in the sequence

- (ii) In order to exploit the degree of preferences implied by the user’s different microbehaviors, we design a behavior activation unit, through which the degree of preferences implied by the user’s different microbehaviors is further quantified
- (iii) We conduct extensive experiments on two real datasets, and the experimental results demonstrate that the IPAKG model has a great improvement over the baseline models

The remainder of this paper is organized as follows. Previous research on sequential recommendation methods and related technologies is discussed in Section 2. In Section 3, the proposed IPAKG approach is explained. Then, in Section 4, the experiments are described and the results are analyzed. Finally, the conclusion and future work are discussed in Section 5.

2. Related Work

In this section, we briefly review three aspects related to our work, namely, general recommendation, sequential recommendation, and knowledge graph-based recommendation methods.

2.1. General Recommendation. Early recommendation systems usually use collaborative filtering models [13] and their variants for recommendation. These models predict a user’s ratings for items by mining the user’s long-term stable preference information, but there are cold-start problems in collaborative filtering-based models. In order to solve the problem of data sparsity, a model based on matrix factorization [14] is proposed. In addition, Yang et al. [15] proposed a new sparsity alleviation algorithm for the recommendation model to solve the sparsity problem by addressing the zero values. With the development of deep learning, the models based on deep neural networks are widely used in recommendation systems. Wu et al. [16] proposed a collaborative noise reduction autoencoder model called CDAE, which combines the traditional matrix factorization model with a deep neural network and predicts the user’s rating information through an autoencoder. Lian et al. [17] further

improved the recommendation performance by combining the traditional decomposition machine model with the deep learning model. Togashi et al. [18] proposed a knowledge graph- (KG-) aware recommender based on graph neural networks, which augments labelled samples through pseudo-labelling to tackle the cold-start problems for new users/items. The above-mentioned models show that deep learning-based methods have greater flexibility in learning user and item representations.

2.2. Sequential Recommendation. Given the user's historical interaction records, the purpose of sequential recommendation methods is to predict the items that the user may take interest in in the future based on the historical interaction data. The early sequential recommendation task is mainly based on the Markov chain. Rendle et al. [3] proposed a model called FPMC, which includes both a general Markov chain and a conventional matrix factorization model and recommends the next item to the user through the item information of the user's interaction in the past period of time. He and McAuley [19] combined Markov chains with similarity-based methods and proposed the fossil model, which can significantly improve recommendation performance, especially on sparse datasets. With the development of deep learning, sequential recommendation methods based on deep learning are widely used. Donkers et al. [4] used a recurrent neural network for sequential recommendation and achieved a better performance boost. Quadrana et al. [20] proposed a hierarchical RNN model for cross-session transmission, which can relay the potential hidden state of the terminal RNN between user sessions. Tang and Wang [21] applied the convolutional neural network to sequential recommendation and regarded the embedding representation of the past L items in the user sequence as a photo, which was used as the input of CNN. Thanks to the excellent performance of the attention mechanism in natural language processing, many people apply the attention mechanism to the recommendation system. Kang and McAuley [22] proposed the SASRec model, which mainly uses a two-layer transformer decoder to model the user's sequential behavior information. Sun et al. [23] applied the BERT model to recommendations to encode user preferences. Zhou et al. [24] proposed the RIB model, which models inherently the sequence of microbehaviors and their effects, but their method did not fully explore the user's implicit preference information. Gu et al. [25] adopted LSTM to model the user's microbehaviors. However, they ignored the different transition pattern between items and behaviors. In addition, their method does not take into account the implicit preference information of users. Meng et al. [26] incorporated user microbehaviors and item knowledge into multitask learning for session-based recommendation, which achieved good performance.

2.3. Knowledge Graph-Based Recommendation. With the development of knowledge graph technology, many people consider combining the knowledge graph with the recommendation system and improve the performance of the recommendation system by mining multiple association

relationships between items. Wang et al. [27] proposed a model called the Knowledge Path Recursive Network (KPRN), which uses knowledge graphs for recommendation. KPRN can generate path representations by combining the semantics of entities and relationships, using the order dependency in the path. The relationship can be effectively inferred on the path to infer the basic principles of the interaction between the user and the item. Lei et al. [28] proposed a conversational path reasoning (CPR) model, which can model conversational recommendation as a graphical interactive path reasoning problem. Through user feedback, this method traverses the attribute vertices in an explicit way. At the same time, by using the graph structure, CPR can delete many irrelevant candidate attributes, so that it can hit the attributes that users prefer. Wang et al. [29] capture the rich relationship between user and item by extracting paths from the knowledge graph. The above work combines the knowledge graph and the recommendation system to improve the performance of recommendation and has good interpretability. However, due to the problem of model selection, it is difficult to determine whether these methods effectively capture high-order associations.

3. Proposed Method

In this section, we introduce our proposed IPAKG model in detail. Our purpose is to provide users with a number of recommended items based on their historical interaction records. We first state the notations and task definition, then describe our methods in detail, and finally state the optimization methods.

3.1. Notations and Task Definition

3.1.1. Notations. We first define the notations that need to be used in this paper. In a sequential recommendation system, given user set $U = \{u_1, u_2, \dots, u_{|U|}\}$, item set $I = \{i_1, i_2, \dots, i_{|I|}\}$, where $|U|$ and $|I|$ represent the number of elements in the user collection and the item collection, respectively. The historical item interaction sequence of user u can be $\{i_1^{(u)}, \dots, i_t^{(u)}, \dots, i_T^{(u)}\}$, where $i_t^{(u)}$ indicates that user u interacted with item i at time t , and T indicates the interaction length of the current user. The time here is relative time. In addition, since we consider the influence of user behavior on preferences, we define the behavior set $B = \{b_1, \dots, b_i, \dots, b_{|B|}\}$, where b_i represents the behavior imposed by the user on the item, and $|B|$ represents the total number of behaviors. Behavior set B has only a few finite elements, such as purchases, views, clicks, carts, and comments. Different behaviors represent the user's preferences for the current item. Based on the above definition, the behavior interaction sequence of user u can be represented by $\{b_1^{(u)}, \dots, b_t^{(u)}, \dots, b_T^{(u)}\}$. In addition to the user's item interaction sequence and behavior interaction sequence, the knowledge graph G is also required in our sequential recommendation task. The knowledge graph G is defined on the head entity set V and the relation entity set R and is composed of a large number of triples, namely, $G = \{(h, r, t) \mid h, t \in V, r \in R\}$, where h

TABLE 1: Notations.

Symbol	Description
U	User set
I	Item set
B	Behavior set
$ U $	Number of user set
$ I $	Number of item set
$ B $	Number of behavior set
i_t^u	Item i that user u interacted with at time t
b_t^u	Behavior b that user u imposed at time t
G	Knowledge graph
V	Entity set in G
R	Relationship set in G
h	Head entity in knowledge graph
t	Tail entity in knowledge graph
r	Relationship between head and tail entity
W^r	Transformation matrix of relationship in G
e^h	Embedding of head entity in G
e^t	Embedding of tail entity in G
e^r	Embedding of relation entity in G
W^Q, W^K, W^V	Linear mapping matrices
W_z, W_r, W_h	Parameter matrices
b_z, b_r, b_h	Deviation parameters
α^k	Attention weight
e_X'	Final preference representation
L_G	Loss function related to knowledge graph
L_p	Loss function related to model
L	Final loss function
λ	Regularization coefficient

and t represent the head entity and the tail entity, respectively, and r represents the relationship between the head entity and the tail entity; a knowledge graph triplet states a factual relationship. For example, the triple (Tenet, isDirectedBy, ChristopherNolan) indicates that the movie Tenet is directed by Christopher Nolan. Since our item set I needs to be associated with the knowledge graph, we can think of I as a subset of the knowledge graph G , that is, $I \subset G$. Through the knowledge graph, we can expand the representation space of the item and mine the implicit preferences of users. Relevant symbol definitions are summarized in Table 1.

3.1.2. Task Definition. Based on the above definition, given the user's historical item interaction sequence $\{i_1^u, \dots, i_t^u, \dots, i_T^u\}$, the history behavior interaction sequence corresponding to the item $\{b_1^u, \dots, b_t^u, \dots, b_T^u\}$, the user's portrait, and the knowledge graph G , the task of sequential recommendation is to predict the item i_{T+1}^u that the user u may interact at time-step $T + 1$.

3.2. Implicit Preference Awareness Sequential Recommendation Model Based on Knowledge Graph. Our model architecture is shown in Figure 2. Our model integrates the knowledge graph information and the user's microbehavior characteristics, which can efficiently expand the user's preference representation space. In addition, through the behavioral activation unit, it can capture the degree of the user's preferences for the certain item. Our model mainly consists of five parts, namely, the knowledge graph-embedding representation layer, preference dependence-aware layer, preference-evolving layer, behavior preference activation layer, and preference attention layer. In the following part, we will elaborate on each component separately.

3.2.1. Knowledge Graph-Embedding Representation Layer. In order to fully exploit the user's implicit preferences, we introduce the knowledge graph-embedding technology. The knowledge graph-embedding technology can map the entities and relationships in the graph to a vector representation, while retaining the information of the graph structure, which is an efficient representation method. In order to map the entities and relationships in the knowledge graph into vector representations, we use the widely used knowledge graph-embedding technology TransR method [30], for the knowledge graph triples $(h, r, t) \in G$, $e_h, e_t \in R^k$ represent the embedding representation of the head entity h and the tail entity t in the knowledge graph, and $e_r \in R^m$ represents the embedding representation of the relation r in the knowledge graph. TransR learns the embedding representation of entities and relationships by optimizing $e_h' + e_r \approx e_t'$, where e_h' and e_t' are the mapping representations of e_h and e_t in the relational space r , respectively. Therefore, given the knowledge graph triples (h, r, t) , the score function can be defined as follows:

$$s(h, r, t) = \|W^r e_h + e_r - W^r e_t\|_2^2. \quad (1)$$

Among them, $W^r \in R^{(k \times d)}$ is the transformation matrix of relation r . The purpose is to map the entity from the d -dimensional space to the k -dimensional space of the relation r . The smaller the above-mentioned score function, the more likely is the triplet (h, r, t) to appear in the knowledge graph G . Through the knowledge graph embedding, we obtain the embedding representation vector e_i of the items in the user interaction sequence.

3.2.2. Preference Dependence-Aware Layer. In order to learn the dependencies between different items in the sequence, we introduce the multihead self-attention mechanism [31]. The self-attention mechanism captures the relationship between items in the sequence to improve the presentation ability of items and, at the same time, eliminates the sequence noise data. The scaled dot-product attention is defined as follows:

$$\text{Attention}(Q, K, V) = \text{softmax}\left(\frac{QK^T}{\sqrt{d}}\right)V, \quad (2)$$

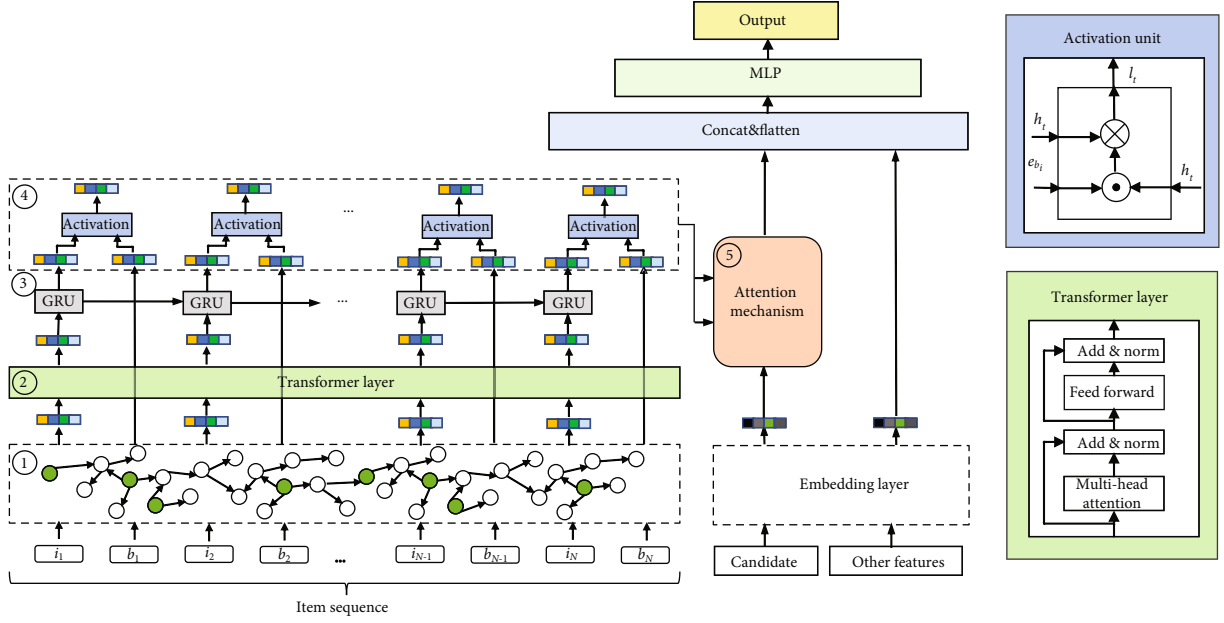


FIGURE 2: Framework of IPAKG. There are mainly five components in IPAKG, including knowledge graph-embedding representation layer, preference dependence-aware layer, preference-evolving layer, behavior preference activation layer, and preference attention layer. The prediction score of each item is obtained through the multilayer perceptron.

where $Q = EW^Q$ means queries; $K = EW^K$ means keys; $V = EW^V$ means values; W^Q , W^K , and W^V are linear mapping matrices; and $E = [e_{i_1}; \dots; e_{i_r}]$ is the stacked matrix of the embedded vector of the knowledge graph. The self-attention of multiple heads can be expressed in the following form:

$$\text{MultiHead}(E) = \text{Concat}(\text{head}_1, \text{head}_2, \dots, \text{head}_h)W^H, \quad (3)$$

$$\text{head}_i = \text{Attention}\left(EW_i^Q, EW_i^Q, EW_i^Q\right), \quad (4)$$

where h is the number of heads. Then, the above results are passed through pointwise Feed-Forward Networks (FFN) to further increase the nonlinearity of the model. In order to avoid over-fitting and to learn feature representation hierarchically, we use dropout and LeakyReLU, so the output of self-attention and FNN is as follows:

$$M = \text{LayerNorm}(E + \text{Dropout}(\text{MultiHead}(E))), \quad (5)$$

$$F = \text{LayerNorm}(M + \text{Dropout}(\text{LeakyReLU}(MW^1 + b^1)W^2 + b^2))). \quad (6)$$

Among them, W^1 , b^1 , W^2 , and b^2 are learning parameters. Through the preference dependence-aware layer, the item representation in the sequence contains the relationship information between different items.

3.2.3. Preference-Evolving Layer. The user's sequential interaction behavior includes the dynamic changes of user preferences and the preference dependencies. Therefore, in the preference-evolving layer, we model the dynamic evolution of preferences and the dependencies between preferences

through recurrent neural networks. We use GRU to model the dynamic evolution of the user's preferences and the dependence between preferences. Compared with LSTM, GRU has fewer parameters, so the convergence speed is faster and the iteration speed can be accelerated. The formula for GRU is as follows:

$$z_t = \sigma(W_z \cdot [h_{t-1}, e_{i_t}] + b_z), \quad (7)$$

$$r_t = \sigma(W_r \cdot [h_{t-1}, e_{i_t}] + b_r), \quad (8)$$

$$\tilde{h}_t = \tanh(W_h[r_t * h_{t-1}, e_{i_t}] + b_h), \quad (9)$$

$$h_t = (1 - z_t) * h_{t-1} + z_t * \tilde{h}_t, \quad (10)$$

where σ is the sigmoid activation function; $*$ is the element-wise multiplication of the vector; W_z , W_r , and $W_h \in R^{d_H \times d_I}$ are the parameter matrix; b_z , b_r , and $b_h \in R^{d_H}$ are the deviation parameters; e_{i_t} is the input of the GRU; and h_t is the t^{th} hidden state vector. Through the recurrent neural network, the user's dynamic evolving preference and dependence between different preferences can be obtained.

3.2.4. Behavior Preference Activation Layer. In sequential recommendation, the behaviors that users impose on different items are different, and such different behaviors imply the degree of preferences for the certain item. For example, the user's purchase behavior implies that the user has a strong preferences or demand for the current item, while browsing behavior merely indicates that the user has certain preferences for the current item. Therefore, it is of great significance to quantify user's different behavior information. In order to model the user's preference intensity implied by the user's different behavior, we introduce the behavioral

preference activation unit. The formula of the behavioral activation unit is as follows:

$$I_i = (h_t \odot e_{b_i}) \cdot h_t. \quad (11)$$

Among them, \odot represents the inner product of the vector, and e_{b_i} represents the embedded representation of the user behavior. Through the behavior activation unit, we quantify the user's different behaviors into the user's degree of preferences for the current item.

3.2.5. Preference Attention Layer. The similarity between the target item and the items in the sequence significantly affects whether the user will interact with the target item. In order to obtain the influence weight of different items in the user's historical interaction sequence on the target item, we introduce the attention mechanism [32]. The preferences after adjustment by the attention mechanism is expressed as follows:

$$\alpha_k = \frac{\exp(I_k W_{e_x})}{\sum_k^T \exp(I_k W_{e_x})}, \quad (12)$$

$$e'_x = \sum_k^T \alpha_k I_k. \quad (13)$$

Among them, W is the parameter matrix, e_x is the embedded representation of the target item, and e'_x is the final preference representation of the user. Finally, the feature-embedding vector, preference representation vector and target item-embedding vector undergo Concat and flatten operations, and then the final prediction result is obtained through the multilayer perceptron.

3.3. Optimization. Our objective function includes the knowledge graph-embedding loss part and the prediction loss part. In the knowledge graph-embedding part, we use the TransR method, which considers the relative order relationship between valid triples and invalid triples and uses the pairwise ranking loss function to make the difference between the scores of these two triples as large as possible. The loss function can be expressed as

$$L_G = \sum_{h,r,t,t'} -\ln \sigma(s(h,r,t') - s(h,r,t)). \quad (14)$$

Among them, $T = \{(h,r,t,t') \mid (h,r,t) \in G, (h,r,t') \notin G\}$, triples (h,r,t') are obtained by randomly replacing the tail entity of the triple (h,r,t) in the knowledge graph G , and $\sigma(\dots)$ is the sigmoid activation function. In order to predict whether a certain user will interact with the item, we treat it as a two-classification problem. In order to train the model, we use the cross-entropy loss function,

$$L_p = -\frac{1}{N} \sum_{(x,y) \in D} (y \log p(x) + (1-y) \log (1-p(x))). \quad (15)$$

TABLE 2: Statistics of Amazon (electronics) and Tmall datasets.

	Amazon (electronics)	Tmall	
User-item interactions	#users	11032	33252
	#items	8865	40865
	#ratings	223654	863252
	#sparsity	99.79%	99.93%
Knowledge graph	#entity	43261	145806
	#relation	22	26
	#triple	924352	2863546

Among them, D is the training set; the number of samples is N ; y is the real label, which represents whether the user has interacted with the item; and $p(x)$ is the output value of the sigmoid function, which represents the current item predicted by the model to be interacted by the user probability. The final objective function can be expressed as

$$L = L_G + L_p + \lambda \|\theta\|_2^2. \quad (16)$$

Among them, λ is the regularization coefficient, and θ is the model parameter set. In order to prevent over-fitting, we adopt the L_2 regularization. In training, we use minibatch Adam [33] to optimize the embedding loss and prediction loss. Adam is a widely used optimizer that can adaptively control the learning rate.

4. Experiment

In this section, we first introduce the experimental dataset, the baseline model, and the evaluation metrics of the experiment, and then, we analyze the experimental results and compare them with the baseline models. In addition, we also conduct an ablation test.

4.1. Datasets and Metrics. We use two commonly used public datasets to verify the effect of my proposed IPAKG model. The statistical information of the dataset is shown in Table 2. The first dataset is the Amazon dataset which comes from the Amazon e-commerce platform; this dataset contains millions of raw data and review information about products. It is a widely used benchmark dataset [34, 35]. We conducted experiments on the Amazon electronics dataset, a subset of the Amazon dataset. In order to adapt to our scenario, we processed the data to filter out those users with less than 30 item interactions and those items with less than 20 occurrences. The second dataset is Tmall that comes from the Tmall e-commerce platform and is a competition dataset provided by IJCAI-15. This dataset contains user behavior information, such as clicks, browses, and purchases. We filter out those users with less than 40 item interactions and those items with less than 20 occurrences. For each user, we sorted the items according to the timestamp.

In order to construct the knowledge base, we refer to the past work [36] and adopt Freebase data dumps. In order to collect relevant factual information from Freebase, we keep those triples associated with the entities mapped by the items

in the dataset. Note that not all knowledge in the knowledge base is useful, so we filter out the relationships that appear with low frequency. In order to evaluate our method, we refer to past work [5, 37] and adopt a series of widely used evaluation metrics, including the hit ratio (HR), normalized discounted cumulative gain (NDCG), and mean reciprocal rank (MRR).

- (i) *HR*: hit ratio gives the percentage of users that can receive at least one correct recommendation, which has been widely used in previous work.

$$\text{HR@K} = \frac{1}{M} \sum_u I\left(\left|R_u \cap T_u\right|\right), \quad (17)$$

where $I(x)$ is an indicator function whose value is 1 when $x > 0$ and 0 otherwise. R_u is the generated recommendation list for user u ; T_u is the item set that user u interacted with in the test set. M is the number of samples.

- (ii) *NDCG*: normalized discounted cumulative gain evaluates ranking performance by taking the positions of correct items into consideration.

$$\text{NDCG@K} = \frac{\text{DCG}}{\text{IDCG}}, \quad (18)$$

$$\text{DCG@K} = \sum_{i=1}^K \frac{\text{rel}_i}{\log_2(i+1)}, \quad (19)$$

where rel_i represents the relevance of the i^{th} recommendation items. If the i^{th} item is selected by the user, then $\text{rel}_i = 1$; otherwise, $\text{rel}_i = 0$. IDCG is a normalized DCG.

- (iii) *MRR*: mean reciprocal rank is a popular ranking metric to measure recommendation quality by finding out how far from the top of the recommendation list the first successfully predicted location is.

$$\text{MRR@K} = \frac{1}{M} \sum_u \frac{1}{\text{ran } k_i}, \quad (20)$$

where rank_i refers to the rank position of the first relevant item for target user u in the recommended list.

4.2. Baseline and Parameter Settings. In order to prove the effectiveness of our proposed method, we compared the proposed IPAKG method with the following methods.

- (i) *FM* [38]: this is a typical similarity-based method that takes into account the second-order interactive information of the input features. In addition, this method is the basis of other baselines and has excellent performance on many benchmark datasets.

- (ii) *BPR* [14]: BPR is a classic method that uses matrix factorization to learn personalized ranking from implicit feedback.
- (iii) *GRU4Rec* [5]: this method improves the GRU network for session-based recommendation, which uses a session-parallel minibatch training process and also uses ranking-based loss functions to train the model.
- (iv) *GRU4Rec+* [39]: this is an improved version of GRU4Rec by implementing a new loss function and sampling approach
- (v) *SASRec* [22]: this method uses a self-attention mechanism with a left-to-right transformer to capture useful patterns in the user's sequences.
- (vi) *BERT4Rec* [23]: this method uses the bidirectional transformer model to learn the temporal behavior of users, which is a state-of-the-art sequential recommendation method.
- (vii) *KTUP* [36]: this is a translation-based user preference model, which transfers the entity embedding and relation embedding learned from knowledge graph to the user preference model and simultaneously training two different tasks.

Among them, BPR and FM are traditional recommendation methods that only consider user feedback without considering sequential information, while GRU4Rec, GRU4Rec+, SASRec, and BERT4Rec are sequential recommendation methods based on neural networks, and KTUP is a recommendation method based on neural networks and knowledge graph.

The experimental environment is CPU Intel (R) Core (TM) i9-9980XE @3.00 GHz, with 128 GB memory and two Titan XP graphics cards. We use the scientific computing library NumPy and SciPy for data processing and use TensorFlow to implement our algorithm. We randomly divide the training set, validation set, and test set with the ratio of 7:2:1 and ensure that each user has at least one item in the test set. For hyperparameters, we apply a grid search to find the best settings for each task. Specifically, the learning rate is searched in $\{0.0001, 0.001, 0.005, 0.01, 0.05\}$, the coefficient of L_2 regularization is searched in $\{10^{-5}, 10^{-4}, 10^{-3}, \dots, 10^1, 10^2\}$, the embedding size is searched in $\{32, 64, 96, 128, 256\}$, and the optimization methods include Adam and SGD. Finally, the learning rate is set to 0.001, L_2 coefficient is set to 10^{-3} , embedding size is set to 96, and the optimization method is set to Adam. For the rest of those parameters, we follow the original way for the setup of the parameters which have been proposed by their authors.

4.3. Performance Evaluation. We compare the performance of our proposed IPAKG method with all other baselines. The results on two datasets are reported on Table 3. From the results, we have the following observations.

In general, our proposed model obtains the best results in all five evaluation metrics on two datasets, which proves the

TABLE 3: Performance comparison of difference recommendation methods.

Models	Amazon (electronics)					Tmall				
	MRR	HR@10	HR@20	NDCG@10	NDCG@20	MRR	HR@10	HR@20	NDCG@10	NDCG@20
FM	0.0307	0.0473	0.0501	0.0387	0.0465	0.0865	0.1108	0.1193	0.0921	0.0976
BPR	0.0421	0.0787	0.0812	0.0589	0.0682	0.1123	0.1425	0.1634	0.1236	0.1398
GRU4Rec	0.0611	0.0923	0.1011	0.0724	0.0854	0.1522	0.1822	0.1903	0.1622	0.1701
GRU4Rec+	0.0786	0.1087	0.1103	0.0822	0.0943	0.1632	0.1944	0.2011	0.1776	0.1804
SASRec	0.0903	0.1203	0.1298	0.0921	0.0987	0.1782	0.2101	0.2187	0.1856	0.1911
BERT4Rec	0.0976	0.1358	0.1398	0.1013	0.1127	0.1956	0.2217	0.2302	0.2014	0.2176
KTUP	0.1067	0.1396	0.1423	0.1201	0.1288	0.2189	0.2298	0.2354	0.2133	0.2199
IPAKG	0.1123	0.1487	0.1533	0.1286	0.1301	0.2234	0.2407	0.2501	0.2276	0.2315

TABLE 4: Ablation study on two datasets.

Models	Amazon (electronics)					Tmall				
	MRR	HR@10	HR@20	NDCG@10	NDCG@20	MRR	HR@10	HR@20	NDCG@10	NDCG@20
IPAKG-B-KG	0.0776	0.0989	0.1043	0.0824	0.0973	0.1612	0.1844	0.1911	0.1736	0.1802
IPAKG-KG	0.0813	0.1058	0.1298	0.0913	0.1027	0.1812	0.2001	0.2187	0.1826	0.1896
IPAKG-B	0.0967	0.1226	0.1401	0.1001	0.1138	0.2011	0.2298	0.2354	0.2119	0.2107
IPAKG	0.1123	0.1487	0.1533	0.1286	0.1301	0.2234	0.2407	0.2501	0.2276	0.2315

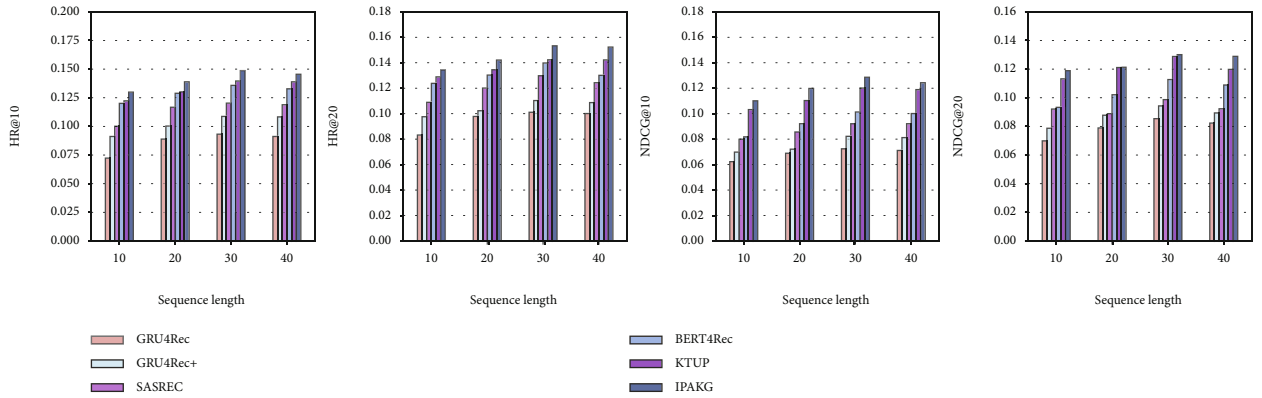


FIGURE 3: The effect of sequence length on results (Amazon electronics).

effectiveness of our model. Specifically, firstly, the IPAKG model and KTUP model both use the knowledge graph, but our model achieves better performance. This is mainly because our model uses the attention mechanism to model the interactive relationship and dynamic evolution of the user's preferences, which makes the user's preference representation more accurate. In addition, we also add user behavior information to model the user's preference degree on the certain item. Therefore, although our model and the KTUP model are both based on knowledge base technology, the model we proposed obtains better recommendation performance. Secondly, IPAKG has better performance compared to GRU4Rec and GRU4Rec+. One possible reason is that these two methods are based on conversational models and do not explicitly model the general preference information of users. Thirdly, our proposed method achieves better performance than SASRec and BERT4Rec which are based on the attention mechanism. One of the main reasons is that

our model integrates the information of the knowledge graph, through which the user's representation space are further expanded and the user's implicit preferences are fully exploited. Fourth, the above models obtain better experimental results on the Tmall dataset compared to the Amazon electronics dataset. This is mainly because the user interaction records of the Amazon electronics dataset are relatively sparse, which affects the representation of the data.

In addition, the performance of GRU4Rec+ on the above two datasets is significantly better than GRU4Rec. This is because GRU4Rec+ not only captures the sequence relationship in the user's interaction sequence but also has a better superior objective function. All the methods perform better than the traditional BPR and FM methods. This is because these two methods only model the user's general preferences and cannot model the user's sequential and dynamic preferences, which makes the preference representation insufficient. Furthermore, the main reason that the BERT4Rec

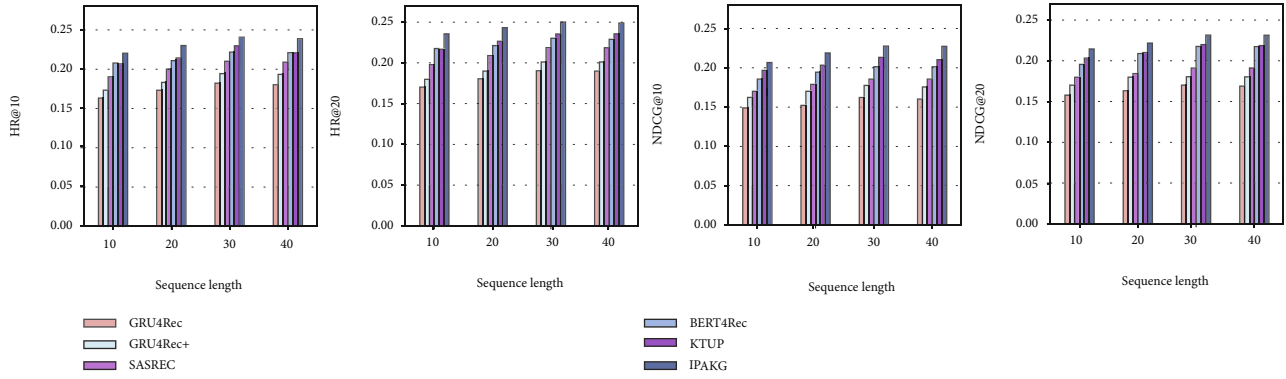
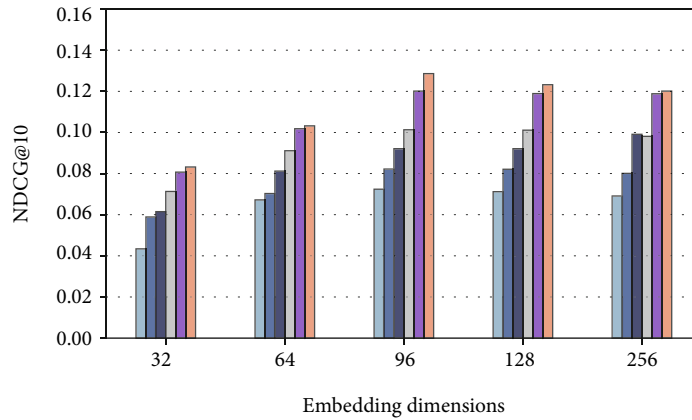
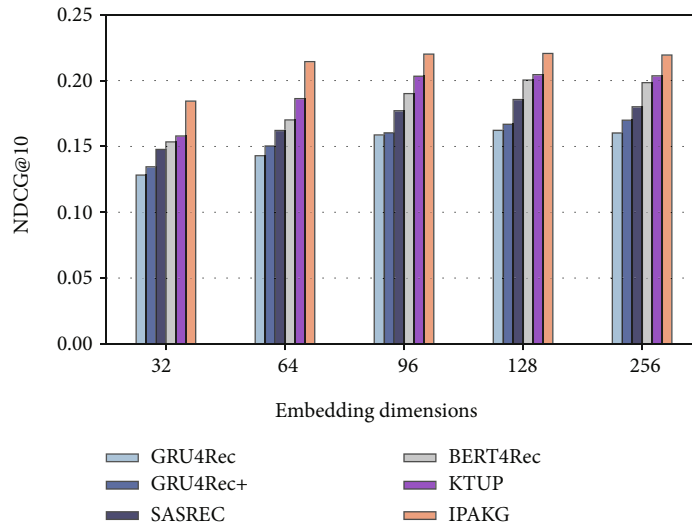


FIGURE 4: The effect of sequence length on results (Tmall).



(a) Amazon electronics



(b) Tmall

FIGURE 5: NDCG@10 values on different embedding dimensions.

model performs better than SASRec is that BERT4Rec can jointly predict the target item based on the context information on the left and right sides, so it can achieve better performance.

4.4. Ablation Study. In order to verify the contribution of each main module of our model to the overall performance,

we conduct an ablation study. We first remove the behavioral activation module separately from the original model, which means that we no longer consider the degree of preferences on items implied by the user’s different behaviors, and we call this modified model IPAKG-B. In order to verify the contribution of the knowledge graph-embedding technology to the model, we removed the knowledge graph-embedding model

and replaced it with conventional embedding technology. In this case, we did not consider the expansion information of the user's preferences and implicit preferences; we call this modified model IPAKG-KG. Finally, we remove the knowledge graph-embedding module and behavioral activation module at the same time, which means that the remaining model becomes a conventional sequential recommendation model based on recurrent neural network and attention mechanism. We call this modified model IPAKG-B-KG. The experimental results of the ablation study are shown in Table 4.

Based on the above experimental results, we have the following findings. First of all, when we removed the knowledge graph-embedding module and behavior activation module, the performance of the model is obvious decline, which means that both the knowledge graph-embedding module and the behavioral activation module play a significant role on the performance of the model. Secondly, the user's behavior activation module has a smaller impact on the model performance than the knowledge graph-embedding module. This means that the user's implicit preferences and expanded preferences have a more important influence on the recommendation. Thirdly, after removing the knowledge graph-embedding module and behavior activation module, the overall performance of the model is between GRU4Rec and GRU4Rec+. This is because that these models have a relatively similar structure, and thus, their performance is relatively similar.

4.5. Analysis of Main Parameters

4.5.1. The Effect of Sequence Length on Experimental Results.

In order to study the impact of different interaction lengths on the recommendation performance, we conduct experiments on two datasets. Figures 3 and 4 report the results of different sequence lengths on the performance of each model. It can be seen from the experimental results that for the Amazon electronics dataset, each model has better performance when the sequence length is about 40, and for the Tmall dataset, each model performs better when the sequence length is about 60. This means that the optimal sequence length depends on the characteristics of the dataset. When the length of the sequence is too short, the model only capture the user's recent preferences, and when the length of the sequence is too long, certain noise data may be introduced, both of which are not conducive to the performance of the model.

4.5.2. The Impact of Embedding Dimensions on Results.

Figure 5 shows the impact of different embedding dimensions on the recommendation performance. The hidden dimension d varies from 32 to 256, while the other optimal hyperparameters remain unchanged. The most obvious observation from these subgraphs is that the performance of each model does not increase as the dimension increases. Larger hidden dimensions do not necessarily lead to better model performance, especially for these datasets with sparse data. This may be caused by overfitting. As can be seen from the figure, the knowledge graph-based methods (that is,

KTUP and IPAKG) have relatively better performance than other methods on the two datasets. For our proposed IPAKG model, even if the hidden dimension is relatively small, our model performance is relatively better than other models.

5. Conclusion

In this paper, we propose a novel sequential recommendation method called IPAKG based on knowledge graph for next-item recommendation task. This method expands the representation space of the item by introducing the knowledge graph-embedding technology and fully exploits user's implicit preferences. Furthermore, the user's sequential behavior information is modeled through the behavioral activation unit, by which the degree of the user's preferences on certain items is fully quantified, which makes the user's preference representation more accurate. The empirical results demonstrate that our model can significantly outperform the baseline models on two real-world datasets. In addition, we conduct a detailed analysis on the IPAKG model to illustrate the effectiveness of our method. At present, our method mainly considers the extended information of user interaction items but does not model the information of similar users. In the next step, we will consider using the knowledge graph to further model the information of similar users to further improve the performance of recommendation.

Data Availability

The original dataset used in this work is available from the corresponding author on request.

Conflicts of Interest

The authors declare that they have no conflicts of interest.

Acknowledgments

This work is supported partly by the National Natural Science Foundation of China under Grant No. 61772285 and the Jiangsu Key Laboratory of Big Data Security and Intelligent Processing.

References

- [1] B. Hidasi, M. Quadrana, A. Karatzoglou, and D. Tikk, "Parallel recurrent neural network architectures for feature-rich session-based recommendations," in *Proceedings of the 10th ACM conference on recommender systems*, pp. 241–248, New York, NY, USA, 2016.
- [2] P. Wang, J. Guo, Y. Lan, J. Xu, S. Wan, and X. Cheng, "Learning hierarchical representation model for nextbasket recommendation," in *Proceedings of the 38th International ACM SIGIR conference on Research and Development in Information Retrieval*, pp. 403–412, New York, NY, USA, 2015.
- [3] S. Rendle, C. Freudenthaler, and L. Schmidt-Thieme, "Factorizing personalized Markov chains for next-basket recommendation," in *Proceedings of the 19th international conference on World wide web*, pp. 811–820, New York, NY, USA, 2010.

- [4] T. Donkers, B. Loepp, and J. Ziegler, "Sequential user-based recurrent neural network recommendations," in *Proceedings of the Eleventh ACM Conference on Recommender Systems*, pp. 152–160, New York, NY, USA, 2017.
- [5] B. Hidasi, A. Karatzoglou, L. Baltrunas, and D. Tikk, "Session based recommendations with recurrent neural networks," 2015, <https://arxiv.org/abs/1511.06939>.
- [6] C.-Y. Wu, A. Ahmed, A. Beutel, A. J. Smola, and H. Jing, "Recurrent recommender networks," in *Proceedings of the tenth ACM international conference on web search and data mining*, pp. 495–503, New York, NY, USA, 2017.
- [7] A. Yan, S. Cheng, W.-C. Kang, M. Wan, and J. McAuley, "Cos-Rec: 2D convolutional neural networks for sequential recommendation," in *Proceedings of the 28th ACM International Conference on Information and Knowledge Management*, pp. 2173–2176, New York, NY, USA, 2019.
- [8] X. Huang, S. Qian, Q. Fang, J. Sang, and C. Xu, "CSAN: contextual self-attention network for user sequential recommendation," in *Proceedings of the 26th ACM international conference on Multimedia*, pp. 447–455, New York, NY, USA, 2018.
- [9] W. Ye, S. Wang, X. Chen, X. Wang, Z. Qin, and D. Yin, "Time matters sequential recommendation with complex temporal information," in *Proceedings of the 43rd International ACM SIGIR Conference on Research and Development in Information Retrieval*, pp. 1459–1468, New York, NY, USA, 2020.
- [10] C. Zhou, J. Bai, J. Song et al., "ATRank: an attention-based user behavior modeling framework for recommendation," *Proceedings of the AAAI Conference on Artificial Intelligence*, vol. 32, no. 1, 2018.
- [11] R. Ren, Z. Liu, Y. Li et al., "Sequential recommendation with self-attentive multi-adversarial network," in *Proceedings of the 43rd International ACM SIGIR Conference on Research and Development in Information Retrieval*, pp. 89–98, New York, NY, USA, 2020.
- [12] J. Li, Y. Wang, and J. McAuley, "Time interval aware self-attention for sequential recommendation," in *Proceedings of the 13th International Conference on Web Search and Data Mining*, pp. 322–330, New York, NY, USA, 2020.
- [13] Y. Koren, "Factorization meets the neighborhood: a multifaceted collaborative filtering model," in *Proceedings of the 14th ACM SIGKDD international conference on Knowledge discovery and data mining*, pp. 426–434, New York, NY, USA, 2008.
- [14] S. Rendle, C. Freudenthaler, Z. Gantner, and L. Schmidt-Thieme, "BPR: Bayesian personalized ranking from implicit feedback," 2012, <https://arxiv.org/abs/1205.2618>.
- [15] X. Yang, S. Zhou, and M. Cao, "An approach to alleviate the sparsity problem of hybrid collaborative filtering based recommendations: the product-attribute perspective from user reviews," *Mobile Networks & Applications*, vol. 25, no. 2, pp. 376–390, 2020.
- [16] Y. Wu, C. DuBois, A. X. Zheng, and M. Ester, "Collaborative denoising auto-encoders for top-n recommender systems," in *Proceedings of the ninth ACM international conference on web search and data mining*, pp. 153–162, New York, NY, USA, 2016.
- [17] J. Lian, X. Zhou, F. Zhang, Z. Chen, X. Xie, and G. Sun, "xDeepFM: combining explicit and implicit feature interactions for recommender systems," in *Proceedings of the 24th ACM SIGKDD International Conference on Knowledge Discovery & Data Mining*, pp. 1754–1763, New York, NY, USA, 2018.
- [18] R. Togashi, M. Otani, and S. Satoh, "Alleviating cold-start problems in recommendation through pseudo-labelling over knowledge graph," in *Proceedings of the 14th ACM International Conference on Web Search and Data Mining*, pp. 931–939, New York, NY, USA, 2021.
- [19] R. He and J. McAuley, "Fusing similarity models with Markov chains for sparse sequential recommendation," in *2016 IEEE 16th International Conference on Data Mining (ICDM)*, pp. 191–200, Barcelona, Spain, 2016.
- [20] M. Quadrana, A. Karatzoglou, B. Hidasi, and P. Cremonesi, "Personalizing session-based recommendations with hierarchical recurrent neural networks," in *Proceedings of the Eleventh ACM Conference on Recommender Systems*, pp. 130–137, New York, NY, USA, 2017.
- [21] J. Tang and K. Wang, "Personalized top-n sequential recommendation via convolutional sequence embedding," in *Proceedings of the Eleventh ACM International Conference on Web Search and Data Mining*, pp. 565–573, New York, NY, USA, 2018.
- [22] W.-C. Kang and J. McAuley, "Self-attentive sequential recommendation," in *2018 IEEE International Conference on Data Mining (ICDM)*, pp. 197–206, Singapore, 2018.
- [23] F. Sun, J. Liu, J. Wu et al., "BERT4Rec: sequential recommendation with bidirectional encoder representations from transformer," in *Proceedings of the 28th ACM international conference on information and knowledge management*, pp. 1441–1450, New York, NY, USA, 2019.
- [24] M. Zhou, Z. Ding, J. Tang, and D. Yin, "Micro behaviors: A new perspective in e-commerce recommender systems," in *Proceedings of the eleventh ACM international conference on web search and data mining*, pp. 727–735, New York, NY, USA, 2018.
- [25] Y. Gu, Z. Ding, S. Wang, and D. Yin, "Hierarchical user profiling for e-commerce recommender systems," in *Proceedings of the 13th International Conference on Web Search and Data Mining*, pp. 223–231, New York, NY, USA, 2020.
- [26] W. Meng, D. Yang, and Y. Xiao, "Incorporating user micro-behaviors and item knowledge into multi-task learning for session-based recommendation," in *Proceedings of the 43rd International ACM SIGIR Conference on Research and Development in Information Retrieval*, pp. 1091–1100, New York, NY, USA, 2020.
- [27] X. Wang, D. Wang, C. Xu, X. He, Y. Cao, and T.-S. Chua, "Explainable reasoning over knowledge graphs for recommendation," *Proceedings of the AAAI Conference on Artificial Intelligence*, vol. 33, no. 1, pp. 5329–5336, 2019.
- [28] W. Lei, G. Zhang, X. He et al., "Interactive path reasoning on graph for conversational recommendation," in *Proceedings of the 26th ACM SIGKDD International Conference on Knowledge Discovery & Data Mining*, pp. 2073–2083, New York, NY, USA, 2020.
- [29] X. Wang, X. He, Y. Cao, M. Liu, and T.-S. Chua, "KGAT: Knowledge graph attention network for recommendation," in *Proceedings of the 795 25th ACM SIGKDD International Conference on Knowledge Discovery & Data Mining*, pp. 950–958, New York, NY, USA, 2019.
- [30] Y. Lin, Z. Liu, M. Sun, Y. Liu, and X. Zhu, "Learning entity and relation embeddings for knowledge graph completion," *Proceedings of the AAAI Conference on Artificial Intelligence*, vol. 29, no. 1, 2015.
- [31] A. Vaswani, N. Shazeer, N. Parmar et al., "Attention is all you need," 2017, <https://arxiv.org/abs/1706.03762>.

- [32] D. Bahdanau, K. Cho, and Y. Bengio, "Neural machine translation by jointly learning to align and translate," 2014, <https://arxiv.org/abs/1409.0473>.
- [33] D. P. Kingma and J. Ba, "Adam: a method for stochastic optimization," 2014, <https://arxiv.org/abs/1412.6980>.
- [34] R. He and J. McAuley, "Ups and downs: modeling the visual evolution of fashion trends with one-class collaborative filtering," in *Proceedings of the 25th international conference on world wide web*, pp. 507–517, New York, NY, USA, 2016.
- [35] J. McAuley, C. Targett, Q. Shi, and A. Van Den Hengel, "Image-based recommendations on styles and substitutes," in *Proceedings of the 38th international ACM SIGIR conference on research and development in information retrieval*, pp. 43–52, New York, NY, USA, 2015.
- [36] Y. Cao, X. Wang, X. He, Z. Hu, and T.-S. Chua, "Unifying knowledge graph learning and recommendation: towards a better understanding of user preferences," in *The world wide web conference*, pp. 151–161, New York, NY, USA, 2019.
- [37] X. Chen, H. Xu, Y. Zhang et al., "Sequential recommendation with user memory networks," in *Proceedings of the eleventh ACM international conference on web search and data mining*, pp. 108–116, New York, NY, USA, 2018.
- [38] S. Rendle, Z. Gantner, C. Freudenthaler, and L. Schmidt-Thieme, "Fast context-aware recommendations with factorization machines," in *Proceedings of the 34th international ACM SIGIR conference on Research and development in Information Retrieval*, pp. 635–644, New York, NY, USA, 2011.
- [39] B. Hidasi and A. Karatzoglou, "Recurrent neural networks with top-k gains for session-based recommendations," in *Proceedings of the 27th ACM international conference on information and knowledge management*, pp. 843–852, New York, NY, USA, 2018.

Research Article

A Novel Approach of Intelligent Computing for Multiperson Pose Estimation with Deep High Spatial Resolution and Multiscale Features

Haiquan Wang,¹ Xiangyang Wang,² Yijie Shi,² Yanping Li ,² Chunhua Qian ,³ and Rui Wang ²

¹Department of General Surgery, Shanghai General Hospital of Shanghai Jiaotong University, Shanghai 200080, China

²Key Laboratory of Specialty Fiber Optics and Optical Access Networks, Joint International Research Laboratory of Specialty Fiber Optics and Advanced Communication, School of Communication and Information Engineering, Shanghai University, 200444 Shanghai, China

³Department of Endocrinology and Metabolism, Shanghai Tenth People's Hospital, Tongji University, School of Medicine, Shanghai 200072, China

Correspondence should be addressed to Yanping Li; yanpingli@shu.edu.cn, Chunhua Qian; chqian2003@126.com, and Rui Wang; rwang@shu.edu.cn

Received 5 April 2021; Revised 30 May 2021; Accepted 22 June 2021; Published 7 July 2021

Academic Editor: Xiangjie Kong

Copyright © 2021 Haiquan Wang et al. This is an open access article distributed under the Creative Commons Attribution License, which permits unrestricted use, distribution, and reproduction in any medium, provided the original work is properly cited.

Currently, human pose estimation (HPE) methods mainly rely on the design framework of Convolutional Neural Networks (CNNs). These CNNs typically consist of high-to-low-resolution subnetworks (encoder) to learn semantic information and low-to-high subnetworks (decoder) to raise the resolution for keypoint localization. Because too low-resolution feature maps in encoder will inevitably lose some spatial information, which cannot be recovered in the upsampling stages, keeping high spatial resolution features is critical for human pose estimation. On the other hand, due to scale variation of human body parts, multiscale features are also very important for human pose estimation. In this paper, a novel backbone network is proposed specifically for HPE, named High Spatial Resolution and Multiscale Networks (HSR-MSNet), which maintain high spatial resolution features in deeper layers of the encoder and meanwhile construct multiscale features within one single residual block via subgroup splitting and fusion of feature maps. Experiments show that our approach outperforms other state-of-the-art methods with more accurate keypoint locations on COCO dataset.

1. Introduction

Human pose estimation (HPE) is one of the most fundamental tasks in computer vision—which is aimed at predicting the locations of body joints from input images. Recently, the human pose estimation methods based on Convolutional Neural Networks (CNNs) have achieved a great breakthrough [1–6], since CNNs have the powerful ability to learn rich convolutional feature representations [7]. For example, for single-person pose estimation, the state-of-the-art models have improved the performance from less than 50% PCKh@0.5 to more than 90% PCKh@0.5 [8–12] on the MPII benchmark

[13]. However, multiperson pose estimation still faces two main challenges:

- (1) There may be occlusion between different people, which will cause ambiguities of joints
- (2) Some invisible joints are hard to be predicted

In order to solve these challenges, existing methods, such as CPN [14] and SimpleBaseline [15], employ ResNet [16] as the backbone to obtain feature maps with large downsampling. However, too large downsampling will cause image spatial information loss [17], leading to difficulties for joint

context recovery. On the other hand, due to camera view change or foreshortening, scales of different body parts may still be inconsistent, even if training images are warped to the same scale [9]. Therefore, scale variation of human body parts is also one of the main challenges. Previous works [9, 10, 18] have shown that multiscale or pyramid features are beneficial for solving the problems caused by scale changes.

In this paper, a novel backbone network is proposed specifically for HPE, named High Spatial Resolution and Multiscale Networks (HSR-MSNet). The network could maintain high spatial resolution features in deeper layers while keeping large receptive fields and construct multiscale features within one single residual block by channel split and fusion. Experiments on COCO keypoint detection dataset demonstrate the effectiveness of HSR-MSNet. At the same time, the network architecture of HSR-MSNet is very lightweight, which means that it will be possible to implement functions similar to MobileNet [19] on Internet-of-Things (IoT) devices.

2. Related Works

2.1. Single-Person Pose Estimation. DeepPose [5] is the first human pose estimation method based on deep learning, which treats the body joint as a CNN-based regression problem, and its backbone consists of a softmax classifier, five convolution layers, and two fully connected layers. Subsequent methods mostly apply heatmaps that could characterize the probability of each keypoint at different locations for pose estimation [20]. The accurate location of a keypoint is further estimated by selecting the maximum value in the aggregation heatmaps. Convolutional Pose Machine (CPM) [21] is a multistage architecture where the belief maps and image features generated in the previous stage are served as input for the next stage [22]. For CPM, large receptive fields are used to learn long-range spatial relationships and the gradient vanishing problem is eliminated by using intermediate supervision. The features of stacked hourglass network [23] (Hourglass) are processed across all scales and consolidated to best capture the various spatial relationships associated with the body [23]. The above two models (CPM and Hourglass) achieve state-of-the-art performance, which all adopt intermediate supervision to generate detailed heatmaps for the joint locations.

2.2. Multiperson Pose Estimation. Multiperson pose estimation is a more challenging problem than single-person pose estimation for many computer vision applications. Due to occlusion and complex background, it is difficult to obtain accurate location results for multiperson pose estimation. A common approach is bottom-up, which detects human joints throughout the image region and then makes the groups of joint candidates for each person. The main problem of the bottom-up approach is to model the joint-to-individual associations [24]. Cao et al. [25] proposed a novel model to detect the 2D pose of several people in an image, which uses a non-parametric representation (Part Affinity Fields (PAFs)) to associate body parts with individuals in the given image. The architecture is aimed at learning part positions and their

association jointly by two branches of the same sequential prediction process.

Another pipeline to multiperson pose estimation is top-down [14, 15, 26, 27], which first detects each person in the image and then conducts single-person pose estimation for each single person. This top-down approach is not suitable when crowds are in close proximity, because it will result in significant overlap between bounding box regions of people. Fang et al. [27] proposed a novel regional multiperson pose estimation (RMPE) framework, which applies SSD [28] or Faster RCNN [29] to locate persons in an image and uses Hourglass [23] to predict pose of each people. Wei et al. [21] proposed the Cascaded Pyramid Network (CPN) for multiperson pose estimation, which uses Mask RCNN [25] to detect persons and then designs CPN to predict each person's pose.

2.2.1. High Spatial Resolution Features. Some state-of-the-art human pose estimation architecture, such as Hourglass [23], CPN [14], and SimpleBaseline [15], are shown in Figure 1. These CNN-based methods are typically encoder-decoder architecture, which consists of high-to-low resolution subnetworks (encoder) to learn semantic information and low-to-high subnetworks (decoder) to raise the resolution for the keypoint locations. Hourglass stacks multiple encoder-decoder subnetworks together to get progressively refined heatmaps. The "RefineNet" of CPN plays the role to explore the context information of "hard" keypoints to further improve the performance. SimpleBaseline simply takes ResNet as its backbone and adds additional deconvolution layers to raise the resolution of feature maps to predict keypoint heatmaps.

Because too low-resolution feature maps in encoder will inevitably lose some spatial information, which cannot be recovered in the upsampling stages, keeping high spatial resolution features is critical to improve the performance of human pose estimation.

In [30], DetNet maintains high spatial resolution in deeper layers to deal with the problem that large downsampling factors may compromise the location capability. Sun et al. [18] proposed the High-Resolution Net (HRNet) that consists of parallel high-to-low resolution subnetworks with multiscale feature fusion, which learns reliable high-resolution features by maintaining high-resolution representations through the whole networks. The information is exchanged repeatedly across multiresolution subnetworks, each of which receives information from other parallel ones.

2.2.2. Multiscale Features. Multiscale features are very important for pose estimation due to scale variation of human body parts. Most existing methods [14, 29] represent the multiscale features in a layer-wise manner fusing different level (scale) features together.

PyraNet proposed by Pishchulin et al. [8] and Res2Net proposed by Gao et al. [31] both construct multiscale features within one single residual block. By means of extending residual block to multiscale pyramids, PyraNet [8] designs Pyramid Residual Modules (PRMs) to enhance the invariance in scales. Multiscale features are obtained by applying

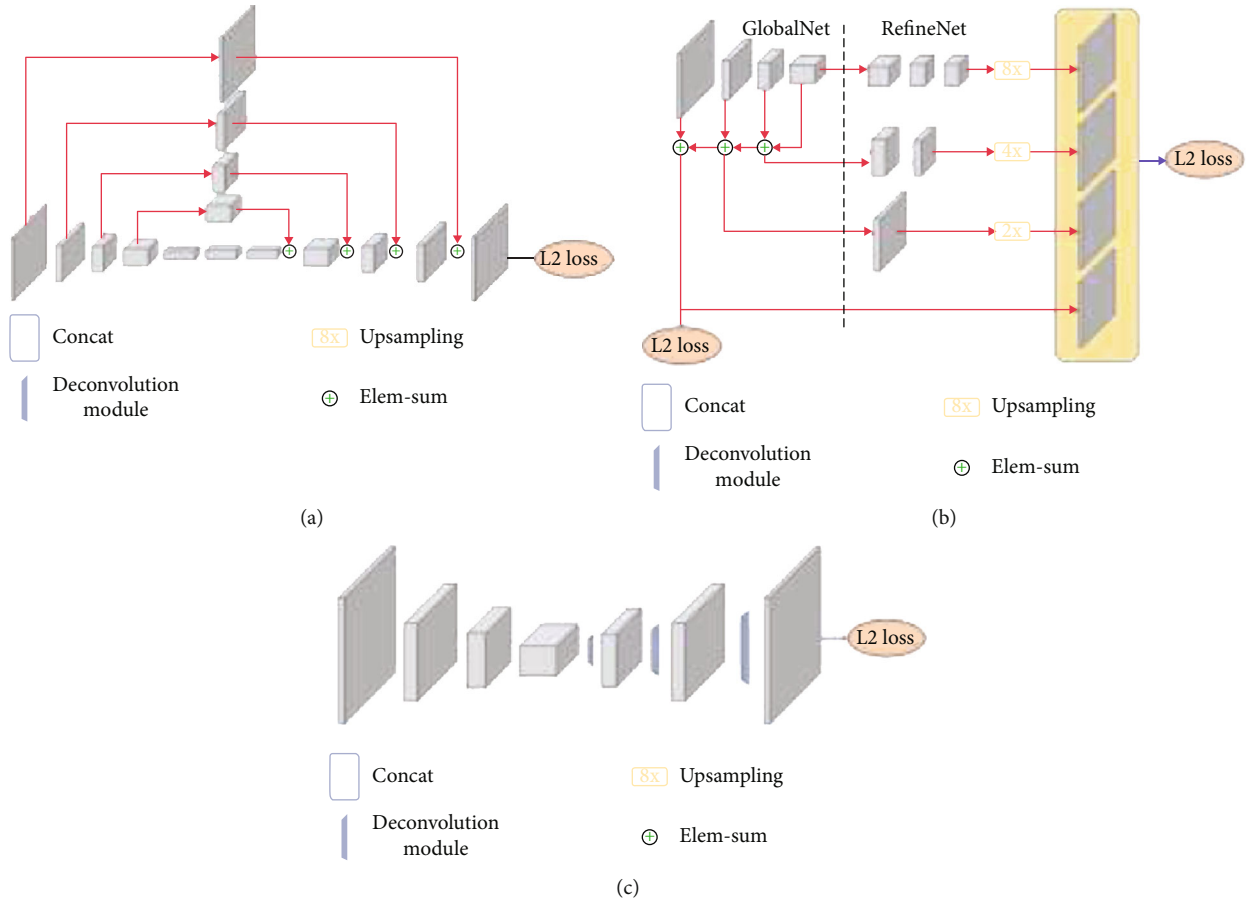


FIGURE 1: Some state-of-the-art pose estimation architecture: (a) Hourglass; (b) CPN; (c) SimpleBaseline.

different subsampling on input features in a multibranch residual block. Res2Net [31] represents multiscale features at a granular level and increases the range of receptive fields for each network layer. Specifically, Res2Net implements multiscale features via splitting channels of feature maps into subgroups and fusing these channel groups hierarchically. It has been proven that Res2Net can boost many backbone networks in some vision tasks, including object detection, semantic segmentation [32, 33], and salient object detection [29].

3. Our Approach

Similar to the previous works [14, 15, 25], we adopt the top-down pipeline for multiperson pose estimation, as illustrated in Figure 2. The whole framework consists of two parts: human detection and human pose estimation. First, a human detector is used to find all persons in the input image and generate a set of human bounding boxes. Then, a human pose estimation approach is applied to predict the keypoints for each single person by dealing with those human bounding boxes.

3.1. Human Detection. The state-of-the-art object detection method, YOLOv3 [34], is utilized for human detection. All eighty categories from the COCO dataset [35] are utilized

to train YOLOv3, but only human bounding boxes are used for our model. In the network of YOLOv3, 53 convolution layers with some shortcut connections are used for image feature extraction and the size of feature map can be adjusted through the convolution stride. Drawing on the idea of feature pyramid networks, YOLOv3 uses multiple scales to detect objections with different sizes, the finer the grid cell, the finer the object can be detected. In addition, the softmax is replaced with logistic classifier; in this way, multilabel object detection can be supported when detecting objects. More detail about YOLOv3 could be found in [34].

3.2. Human Pose Estimation with High Spatial Resolution Features

3.2.1. Motivation. Backbone networks play an important role in human pose estimation because of their abilities to extract effective features from the input images, which is critical for classification and keypoint localization. ResNet [16], as a traditional backbone network, has been widely used [36] and achieved outstanding performance in many state-of-art networks for human pose estimation such as SimpleBaseline [15] and CPN [14]. Accordingly, ResNet has high efficiency for image feature extraction. However, there still exist the following shortcomings when ResNet is used as the backbone network for human pose estimation.

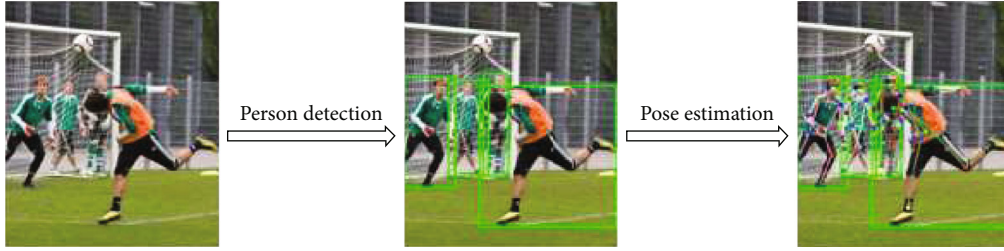


FIGURE 2: Top-down pipeline for multiperson pose estimation.

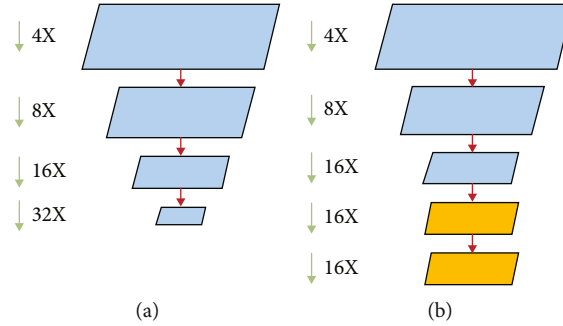


FIGURE 3: Comparisons of different backbones used in human pose estimation: (a) ResNet backbone; (b) HSRNet backbone.

- (1) Poor accuracy of keypoint localization. There are five stages in ResNet, and in each stage, the feature maps are sampled down. Compared to the input image, the feature maps have strides of 32 with strong semantic information and have large valid receptive fields, which bring a great performance in classification task. However, the downsampling with 32 strides may lead to the loss of local information and further affect the accuracy of keypoint localization in human pose estimation
- (2) Invisibility of small joints. Another drawback of large stride is the missing of small keypoints. For some occluded joints which contain less information, the spatial resolution of input image is greatly reduced when the large stride feature maps are extracted
- (3) Ambiguities. In the case of occlusion between multiple persons, one human bounding box may contain the keypoints of other persons. There exists the loss of the context information while the input image is converted into feature maps with large strides. It is hard to distinguish which keypoints belong to the right person without the context information

To solve these problems, inspired by DetNet [30], we reserve the first four stages of ResNet and replace the fifth stage with two new stages, as shown in Figure 3(b), named as HSRNet (High Spatial Resolution Network). In these two stages, the feature maps are no longer sampled down and the valid receptive fields are expanded. Thus, we can not only ensure the classification of each keypoint but also reserve more semantic information of the feature maps, which will be helpful to improve the accuracy of keypoint localization.

3.2.2. Our Model for Keypoint Localization. A simple network structure is adopted in our model, as shown in Figure 4(b). Firstly, we use HSRNet as backbone network to generate feature maps with semantic information. Then, a few deconvolutional layers with batch normalization and ReLU activation are applied to generate heatmaps from the low-resolution feature maps. Finally, Mean Squared Error (MSE) is used as the loss between the predicted heatmaps and target heatmaps. The target heatmaps for keypoints are generated by applying a Gaussian centered at the ground-truth location of keypoints. Compared with SimpleBaseline [15], HSRNet is adopted to replace the original ResNet. Since the size of output feature maps of HSRNet and ResNet is different, the deconvolutional layer is reduced to keep the same size of feature map.

As shown in Figure 5(b), HSRNet is our backbone network with two new stages based on the existing ResNet [16]. As shown in Figure 6, in the two new stages, original bottlenecks A and B are slightly altered into two new bottlenecks C and D. Original 3×3 convolution layer is converted into a convolution layer with dilation of 2. And the bottleneck C does not have a downsampling, which ensures that the size of feature maps will not change during these two new stages. Similar to ResNet, the stack method is applied, and original bottlenecks A and B are replaced by bottlenecks C and D, as shown in Figure 5. Since the fifth stage in ResNet has a downsampling with a stride of 2, if only a new stage is used, it will reduce the valid receptive field, leading to a negative effect for human pose estimation. Therefore, we utilize two new stages to gain feature maps of higher spatial resolution, simultaneously without sacrificing valid receptive field.

3.3. Human Pose Estimation with Multiscale Features. Based on Res2Net [31], we design a new multiscale module

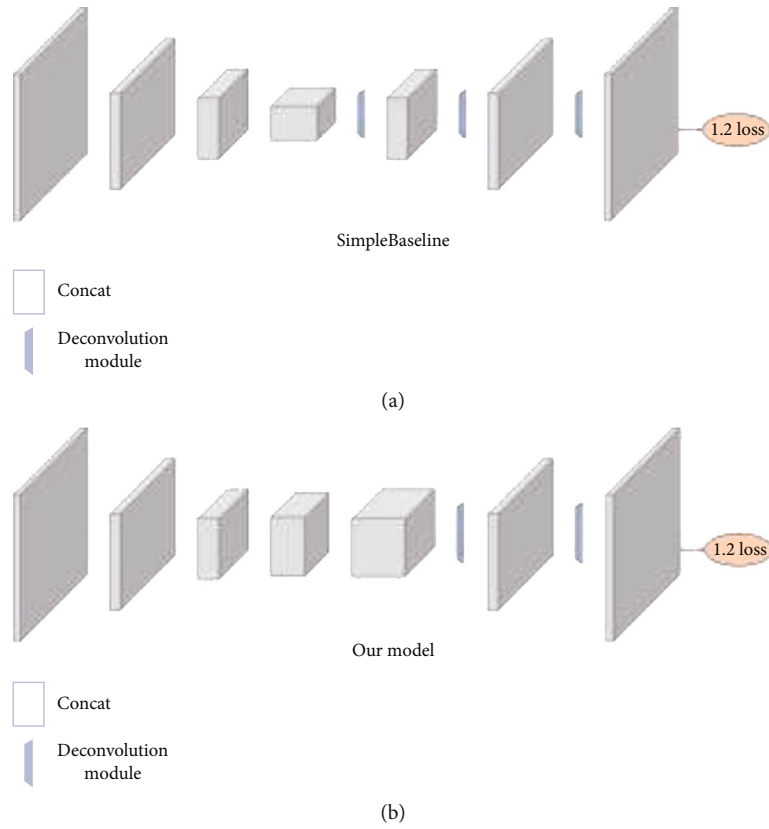


FIGURE 4: Illustration of network architecture for human pose estimation: (a) SimpleBaseline; (b) our model.

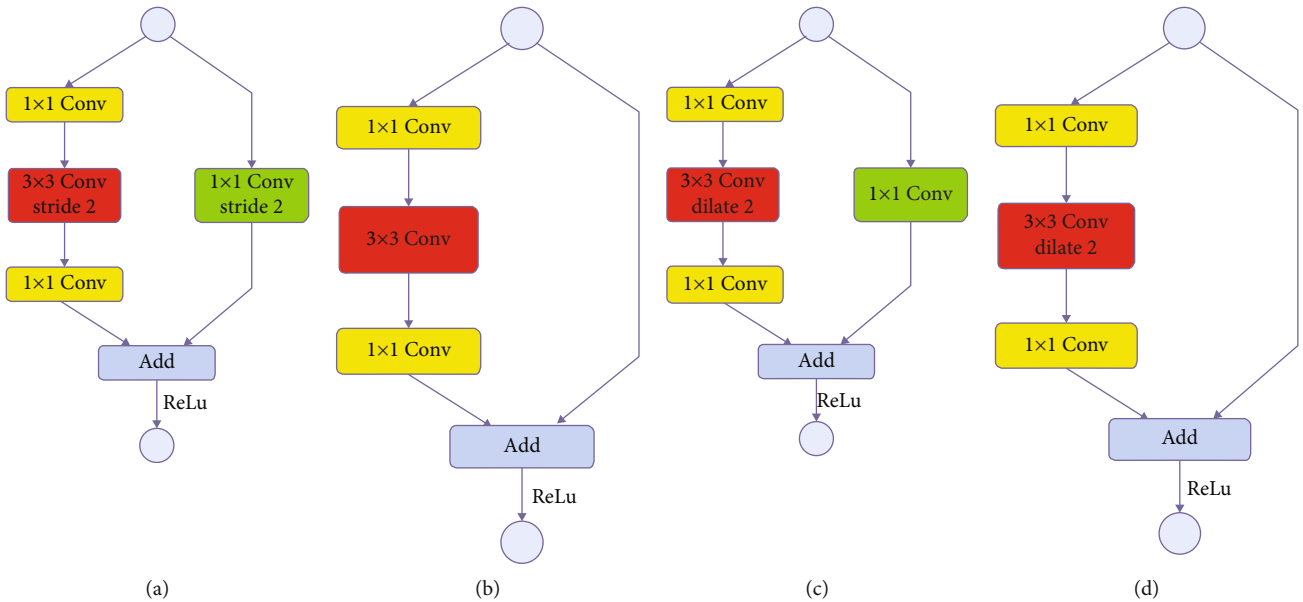


FIGURE 5: Detailed structures of different bottlenecks: (a) original bottleneck with 1×1 Conv; (b) original bottleneck; (c) dilated bottleneck with 1×1 Conv; (d) dilated bottleneck.

(MSNet) (as shown in Figure 7(b)) specifically and further integrate it into HSRNet to learn multiscale features. Our entire framework is named as HSR-MSNet.

The structure of Res2Net [31] is shown in Figure 7(a). Res2Net uses hierarchical groups of 3×3 convolution filters to extract multiscale features. Specifically, Res2Net

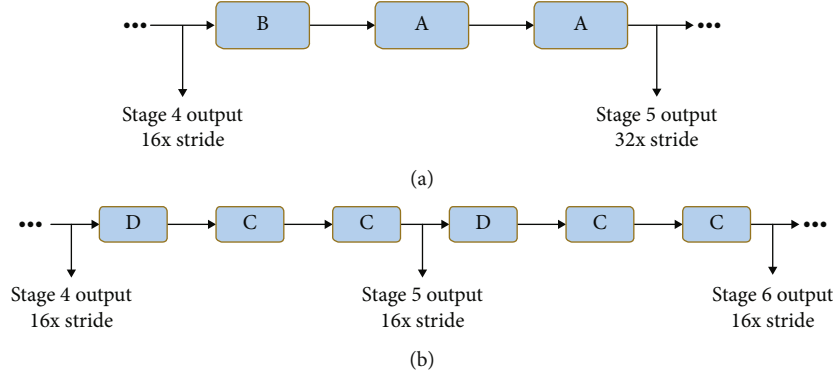


FIGURE 6: Detailed structures of ResNet and HSRNet. A, B, C, and D are bottlenecks illustrated in Figure 5. HSRNet follows the same design as ResNet before stage 4, while keeping spatial size after stage 6. (a) The fifth stage of ResNet; (b) two new stages of HSRNet.

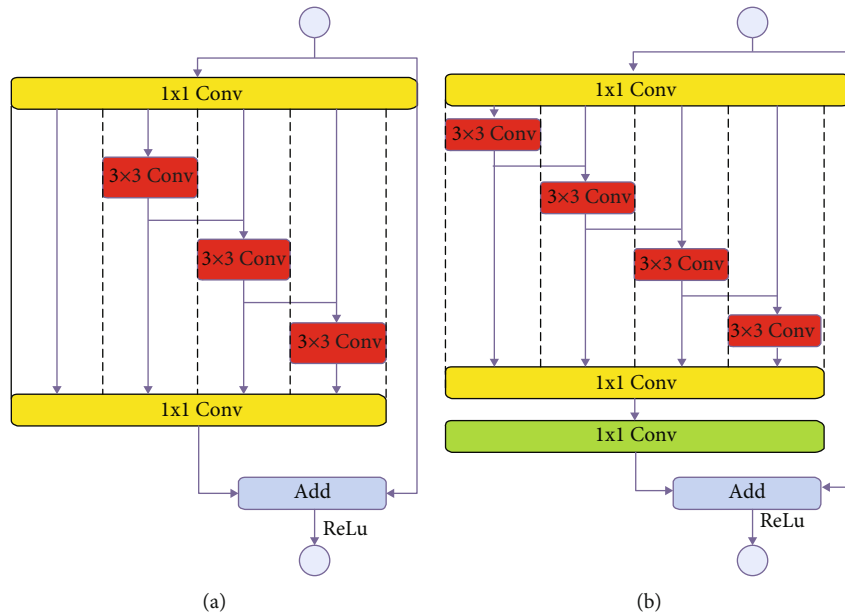


FIGURE 7: Comparison of two multiscale building blocks: (a) original Res2Net block; (b) our proposed MSNet.

implements multiscale features by splitting channels of feature maps into subgroups (3 groups as shown in Figure 7(a)) and fuses these channel groups hierarchically. Since we have retained the first four stages of ResNet, Res2Net module can be easily integrated into the first four stages of our network backbone. As shown in Figure 7(b), we add a 3×3 convolution layer compared with Res2Net, in order to increase the receptive fields. In addition, we use multiple smaller scale 3×3 convolution layers to replace the 3×3 convolution layer with stride 2. There are two advantages in this network structure. Firstly, multiple smaller 3×3 convolution layers can learn more context information of keypoints compared with one convolution layer with stride 2, especially for small-scale persons. Since the output feature maps of stage 4 are 16x strides with respect to input image, the convolution layer with stride 2 will be more difficult to extract semantic features for small-scale persons in detail. Secondly, the MSNet module can extract deep seman-

tic features in multiscale style, while keeping large receptive fields. We denote the output feature maps of the 3×3 convolutional layer $Conv()$ as y_i , $i \in \{1, 2, \dots, n\}$, where n is the total numbers of subgroups that the feature maps are split into evenly. Then, y_i could be expressed as

$$y_i = \begin{cases} Conv(x_i), & i = 1, \\ Conv(x_i + y_{i-1}), & 1 < i \leq n, \end{cases} \quad (1)$$

where x_i denotes the results of input feature maps x after 1×1 convolution and split evenly.

Among the multiscale features, not all the features are equally valid for human pose estimation. In order to balance the relationship among channel features, we add a SE (Squeeze-and-Excitation) block [37] before the residual connections (Figure 7(b)), which can learn the importance of each feature channel and promote important features while

TABLE 1: Comparisons on the COCO val2017 dataset.

Method	Backbone	Input size	Deconv. layers	Deconv. kernel size	AP
a	ResNet-50	256×192	3	4	70.4
b	ResNet-101	256×192	3	4	71.4
c	ResNet-152	256×192	3	4	72.0
d	ResNet-50	256×192	3	2	70.1
e	ResNet-50	256×192	3	3	70.3
f	ResNet-50	384×288	3	4	72.7
g	HSRNet-59	256×192	2	4	71.4
h	HSRNet-110	256×192	2	4	71.8
i	HSRNet-161	256×192	2	4	72.6
j	HSRNet-59	256×192	2	2	70.9
k	HSRNet-59	256×192	2	3	71.2
l	HSRNet-59	384×288	2	4	73.2

suppressing the less useful features for the current vision task. As a result, the final formula of our MSNet module could be written as

$$f = \text{Re Lu}(x + K(y)), \quad (2)$$

where y represents the concatenation of $y_i (i \in \{1, 2, \dots, n\})$, f represents the final output feature maps, ReLu is the activation layer we used, and $K()$ represents the SE block and 1×1 convolution layer.

4. Experiments

4.1. Datasets. We evaluate our model on popular MS COCO benchmark [35]. There are more than 200K images and 250K person instances labeled with keypoints in the COCO dataset which contain train set, validation set, and test set. 150K person instances are publicly available for training and validation. Our models are only trained on COCO train2017 dataset (includes 57K images and 150K person instances), no extra data involved, and ablation studies are conducted on the COCO val2017 dataset. Finally, we report the results on COCO test-dev2017 set to make a fair comparison with the public state-of-the-art methods.

4.2. Model Training and Inference. Our models are trained on the NVIDIA Tesla P100 GPU using PyTorch and optimized by Adam algorithm with a batch size of 32 for 140 epochs. The learning rate is initialized as 0.0001 and decreased by a factor of 0.1 at 90th and 120th epoch. The ground-truth human box is made to a fixed aspect ratio, which is height : width = 4 : 3 by extending the box in height or width. It is then cropped from the image and resized to a fixed resolution. The default resolution is 256×192 , which is the same as the state-of-the-art methods [14, 15] for a fair comparison. During the model training, we use a pretrained model trained on ImageNet classification task [1].

We test HSR-MSNet with 59, 110, and 161 layers, named HSR-MSNet-59, HSR-MSNet-110, and HSR-MSNet-161,

respectively. HSR-MSNet-59 is derived from [18], which can be download at https://github.com/guoruoqian/DetNet_pytorch. For HSR-MSNet-110 and HSR-MSNet-161, we adopt to initial the parameters of the first four stages from ResNet pretrained models [16].

The standard COCO metrics [35] are used to evaluate our approach, including AP (averaged precision), OKS (object keypoint similarity) thresholds, AP_{50} and AP_{75} (AP at different IoU (Intersection over Union) thresholds), AP_m and AP_l (AP at different scales: middle and large), and AR (average recall). The OKS plays the same role as the IoU in object detection, which is calculated from the distance between predicted keypoints and ground-truth keypoints normalized by scale of the person.

4.3. Quantitative Results. The experiments with HSRNet and HSR-MSNet are implemented to investigate the effectiveness of keeping high spatial resolution features and multiscale features for human pose estimation, respectively.

4.3.1. High Spatial Resolution Features. For the experiments with HSRNet, a human detector is introduced with AP 56.4 on COCO val2017, and the performance of ResNet and HSRNet with various options is listed in Table 1. Since the feature maps of HSRNet have higher spatial resolution than ResNet, two deconvolution layers are utilized to maintain the same size of output heatmaps. Methods a, b, c, d, e, g, h, i, j, and k with 256×192 input size eventually generate 64×48 heatmaps, and methods f and l with 384×288 input size generate 96×72 heatmaps.

- (1) Size-varied backbone. Methods a, b, and c and g, h, and i compare the results of HSRNet and ResNet by size-varied backbones, which illustrate that HSRNet is better than ResNet by 0.4 AP at least in comparable size of backbones. Similar to ResNet, the larger the size of HSRNet backbone, the better the performance. As can be seen from Table 1, AP increases 0.4 from

TABLE 2: Comparisons on the COCO val2017 dataset.

Method	Backbone	Input size	Deconv. layers	Deconv. kernel size	AP
a	HSRNet-59	256 × 192	2	4	71.4
b	HSRNet-59	384 × 288	2	4	73.2
c	HSR-MSNet-59	256 × 192	2	4	71.5
d	HSR-MSNet-59	384 × 288	2	4	73.3

TABLE 3: Comparisons with Hourglass, CPN, and SimpleBaseline on the COCO val2017 dataset.

Method	Backbone	Input size	OHKM	AP
8-stage Hourglass	—	256 × 192	N	66.9
8-stage Hourglass	—	256 × 256	N	67.1
CPN	ResNet-50	256 × 192	N	68.6
CPN	ResNet-50	384 × 288	N	70.6
CPN	ResNet-50	256 × 192	Y	69.4
CPN	ResNet-50	384 × 288	Y	71.6
SimpleBaseline	ResNet-50	256 × 192	N	70.4
SimpleBaseline	ResNet-50	384 × 288	N	72.2
Ours	HSRNet-59	256 × 192	N	71.4
Ours	HSRNet-59	384 × 288	N	73.2

HSRNet-59 to HSRNet-110 and 1.2 from HSRNet-59 to HSRNet-161

- (2) Various kernel sizes of deconvolution layers. Methods a, d, and e and j, i, and k prove that HSRNet also outperforms ResNet by at least 0.8 AP with various kernel sizes of deconvolution layers. AP increases 0.3 from kernel size 2 to 3 and 0.5 from kernel size 2 to 4 in HSRNet-59
- (3) Different sizes of input images. a and f and g and l methods illustrate that the higher the resolution of input images, the better the performance. In addition, HSRNet improves 1 AP compared with ResNet

Since HSRNet has more parameters than ResNet in comparable size of backbone, it may be hard to demonstrate that HSRNet structure is better than ResNet. However, it is worth noting that AP of methods b and g are the same. The performance is comparable between HSRNet-59 and ResNet-101, which implies the ability of high spatial resolution to improve the performance of human pose estimation significantly.

4.3.2. Multiscale Features. The experiments are implemented with HSR-MSNet and compared with HSRNet to show the importance of multiscale features for human pose estimation, as shown in Table 2.

A human detector is adopted with AP 56.4 on COCO val2017. Due to the fact that HSR-MSNet can extract semantic features with multiscale and assign weights to these features by the SE module, HSR-MSNet has a better performance than HSRNet with the same parameters which is improved by 0.1AP. Obviously, multiscale features play

an important role in human pose estimation, because it requires an understanding of large-scale features for the classification of keypoints, as well as small-scale features for localization of keypoints. SE block is also indispensable since it can assign weights to different features and make the most effective features prominent among others. The combination of multiscale features and weight distribution can further improve human pose estimation.

4.3.3. Comparisons with Other State-of-the-Art Methods. The results of HSRNet and other state-of-the-art models including Hourglass [23], CPN [14], and SimpleBaseline [15] on the COCO val2017 dataset are shown in Table 3. For fair comparison, a human detector provided by SimpleBaseline is introduced with 56.4 AP, which is comparable to Hourglass and CPN with 55.3 AP.

Our method exceeds Hourglass by 4.5 AP in the same input size of 256 × 192. Compared with CPN, our method outperforms CPN without OHKM by more than 2.6 AP and CPN with OHKM by 1.6 AP. Although our model is based on SimpleBaseline, it has been proved in Table 1 that our method performs better than SimpleBaseline. It is obvious that these performance gains are benefited from keeping high spatial resolution in deeper layers of the backbone encoder networks.

To gain a better performance, a human detector of 60.9 AP is applied to obtain human bounding boxes on COCO test2017 dataset. For reference, CPN uses a human detector with person detection AP of 62.9 on COCO minival split dataset and SimpleBaseline uses a human detector of 60.9 AP on COCO std-dev split dataset. As shown in Table 4, CPN uses the ResNet-Inception and SimpleBaseline uses

TABLE 4: Comparison experiments on the COCO test2017 dataset. Results of compared methods are cited from [15].

Method	Backbone	Input size	AP	AP ₅₀	AP ₇₅	AP _m	AP _l	AR
G-RMI [38]	ResNet-50	256 × 192	64.9	85.5	71.3	62.3	70.0	69.7
CPN	ResNet-Inception	384 × 288	72.1	91.4	80.0	68.7	77.2	78.5
FAIR* [37]	ResNeXt-101-FPN	—	69.2	90.4	77.0	64.9	76.3	75.2
G-RMI*	ResNet-152	384 × 288	71.0	87.9	77.7	69.0	75.2	70.6
oks* [37]	—	—	72.0	90.3	79.7	67.6	78.4	77.2
Bangbangren* [37]	ResNet-101	—	72.8	89.4	79.6	68.6	80.0	78.7
CPN*	ResNet-Inception	384 × 288	73.0	91.7	80.9	69.5	78.1	79.0
SimpleBaseline	ResNet-152	384 × 288	73.7	91.9	81.1	70.3	80.0	79.0
Ours	HSRNet-59	384 × 288	72.6	91.2	79.9	69.0	78.9	77.8
Ours	HSR-MSNet-59	384 × 288	72.8	91.2	80.5	69.6	79.0	78.3

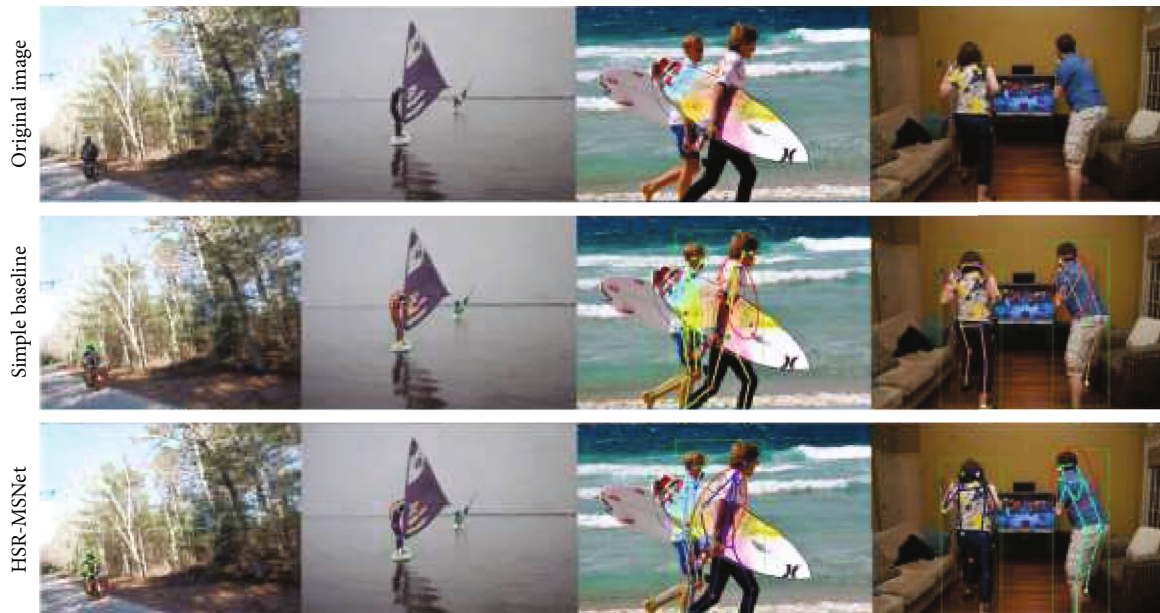


FIGURE 8: Qualitative comparisons on the COCO test2017 dataset.

ResNet-152 for human pose estimation. Our method only utilized a small backbone but outperforms some state-of-the-art models including G-RMI [38] and FAIR* [37] and achieves a potential performance of 72.6 AP and 72.8 AP.

Since our model is based on SimpleBaseline, the changes we made are very slight, which have a negligible impact on the overall parameters of the model. In other words, compared to SimpleBaseline, the computational complexity of our model is almost the same.

4.4. Qualitative Comparisons. Some qualitative comparison results on the COCO test2017 dataset are shown in Figure 8. We compare our approach with SimpleBaseline [15] and use comparable model to predict the keypoints for fair comparison. SimpleBaseline utilizes ResNet-50 as backbone, and our method is HSR-MSNet-59. As shown in Figure 8, the first row contains some original images of the COCO test2017 dataset, the second row is the

results predicted by SimpleBaseline [15], and the third row is our results.

It is obvious that our method can better predict the keypoints of partially occluded or small people by utilizing higher resolution and multiscale feature maps. As the first column of Figure 8 has shown, our method can perceive and predict the keypoints more accurately for small people. For complex backgrounds, the second column illustrates that our method can separate the person from the background easily with high-resolution feature maps to avoid misidentification. In addition, our method can accurately predict the “hard” joints that are occluded or invisible in the third and fourth columns of Figure 8. Especially in the third column, HSR-MSNet makes it easier to detect the left arm which is heavily occluded in this image and gives a more accurate prediction. It is attributed to the ability of HSR-MSNet to mine more context information of “hard” joints.

5. Conclusion

In this paper, a novel backbone network, named HSR-MSNet, is proposed specifically for human pose estimation, which maintains high spatial resolution features in deeper layers of the encoder while still keeping large receptive fields. We also design a building module to learn multiscale features within one single residual block by splitting channels of feature maps into subgroups and then fuse these channel groups hierarchically. For multiperson pose estimation, our model can learn efficient context information of “hard” joints, due to partial occlusion or small scale of persons. Experiments on the COCO keypoint detection dataset show that our model outperforms other state-of-the-art methods, such as Hourglass [23], CPN [14], and SimpleBaseline [15] with respect to standard COCO metrics. At next steps, we will focus on evaluating our model on other human datasets, such as MPII dataset, and then further experiments on lightweight devices.

Data Availability

The data that support the findings of this study are openly available in COCO at doi:10.1007/978-3-319-10602-1_48, reference number [29].

Conflicts of Interest

The authors declare that they have no conflicts of interest.

Acknowledgments

This work was supported by the National Natural Science Foundation of China grant 61771299.

References

- [1] A. Krizhevsky, I. Sutskever, and G. E. Hinton, “ImageNet classification with deep convolutional neural networks,” *Communications of the ACM*, vol. 60, no. 6, pp. 84–90, 2017.
- [2] N. Kalchbrenner, E. Grefenstette, and P. Blunsom, “A convolutional neural network for modelling sentences,” 2014, <https://arxiv.org/abs/1404.2188>.
- [3] Y. Kim, “Convolutional neural networks for sentence classification,” 2014, <https://arxiv.org/abs/1408.5882>.
- [4] S. Ji, W. Xu, M. Yang, and K. Yu, “3d convolutional neural networks for human action recognition,” *IEEE Transactions on Pattern Analysis and Machine Intelligence*, vol. 35, no. 1, pp. 221–231, 2012.
- [5] A. Toshev and C. Szegedy, “DeepPose: human pose estimation via deep neural networks,” 2013.
- [6] Z. Bi, L. Yu, H. Gao, P. Zhou, and H. Yao, “Improved VGG model-based efficient traffic sign recognition for safe driving in 5G scenarios,” *International Journal of Machine Learning and Cybernetics*, vol. 3, 2020.
- [7] Y. LeCun, Y. Bengio, and G. Hinton, “Deep learning,” *Nature*, vol. 521, no. 7553, pp. 436–444, 2015.
- [8] L. Pishchulin, M. Andriluka, P. Gehler, and B. Schiele, “Strong appearance and expressive spatial models for human pose estimation,” in *2013 IEEE International Conference on Computer Vision*, pp. 3487–3494, Sydney, NSW, Australia, 2014.
- [9] W. Yang, S. Li, W. Ouyang, H. Li, and X. Wang, “Learning feature pyramids for human pose estimation,” in *2017 IEEE International Conference on Computer Vision (ICCV)*, pp. 1281–1290, Venice, Italy, 2017.
- [10] L. Ke, M. C. Chang, H. Qi, and S. Lyu, “Multi-scale structure-aware network for human pose estimation,” in *2018 25th IEEE International Conference on Image Processing (ICIP)*, pp. 713–728, Athens, Greece, 2018.
- [11] W. Tang, P. Yu, and Y. Wu, “Deeply learned compositional models for human pose estimation,” in *Computer Vision – ECCV 2018. ECCV 2018*, pp. 190–206, Springer, 2018.
- [12] H. Zhang, H. Ouyang, S. Liu et al., “Human pose estimation with spatial contextual information,” 2019, <https://arxiv.org/abs/1901.01760>.
- [13] M. Andriluka, L. Pishchulin, P. Gehler, and B. Schiele, “2D Human pose estimation: new benchmark and state of the art analysis,” in *2014 IEEE Conference on Computer Vision and Pattern Recognition*, pp. 3686–3693, Columbus, OH, USA, 2014.
- [14] Y. Chen, Z. Wang, Y. Peng, Z. Zhang, G. Yu, and J. Sun, “Cascaded pyramid network for multi-person pose estimation,” in *2018 IEEE/CVF Conference on Computer Vision and Pattern Recognition*, pp. 7103–7112, Salt Lake City, UT, USA, 2018.
- [15] B. Xiao, H. Wu, and Y. Wei, “Simple baselines for human pose estimation and tracking,” in *Computer Vision – ECCV 2018. ECCV 2018*, pp. 472–487, Springer, 2018.
- [16] K. He, X. Zhang, S. Ren, and J. Sun, “Deep residual learning for image recognition,” in *2016 IEEE Conference on Computer Vision and Pattern Recognition (CVPR)*, pp. 770–778, Las Vegas, NV, USA, 2016.
- [17] J. Chen, H. Ying, X. Liu et al., “A transfer learning based super-resolution microscopy for biopsy slice images: the joint methods perspective,” *IEEE/ACM Transactions on Computational Biology and Bioinformatics*, vol. 18, no. 1, pp. 103–113, 2020.
- [18] K. Sun, B. Xiao, L. Dong, and J. Wang, “Deep high-resolution representation learning for human pose estimation,” in *2019 IEEE/CVF Conference on Computer Vision and Pattern Recognition (CVPR)*, pp. 5693–5703, Long Beach, CA, USA, 2019.
- [19] A. Howard, M. Sandler, and G. Chu, “Searching for MobileNetv3,” in *2019 IEEE/CVF International Conference on Computer Vision (ICCV)*, pp. 1314–1324, Seoul, Korea, 2019.
- [20] J. J. Tompson, A. Jain, Y. LeCun, and C. Bregler, “Joint training of a convolutional network and a graphical model for human pose estimation,” 2014, <https://arxiv.org/abs/1406.2984>.
- [21] S.-E. Wei, V. Ramakrishna, T. Kanade, and Y. Sheikh, “Convolutional pose machines,” in *2016 IEEE Conference on Computer Vision and Pattern Recognition (CVPR)*, pp. 4724–4732, Las Vegas, NV, USA, 2016.
- [22] T. L. Munea, Y. Z. Jembre, H. T. Weldegebriel, L. Chen, C. Huang, and C. Yang, “The progress of human pose estimation: a survey and taxonomy of models applied in 2D human pose estimation,” *IEEE Access*, vol. 8, pp. 133330–133348, 2020.
- [23] A. Newell, K. Yang, and J. Deng, “Stacked hourglass networks for human pose estimation,” in *Computer Vision – ECCV 2016. ECCV 2016*, pp. 483–499, Springer, 2016.
- [24] B. Li, K. Liu, Y. Ji, J. Yang, and C. Liu, “Selective complementary features for multi-person pose estimation,” in *2020 IEEE international conference on image processing (ICIP)*, pp. 623–627, Abu Dhabi, United Arab Emirates, 2020.

- [25] Z. Cao, T. Simon, S. E. Wei, and Y. Sheikh, "Realtime multi-person 2d pose estimation using part affinity fields," in *2017 IEEE Conference on Computer Vision and Pattern Recognition (CVPR)*, pp. 7291–7299, Honolulu, HI, USA, 2016.
- [26] K. He, G. Gkioxari, P. Dollár, and R. Girshick, "Mask R-CNN," *IEEE Transactions on Pattern Analysis & Machine Intelligence*, no. 2, pp. 386–397, 2020.
- [27] H.-S. Fang, S. Xie, Y.-W. Tai, and C. Lu, "RMPE: regional multi-person pose estimation," in *2017 IEEE International Conference on Computer Vision (ICCV)*, pp. 2334–2343, Venice, Italy, 2017.
- [28] W. Liu, D. Anguelov, D. Erhan et al., "SSD: Single shot multi-box detector," in *European conference on computer vision*, pp. 21–37, Amsterdam, The Netherlands, 2016.
- [29] S. Ren, K. He, R. Girshick, and J. Sun, "Faster R-CNN: towards real-time object detection with region proposal networks," *IEEE Transactions on Pattern Analysis and Machine Intelligence*, vol. 39, no. 6, pp. 1137–1149, 2017.
- [30] Z. Li, C. Peng, G. Yu, X. Zhang, Y. Deng, and J. Sun, "DetNet: a backbone network for object detection," 2018, <https://arxiv.org/abs/1804.06215>.
- [31] S. Gao, M.-M. Cheng, K. Zhao, X.-Y. Zhang, M.-H. Yang, and P. H. S. Torr, "Res2net: a new multi-scale backbone architecture," *IEEE Transactions on Pattern Analysis and Machine Intelligence*, vol. 43, no. 2, pp. 652–662, 2021.
- [32] J. Xiao, H. Xu, H. Gao, M. Bian, and Y. Li, "A weakly supervised semantic segmentation network by aggregating seed cues: the multi-object proposal generation perspective," *ACM Transactions on Multimedia Computing, Communications, and Applications*, vol. 17, no. 1s, pp. 1–19, 2021.
- [33] J. Xiao, H. Xu, W. Zhao, C. Cheng, and H. H. Gao, "A prior-mask-guided few-shot learning for skin lesion segmentation," *Computing*, pp. 1–13, 2021.
- [34] J. Redmon and A. Farhadi, "YOLOv3: an incremental improvement," 2018, <https://arxiv.org/abs/1804.02767>.
- [35] T.-Y. Lin, M. Maire, S. Belongie et al., "Microsoft COCO: common objects in context," in *Computer Vision – ECCV 2014. ECCV 2014*, pp. 740–755, Springer, 2014.
- [36] Z. Cao, C. Sun, W. Wang, X. Zheng, J. Wu, and H. Gao, "Multi-modality fusion learning for the automatic diagnosis of optic neuropathy," *Pattern Recognition Letters*, vol. 142, pp. 58–64, 2021.
- [37] J. Hu, L. Shen, S. Albanie, G. Sun, and E. Wu, "Squeeze-and-excitation networks," *IEEE Transactions on Pattern Analysis and Machine Intelligence*, vol. 42, no. 8, pp. 2011–2023, 2020.
- [38] G. Papandreou, T. Zhu, N. Kanazawa et al., "Towards accurate multi-person pose estimation in the wild," in *2017 IEEE Conference on Computer Vision and Pattern Recognition (CVPR)*, pp. 4903–4911, Honolulu, HI, USA, 2017.

Research Article

Research on Named Entity Recognition of Electronic Medical Records Based on RoBERTa and Radical-Level Feature

Yue Wu , Jie Huang , Caie Xu, Huilin Zheng , Lei Zhang, and Jian Wan 

School of Information and Electronic Engineering, Zhejiang University of Science and Technology, Zhejiang Hangzhou 310023, China

Correspondence should be addressed to Jian Wan; wanjian@zust.edu.cn

Received 11 May 2021; Revised 6 June 2021; Accepted 16 June 2021; Published 28 June 2021

Academic Editor: Honghao Gao

Copyright © 2021 Yue Wu et al. This is an open access article distributed under the Creative Commons Attribution License, which permits unrestricted use, distribution, and reproduction in any medium, provided the original work is properly cited.

Clinical named entity recognition (CNER) identifies entities from unstructured medical records and classifies them into predefined categories. It is of great significance for follow-up clinical studies. Most of the existing CNER methods fail to give enough thought to Chinese radical-level characteristics and the specialty of the Chinese field. This paper proposes the Ra-RC model, which combines radical features and a deep learning structure to fix this problem. A bidirectional encoder representation of transformer (RoBERTa) is utilized to learn medical features thoroughly. Simultaneously, we use the bidirectional long short-term memory (BiLSTM) network to extract radical-level information to capture the internal relevance of characteristics and stitch the eigenvectors generated by RoBERTa. In addition, the relationship between labels is considered to obtain the optimal tag sequence by applying conditional random field (CRF). The experimental results demonstrate that the proposed Ra-RC model achieves F1 score 93.26% and 82.87% on the CCKS2017 and CCKS2019 datasets, respectively.

1. Introduction

Named entity recognition (NER) refers to the extraction of specific entities from unstructured texts, which plays a vital role in subsequent tasks, such as constructing knowledge graphs and personalized recommendation systems [1–3]. In recent years, with the rapid development of medical information technology, textual data of electronic medical records (EMRs) keep on increasing. As a fundamental Chinese medical information extraction task, named entity recognition of Chinese clinical EMRs has attracted extensive attention [4].

NER of clinical EMRs relates to the automatic discovery of all kinds of named entities closely associated with patients' health from EMRs, such as disease, drugs, or symptoms. Early researches in the CNER tasks mainly use lexicon-based and rule-based approaches [5, 6]. And then, a lot of statistical models are used for CNER [7, 8]. With the substantial increase in hardware computing power, the deep learning method has been successfully applied to CNER. At present, many research approaches have focused on exploring a generic domain model for migration. Traditional bidirectional long short-term memory networks [9, 10] and unsu-

pervised pretraining of language models [11–14] are widely migrated to the CNER field. Both neural network algorithms have accomplished state-of-art achievement on the regular named recognition field. However, these models also have a room for improvement. First, the generality of the LSTM network leads to the model has no adequate capacity to extract features, where the extracted features are limited by the correctness of the dataset annotation and the context information. Second, the released versions of the pretraining model are more suitable for the general Chinese entity extraction. Both of them do not adapt to the characteristics of the EMR dataset, which underperforms on the task of medical entity extraction.

Moreover, the identification of Chinese clinical named entity recognition has been problematic. Firstly, many clinical named entities are multiword, and some of them are even being very long. It is not easy to distinguish the word boundaries of medical multiword in Chinese. What is more, the identical word and phrase can be divided into different kinds of named entities, for example, stroke can be delegated a modifier, and it can be additionally classified into particular disease and disease class and so on [15]. In addition, some

specific types of medical entities often have characteristics different from the general ones, especially in the radical-level characteristics of the entity. For instance, many characters of disease entities tend to have “疒” radicals, such as “病,” and “痛.” In ancient Chinese characters, “月” is related to human organs and flesh. Furthermore, many entities that consist of body parts often have “月” radicals, such as “脏,” “脑,” and “骨.” These radical-level characteristics also have a significant reference value in determining labels, especially in complex medical entities consisting of multiple categories, such as the disease entity of “body parts and symptoms” format. However, this information has not been fully utilized by the regular named entity recognition model.

To address these issues, we propose a Ra-RC model which combines radical information with a deep learning structure. Above all, we adopt BiLSTM to encode radical characteristics. Simultaneously, RoBERTa is utilized to capture the characteristics of medical texts and generate characteristic representations. After that, we concatenate radical representations and characteristic representations and then use CRF to get predictive label sequences. Our proposed method has extensively evaluated its feasibility and utility on the CCKS2017 dataset and CCKS2019 dataset.

The main contribution can be summarized as follows:

- (1) Considering the particularity of the medical entity and the underutilization of the radical-level information, we use BiLSTM to extract the radical characteristics
- (2) Integrate radical-level information and deep learning model to solve the poor extraction performance of medical entities caused by migrating the general deep learning model
- (3) The experimental results show that the Ra-RC model has a good performance on both datasets

2. Related Work

2.1. Clinical Named Entity Recognition. NER of EMRs has not only crucial practical significance but also high academic research value. Academics have done much research on it. At present, there are a large number of researches on NER in English clinical EMRs [16, 17]. For example, aiming at the lack of enough annotated data, Yang et al. [18] and Peters et al. [19] used transfer learning and semisupervised learning to extract entities, which could significantly improve the performance. There are many high-quality annotated data in the field of English CNER, such as JNLPBA, BC2GM, and NCBI. Due to the lack of high-quality EMRs and many nonstandard abbreviations, the Chinese CNER domain NER task is difficult [20].

An end-to-end deep learning method can be used to explore deeper features. The main network structure of this method is BiLSTM combined with CRF [21]. Li et al. [22] proposed a conditional random field algorithm that integrated characters, speech, and dictionary features based on establishing a medical dictionary. The experiments showed that these features were conducive to improving the CNER

effect. Wang et al. [23] integrated dictionary features into the BiLSTM-CRF, and the results showed that prior knowledge helped improve the performance of the BiLSTM-CRF. Liu et al. [24] compared the CRF model requiring manual features with the LSTM-CRF without manual features and found that the F1 score of the LSTM-CRF on the i2b2 2010, 2012, and 2014 corpora was better than that of CRF.

However, the above CNER methods based on a deep neural network could not model the polysemy of words. That is, they could not solve the problem of polysemy. Therefore, Devlin et al. proposed a bidirectional encoder representation from transformer pretrained language model (BERT), which used bidirectional transformer encoders to capture potential semantic relations and generated a pretrained language model. Based on BERT, Liu et al. put forward the RoBERTa model to enhance the performance of BERT. And then, Lan et al.'s ALBERT model, a lightweight BERT model, was put forward for using two strategies to reduce the size of BERT. Dai et al. [25] compared the model performance after Word2vec and BERT were fused with BiLSTM-CRF, and the experiment showed that the model performance would be better if BERT was fused with the traditional BiLSTM-CRF model. However, these models failed to consider the characteristics of medical datasets thoroughly, and the performance on medical entity extraction was not highly effective.

2.2. Radical-Level Information. The specialization of the medical field leads to the particular linguistic structure of medical texts. Many experts have investigated on this characteristic. Peng et al. [26] put forward two types of Chinese radical-level hierarchical embeddings, and experimental results showed that radical-level semantics and sentiments on the sentence-level classification of emotions were better than char embeddings and word embeddings. A new deep learning technology referred to as “Radical Embedding” was proposed, and Shi et al. [27] conducted three experiments to verify its effectiveness. The results showed that the effect of radical embeddings was the same as competing methods and sometimes even better. Yin et al. [28] proposed BiLSTM-CRF based on radical features and used self-attention to capture character dependence. A new strategy was proposed to integrate dictionary information with characteristic presentation from BERT, and the F1 value of this method reached 91.60% and 89.56% on CCKS2017 and CCKS2018, respectively. However, in the existing researches, the information of radical has not been fully utilized.

3. Methods

3.1. Radical Characteristics. The Chinese electronic medical record datasets are different from the other datasets. In the CCKS2017 and CCKS2019 datasets, the frequency of radical-level feature is shown in Figure 1.

As the introduction mentioned, the radical “月” is often associated with the human organ, the radical “疒” is often related with the disease, and the radical “口” frequently appears in symptom entities. As shown in Figure 1, the Chinese five elements “metal, wood, water, fire, and earth” are

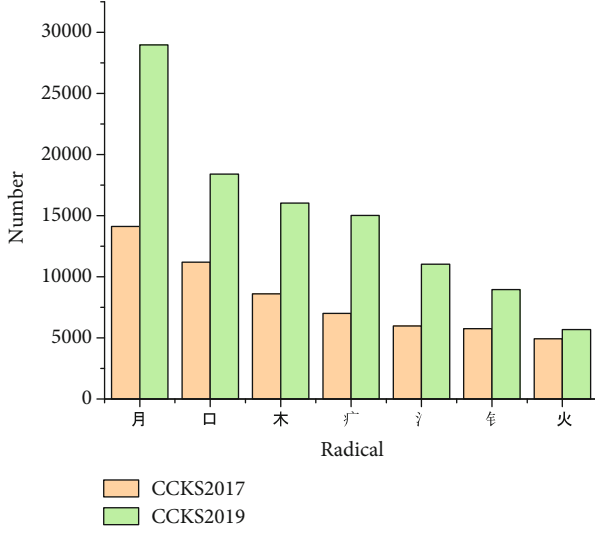


FIGURE 1: The occurrence frequency of each radical feature.

often included in medical entities. For example, “车” correlates with microelement and drug names such as “钙” and “铁.” “木” is related to “查体” and “脑血栓” and the name of the Chinese patent medicine. “讠” is associated with body fluids (plasma, tissue fluid, and lymphatic fluid) and symptoms such as “渗” and “溶.” “火” has a relationship with inflammation-related entities such as “病灶” and “骨髓炎.” “土” relates to modification words of a body part such as “壁” and “型.” These radical features play an essential role in identifying medical entities [29].

The sources of the radicals include two parts: local dictionaries and Baidu Chinese dictionaries (<https://hanyu.baidu.com>). The local dictionary is created by crawling the familiar words of Xinhua Dictionary (<http://xh.5156edu.com/>). Thus, it generates a dictionary of key-value pairs in the form of “chars-radicals.”

3.2. Design of Architecture. The proposed Ra-RC framework for the clinical named entity recognition task is shown in Figure 2. The framework mainly includes BiLSTM for radical-level representation, sequence modeling, and label inference layer. We train RoBERTa on both datasets where radical representations are extracting from BiLSTM. After that, we concatenate the char representations and radical-level representations and then feed them into CRF to decode.

3.2.1. BiLSTM for Radical-Level Representation. To make the most of the radical information, it needs to be extracted by a deep learning framework. From the perspective of theoretical and practical effects, both BiLSTM and RoBERTa are more suitable for feature extraction tasks, and RoBERTa enhances the performance based on BERT to have better expression ability. Therefore, this paper chooses these technologies to get contextual semantic information.

Figure 3 shows an overview of the radical-BiLSTM model. Formally, the inputs contain two parts: word embedding and radical embedding. Firstly, each word finds its corresponding radicals using a mapping dictionary which was

constructed. Secondly, both words and radicals pass through the same trainable matrix of the lookup layer. Afterward, for the preliminary representations of radical messages, we concatenate both embeddings recorded as X_i , and then feed X_i into the BiLSTM network to extract the feature.

As shown in Figure 3, the radical-level representation $X_i = (x_1, x_2, \dots, x_n)$ is taken as an input to the BiLSTM network. The BiLSTM network has two kinds of LSTM cells [30] that extract the feature in the forward (\vec{h}) and backward (\overleftarrow{h}) directions. The i^{th} characters $H_{Li} = (h_{l1}, h_{l2}, \dots, h_{ld})$ are the output of hidden state in the backward direction, and the $H_{Ri} = (h_{r1}, h_{r2}, \dots, h_{rd})$ is obtained after the forward LSTM. Afterwards, we can get the complete output hidden state $C_i = [(H_{Li}, H_{Ri})]$ of each position i by concatenating H_{Li} and H_{Ri} . An LSTM cell is made up of three gates which are used to select semantic information. The implement of LSTM cell is

$$i_t = \sigma(W_{xi}x_t + b_{ii} + W_{hi}h_{t-1} + b_{hi}), \quad (1)$$

$$f_t = \sigma(W_{xf}x_t + b_{if} + W_{hf}h_{t-1} + b_{hf}), \quad (2)$$

$$o_t = \sigma(W_{xo}x_t + b_{io} + W_{ho}h_{t-1} + b_{ho}), \quad (3)$$

$$\tilde{c}_t = \tanh(W_{xc}x_t + b_{ic} + W_{hc}h_{t-1} + b_{hc}), \quad (4)$$

$$c_t = f_t c_{t-1} + i_t \tilde{c}_t, \quad (5)$$

$$h_t = o_t \tanh(c_t), \quad (6)$$

where $\sigma(\cdot)$ denotes element-wise Sigmoid function and $\tanh(\cdot)$ denotes hyperbolic tangent functions. w is a weight matrix, and b is bias. i_t , O_t , and f_t are called input gate, output gate, and forget gate, respectively.

The output of the BiLSTM network is referred to as C_i , and characteristic representations, which are called P_i , are extracted from RoBERTa. The final representations O_i splice C_i and P_i together.

3.2.2. Sequence Modeling. We use the famous architecture of RoBERTa, which consists of the bidirectional transformer encoder for feature extraction and sentence modeling. As an autocoding language model, the model can introduce noise data to reconstruct the original data. It randomly selects some words to be predicted through the Mask language model mechanism and shields them with the [MASK] symbol. The training process is shown in Figure 4. Firstly, input sentences are segmented and annotated according to character level.

Secondly, the sentence is processed as a distributed representation $Y = (Y_1, Y_2, \dots, Y_t, \dots, Y_n)$, consisting of token embedding, segment embedding, and position embedding. Y_t indicates the input status of each character:

$$Y_t = Y_{\text{token_emb}} + Y_{\text{seg_emb}} + Y_{\text{pos_emb}}. \quad (7)$$

The transformer encoder is the most core component of the RoBERTa pretraining model, where multiheaded attention is the most critical module of the transformer unit.

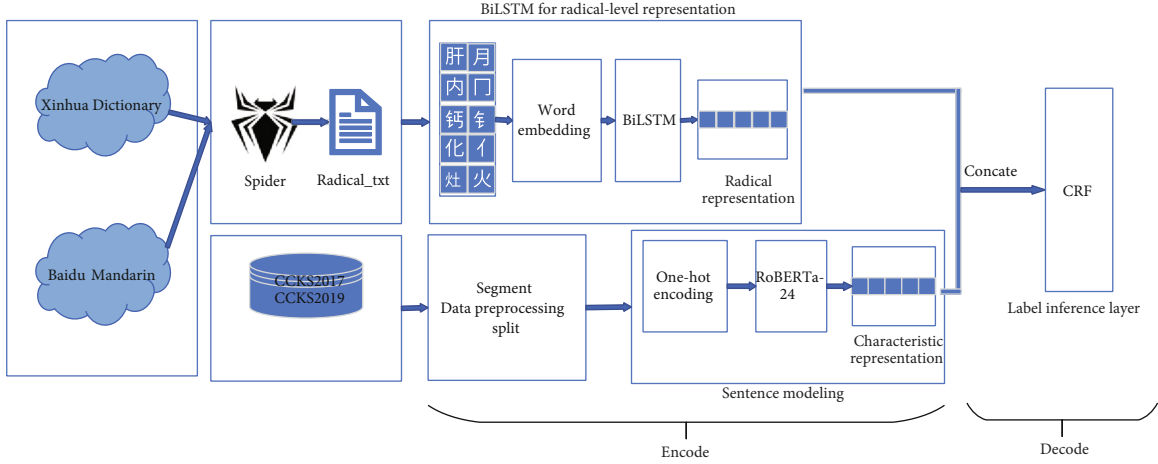


FIGURE 2: Ra-RC framework of CNER.

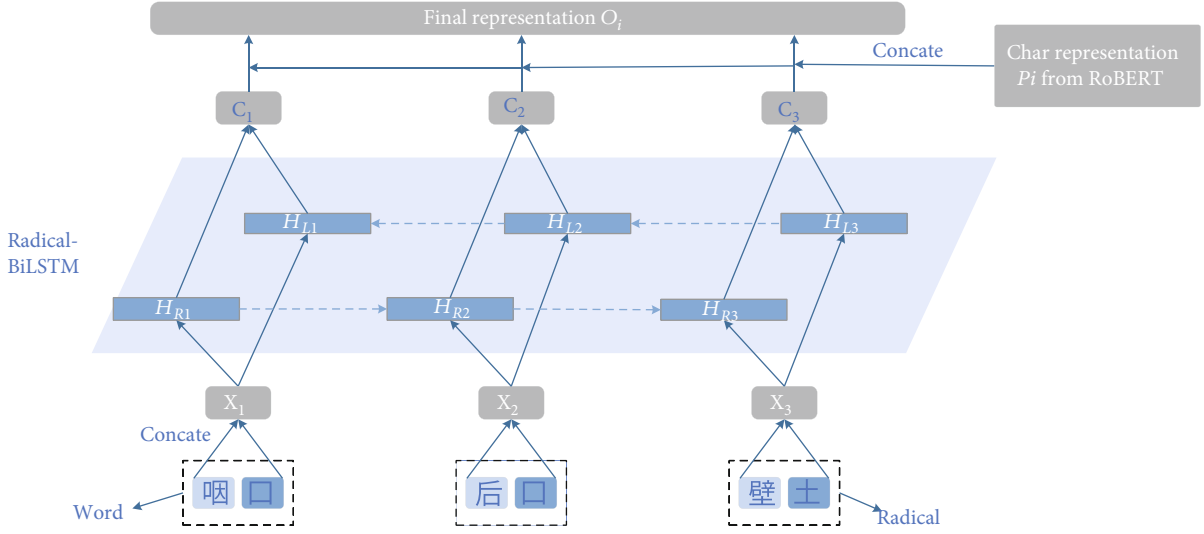


FIGURE 3: The model of radical-BiLSTM.

The multiheaded attention mechanism is utilized to capture character dependencies. The calculation of the single-head attention mechanism is shown in equation (8).

$$\text{head}_i = \text{Attention} \left(Y_t W_i^Q, Y_t W_i^K, Y_t W_i^V \right). \quad (8)$$

where W_i^Q , W_i^K , and W_i^V are the weight parameters for i^{th} calculation, respectively.

Then, the results of i^{th} calculations are stitched together. Moreover, we linearly transformed once more to obtain the results of the multiheaded attention calculation. The specific formula is shown in equation (9), where W^o is the weight parameter.

$$\text{MultiHead}(Q, K, V) = \text{Concat}(\text{head}_1, \text{head}_2, \dots, \text{head}_n) W^o. \quad (9)$$

3.2.3. *Label Inference Layer.* Finally, we use a sequential CRF [31] layer to infer the correct tag sequence. $S = \{w_1, w_2, w_3, \dots, w_n\}$ represents the tag sequence, $y = \{y_1, y_2, y_3, \dots, y_n\}$ score corresponding to the $S = \{w_1, w_2, w_3, \dots, w_n\}$ sequence.

$$s(S, y) = \sum_{i=1}^n E_{i, y_i} + \sum_{i=1}^{n+1} T_{y_{i-1}, y_i}, \quad (10)$$

where E is the emission matrix output by the RoBERTa layer, and $E_{i,j}$ represents the probability that the i^{th} word is classified into the j^{th} label; T is the transition matrix, and $T_{i-1,i}$ refers to the score transferred from label $i-1$ to i ; and $s(S, y)$ refers to the score of the label prediction sequence y generated by the input sequence S .

In a given input sequence S , the CRF model is trained using the maximized log-likelihood function. The formulas

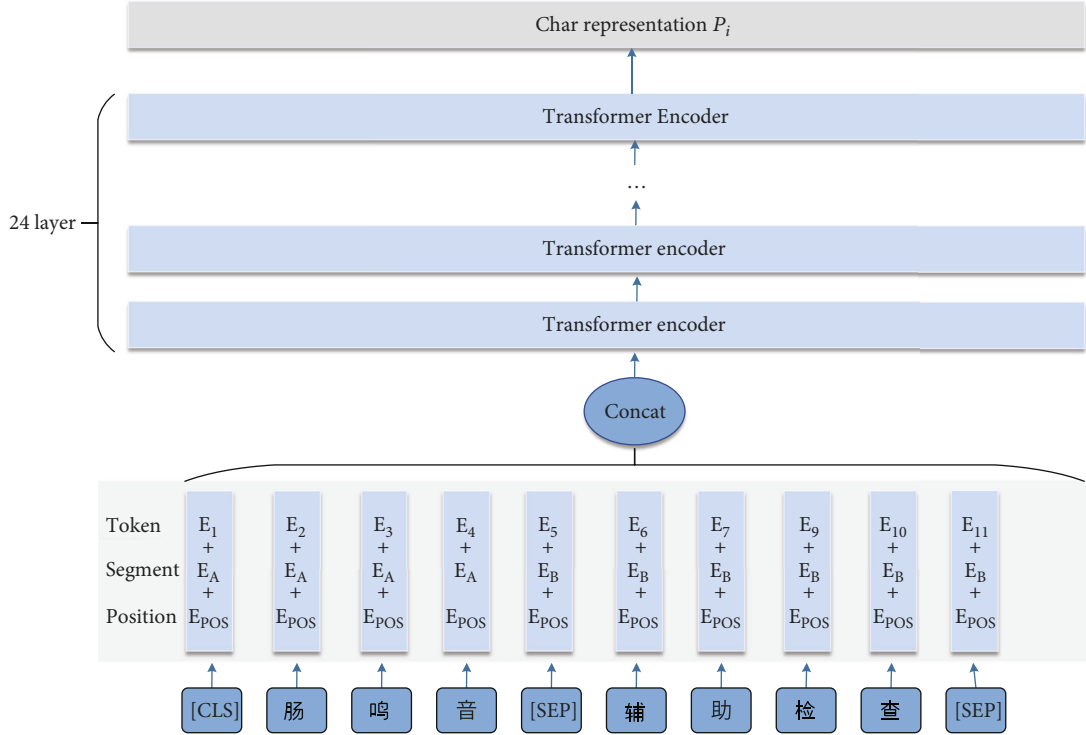


FIGURE 4: The RoBERTa for sentence modelling.

are shown in equations.

$$p(y | S) = \frac{e^{s(S,y)}}{\sum_{\tilde{y} \in Y_X} e^{s(S,\tilde{y})}}, \quad (11)$$

$$\log(p(y | S)) = s(S, y) - \log \left(\sum_{\tilde{y} \in Y_X} e^{s(S,\tilde{y})} \right). \quad (12)$$

The higher the $s(S, y)$ score, the greater the probability. Besides, Y_X is the sequence of all the possible tags for a given sentence S , and $\log(p(y | S))$ is the defined loss function.

In the decoding process, the Viterbi algorithm is used to solve the CRF global optimal sequence label. The formula is given below, where y^* is the sequence in which the score function achieves the maximum value.

$$y^* = \arg \max_{\tilde{y} \in Y_X} s(X, \tilde{y}). \quad (13)$$

4. Experiments

4.1. Datasets. In this study, the CCKS2017 and CCKS2019 datasets are utilized to conduct experiments. The datasets contain actual EMR data, and a professional medical team manually annotated all EMR corpora. As we did not participate in the competition, the CCKS2017 dataset is incomplete. The numbers of the various types of medical entities are given in Figure 5.

The Beginning, Inside, Outside (BIO) sequence labeling system, a standard labeling strategy in the NER field, is

adopted in this study. Note that “B” means the starting position of the medical entity, “I” represents the middle position of the medical entity, and “O” indicates that it is not a medical entity, such as “B-X,” “I-X,” and “O,” where X represents the type of medical entity.

4.2. Evaluation. In this experiment, accuracy (P), recall rate (R), and F1 score are used as the comprehensive evaluation indexes of NER. The specific formulas are shown as follows:

$$P = \frac{TP}{TP + FP} \times 100\%, \quad (14)$$

$$R = \frac{TP}{TP + FN} \times 100\%, \quad (15)$$

$$F_1 \text{ Measure} = \frac{2PR}{P + R} \times 100\%, \quad (16)$$

where TP is the number of correctly identified medical entities, FP is the number of unrelated medical entities identified, and FN is the number of unknown medical entities.

4.3. Environment. In this experiment, the NER model is based on the TensorFlow framework. Besides, the hardware and software environments are listed in Table 1.

4.4. Result and Discussion. In the experiment, the ratio of the training set to the test set is 5 : 1. The relevant parameters are set as follows: Radical embedding is initialized from a uniform distribution, where the embedding dim is set to 128. The hidden size of BiLSTM is 128. Char embedding is initialized via a pretrained model. The parameters of pretrained are

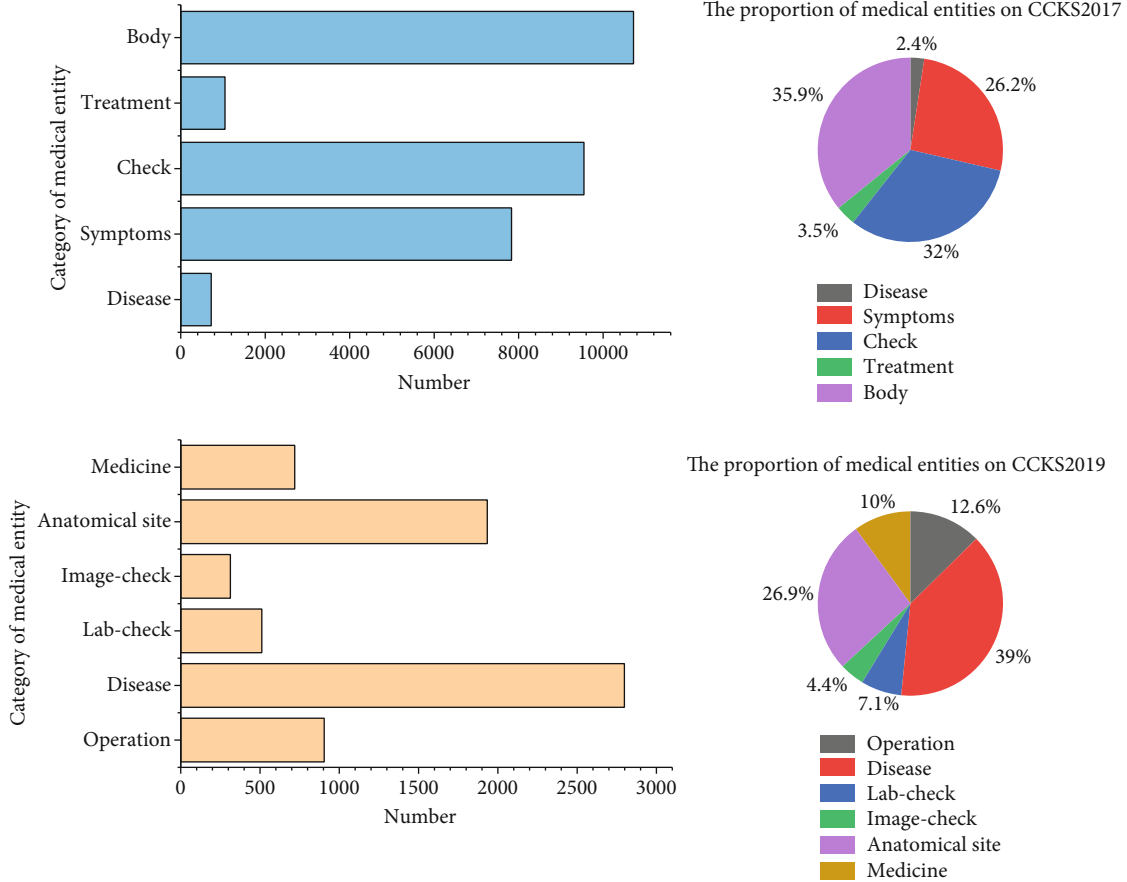


FIGURE 5: The numbers and proportion of both datasets.

TABLE 1: Experimental environment settings.

Item	Environment
Operating system	Ubuntu 18.04.5 LTS
CPU	i7-8700 @3.20GHz
GPU	NVIDIA GeForce RTX 2080Ti
Memory	31G
Python version	3.6
TensorFlow version	TensorFlow1.13.0
Keras version	2.2.4

all default parameters. Adam optimization algorithm [32] is adopted to optimize the model and the learning rate of $1E-5$.

4.4.1. Compare Three Pretraining Models. To better integrate with the radical-level information, three pretraining models are trained and tested on the extraction of medical entities, and then, the best one was selected as our baseline model.

As observed in Tables 2 and 3, RoBERTa has the best effect of extracting entities. This reason is that RoBERTa has more data, more steps, and a large batch than BERT. Moreover, the RoBERTa-wwm-ext-large model has a 24-tier transformer to get a more robust capability of feature extraction.

4.4.2. Ablation Experiments. We take RoBERTa-CRF as the baseline model, and the comparison after adding the radical information is shown in Tables 4 and 5. RC stands for RoBERTa-CRF, and Ra-RC means adding radical information.

The extraction results of medical entities of CCKS2017 are shown in Table 4. The F1 values of the ‘‘Symptom’’ and ‘‘Check’’ categories are the highest, which are ‘‘96.53’’ and ‘‘96.36,’’ respectively. Nevertheless, the recognition effect on ‘‘Treatment’’ is lacking, indicating that this type of entity is difficult to recognize. According to Figure 1, the sample size of this type of entity is small, accounting for only 3.60%. Hence, the neural network does not have enough samples to learn features, and the structure of entities is like the ‘‘Disease’’ entity, which is prone to classification errors. For example, consider ‘‘输卵管结扎术’’ and ‘‘输卵管结扎术后,’’ they belong to different entity classes, where the former belongs to the ‘‘disease and diagnosis’’ entity class and the latter belongs to the ‘‘Treatment’’ entity class. On the whole, we can observe that our Ra-RC model based on radical-level information that BiLSTM extracts achieves the best performance with the F1 value of 93.26%, the precision of 94.14%, and the recall of 92.39% on the CCKS2017 dataset. The F1 value of the RA-RC is 1.2% higher than that of RC. In view of entity categories, the F1 values of all categories are higher than RC except for ‘‘Disease’’ and ‘‘Treatment.’’

TABLE 2: Comparison of three pretraining models on CCKS2017.

Model	Precision	Recall	F1 score
BERT+CRF	89.78	91.64	90.70
ALBERT+CRF	89.12	91.38	90.24
RoBERTa-wwm-ext+CRF	92.62	90.35	91.47
RoBERTa-wwm-ext-large+CRF	92.79	91.34	92.06

TABLE 3: Comparison of three pretraining models on CCKS2019.

Model	Precision	Recall	F1 score
BERT+CRF	81.82	79.33	80.56
ALBERT+CRF	81.91	77.68	79.74
RoBERTa-wwm-ext+CRF	81.83	79.33	80.55
RoBERTa-wwm-ext-large+CRF	82.29	79.69	80.97

TABLE 4: Comparison of RC and Ra-RC on CCKS2017.

		RC	Ra-RC
Disease	<i>P</i>	90.29	89.44
	<i>R</i>	89.76	89.17
	F1	90.02	89.31
Symptoms	<i>P</i>	94.08	95.00
	<i>R</i>	98.62	98.11
	F1	96.30	96.53
Check	<i>P</i>	95.52	95.73
	<i>R</i>	96.04	97.00
	F1	95.78	96.36
Treatment	<i>P</i>	60.97	61.25
	<i>R</i>	70.42	69.01
	F1	65.35	64.90
Body	<i>P</i>	89.14	89.29
	<i>R</i>	90.67	90.79
	F1	89.90	90.03
Total	<i>P</i>	92.79	94.14
	<i>R</i>	91.34	92.39
	F1	92.06	93.26

At the same time, the extraction results of medical entities of CCKS2019 are shown in Table 5. It can be seen from Table 5 that the Ra-RC model combining radical-level information has an improvement of 1.9% in terms of F1 value compared with the RC model, which is without radical-level information on the CCKS2019 dataset. All types of entities have increased except for the “disease” entity. “Medicine” has the best recognition performance of all entities where the F1 score reaches 92.77%. However, the recognition effect on the entity class of “Lab-Check” is insufficient, because some entities of “lab-check” in which the composition is complex often cause an error in boundary judgment. For instance,

TABLE 5: Comparison of RC and Ra-RC on CCKS2019.

		RC	Ra-RC
Image-check	<i>P</i>	78.48	81.23
	<i>R</i>	84.09	85.71
	F1	81.19	83.41
Operation	<i>P</i>	81.25	79.61
	<i>R</i>	75.00	77.56
	F1	78.00	78.57
Medicine	<i>P</i>	87.79	93.27
	<i>R</i>	89.23	92.27
	F1	88.50	92.77
Disease	<i>P</i>	80.02	78.74
	<i>R</i>	78.59	79.00
	F1	79.30	78.87
Lab-check	<i>P</i>	72.46	74.28
	<i>R</i>	66.28	69.96
	F1	69.23	72.06
Anatomical site	<i>P</i>	78.90	82.67
	<i>R</i>	86.57	85.23
	F1	82.55	83.93
Total	<i>P</i>	82.29	83.31
	<i>R</i>	79.69	82.44
	F1	80.97	82.87

these entities are always composed of “letters and other characters,” such as “CEA,” “F/T,” “T-PSA,” and “CA125.” Moreover, some image-check entities are made up of letters, such as “OR” and “CT”. Due to the similarity of “image-check” and “lab-check” structures, the model cannot analyze the boundary between two kinds of entity classes.

In order to further compare the performance of RC and RA-RC, we also calculate the F1 value, recall, and precision of different methods, as shown in Figure 6. The RC (17) and RA-RC (17) represent that experiments conducting on the CCKS2017 dataset, RC (19) and RA-RC (19) are evaluated on the CCKS2019 dataset. In Figure 6, the F1 score of the Ra-RC model is higher than RC on both datasets.

4.4.3. Comparative Experiment with Existing Research Work.

In addition to the basic model described above, several researchers have conducted CNER studies on both datasets. For example, Li et al. [33] use a BiLSTM-CRF model combined with specialized word embeddings for CNER tasks. They use health domain datasets to create more prosperous and robust word embeddings. In addition to this, external health domain vocabulary is used to improve entity recognition results. Ouyang et al. [34] use the BiLSTM-CRF model combining the n -gram algorithm to the CNER tasks. At the same time, they introduce three types of external information as inputs to the model. Qiu et al. [35] use Chinese characters and dictionary features as input and then feed them into the

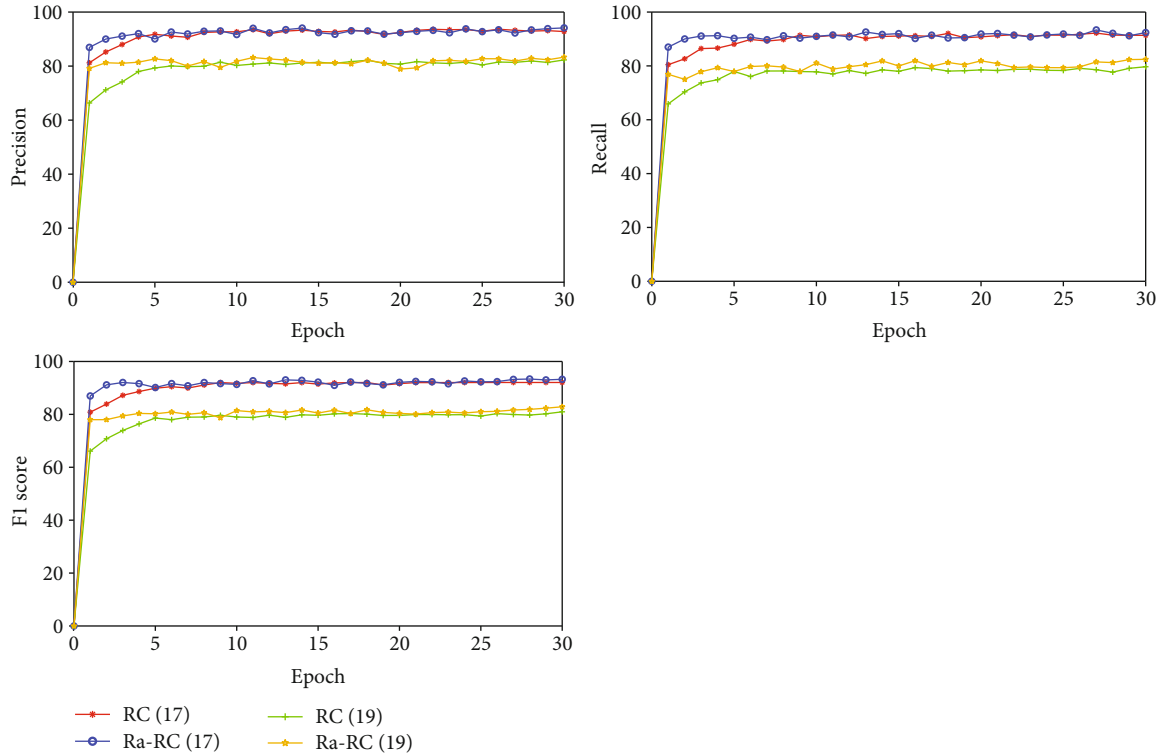


FIGURE 6: Evaluation results of RC and Ra-RC on the CCKS2017 and CCKS2019 datasets.

TABLE 6: Comparison of different methods on CCKS2017.

Method	Precision	Recall	F1 score
Li et al. [33]	—	—	87.95
Ouyang et al. [34]	—	—	88.85
Qiu et al. [35]	90.63	92.02	91.32
Tang et al. [36]	88.60	94.25	91.34
Wang et al. [23]	90.83	91.64	91.24
Luo et al. [4]	—	—	91.75
Yin et al. [28]	92.30	93.28	92.79
Yin et al. [28] *	92.27	93.73	93.00
Ours	94.14	92.39	93.26

residual dilated convolutional neural network combined with CRF to identify the entity. Tang et al. [36] propose a method that combines language model and multihead attention. Firstly, the sentence vectors are fed into BiGRU and the pre-trained model. After that, this paper concatenates the output of them. Moreover, the output is given to the block of BiGRU and multihead attention. Wang et al. [23] construct a medical domain dictionary using relevant medical resources and then integrate the dictionary features and word vectors into the BiLSTM-CRF model to identify entities. Luo et al. [4] propose a CNER method that is based on ELMo and multitask learning. The ELMo is trained by adding the stroke features as input. Simultaneously, multitask learning is used to make full use of existing data to improve the model's performance. Yin et al. [28] propose the AR-CCNER model. The radical

feature is extracted by the convolutional neural network (CNN). At the same time, this paper uses BiLSTM-attention to capture contextual features and the dependency between characters.

The experimental results are shown in Table 6. However, although all experiments are based on the CCKS2017 dataset, our dataset may not be the same as those of above researchers because we did not participate in the competition.

The results show that the Ra-RC achieves better precision and F1 score on the CCKS2017 dataset. Li et al.'s [33] model performs the worst because their approach is based on word segmentation, which causes the model to fail to identify word boundaries well. The latter is much larger than the former compared to the character set and the word set. This means that the corpus is not sufficient for the model to learn word embedding information effectively. What is more, the results show that the model of Yin et al. [25], which combines radical information and performs well on CCKS2017. The F1 score of the model has achieved 92.79%. This also proves that the radical feature is helpful for entity extraction. Moreover, they use self-attention to capture intercharacter dependencies, enhancing the extraction ability of entity, and the F1 score of the model has achieved 93.00%. However, this method is not compared with the pretraining model, which is the mainstream model in the CNER field. We compare the entity extraction effects of three pretraining models (BERT/ALBERT/RoBERTa) on the CCKS2017 dataset and combine them with another mainstream CNER technique (BiLSTM) to improve performance. The results show that pretraining the model helps to improve the performance of the model.

TABLE 7: Comparison of different methods on CCKS2019.

Method	Precision	Recall	F1 score
BERT-IDCNN-MHA-CRF (Liang et al. [37])	82.63	82.23	82.43
BiLSTM-CRF (baseline)	81.49	80.52	81.00
IDCNN-CRF (baseline)	80.56	81.47	81.01
Ours	83.31	82.44	82.87

The comparison of the CCKS2019 dataset is shown in Table 7. The experimental results show that the proposed model is superior to the baseline model in P , R , and $F1$ values. The $F1$ value of our model is slightly higher than the value of the model that Liang et al. [37] proposed, which indicates that the recognition ability of both is similar.

5. Conclusions

Aiming at the problem of insufficient medical entity extraction effect caused by the migration of the generic algorithm, we propose the Ra-RC model, which combines radical information extracted by BiLSTM with characteristic capturing by the pretrained model. To achieve a better entity extraction effect, we train three pretrained models for comparison. In addition, we introduce the radical feature, which can be seen as morphological information to enhance semantic information. After that, we concatenate both vectors and then feed them into CRF to get the corresponding label sequences. The experimental results on both datasets show that the Ra-RC method in this paper is superior to the baseline model.

A follow-up study will focus on how to distinguish entities more accurately with similar text structures. In addition, we will use this method in the following tasks, such as medical relation extraction and medical knowledge graph construction.

Data Availability

We have used the CCKS2017 and CCKS2019 datasets for our experiments. And datasets can be downloaded through the following link: <https://github.com/baiyewww/Data>.

Conflicts of Interest

The authors declare no conflicts of interest.

Acknowledgments

This work was supported by the National Natural Science Foundation of China (Grant no. 61972358) and Zhejiang Provincial Key Research and Development Program Project (Grant 2020C03071).

References

- [1] Y. Yin, Q. Huang, H. Gao, and Y. Xu, "Personalized APIs recommendation with cognitive knowledge mining for industrial systems," *IEEE Transactions on Industrial Informatics*, vol. 17, no. 9, pp. 6153–6161, 2020.
- [2] Y. Yin, Z. Cao, Y. Xu, H. Gao, R. Li, and Z. Mai, "QoS prediction for service recommendation with features learning in mobile edge computing environment," *IEEE Transactions on Cognitive Communications and Networking*, vol. 6, no. 4, pp. 1136–1145, 2020.
- [3] X. X. Yang, S. J. Zhou, and M. Cao, "An approach to alleviate the sparsity problem of hybrid collaborative filtering based recommendations: the product-attribute perspective from user reviews," *ACM/Springer Mobile Networks and Applications (MONET)*, vol. 25, no. 2, pp. 376–390, 2020.
- [4] L. Luo, Z. H. Yang, Y. W. Song, and N. L. H. F. Lin, "Chinese clinical named entity recognition based on stroke ELMo and multi-task learning," *Chinese Journal of Computers*, vol. 43, no. 10, pp. 1943–1957, 2020.
- [5] M. Song, H. Yu, and W. S. Han, "Developing a hybrid dictionary-based bio-entity recognition technique," *BMC medical informatics and decision making*, vol. 15, no. 1, pp. 1–8, 2015.
- [6] A. Coden, G. Savova, I. Sominsky et al., "Automatically extracting cancer disease characteristics from pathology reports into a disease knowledge representation model," *Journal of Biomedical Informatics*, vol. 42, no. 5, pp. 937–949, 2009.
- [7] D. Li, G. Savova, and K. Kipper-Schuler, "Conditional random fields and support vector machines for disorder named entity recognition in clinical texts," *Workshop on Current Trends in Biomedical Natural Language Processing*, pp. 94–95, 2008.
- [8] Y. Feng, C. Ying-Ying, Z. Gen-Gui, L. H. Wen, and L. Ying, "Intelligent recognition of named entity in electronic medical records," *Chinese Journal of Biomedical Engineering*, vol. 30, no. 2, pp. 256–262, 2011.
- [9] M. Miwa and M. Bansal, "End-to-end relation extraction using LSTMs on sequences and tree structures," *54th Annual Meeting of the Association for Computational Linguistics (Volume 1: Long Papers)*, vol. 2, pp. 1105–1116, 2016.
- [10] Z. Huang, W. Xu, and K. Yu, "Bidirectional LSTM-CRF models for sequence tagging," 2015, <https://arxiv.org/abs/1508.01991>.
- [11] X. P. Qiu, T. X. Sun, Y. G. Xu, Y. F. Shao, N. Dai, and X. J. Huang, "Pre-trained models for natural language processing: a survey," *Science China Technological Sciences*, vol. 63, no. 10, pp. 1872–1897, 2020.
- [12] Z. Z. Lan, M. Chen, S. Goodman, G. Kevin, S. Piyush, and R. Soricut, "ALBERT: a lite BERT for self-supervised learning of language representations," *ICLR*, pp. 1–16, 2020.
- [13] J. Devlin, M. W. Chang, K. Lee, and K. Toutanova, "BERT: pre-training of deep bidirectional transformers for language understanding," pp. 4171–4186, 2018, <https://arxiv.org/abs/1810.04805>.
- [14] Y. H. Liu, M. Ott, N. Goyal et al., "RoBERTa: a robustly optimized BERT pretraining approach," 2019, <https://arxiv.org/abs/1907.11692>.

- [15] P. D. Soomro, S. Kumar, A. A. Banbhrani, A. A. Shaikh, and H. Raj, "Bio-NER: biomedical named entity recognition using rule-based and statistical learners," *International Journal of Advanced Computer Science and Applications*, vol. 8, no. 12, pp. 163–170, 2017.
- [16] G. H. Xu, C. Y. Wang, and X. F. He, "Improving clinical named entity recognition with global neural attention," in *Asia-Pacific Web (APWeb) and Web-Age Information Management (WAIM) Joint International Conference on Web and Big Data*, vol. 11642, Cham, 2019.
- [17] R. Chalapathy, E. Z. Borzeshi, and M. Piccardi, "Bidirectional LSTM-CRF for clinical concept extraction," pp. 7–12, 2016, <https://arxiv.org/abs/1611.08373>.
- [18] Z. Yang, R. Salakhutdinov, and W. W. Cohen, "Transfer learning for sequence tagging with hierarchical recurrent networks," pp. 1–10, 2017, <https://arxiv.org/abs/1703.06345>.
- [19] M. E. Peters, W. Ammar, C. Bhagavatula, and R. Power, "Semi-supervised sequence tagging with bidirectional language models," *55th Annual Meeting of the Association for Computational Linguistics*, pp. 1756–1765, 2017.
- [20] J. Qiu, Q. Wang, Y. Zhou, T. Ruan, and J. Gao, "Fast and accurate recognition of Chinese clinical named entities with residual dilated convolutions," in *2018 IEEE International Conference on Bioinformatics and Biomedicine (BIBM)*, pp. 935–942, Madrid, Spain, 2019.
- [21] G. Wu, G. Tang, Z. Wang, Z. Zhang, and Z. Wang, "An attention-based BiLSTM-CRF model for Chinese clinic named entity recognition," *IEEE Access*, vol. 7, pp. 113942–113949, 2019.
- [22] X. Li, H. Zhang, and X. H. Zhou, "Chinese clinical named entity recognition with variant neural structures based on BERT methods," *Journal of Biomedical Informatics*, vol. 107, p. 103422, 2020.
- [23] Q. Wang, Y. Zhou, T. Ruan, D. Gao, Y. Xia, and P. He, "Incorporating dictionaries into deep neural networks for the Chinese clinical named entity recognition," *Journal of biomedical informatics*, vol. 92, article 103133, 2019.
- [24] Z. Liu, M. Yang, X. L. Wang et al., "Entity recognition from clinical texts via recurrent neural network," *BMC medical informatics and decision making*, vol. 17, Suppl 2, p. 67, 2017.
- [25] Z. Dai, X. Wang, P. Ni, Y. Li, G. Li, and X. Bai, "Named entity recognition using BERT BiLSTM CRF for Chinese electronic health records," in *2019 12th international congress on image and signal processing, biomedical engineering and informatics (cisp-bmei)*, Suzhou, China, 2019.
- [26] H. Peng, E. Cambria, and X. Zou, "Radical-based hierarchical embeddings for Chinese sentiment analysis at sentence level," in *The Thirtieth International Flairs Conference*, pp. 347–352, Marco Island, Florida, 2017.
- [27] X. Shi, J. Zhai, X. Yang, Z. Xie, and C. Liu, "Radical embedding: delving deeper to Chinese radicals," in *Proceedings of the 53rd Annual Meeting of the Association for Computational Linguistics and the 7th International Joint Conference on Natural Language Processing (Volume 2: Short Papers)*, vol. 10, pp. 594–598, Beijing, China, 2015.
- [28] M. Yin, C. Mou, K. Xiong, and J. Ren, "Chinese clinical named entity recognition with radical-level feature and self-attention mechanism," *Journal of biomedical informatics*, vol. 98, article 103289, 2019.
- [29] J. Z. Wang, "The generation, development and evolution of radicals and their types," *Traditional Chinese Medicine Culture*, vol. 1, no. 5–8, 1990.
- [30] S. Hochreiter and J. Schmidhuber, "Long short-term memory," *Neural Computation*, vol. 9, no. 8, pp. 1735–1780, 1997.
- [31] J. D. Lafferty, A. McCallum, and F. C. N. Pereira, "Conditional random fields: probabilistic models for segmenting and labeling sequence data," in *ICML '01 Proceedings of the Eighteenth International Conference on Machine Learning*, pp. 282–289, Williamstown, MA, USA, 2001.
- [32] A. Graves and J. Schmidhuber, "Framewise phoneme classification with bidirectional LSTM and other neural network architectures," *Neural Networks*, vol. 18, no. 5–6, pp. 602–610, 2005.
- [33] Z. Li, Q. Zhang, Y. Liu, D. Feng, and Z. Huang, "Recurrent neural networks with specialized word embedding for Chinese clinical named entity recognition," *CEUR Workshop Proceedings*, pp. 55–60, 2017.
- [34] E. Ouyang, Y. Li, L. Jin, Z. Li, and X. Zhang, "Exploring n-gram character presentation in bidirectional RNN-CRF for Chinese clinical named entity recognition," *CEUR Workshop Proceedings*, pp. 37–42, 2017.
- [35] J. Qiu, Y. Zhou, Q. Wang, T. Ruan, and J. Gao, "Chinese clinical named entity recognition using residual dilated convolutional neural network with conditional random field," *IEEE Transactions on Nanobioscience*, vol. 18, no. 3, pp. 306–315, 2019.
- [36] G. Q. Tang, D. Q. Gao, T. Ruan, Q. Ye, and Q. Wang, "Clinical electronic medical record named entity recognition incorporating language model and attention mechanism," *Computer Science*, vol. 47, no. 3, pp. 211–216, 2020.
- [37] W. Liang, Y. H. Zhu, F. Zhan, and X. B. Ji, "Named entity recognition of electronic medical records based on BERT," *Journal of Hunan University of Technology*, vol. 34, no. 4, pp. 54–62, 2020.

Research Article

Story Generation Using Knowledge Graph under Psychological States

Feifei Xu , Xinpeng Wang , and Shanlin Zhou 

College of Computer Science and Technology, Shanghai University of Electric Power, Shanghai, China

Correspondence should be addressed to Xinpeng Wang; wangxinpeng@mail.shiep.edu.cn

Received 18 February 2021; Revised 17 March 2021; Accepted 29 March 2021; Published 28 April 2021

Academic Editor: Honghao Gao

Copyright © 2021 Feifei Xu et al. This is an open access article distributed under the Creative Commons Attribution License, which permits unrestricted use, distribution, and reproduction in any medium, provided the original work is properly cited.

Story generation, aiming to generate a story that people could understand easily, captures increasing researchers' attention in recent years. However, a good story usually requires interesting and emotional plots. Previous works only consider a specific or binary emotion like positive or negative. In our work, we propose a Knowledge-Aware Generation framework under Controllable Conditions (K-GuCCI). The model assigns a change line of psychological states to story characters, which makes the story develop following the setting. Besides, we incorporate the knowledge graph into the model to facilitate the coherence of the story. Moreover, we investigate a metric AGPS to evaluate the accuracy of generated stories' psychological states. Experiments exhibit that the proposed model improves over standard benchmarks, while also generating stories reliable and valid.

1. Introduction

Story generation has been an emerging theme in natural language processing technologies [1–3]. Much of the research has examined the coherence, rationality, and diversity of the generated stories. Huang et al. and Song et al. [4, 5] and Luo et al. [6] argued that assigning emotions in text generation could enrich the texts and full of variety. From psychological theories, Figure 1 shows the fine-grained psychological states involved in an individual. Figure 1(a) displays the motivation of folks described by the two popular theories: the “Hierarchy of Needs” of Maslow [7] on the left, and the “Basic Motives” of Reiss [8] on the right. “Hierarchy of Needs” proposed by Maslow use such terms as *physiological needs*, *stability*, *love/belonging*, *esteem*, and *spiritual growth* to describe the evolution of human motivation. There are nineteen fine-grained categories that include a variety of motives in Reiss, which is richer than that in Maslow. Plutchik [9], also called the “Wheel of Emotions”, has eight motions shown in Figure 1(b). Xu et al. [10] propose a novel model called SoCP, which uses the theories to generate an emotional story. Nevertheless, it still lacks richness and coherence.

Knowledge graph, known for better semantic understanding, is a key factor in the success of natural language

processing. External knowledge can be introduced to increase the richness of the texts in story generation. Zhou et al. [11] use a large-scale commonsense knowledge in neural conversation generation with a Graph Attention approach, which can better interpret the semantics of an entity from its neighboring entities and relations.

Accordingly, we propose a model called K-GuCCI, which leverages the knowledge graph to enhance the coherence of story generation and psychological theories to enrich the emotion of stories. Table 1 shows an example of a generated story. Our proposed model under controllable conditions can generate stories with multiple fine-grained psychological states of multiple characters by assigning emotional change lines to the characters in the story. We design a Character Psychological State Controller (CPSC). Each time step in the decoder selects a character who will be described at the current time step and corresponding psychological state we assigned manually from many characters in the story. The selected character's psychological state will then be controlled and determined. For generating coherent stories easily, we introduce the external knowledge that can facilitate language understanding and generation. ConceptNet is a commonsense semantic network that consists of triples with head, relation, and tail, which can be represented as $g = (h,$

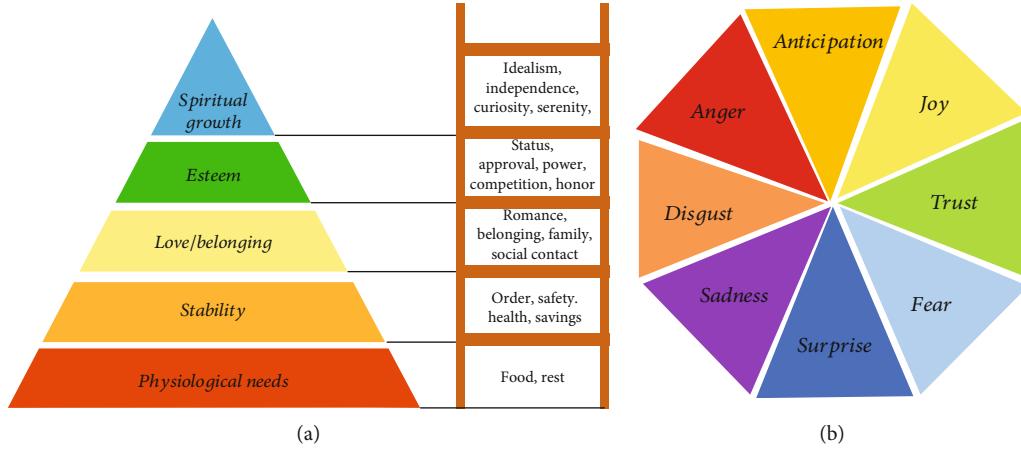


FIGURE 1: We take the psychological states consisting of Maslow, Reiss, and Plutchik three theories as our controllable conditions. The pyramid in (a) shows the five categories of Maslow from the physiological to the spiritual level. The right ladder represents the Reiss motives as a subset of Maslow. Plutchik’s wheel of emotions in (b) represents the eight basic dimensions of emotions.

TABLE 1: An example of our story generation. The input sentence is the beginning of the story. “Jervis” and “girlfriend” are the characters in the story. We have three psychological theories, like “Plutchik,” “Maslow,” and “Reiss.” For Plutchik, each character has an emotional change line assigned manually. The characters will share identical motivations based on Maslow and Reiss. The following table shows an example of the story.

Input	Jervis has been single for a long time.	
Characters	Jervis, girlfriend	
Plutchik	Jervis	Sadness–anticipation–joy–joy–joy
	Girlfriend	None–none–joy–joy–joy
Maslow	Love	
Reiss	Contact, romance	
Story	Jervis has been single for a long time.	
	He wants to have a girlfriend.	
	One day he meets a nice girl at the grocery store.	
	They begin to date.	
	Jervis is happy that he is no longer single.	

r, t). The head and tail can be connected by their relation, where we apply this method to build a bridge of story context and next story sentence. Inspired by the Graph Attention [11], we design a knowledge-enhanced method to represent the knowledge triples. The method treats the knowledge triples as a graph, from which we can better interpret the semantics of an entity from its neighboring entities and relations. For the reason of the particularity of our model, the evaluation metric of the accuracy of psychological state control is investigated.

Our contributions are as follows:

- (i) We develop three psychological theories as controllable conditions, which are used to describe characters in the stories
- (ii) To enhance the semantic and richness of the story, we introduce the external knowledge graph into the generation model

- (iii) We propose a model K-GuCCI, which utilizes external knowledge to enhance story generation’s coherence while ensuring the controllability of conditions. We design a character psychological state controller that achieves fine-grained psychological state control of the characters in the story
- (iv) We explore a novel evaluation metric for the accuracy rate of psychological state control
- (v) The experimental results demonstrate superior performance in various evaluating indicators and can generate more vivid and coherent stories with fine-grained psychological states of multiple characters. We also verify the effectiveness of the designed modules

2. Related Work

2.1. Text Generation with External Knowledge. Introducing external knowledge to natural language tasks is a trend in recent several years. Semantic information can be enhanced by external knowledge to help complete many works, particularly important in story generation. Chen et al. [12] utilize external knowledge to enhance neural data-to-text models. Relevant external knowledge can be attended by the model to improve text generation. Wang et al. [13] introduce the knowledge base question answering (KBQA) task into dialogue generation, which facilitates the utterance understanding and factual knowledge selection. Zhou et al. [11] first attempt to use large-scale commonsense knowledge in conversation generation. They design a graph attention mechanism in encoder and decoder, which augments the semantic information and facilitates a better generation. Guan et al. [14] focus on generating coherent and reasonable story endings by using an incremental encoding scheme. All of the above works show the effectiveness of introducing external knowledge. In our work, the proposed model K-GuCCI mainly focuses on the characters’ psychological state.

2.2. Story Generation under Conditions. Story generation has attracted much attention recently. Jain et al. [15] leverage a sequence-to-sequence recurrent neural network architecture to generate a coherent story from independent descriptions. The standalone textual descriptions describing a scene or event are converted to human-like coherent summaries. Fan et al. [2] explore coarse-to-fine models that first generate sequences of predicates and arguments conditioned upon the prompt and then generate a story with placeholder entities. Finally, the placeholders are replaced with specific references. Fan et al. [1] propose a hierarchical model that can build coherent and fluent passages of text about a topic. Yu et al. [16] propose a multipass hierarchical CVAE generation model, targeting to enhance the quality of the generated story, including wording diversity and content consistency. A lot of emotional text generation tasks have emerged in recent years. Xing et al. [17] use a sequence-to-sequence structure with topic information to produce exciting chatbots responses with rich information. Ghosh et al. [18] generate conversational text conditioned on affect categories, which customize the degree of emotional content in generated sentences through an additional design parameter. There are also some generation tasks with emotion or sentiment [4, 19, 20]. They only use a specific or binary emotion like positive or negative to express emotion or sentiment. Unlike the above works, we aim to generate a story with different characters' psychological states change, including multiple motivations and emotions. We use [21] as our dataset that composes of a five-sentence story. The characters' motivations and emotions in the story will change with the development of the story plot. Paul and Frank [22] also use the dataset to do a sentiment classification task according to the psychological state.

3. Methodology

Figure 2 shows an overview of the K-GuCCI model. The proposed model can generate vivid and coherent stories under controllable conditions. We assign the multiple fine-grained psychological states of characters as controllable conditions. We perform story generation using a Seq2Seq structure [23] with external knowledge using graph attention method, where BiLSTM [24] and LSTM [25] are used as encoder and decoder, respectively. We design a Character Psychological State Controller (CPSC) module to control each character's fine-grained psychological state.

3.1. Problem Formulation. Formally, the input is a text sequence $X = (x_1^c, \dots, x_n^c)$ that is a beginning of the story, which consists of n words. We also take story context $C = (x_1^c, \dots, x_m^c)$ consisting of m words as input to increase the coherence of the story, which represents historical story sentences of the input sentence X . We represent the external knowledge as $K = ([h_1, r_1, t_1], \dots, [h_j, r_j, t_j])$, where $[h_i, r_i, t_i]$ is the triple consisting of head, relation, and tail. Meanwhile, we quantify a psychological state score of each character for three theories Plutchik, Maslow, and Reiss: $S^{pmr} = (S_1^p, S_1^m, S_1^r), \dots, (S_j^p, S_j^m, S_j^r)$, where j is the characters' number in the story. The output

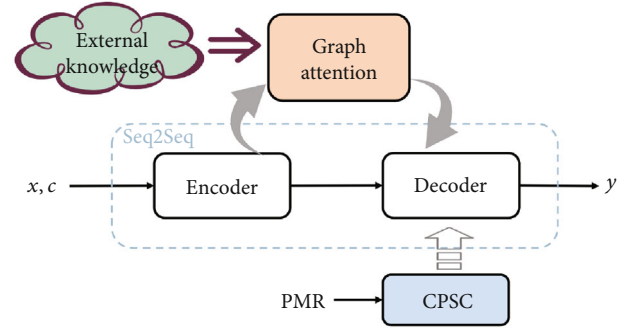


FIGURE 2: The architecture of K-GuCCI model. We introduce external knowledge into the model that improves the richness of the model. The PMR is a quantified psychological state matrix, and the Character Psychological State Controller (CPSC) is designed to generate the story following the setting psychological states for characters.

target is another text sequence $Y = (y_1, \dots, y_k)$ that consists of k words. The task is then formulated as calculating the conditional probability $P(Y | [X, C], PMR, K)$, where PMR represents the psychological state.

3.2. Character Psychological State Controller. The Character Psychological State Controller is used to control which and how much characters' psychological state can be used to describe the story. For psychological state, because it is composed of multiple psychological states, we quantify the psychological state so that it can be accepted by the model.

3.2.1. Psychological State Representation. We quantify a psychological state as a PMR matrix that is used to describe the fine-grained psychological state of characters in the story. As shown in Figure 3, we just display Plutchik score of each character for the third sentence in the story, where the score "0" denotes no current emotion. The higher the score, the richer the current emotion. We normalize these scores and then build a vector for each emotion or motivation. We set the characters number as maximum n for processing different characters in the stories. We concatenate them as multiple characters score matrix, i.e., Plutchik score S^p , Maslow score S^m , and Reiss score S^r . Then, a word vector matrix for the three psychological states is randomly initialized as V^p , V^m , and V^r , respectively. Figure 3 shows the Plutchik score matrix S^p and word vector matrix V^p . For the Plutchik score matrix S^p , we pad the matrix with less than the maximum number of characters. Each row represents a character, and each column represents a score for each emotion. For word vector matrix V^p , each row expresses a representation of an emotion. The word vector matrix will be multiplied by the characters score matrix; then, the product will be mapped into a low dimension space. We obtain the Plutchik matrix, the Maslow matrix, and the Reiss matrix subsequently. The formulation is as follows:

$$P_i = W_p (S_i^p \times V_i^p) + b_p, \quad (1)$$

$$M_i = W_m (S_i^m \times V_i^m) + b_m, \quad (2)$$

Story: Gina wanted a unicorn folder like her friend Tami
 She had never seen anything like it.
 She had already been in trouble for talking while the teacher was.
 So she decide to wait till the teacher was done teaching.
 Once the teacher finished she asked Tami about the folder.

Character : Teacher, Gina, Tami

Plutchik score :

	Joy	Trust	Fear	Surprise	Sadness	Disgust	Anger	Anticipation
Teacher	0	0	0	5	0	6	8	0
Gina	0	0	0	0	0	0	0	4
Tami	0	4	7	0	4	0	0	0

	Joy	Trust	Fear	Surp rise	Sadn ess	Disg ust	Anger	Antici pation
Teacher	0	0	0	0.6	0	0.7	1	0
Gina	0	0	0	0	0	0	0	1
Tami	0	0.6	1	0	0.6	0	0	0
None
None	0	0	0	0	0	0	0	0

S^p

$n \times 8$

	Joy	Trust	Fear	Surprise	Sadness	Disgust	Anger	Anticipation
Joy								
Trust								
Fear								
Surprise								
Sadness								
Disgust								
Anger								
Anticipation								

V^p

$8 \times \text{hidden_size}$

FIGURE 3: An example of constructing the PMR matrix. We just attend to the third sentence in blue in the story. There are three characters in this story. The table above shows the Plutchik score for each character in the dataset. The matrix in orange and in green displays the Plutchik score matrix S^p and Plutchik word vector matrix V^p , respectively.

$$R_i = W_r(S_i^r \times V_i^r) + b_r, \quad (3)$$

where W_p , W_m , and W_r are the weight matrices. b_p , b_m , and b_r indicate the biases, and i is the i -th character. The Plutchik, Maslow, and Reiss matrices will be concatenated as characters PMR matrix for the convenience of calculation:

$$PMR_i = W_{pmr}(S_i^{pmr} \times V_i^{pmr}) + b_{pmr}. \quad (4)$$

3.2.2. Controllable Psychological State. We control the multiple characters' psychological states by first selecting a character who will be described at each decoder time step, and then, the selected character's psychological state will be controlled using an attention method.

At each step t of decoder, we use a feed-forward layer to compute a character gate vector g_t^{char} . The *softmax* activation is used to calculate a probability distribution of characters in the story; then, a *one-hot* mechanism picks up a character with maximum probability o_t^{char} . We multiply the PMR_i with the o_t^{char} to obtain the character's psychological states:

$$g_t^{\text{char}} = \text{softmax}(W_g[y_{t-1}; h_{t-1}; c_t]), \quad (5)$$

$$o_t^{\text{char}} = \text{one-hot}(g_t^{\text{char}}), \quad (6)$$

$$s_t^{\text{char}} = o_t^{\text{char}} \times PMR_i, \quad (7)$$

where W_g is the weight matrix, y_{t-1} is the input word, h_{t-1} is the decoder hidden state, and c_t is the context

vector. After that, we calculate a psychological state vector c_t^{PMR} at step t which is taken as the final condition to control model generation.

$$e_{t,i} = V_a^T \tanh(W_a s_t^{\text{char}} + U_a h_{PMR,i}), \quad (8)$$

$$\alpha_{t,i} = \frac{\exp(e_{t,i})}{\sum_{i=1}^c \exp(e_{t,i})}, \quad (9)$$

$$c_t^{PMR} = \sum_{i=1}^c \alpha_{t,i} PMR_i, \quad (10)$$

where W_a and U_a are the weight matrices, t is the time step, i is the i -th character, and c is the number of characters.

3.3. Knowledge-Enhanced Generation Model

3.3.1. Knowledge Encoding. In order to represent a word more meaningful and a story more coherent, we use knowledge aware representation and attention based on the context to enhance the semantic expression in the encoder. We first calculate a knowledge graph vector c_{kg} which attends to the triple of the words in the knowledge graph, and then a context vector c_{con} to attend to the context information; both of which are as the input with the sentence together. We get a knowledge graph vector c_{kg} by using graph attention [11]. The words in the sentences have their own knowledge representation by triples. In this way, the words can be enriched by their adjacent nodes and their relations. For a context vector

c_{con} , we use attention [26] method, which reflects the relation between the input sentence and its previous context.

$$h^{(i)} = \text{BiLSTM}\left(h^{(i-1)}, [X; C]^{(i)}, c_e^{(i)}\right), \quad (11)$$

where $h^{(i)}$ is the hidden state of the i -th sentence of the story. $c_e^{(i)}$ is the concatenation of the knowledge graph vector $c_{kg}^{(i)}$ and context vector $c_{con}^{(i)}$.

$$c_e^{(i)} = \left[c_{kg}^{(i)}; c_{con}^{(i)} \right], \quad (12)$$

where $c_{con}^{(i)}$ is the context attention vector of i -th sentence. $c_{kg}^{(i)}$ is the knowledge graph vector of the i -th sentence and is formulated as follows:

$$e_k^{(i)} = h^{(i)} W_k g(x)^{(i-1)}, \quad (13)$$

$$\alpha_k^{(i)} = \frac{\exp\left(e_k^{(i)}\right)}{\sum_{i=1}^c \exp\left(e_k^{(i)}\right)}, \quad (14)$$

$$c_{kg}^{(i)} = \sum_{i=1}^k \alpha_k^{(i)} g(x)^{(i-1)}, \quad (15)$$

where $g(x)^{(i-1)}$ is the graph attention vector in [11]. The whole story generation process will always be followed by the knowledge graph vector and context vector, which is the soul that keeps the story coherent.

3.3.2. Incorporating the Knowledge. We concatenate the last time step word embedding vector $e(y_{t-1})$, PMR context c_t^{PMR} , knowledge graph vector c_t^{kg} , and attention context c_t , which represent incorporating the external knowledge and psychological state into the generation model. The LSTM hidden state is updated as follows:

$$h_t = \text{LSTM}\left(\left[e(y_{t-1}); c_t^{PMR}; c_t^{kg}; c_t\right], h_{t-1}\right). \quad (16)$$

We minimize the negative log-likelihood objective function to generate expected sentences.

$$L_{NLL} = -\frac{1}{N} \sum_{i=1}^N \sum_{t=1}^T \log P\left(y_t^{(i)} \mid y_{<t}^{(i)}, X^{(i)}, C^{(i)}, PMR^{(i)}, k^{(i)}\right), \quad (17)$$

where N is the story number in the dataset, and T is the time step of the i -th generated sentence in the decoder. $X^{(i)}$ represents the i -th sentence in the dataset. Similarly, $C^{(i)}$, $PMR^{(i)}$, and $K^{(i)}$ represent the i -th context, i -th PMR matrix, and i -th knowledge triples in the dataset, respectively.

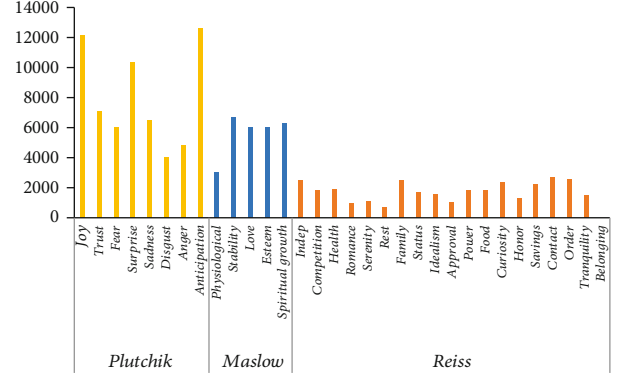


FIGURE 4: The statistic of psychological states. “Anticipation” is the most frequent state in Plutchick’s wheel of emotion, while “belonging” is the least frequent state in the Reiss classification.

TABLE 2: The statistic of character number.

Character number	Sentence number
1	11008
2	6547
3	1254
4	164
5	36
6	1

4. Experiments

4.1. Dataset. The dataset in [21] is chosen as our story corpus, consisting of 4k five-sentence stories. The corpus contains stories where each sentence is not only annotated but also with characters and three psychological theories. Figure 4 displays the statistic of the psychological states. Plutchik’s emotion appears more frequently than Maslow’s and Reiss’s motivation. Particularly, “joy” and “participation” are most in the Plutchik states. The Reiss categories are subcategories of the Maslow categories. We use different methods to process the dataset for *Plutchik*, *Maslow*, and *Reiss*. Three workers who are employed by the original author annotate the original data. Intuitively, the workers will have different viewpoints, so we sum up the Plutchik scores and normalize them. Maslow and Reiss have no repeated words; thus, we use a one-hot vector to represent them. We split the data as 80% for training and 20% for testing. In the test phase, we input the story’s first sentence and the normalized psychological states scores. Table 2 statistics the character number in each story sentence. They are most in the range 1-3, and the largest character number is 6. Thus, we set the character number as 3.

4.2. Baselines. We compare our model with representative baselines to investigate the effectiveness of the K-GuCCI model. The baselines are as follows:

Seq2Seq model introduced by Google in 2014 and has encoder, decoder, and intermediate step as its main components. The model can map input text with fixed length to

TABLE 3: Automatic evaluations of the proposed model and the baseline models. The context-merge and context-independent represent different methods of encoder mentioned in [10]. The former is to encode the context and sentence together, while the latter encodes them separately and then concatenates them.

Model	BLEU				ROUGE			METEOR	AGPS
	B-1	B-2	B-3	B-4	R-1	R-2	R-l		
Seq2Seq	0.202	0.049	0.016	0.007	0.122	0.014	0.117	0.062	0.654
Transformer	0.207	0.053	0.020	0.008	0.139	0.012	0.128	0.069	0.747
Inc-S2S	0.224	0.053	0.017	0.006	0.151	0.013	0.141	0.067	0.825
SoCP+context-merger	0.216	0.056	0.021	0.010	0.144	0.016	0.136	0.067	0.886
SoCP+context-independent	0.232	0.062	0.025	0.011	0.161	0.018	0.151	0.072	0.879
(Ours)K-GuCCI	0.242	0.070	0.029	0.014	0.169	0.022	0.160	0.077	0.914

output text with fixed length. It is widely used in text generation tasks. Our model is improved based on Seq2Seq. Therefore, the Seq2Seq baseline can be used to compare to prove our model’s effect on emotional controllability and fluency.

Inc-S2S is an incremental Seq2Seq model mentioned in [3]. Different from the implementation in [3], we incorporate the psychological states into the model. The story sentences are generated according to the beginning of the story sentence and context. Compared with the Inc-S2S model, the effectiveness of the Character Psychological State Controller can be proved.

Transformer [27] is a novel architecture that aims at solving natural language processing tasks while handling long-range dependencies with ease. Since the Transformer model facilitates more parallelization during training, it has led to the development of pretrained models such as BERT [28], GPT-2 [29], and Transformer-xl [30], which have been trained with huge general language datasets.

GPT-2 [29] shows an impressive ability to write coherent and passionate essays. Its architecture is composed of the decoder-only transformer and it can be trained on a massive dataset. There are many works in natural language generation tasks that use GPT-2-based model.

SoCP [10] proposes a novel model called SoCP, which can generate a story according to the characters’ psychological states. The model is most relative to us. Different from that, our model introduces a knowledge graph to enhance semantic information and promote the coherence of the story.

4.3. Experimental Settings. Based on the above, we fix the character number to three. If the character number is smaller than three, use “none” as a character. The pretrained glove 300 dimension vector is used as our word embedding vector. We map the PMR matrix from a high dimension to a 256 low dimension. We implement the encoder as a two-layer bidirectional LSTM and the decoder as a one-layer LSTM with a 256 hidden size. The batch size is 8, and 0.2 is the dropout [31]. The learning rate of Adam optimizer [32] is initialed as 0.0003.

4.4. Evaluation Metrics. *BLEU* [33] is a metric to quantify the effectiveness of generated text according to compare a candidate sentence of the text to one or more reference label sen-

tences. Although designed for translation, it is commonly utilized for a suite of natural language processing tasks.

ROUGE, stands for Recall Oriented Understudy for Gisting Evaluation, is a set of metrics used for evaluating the automatic text summarization and machine translations. The metrics basically compare the similarity between generated sentences and reference sentences.

METEOR is based on the harmonic mean of unigram accuracy and recall, weighted higher than accuracy with recall. In the more common BLEU metric, the metric will correct some of the issues and also produce a strong correlation with human judgement at the level of the sentence or section.

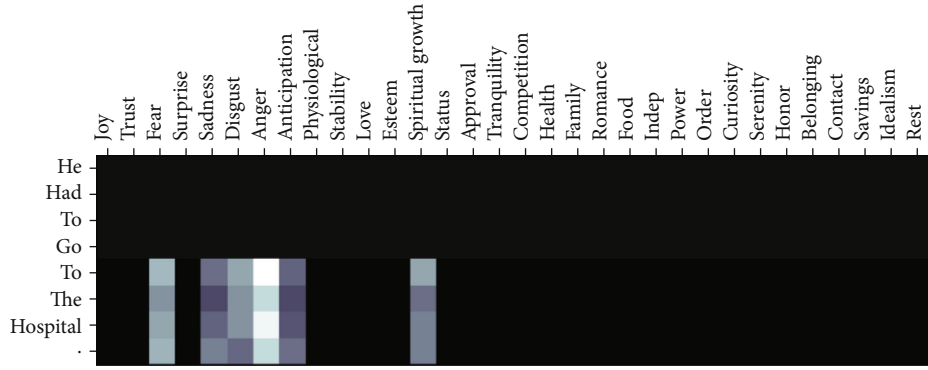
In *AGPS (Accuracy of Generated Psychological State)*, we pretrain a classifier to evaluate the accuracy of the generated psychological state. There are many approaches to train a classifier [34–36]. We utilize bidirectional LSTM to pretrain a classifier to classify the generated sentence like sentiment classification. This demonstrates our model’s capacity to convey emotions. The name of the character Char and the sentence X as input are concatenated. In this fashion, several training pairs with different outputs in similar sentences can be obtained when different characters in a sentence have various psychological states. The compact vector h^{clf} can be accessed by BiLSTM, and then, we utilize two feed-forward layers to compact it into the output size.

$$h^{clf} = \text{BiLSTM}([\text{Char}; X]), \quad (18)$$

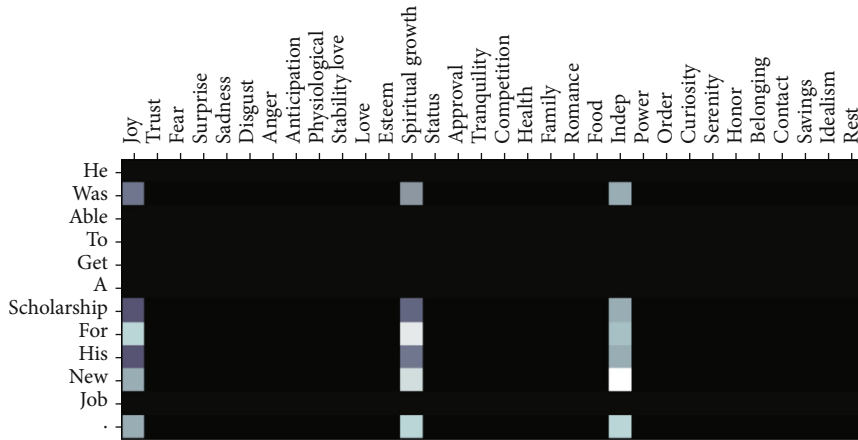
$$p = W_p \left(\text{Relu} \left(W_o \left(h^{clf} \right) + b_o \right) \right) + b_p. \quad (19)$$

4.5. Result Analysis. We have the Seq2Seq framework, the Inc-S2S, and Transformer as the baseline model. We use automatic assessment metrics, including the proposed metric AGPS, to compare our model with baseline models’ effectiveness. The experiments can prove our components and demonstrate the consistency in which the generated sentence psychological states correspond with our previous collection. All matrix’ scores in our model are the highest, as seen in Table 3, which shows the effect of our built modules, and the generated sentences are coherent.

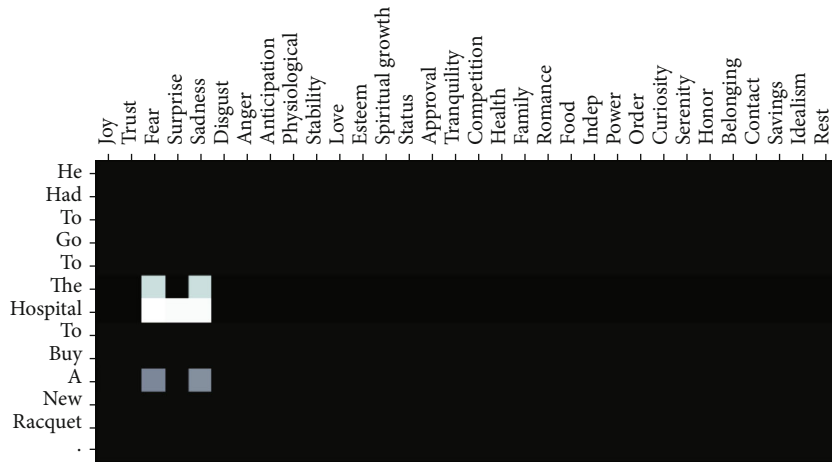
We see that Seq2Seq has better results for BLEU, ROUGE, and METEOR than the Transformer framework.



(a) Attention map 1

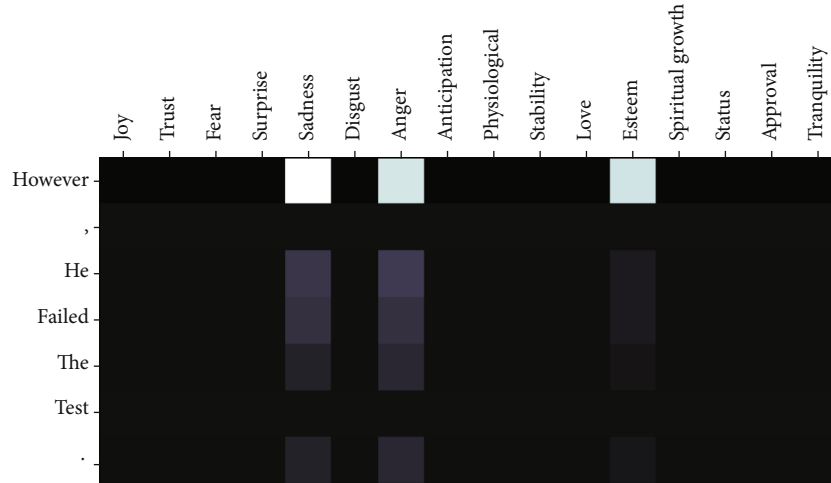


(b) Attention map 2



(c) Attention map 3

FIGURE 5: Continued.



(d) Attention map 4

FIGURE 5: Visualization of our Character Psychological State Controller. The row in the figure is the fine-grained emotion and motivation of the three psychological states, and the column represents the generated sentence. In the graph, the brighter the grid, the more attention there is between rows and columns.

The reason may be that the Seq2Seq model is more appropriate for short texts than Transformer. In addition, the outcomes of our method are better than the SoCP with context-merge method and context-independent method. The effectiveness of external knowledge that can enrich the generated stories is also reflected in this table. Our proposed model, of all the ones, has the best efficiency. The training speed of the Transformer, however, is much higher than that of Seq2Seq. It reflects the benefit of the Transformer in training speed because of the parallelism of operation.

We design AGPS to assess whether the emotion of the generated sentences is consistent with the settings. We intuitively assume that the score without input emotion will be lower. The performance of Inc-s2s is between our model and other models, which shows that our model performs efficiently for our built components.

The result of the K-GuCCI model is better than that of the SoCP model, which shows that the story can be enriched by introducing knowledge.

4.6. Model Effect Analysis

4.6.1. The Effect of the Character Psychological State Controller. We display the attention weight distribution to demonstrate the relation between the generated sentences and psychological states. As seen in Figure 5, the model provides interpretability dependent on the character’s psychological state controller. The brighter the square corresponding to the two words while generating the next word is, the stronger the relationship between them will be. Visualization of the focus maps offers a proof of the model’s ability to recognize which psychological state corresponds to the character. A word may have many different color squares, suggesting that our component can read several characters’ psychological states automatically and can select the psychological states for the character automatically. The black square suggests that no responsible psychological state is

reached because the feeling is not actually conveyed by all words, such as “a” and “the”. The model correctly chooses the elements from the psychological states in the examples displayed. The first example focuses on the emotions of Plutchik, such as “fear” and “anger,” while the second example discusses Maslow and Reiss’s elements, such as “spiritual growth” and “indep.” The term “hospital” is correlated with the Plutchik in the third attention diagram, such as “fear,” “surprise,” and “sadness,” implying that “hospital” is typically associated with a character’s negative emotion. In the fourth attention diagram, the word “however” predicts a vital turning point and negative outcomes that the character will be failed in the exam, which is also compatible with the “depression” and “anger” emotions.

4.6.2. The Effect of the External Knowledge. As seen in Table 4, the evaluation matrix shows that the performance of our model is better than other models. In addition, K-GuCCI demonstrates the effect of external knowledge in Table 4. For example, “necklace” is linked to “like it,” and “losing his mind” is linked to “go to the hospital,” which illustrates that the generated stories are coherent and reasonable. In the meantime, the conditions we set can control the stories while the coherence of the story is assured. With our setting, as we assigned the Plutchik emotional lines, the emotions of the stories will shift.

4.7. Case Study

4.7.1. Comparison with Baseline Models. The examples of stories generated by our model and the baseline models are shown in Table 4. A coherent story can be constructed by the psychological state condition we have given.

We see that it generates typically repetitive sentences by the Seq2Seq model, and it cannot accept all the characters. In Table 4, example 1 produced by the baseline model describes only one character “Jane,” but can generate

TABLE 4: Examples generated by the proposed model and the baseline models.

	Jane bought a new necklace.	The man next door seemed to be losing his mind.
Input	Characters: Jane, friends Plutchik: joy-joy-joy-joy-joy, none-none-joy-none-none Maslow: esteem, love Reiss: approval	Characters: man Plutchik: fear-disgust-surprise-surprise-joy Maslow: spiritual growth Reiss: status
Seq2Seq	She was running it. She was amazed by it. She tried it. She was thankful of Jane with it.	He was very happy to have a new job. He was not sure where he was going. He was not sure where he was going. He was not sure where to go.
Inc-S2S	She was not sure if she wanted to go to the store. She was very happy. She was very happy. She was so happy that she had a good time.	He asked his credit hour he did not know how. He asked his parents would help him some directions. He tied the games and tied miles. He was sad that he realized his card.
Transformer	She decided to do something about it. She did not have any money. She decided to save money. She decided to save up.	He yelled at him. He had to go to the hospital. He asked his girlfriend. She said yes right away.
GPT-2	“I’m not sure if I’m going to be able to wear it anymore,” she said. “I’m not sure if I’m going to be able to wear it anymore.” She said she’s been looking for a way to get rid of the necklace. “I’m not sure if I’m going to be able to wear it anymore,” she said.	“I’m sorry, but I’m not going to be able to go to the hospital,” he said. “I’m not going to be able to go to the hospital.” The man next door was also in shock. “I’m not going to be able to go to the hospital,” he said.
SoCP	She was excited to get a job. Her friend was on the same. She was very happy. She was happy to the best game.	He was very angry and did not want to do. He was a detective man about the problem. The man was not the wrong man. He was able to beat the ball and he was shot.
K-GuCCI	She was a great man. Her friend was very excited. She really liked it. She was very excited.	He was very angry and did not want to go to the hospital. He was very surprised; he was not very tall as he got to the man. He was surprised by the organizers. He was very excited to be nice.

“friends” by the K-GuCCI. In example 2, we see that with our defined psychological state condition, the baseline model cannot vary the story and even have incorrect feelings, but our K-GuCCI model can match it correctly. The GPT-2 model is capable of generating rational phrases but has several repetitions.

Overall, by manipulating the feelings of the characters, our proposed model will generate good stories. There are also some stories that are not coherent, so it is still a challenge for us.

4.7.2. Controllability. The examples in Table 5 show the controllability of generated stories under different psychological state conditions. The first example in Table 5 compares the generated stories under various condition scores using an identical Plutchik element. In specific, we set the Plutchik “joy” with different scores in the first example. Some obvious

terms such as “great,” “excited,” or “really liked” are produced when the score sets 1. As the “joy” score gets lower and lower, the terms produced get more and more negative. When the score is set to 0, some negative terms, such as “nervous” or “not good” are produced. The second example shows the produced stories with various indicators from Plutchik. We assign various Plutchik indicators to “surprise,” “fear,” and “anger.” It produces several words, such as “was surprised” or “shocked” when Plutchik is “surprise.” When Plutchik is “fear,” the words “was afraid of” or “scared” are formed. The term “angry” can be formed when Plutchik is “anger.” In the third case, for the multiple Plutchik metrics, separate scores are assigned. In the third case, in the produced stories, several emotions are portrayed.

The above examples demonstrate the controllability of our model. On the other hand, in the examples mentioned above, several incoherent stories tell us that although the

TABLE 5: Examples of controllable generated stories.

Input sentence	Jane bought a new necklace.		
Character	Jane		
Maslow	Esteem, love		
Reiss	Approval		
Generated stories with the same Plutchik indicator “joy” under different scores			
Joy = 1	Joy = 0.5	Joy = 0	
Jane bought a new necklace.	Jane bought a new necklace.	Jane bought a new necklace.	
She was a great man.	She was a new person; it was a bit huge.	She was a person and it was a bit huge.	
Her friend was very excited.	She was excited.	The man was not good and she was very nervous.	
She really liked it.	She always had been in the car, and it was fun.	She was really wanted it; the baby was gone.	
She was very excited.	She was really allowed to go to the beach.	She was pulled in the car; It was gone.	
Generated stories with different Plutchik indicators			
Surprise = 1	Fear = 1	Anger = 1	
Jane bought a new necklace.	Jane bought a new necklace.	Jane bought a new necklace.	
She was surprised to see what she had been.	She was nervous.	She was nervous.	
The man was upset.	She was nervous.	She was angry about it.	
The man was shocked.	She was afraid and was going to be scared.	She tried to be a person; a man came into the car.	
The man was not friendly.	She was going to the car that was very crowded.	The man was pulled over the police’s car.	
Generated stories with multiple Plutchik indicators			
Trust = 1, joy = 0.5	Sadness = 0.4, anticipation = 0.8	Fear = 1, disgust = 0.5	
Jane bought a new necklace.	Jane bought a new necklace.	Jane bought a new necklace.	
The man was a nice man.	She was very tired and she was not able to go.	She was nervous.	
The man was very good and they were very good.	She was nervous.	She was afraid.	
The man was always had been in the car.	She was nervous and her friends were not allowed to go.	She was afraid and her friends were going to be scared.	
The man was very close in the car.	She was nervous and decided to go to the party.	She was nervous and went to the car; she was very scared	

model performs well in emotion control, it still needs to be improved in coherence.

5. Conclusion

Traditional story generation models can only generate stories with one specific emotion and lack coherence. In this paper, we propose a model called K-GuCCI, which can generate more vivid and coherent stories under controllable conditions. We take the three psychological state theories as our controllable conditions and design a character psychological state controller, which controls the psychological state of multiple characters in the story. We introduce the external knowledge graph to enhance the semantic and richness of stories. In addition, we design an evaluation metric called AGPS to evaluate the accuracy of the generated psychological state. For future work, we will use an advanced pretrained model to generate more coherent texts. In the field of wireless communications and mobile computing, there are many

applications of the recommender system, such as [37–39], and the Internet technology, such as [40–42]. We want to use our method to recognize users’ emotions, generate high-quality text, and serve more Internet applications.

Data Availability

The data that support the findings of this study are available at <https://uwnlp.github.io/storycommonsense/>.

Conflicts of Interest

The authors declare that they have no conflicts of interest.

References

- [1] A. Fan, M. Lewis, and Y. Dauphin, “Hierarchical neural story generation,” in *Proceedings of the 56th Annual Meeting of the*

- Association for Computational Linguistics (Volume 1: Long Papers)*, pp. 889–898, Melbourne, Australia, July 2018.
- [2] A. Fan, M. Lewis, and Y. Dauphin, “Strategies for structuring story generation,” in *Proceedings of the 57th Annual Meeting of the Association for Computational Linguistics*, pp. 2650–2660, Florence, Italy, July 2019.
 - [3] L. Yao, N. Peng, R. Weischedel, K. Knight, D. Zhao, and R. Yan, “Plan-and-write: towards better automatic storytelling,” *Proceedings of the AAAI Conference on Artificial Intelligence*, vol. 33, pp. 7378–7385, 2019.
 - [4] C. Huang, O. Zaiane, A. Trabelsi, and N. Dziri, “Automatic dialogue generation with expressed emotions,” in *Proceedings of the 2018 Conference of the North American Chapter of the Association for Computational Linguistics: Human Language Technologies, Volume 2 (Short Papers)*, pp. 49–54, New Orleans, Louisiana, June 2018.
 - [5] Z. Song, X. Zheng, M. X. Lu Liu, and X. Huang, “Generating responses with a specific emotion in dialog,” in *Proceedings of the 57th Annual Meeting of the Association for Computational Linguistics*, pp. 3685–3695, Florence, Italy, July 2019.
 - [6] F. Luo, D. Dai, P. Yang et al., “Learning to control the fine-grained sentiment for story ending generation,” in *Proceedings of the 57th Annual Meeting of the Association for Computational Linguistics*, pp. 6020–6026, Florence, Italy, July 2019.
 - [7] A. H. Maslow, “A theory of human motivation,” *Psychological Review*, vol. 50, no. 4, pp. 370–396, 1943.
 - [8] S. Reiss, “Multifaceted nature of intrinsic motivation: the theory of 16 basic desires,” *Review of General Psychology*, vol. 8, no. 3, pp. 179–193, 2004.
 - [9] R. Plutchik, “A general psychoevolutionary theory of emotion,” *Theories of Emotion*, vol. 1, pp. 3–31, 1980.
 - [10] F. Xu, X. Wang, Y. Ma et al., “Controllable multi-character psychology-oriented story generation,” in *Proceedings of the 29th ACM International Conference on Information & Knowledge Management, CIKM’20*, pp. 1675–1684, New York, NY, USA, 2020.
 - [11] H. Zhou, T. Young, M. Huang, H. Zhao, J. Xu, and X. Zhu, *Commonsense Knowledge Aware Conversation Generation with Graph Attention*, IJCAI, 2018.
 - [12] S. Chen, J. Wang, X. Feng, F. Jiang, B. Qin, and C.-Y. Lin, “Enhancing neural data-to-text generation models with external background knowledge,” in *Proceedings of the 2019 Conference on Empirical Methods in Natural Language Processing and the 9th International Joint Conference on Natural Language Processing (EMNLP-IJCNLP)*, pp. 3013–3023, Hong Kong, China, 2019.
 - [13] J. Wang, J. Liu, W. Bi et al., “Improving knowledge-aware dialogue generation via knowledge base question answering,” 2019, <https://arxiv.org/abs/1912.07491>.
 - [14] J. Guan, Y. Wang, and M. Huang, “Story ending generation with incremental encoding and commonsense knowledge,” *Proceedings of the AAAI Conference on Artificial Intelligence*, vol. 33, pp. 6473–6480, 2019.
 - [15] P. Jain, P. Agrawal, A. Mishra, M. Sukhwani, A. Laha, and K. Sankaranarayanan, “Story generation from sequence of independent short descriptions,” 2017, <https://arxiv.org/abs/1707.05501>.
 - [16] M.-H. Yu, J. Li, D. Liu et al., *Draft and Edit: Automatic Storytelling through Multi-Pass Hierarchical Conditional Variational Autoencoder*, AAAI, 2020.
 - [17] C. Xing, W. Wu, Y. Wu et al., “Topic augmented neural response generation with a joint attention mechanism,” 2016, <https://arxiv.org/abs/1606.08340>.
 - [18] S. Ghosh, M. Chollet, E. Laksana, L.-P. Morency, and S. Scherer, “Affect-LM: a neural language model for customizable affective text generation,” in *Proceedings of the 55th Annual Meeting of the Association for Computational Linguistics (Volume 1: Long Papers)*, pp. 634–642, Vancouver, Canada, July 2017.
 - [19] H. Zhou, M. Huang, T. Zhang, X. Zhu, and B. Liu, *Emotional Chatting Machine: Emotional Conversation Generation with Internal and External Memory*, AAAI, 2018.
 - [20] X. Zhou and W. Y. Wang, “Mojitalk: generating emotional responses at scale,” in *Proceedings of the 56th Annual Meeting of the Association for Computational Linguistics (Volume 1: Long Papers)*, pp. 1128–1137, Melbourne, Australia, July 2018.
 - [21] H. Rashkin, A. Bosselut, M. Sap, K. Knight, and Y. Choi, “Modeling naive psychology of characters in simple common-sense stories,” in *Proceedings of the 56th Annual Meeting of the Association for Computational Linguistics (Volume 1: Long Papers)*, pp. 2289–2299, Melbourne, Australia, July 2018.
 - [22] D. Paul and A. Frank, “Ranking and selecting multi-hop knowledge paths to better predict human needs,” in *Proceedings of the 2019 Conference of the North American Chapter of the Association for Computational Linguistics: Human Language Technologies, Volume 1 (Long and Short Papers)*, pp. 3671–3681, Minneapolis, Minnesota, June 2019.
 - [23] I. Sutskever, O. Vinyals, and Q. V. Le, “Sequence to sequence learning with neural networks,” in *Proceedings of the 27th International Conference on Neural Information Processing Systems - Volume 2*, pp. 3104–3112, Montreal, Canada, 2014.
 - [24] M. Schuster K. K. Paliwal et al., “Bidirectional recurrent neural networks,” *IEEE Transactions on Signal Processing*, vol. 45, no. 11, pp. 2673–2681, 1997.
 - [25] S. Hochreiter and J. Schmidhuber, “Long short-term memory,” *Neural Computation*, vol. 9, no. 8, pp. 1735–1780, 1997.
 - [26] D. Bahdanau, K. Cho, and Y. Bengio, “Neural machine translation by jointly learning to align and translate,” 2014, <https://arxiv.org/abs/1409.0473>.
 - [27] A. Vaswani, N. Shazeer, N. Parmar et al., “Attention is all you need,” in *Proceedings of the 31st International Conference on Neural Information Processing Systems, NIPS’17*, page 6000–6010, Red Hook, NY, USA, 2017.
 - [28] J. Devlin, M.-W. Chang, K. Lee, and K. Toutanova, “BERT: pre-training of deep bidirectional transformers for language understanding,” in *Proceedings of the 2019 Conference of the North American Chapter of the Association for Computational Linguistics: Human Language Technologies, Volume 1 (Long and Short Papers)*, pp. 4171–4186, Minneapolis, Minnesota, June 2019.
 - [29] A. Radford, J. Wu, R. Child, D. Luan, D. Amodei, and I. Sutskever, “Language models are unsupervised multitask learners,” *OpenAI Blog*, vol. 1, no. 8, p. 9, 2019.
 - [30] Z. Dai, Z. Yang, Y. Yang, J. Carbonell, Q. Le, and R. Salakhutdinov, “Transformer-XL: attentive language models beyond a fixed-length context,” in *Proceedings of the 57th Annual Meeting of the Association for Computational Linguistics*, pp. 2978–2988, Florence, Italy, July 2019.
 - [31] N. Srivastava, G. Hinton, A. Krizhevsky, I. Sutskever, and R. Salakhutdinov, “Dropout: a simple way to prevent neural

- networks from overfitting,” *The Journal of Machine Learning Research*, vol. 15, no. 1, pp. 1929–1958, 2014.
- [32] D. P. Kingma and J. Ba, “Adam: a method for stochastic optimization,” in *Published as a Conference Paper at the 3rd International Conference for Learning Representations*, San Diego, 2015.
- [33] K. Papineni, S. Roukos, T. Ward, and W.-J. Zhu, “BLEU: a method for automatic evaluation of machine translation,” in *Proceedings of the 40th Annual Meeting of the Association for Computational Linguistics*, pp. 311–318, Philadelphia, Pennsylvania, USA, July 2002.
- [34] Y. Zhang, D. Song, P. Zhang, X. Li, and P. Wang, “A quantum-inspired sentiment representation model for twitter sentiment analysis,” *Applied Intelligence*, vol. 49, no. 8, pp. 3093–3108, 2019.
- [35] B. Bansal and S. Srivastava, “Hybrid attribute based sentiment classification of online reviews for consumer intelligence,” *Applied Intelligence*, vol. 49, no. 1, pp. 137–149, 2019.
- [36] J. Khan, A. Alam, J. Hussain, and Y.-K. Lee, “EnSWF: effective features extraction and selection in conjunction with ensemble learning methods for document sentiment classification,” *Applied Intelligence*, vol. 49, no. 8, pp. 3123–3145, 2019.
- [37] X. Yang, S. Zhou, and M. Cao, “An approach to alleviate the sparsity problem of hybrid collaborative filtering based recommendations: the product-attribute perspective from user reviews,” *Mobile Networks and Applications*, vol. 25, pp. 376–390, 2019.
- [38] H. Gao, L. Kuang, Y. Yin, B. Guo, and K. Dou, “Mining consuming behaviors with temporal evolution for personalized recommendation in mobile marketing apps,” *Mobile Networks and Applications*, vol. 25, no. 4, pp. 1233–1248, 2020.
- [39] Y. Yin, Z. Cao, Y. Xu, H. Gao, R. Li, and Z. Mai, “QoS prediction for service recommendation with features learning in mobile edge computing environment,” *IEEE Transactions on Cognitive Communications and Networking*, vol. 6, no. 4, pp. 1136–1145, 2020.
- [40] X. Ma, H. Gao, H. Xu, and M. Bian, “An IoT-based task scheduling optimization scheme considering the deadline and cost-aware scientific workflow for cloud computing,” *EURASIP Journal on Wireless Communications and Networking*, vol. 2019, Article ID 249, 2019.
- [41] H. Gao, W. Huang, and Y. Duan, “The cloud-edge-based dynamic reconfiguration to service workflow for mobile e-commerce environments,” *ACM Transactions on Internet Technology (TOIT)*, vol. 21, no. 1, pp. 1–23, 2021.
- [42] H. Gao, C. Liu, Y. Li, and X. Yang, “V2VR: reliable hybrid-network-oriented V2V data transmission and routing considering RSUs and connectivity probability,” *IEEE Transactions on Intelligent Transportation Systems*, pp. 1–14, 2020.